In-vivo characterization of therapeutic antibodies after subcutaneous injection using a LC-MS based immuno-capture assay

Dissertation

zur Erlangung des akademischen Grades eines
Doktors der Naturwissenschaften
– Dr. rer. nat. –

vorgelegt von

Annika Doell

geboren in Ludwigshafen am Rhein

Angewandte Analytische Chemie
der
University Duisburg-Essen

2019

DOI: 10.17185/duepublico/70594
URN: urn:nbn:de:hbz:464-20191023-084636-2

Die vorliegende Arbeit wurde im Zeitraum von Februar 2016 bis Januar 2019 im Arbeitskreis von Prof. Dr. Oliver J. Schmitz am Institut für Angewandte Analytische Chemie der Universität Duisburg-Essen angefertigt. Jegliche Praktische Arbeiten wurden in der Arbeitsgruppe von Dr. Markus Hollmann in Ludwigshafen bei der Firma AbbVie Deutschland GmbH & Co. KG durchgeführt.

Tag der Disputation: 07. Oktober 2019

Gutachter:	Prof. Dr. Oliver J. Schmitz
	Prof. Dr. Thorsten C. Schmidt
Vorsitzender:	Prof. Dr. Holger Somnitz

Hiermit versichere ich, dass ich die vorliegende Arbeit mit dem Titel

„*In-vivo characterization of therapeutic antibodies after subcutaneous injection using a LC-MS based immuno-capture assay*"

selbst verfasst und keine außer den angegebenen Hilfsmitteln und Quellen benutzt habe, und dass die Arbeit in dieser oder ähnlicher Form noch bei keiner anderen Universität eingereicht wurde.

Ludwigshafen, den 13. März 2019

_____

Annika Doell

Table of Content

Summary

Therapeutic antibodies have become increasingly important in the treatment of autoimmune diseases and different types of cancer. During production and storage the protein molecules can undergo modification due to different degradation reactions, which may decrease biological activity and/or bioavailability of the antibody. Therefore, the analysis of protein modifications on the peptide level using liquid chromatography coupled to mass spectrometry (LC-MS) is a common approach to characterize protein therapeutics. While analysis of *in-vitro* samples is performed routinely, the full characterization of protein therapeutics after *in-vivo* administration is highly challenging due to the low protein amount that is available for analysis. The work described in this thesis focuses on the development of a complete workflow that enables full characterization of therapeutic antibodies after subcutaneous injection. At first, a suitable capture protocol to purify the therapeutic antibody from complex biological matrices was developed in order to remove matrix proteins that may interfere with the mass spectrometric analysis. Best results were achieved using a commercial anti-human capture antibody fragment in combination with streptavidin coated magnetic beads providing capture efficiencies of 90-100%. The obtained results further demonstrated that the protocol works in an unbiased way and allows capturing both, stressed and unstressed material. To localize then the sites of particular modifications, it is a common approach to apply enzymatic digestion followed by LC-MS analysis (peptide map). This peptide map procedure is routinely performed using 250 µg antibody for digestion. However, for *in-vivo* samples only a few hundred nanogram (up to 1 µg) are available for analysis. Therefore, a part of this thesis is also focused on the development of a special digestion protocol suitable for low sample amounts. The final workflow requires less than 1 µg antibody, includes two desalting steps and shows sequence coverages of 95-100%. Thus, compared to standard *in-vitro* approaches a 250-fold reduction of the required amount of antibody was achieved. With the implementation of a nano-LC-MS platform the required sensitivity for the analysis of *in-vivo* samples was realized. Thus, compared to a standard flow LC using 2.1 mm columns, the developed nano-LC platform offers a 300-fold sensitivity increase. Finally, the workflow was successfully applied for the characterization of a therapeutic antibody after subcutaneous injection in both, serum and interstitial fluid. This is the first time that a therapeutic antibody has been extracted from the subcutis of a pig after subcutaneous injection and got fully characterized. Overall, the results revealed the same modifications for both sample types and therefore it can be concluded that the antibody is not modified in the subcutaneous tissue after injection within the first ten hours. The ability to specifically capture and fully characterize therapeutic antibodies from biologic matrices is a major improvement and of high importance for the development of biotherapeutics. This workflow described here lays the foundation for future experiments to answer the question of what happens to antibodies after injection *in-vivo*. Thus, a better understanding of the *in-vivo* processes could contribute to an improved risk assessment of biopharmaceuticals during development, manufacturing and storage.

Zusammenfassung

Die Bedeutung therapeutischer Antikörper in der Krebstherapie sowie zur Behandlung von schweren Autoimmunkrankheiten nimmt stetig zu. Bei der Produktion und Lagerung der Moleküle, kann es jedoch zu verschiedensten Degradationsreaktionen kommen. Diese wiederum können zu einer verminderten biologischen Aktivität, sowie einer reduzierten Bioverfügbarkeit der Antikörper im Patienten führen. Daher ist die Analyse der Moleküle von großer Bedeutung und wird standardmäßig auf Peptidebene mittels Flüssigchromatographie gekoppelter Massenspektrometrie (LC-MS) betrieben. Während die Charakterisierung der Antikörper *in-vitro* Routine ist, stellt ihre Analyse nach Verabreichung *in-vivo* eine große Herausforderung dar. Dies ist vor allem darin begründet, dass der Antikörper nach der Injektion in einer komplexen biologischen Matrix vorliegt und zusätzlich nur in sehr geringen Mengen zur Verfügung steht. Das Ziel dieser Arbeit lag somit in der Entwicklung einer geeigneten Methode zur vollständigen Charakterisierung von therapeutischen Antikörpern nach der subkutanen Injektion. Um den Antikörper nach der Injektion aus der biologischen Matrix zu isolieren, wurde zunächst ein Protokoll zur spezifischen Aufreinigung entwickelt. Die besten Ergebnisse wurden mit einem kommerziellen anti-humanen Capture-Fragment in Kombination mit Streptavidin-beschichteten Magnetic Beads erzielt. Mit Hilfe dieses Protokolls konnten Aufreinigungseffizienzen von 90-100% erreicht werden. Ebenso wurde demonstriert, dass auch modifizierte Antikörper aufgereinigt werden und die Ergebnisse somit unverfälscht sind. Um die genaue Position einer Modifikation im Antikörper zu bestimmen, ist es hilfreich diesen in kleinere Stücke zu schneiden. Ein klassischer Ansatz ist hier der enzymatische Verdau in Peptide (Peptide Map). Während bei *in-vitro* Analysen mehrere hundert Mikrogramm Antikörper eingesetzt werden können, stehen bei *in-vivo* Proben meist nur ein paar hundert Nanogramm bis hin zu einem Mikrogramm zur Verfügung. Der Fokus lag somit auch auf der Entwicklung eines Peptide Map-Protokolls für *in-vivo* Proben. Der finale Ansatz beinhaltet zwei Entsalzungsschritte und benötigt eine absolute Menge an Antikörper von weniger als einem Mikrogram bei einer Sequenzabdeckung von 95-100%. Somit wurde im Vergleich zu *in-vitro* Analysen eine 250-fache Reduzierung der benötigten Menge an Antikörper erreicht. Mit der erfolgreichen Implementierung einer Nano-HPLC-MS Plattform konnte zudem ein 300-facher Sensitivitätsgewinn im Vergleich zu Standard-Fluss Geräten erreicht werden. Das gesamte Protokoll wurde erfolgreich für die Charakterisierung eines therapeutischen Antikörpers nach subkutaner Injektion angewendet und liefert erstmals Erkenntnisse über subkutan auftretenden Modifikationen. Mithilfe dieser Studie kann geschlussfolgert werden, dass der Antikörper innerhalb der ersten zehn Stunden nach der Injektion in der Subkutis nicht modifiziert wird. Die Fähigkeit therapeutische Antikörper spezifisch aus biologischen Matrices aufzureinigen und vollständig zu charakterisieren ist ein großer Benefit für die Entwicklung von Biotherapeutika. Der in dieser Arbeit entwickelte Ablauf legt den Grundstein zur Beantwortung der Frage was mit Antikörpern nach der Injektion passiert. Ein genaueres Verständnis der *in-vivo* Prozesse kann zu einem besseren Produkt-Risiko Verständnis in der Entwicklung, Herstellung und Lagerung führen.

1. Introduction

1.1 General

1.1.1 Antibody structure and function

Antibodies or immunoglobulins (Ig) are Y-shaped glycoproteins composed of four polypeptide chains. Two identical light chains (LC) with a mass of ~25 kDa and two identical heavy chains (HC) with a mass of ~50 kDa are connected by disulfide bonds. Based on the different types of heavy chains α, δ, ε, μ and γ, antibodies can be divided into five different classes IgA, IgD, IgE, IgM and IgG. However, as Ig type G is the major class of antibody molecules and also the type most abundantly used for therapeutic purposes, their structure is discussed in detail (see Figure 1). [1]

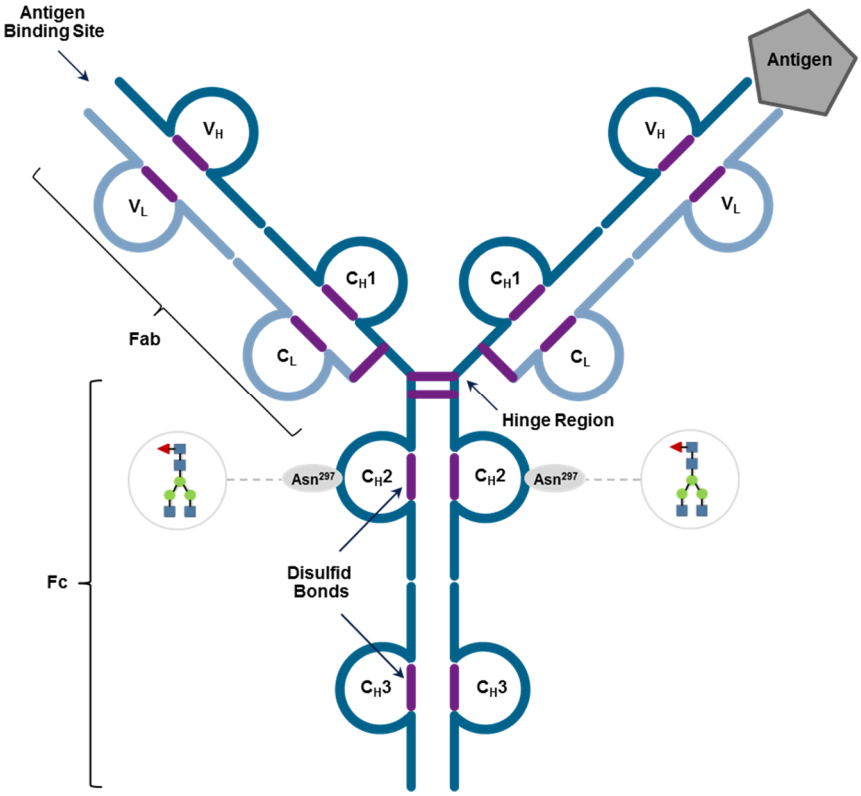

Figure 1 – Structure of an IgG-1 Antibody

An antibody can be displayed as a Y-shaped glycoprotein made up of two identical light (light blue) and heavy chains (dark blue). The polypeptide chains consist of variable (V) and constant (C) part and are connected via disulfide-linkages (purple). The flexible hinge region separates the antibody molecule in the antigen-binding fragment (Fab) and the constant fragment (Fc).

Each polypeptide chain contains a variable (V) region which is different for each antibody. Therefore, the variable parts define the specific antigen-binding properties and offer two identical antigen-binding sites. The binding sites are formed by six hypervariable loops, three from LC and three from HC and are also called complementary-determining regions (CDRs).

In addition to the variable regions, LCs have one and HCs three constant domains (C_H1, C_H2 and C_H3) that are similar for the antibodies of one class. Therefore, the antibody molecule can be divided into an antigen-binding fragment (Fab) and a constant fragment (Fc) that is involved in effector functions of the immune system. The Fab and Fc part are connected by an amino acid series rich in proline, serine and threonine. The so called hinge-region provides a high flexibility to the antibody molecule as it imparts lateral and rotational movement.

As antibodies are specific proteins of the humoral immune system they recognize and defend vertebrates against pathogens. Viral proteins, toxins, parasites or microorganisms that enter the body are detected as foreign molecules/pathogens. Either, a microorganism or a molecule itself, or a part of it (e.g. surface proteins of bacteria or their fragments), are recognized by the immune system and called antigens. In order to produce specific antibodies against the antigen, the immune system needs to be activated. In a first step, B-lymphocytes which are specific cells of the immune system, bind the antigen via a membrane-bound antibody. This antibody is part of the B-cell receptors (BCR) and the binding of the antigen leads to an activation of a complex immune cascade. At the end of this cascade specific antibodies against the antigen are produced. The antibodies bind the foreign molecule via their antigen-binding sites, building antibody-antigen complexes. Those complexes are recognized via the Fc part of the IgGs by specific receptors, FcγR on macrophages and get degraded. [2, 3]
Thus, the Fc-part of the antibody molecule exerts different functions including activation of the complement cascade, antibody dependent cellular cytotoxicity (ADCC) and opsonization of the target cell via binding to FcγR. [4, 5]

A distinction is made between polyclonal and monoclonal antibodies (mAb). Polyclonal antibodies (pAbs) are a mixture of antibodies synthesized by many different B-cells that recognize different epitopes of one antigen. The region of the antigen where binding to the antibody occurs is called epitope whereas the amino acid residues of the antibody that are in direct contact to the antigen are called paratope. In contrast to pAbs, monoclonal antibodies (mAbs) are produced by a population of identical B-cells generated from a single clone and therefore all recognize the same epitope of the respective antigen. [6]

1.1.2 Antibody recycling

Besides binding to FcγRs the Fc-region is involved in another important receptor binding. The neonatal Fc-Receptor (FcRn) mediates maternal IgG transport across the intestinal epithelium of neonatal rodents and the placenta in humans. As a consequence, humoral immunity of the mother is conferred to the newborn or fetus. [7-9]

The FcRn receptor is also called Brambell-receptor as this phenomenon was first postulated by Brambell in 1966 [10].

The receptor is responsible for the prolonged half-life of mAbs *in-vivo* due to a specific salvage pathway. In 1964 Spiegelberg and co-workers found the half-life of the Fc-portion to be closely related to the intact IgG, whereas the Fab-Fragment is removed rapidly [11]. This finding already indicated the importance of the Fc-region in the recycling process of antibodies. Further investigations revealed that the binding of FcRn and the Fc-region of IgGs is pH-dependent [12, 13].

As shown in Figure 2 endothelial cells internalize IgGs from serum and form endocytic vesicles.

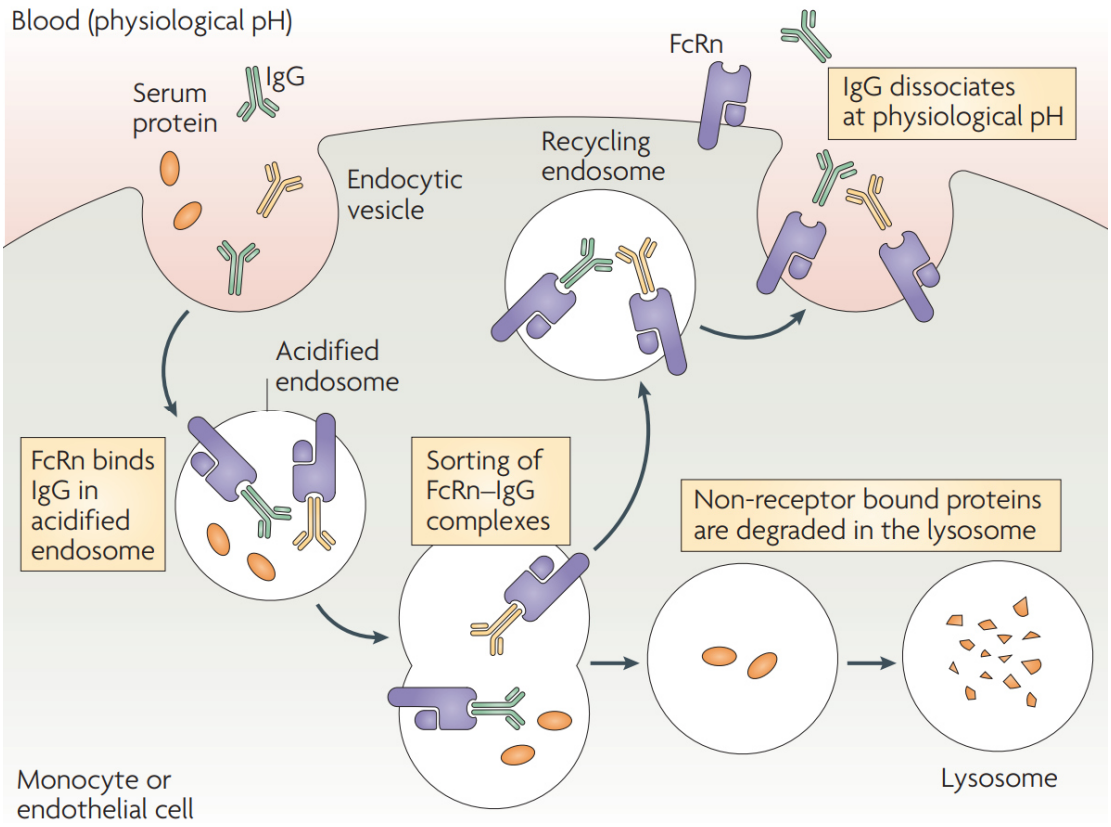

Figure 2 – FcRn-mediated antibody salvage

Serum IgGs get internalized by endosomes and bind to FcRn receptors in an acidified environment. Non-receptor bound serum proteins undergo lysosomal degradation whereas FcRn-bound IgGs get transported back to the cell surface. At physiological pH of 7.4, the IgG gets released from the FcRn, as the binding shows a specific pH-dependency (copied with permission from Roopenian et al. [14]).

In acidified endosomes (pH 6) the intact IgG gets bound by the FcRn and is thus protected from lysosomal degradation. Other serum proteins that are not bound to the receptor undergo lysosomal degradation. The recycled IgG is transported back to the cell surface and released at physiological pH conditions (pH 7.4). This salvage pathway is the reason for the extended half-life of serum IgGs compared to other proteins. [14]

1.1.3 Production of monoclonal antibodies

The foundational technology in the production of mAbs with predefined specificity was the hybridoma technique developed by Milstein and Köhler [15]. In a first step a mouse was immunized with a specific antigen provoking an immune response and the production of B-Cells. The B-cells were isolated from the spleen and fused to immortalized murine myeloma cells that lack the ability to produce a specific enzyme, the hypoxanthine-guanine phosphoribosyltransferase. Due to a gene mutation, myeloma cells are not able to produce the enzyme required for the nucleotide salvage pathway. This deficiency was used as a selection marker to differentiate between successful hybridomas, and unfused myeloma and B-cells [15, 16].

Incubation of the fused cells in hypoxanthine-aminopterin-thymidine medium (HAT) blocks the de novo synthesis of nucleotides, and kills unfused myeloma cells as they lack the ability to produce nucleotides. Although, B-cells are able to produce nucleotides, they die due to their short live time in cell culture. Only the hybridoma cells are able to survive culture in HAT-medium, due to the B-cell ability to produce nucleotides and the immortality from the myeloma cells. In this way, permanent antibody secreting hybridoma cell lines are produced. [16]

As the “mouse hybridoma technique” represented the first milestone in antibody engineering, in 1984 Köhler, Milstein and Jerne awarded the Nobel Prize in Physiology or Medicine [17].

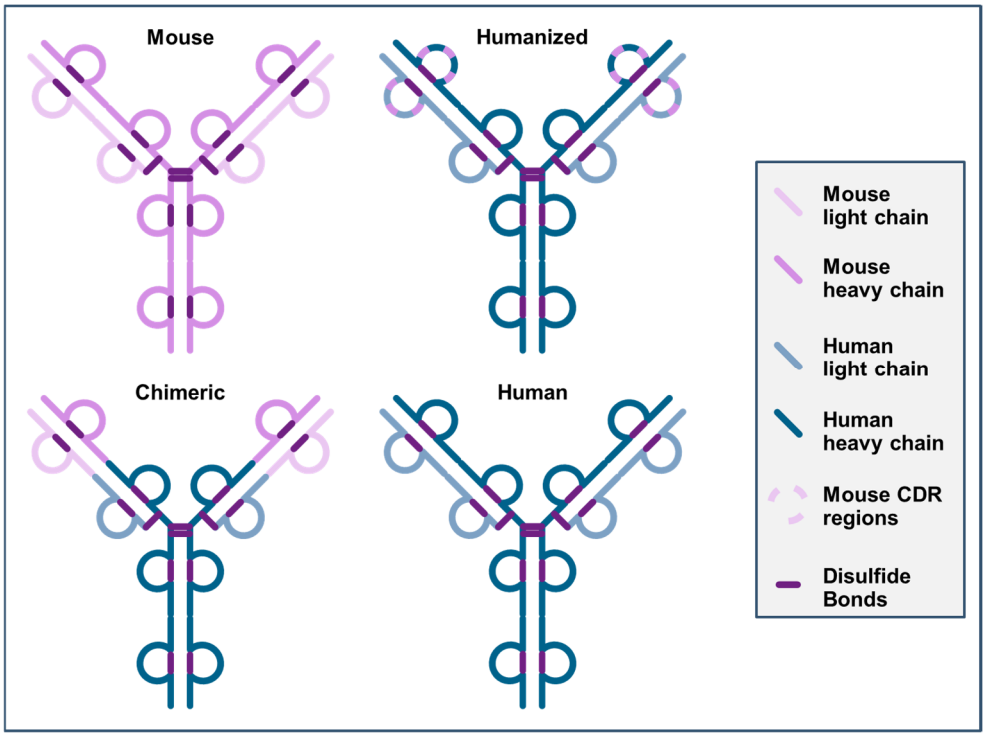

Figure 3 – Antibody Engineering

Mouse antibodies are generated using the mouse hybridoma technique. By genetic engineering the variable domains of a mouse mAb were joined to human constant domains to produce chimeric antibodies. For the production of humanized mAbs, only the CDR regions from a mouse mAb were grafted into a human IgG. By phage display technology or the transgenic approach it became possible to produce fully human antibodies without murine sequences.

However, the murine antibodies produced by the hybridoma technique showed immunogenicity when used as therapeutic agents in humans. The human immune system quickly responds to the murine mAbs and produces human antibodies against the mouse antibody (HAMA). As a consequence, the therapeutic murine antibody is cleared from the bloodstream, and by this the effectiveness is reduced. [3, 18]

To reduce immunogenicity, the variable domains of a mouse mAb were joined to human constant domains building a "chimeric" antibody [19]. A further step was made in 1986 by grafting the CDRs of a murine antibody into a human antibody. The "humanized" antibodies contain only the proportion of mouse sequence involved in antigen binding and are therefore less immunogenic. However, the humanized mAbs often showed reduced binding affinity compared to the original murine mAb. Additional changes were required in the framework regions flanking the CDRs to restore full affinity (see Figure 3). [20]

The direct production of fully human mAbs became possible with the development of phage display technology by Smith *et al.* [21]. In phage display technology foreign genes were inserted into a gene of filamentous bacteriophages which codes for the protein pIII. This protein is a minor coat protein and is expressed on the surface of the phages. To express the foreign protein in a native form with functional integrity, the gene of interest needs to be inserted in the coding regions for the amino and carboxyl domains of pIII [22]. In 1990, McCafferty *et al.* applied the phage display technology for the production of complete antibody variable domains and by this revolutionized the process of antibody engineering [15, 23]. Recently, the Royal Swedish Academy of Sciences awarded the Nobel Prize in Chemistry to Smith and Winter for the phage display of peptides and antibodies [24].
An alternative way to produce fully human mAbs, is the transgenic approach using humanized mice. Endogenous Ig genes are silenced, whereas the human counterparts are introduced into mice at germ line level. Immunization against the antigen and isolation of B-cells is then performed as earlier described in hybridoma technology. [15, 25]

1.1.4 Application of therapeutic mAbs in medicine

The approval of the first therapeutic antibody in 1986 was the beginning of a revolution of the pharmaceutical industry. Muronomab-CD3 (Orthoclone OKT-3) was produced using the hybridoma technique and was applied for prevention of kidney transplant rejection. However, as the antibody originated from mouse, immune reactions were observed in 50% of the patients. The next step was taken in 1994 with the approval of abciximab (ReoPro), the first chimeric antibody. This molecule showed reduced immunogenicity of 1 – 14%. Three years later, the humanized antibody daclizumab (Zenapax) was approved with immunogenicity levels of 14 – 34% [26].

In 2002 the first fully human antibody adalimumab (Humira) isolated by phage display technology, was approved [26, 27]. Four years later the American Food and Drug Administration (FDA) approved panitumumab, the first fully human mAb produced by transgenic mice [28].

Due to the ongoing technological progress, safety and efficacy of therapeutic antibodies could be increased over the last 30 years [26]. The drawbacks of high immunogenicity and short half-lives could be overcome by the advancing technology. With the development of biologics, new treatment opportunities were created targeting areas were traditional therapies have failed. Thus, most therapeutic antibodies are used in the treatment of autoimmune and inflammatory diseases as well as in oncology. [27]

A specific class of engineered antibodies, developed especially for the treatment of oncologic diseases, is called antibody-drug conjugates (ADC). An ADC is a combination of a therapeutic antibody and a small molecule drug like e.g. auristatins or calicheamycins. Via the therapeutic antibody the ADC is directed to the tumor cell and binds to the antigen. After internalization of the ADC, the cytotoxic drug is released by proteolytic cleavage or lysosomal degradation of the linker at the site of the tumor cell. This leads depending of the drug to either microtubule inhibition or damage of the tumor cell DNA and finally to cell death of the tumor cell. Thus, the small molecule drug is released directly at the target cell which is less toxic than a systemic application of the drug alone. [29]

Brentuximab vedotin was the first ADC approved for the US-market. The chimeric mAb against receptor CD30 carries the anti-mitotic agent monomethyl auristatin E (MMAE) and is applied in the treatment of lymphomas [15].
After binding to CD30 on lymphoma cells, brentuximab vedotin is internalized by the formation of clathrin coated particles into endosomes (see Figure 4). In the lysosome the drug linker is cleaved by proteases and MMAE is released. The free drug enters the cytosol and binds the microtubuli, leading to depolymerization and cell death. Via drug transporters in the cell membrane, MMAE can also exit the cell and enter neighboring cells, called bystander effect. [30]

Overall, therapeutic antibodies and other biologics can be categorized into five groups based on their mechanism of action. The first group comprises cytotoxic mAbs that induce death of cells with aberrant function, which is the primary goal in autoimmune disease or cancer therapy. The second group describes mAbs modulating cell activation/interaction. Those antibodies have been successfully applied in the treatment of organ transplant rejection or autoimmune diseases by blocking T-cell activation. Another mode of action is the blockage of growth receptors in e.g. tumor treatment by mAbs preventing cell growth and proliferation. Furthermore, mAbs can be directed against pro-inflammatory cytokines

modulating immune signaling. The last group is built by mAbs neutralizing foreign entities such as fusion proteins of viral infections. [15]

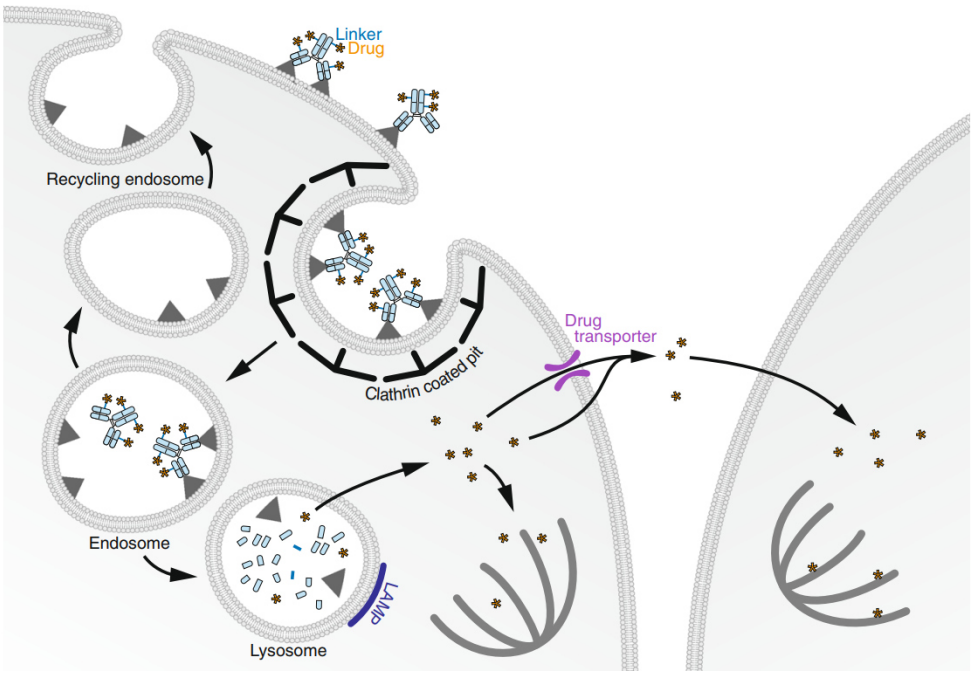

Figure 4 – Brentuximab vedotin: Mode of action

Brentuximab vedotin binds the antigen CD30 on Hodgkin lymphoma cells and is then internalized as clathrin coated particle until it reaches the endosomes. The linker is cleaved by proteases in the lysosome and the MMAE is released. The drug exits the lysosome and binds the microtubuli in the cytosol, leading to depolymerization and finally death of the cell. MMAE can also act on neighboring cell, which is called bystander effect. (copied with permission from Chalouni et al. [30])

1.1.5 Specification and comparability assessment of biotherapeutics

To ensure the worldwide development of safe and effective biotherapeutics of high quality, a global harmonization is essential. The International Council for Harmonization of Technical Requirements for Pharmaceuticals for Human Use (ICH) brings together regulatory agencies and industrial associations for the development of harmonized guidelines for global pharmaceutical development. These guidelines focus on the topics safety, quality and efficacy of pharmaceutical products. [31]

During the development of a biotherapeutic, starting from early to late stages, it is highly likely that the production process is continually optimized. Reasons for those changes can be the implementation of new and improved techniques, but also evolving regulatory requirements. However, independent on the reason of process change, the quality of the pharmaceutical should not be affected. Therefore, comparability studies between the products prior and after process changes are required, to ensure consistent quality. According to ICH Guideline Q6B, for each biotechnological product a certain

specification is proposed and justified by the manufacturer, to which a drug should conform to guarantee the quality and consistency of the product for its intended use. It is defined by a list of tests and analytical procedures including the appropriate acceptance ranges, limits or other criteria for each test. These critical standards are approved by the regulatory authorities as conditions of approval. [32]
Therefore, ICH guideline pharmaceutical development Q8 expects the identification of so-called Critical Quality Attributes (CQA). *"A CQA is a physical, chemical, biological, or microbiological property or characteristic that should be within an appropriate limit, range, or distribution to ensure the desired product quality"* [33].
Furthermore, a distinction is made between product-related substances and product-related impurities, as described in ICH guideline Q6B. Active molecular variants that do not influence safety and efficacy of the drug product are regarded as product-related substances. In contrast to this, molecular variants that have deleterious effects on activity, efficacy or safety, are defined as product-related impurities. Thus, it is important to define the different characteristics and variants as quality attributes and specify the numeric ranges that the product need to conform.[32]

Historically, the characterization of proteins was performed by Edman degradation, ultra violet and visible spectrometric methods as well as electrophoretic analysis, like SDS-PAGE [34]. However, with the approval of Insulin as the first recombinant protein therapeutic in 1982 the number of analytical tests for the characterization of proteins started to increase [35]. Nowadays, an arsenal of different established analytical methods is available that include techniques for the characterization of physicochemical properties, biological activity, immunochemical properties, purity and impurities [32]. Table 1 lists some common analytical techniques used for the batch release of protein therapeutics.

Table 1 – Common techniques for the batch release of protein therapeutics

Attribute	Common batch release methods
Identity	Peptide Map (LC-UV)
Glycosylation	HILIC
Molecular weight, Size	SEC, SDS-PAGE, MS
Charge	CE, IEX, IEF
Extinction coefficient	UV/visible Spectrophotometry
Homogeneity, purity	SDS-PAGE, IEF
Higher order structure	CD, DSC
Potency	Cell-based assay

HILIC = hydrophilic interaction liquid chromatography, SEC = size exclusion chromatography, SDS-PAGE = sodium dodecyl sulfate polyacrylamid gel electrophoresis, MS = mass spectrometry, CE = capillary electrophoresis, IEX = ion exchange chromatography , IEF = isoelectric focusing, UV = ultra violet, CD = circular dichroism, DSC = differential scanning calorimetry

Confirmation of the identity of biotherapeutics is routinely performed by peptide mapping [36-39]. Thereby, the protein is digested using suitable enzymes such as trypsin or lys-C that recognize specific amino acid sequences to perform the peptide bond cleavage. Therefore, the expected set of peptides produced by the digestion with a particular proteolytic enzyme can be deducted from the knowledge of therapeutic protein sequence. The peptides are then separated by reversed phase High Performance Liquid Chromatography (RP-HPLC) and analyzed by ultra violet/visible (UV/vis) absorbance [40]. Although, mass spectrometry (MS) based peptide mapping has been used for several decades in the extended characterization of proteins, release testing has been performed by the classical UV-detection. [36-39]

Conventional assays used for lot release were generally designed to monitor one type of CQA [41, 42]. Thus, SDS-PAGE is used to determine homogeneity and purity, while several chromatographic techniques such as hydrophilic interaction (HILIC), ion exchange (IEX) or size-exclusion chromatography (SEC) are used for the analysis of glycosylation pattern, charge variants or aggregates, respectively [43-45].

In 2015, Rogers *et al.* (Amgen, CA, USA) described LC-MS/MS based peptide mapping as a multiple attribute method (MAM) that has the potential to replace several classical assays leading to an improved control strategy [46]. The idea to use MAM in quality control and release testing is to assess more attributes with fewer methods. Therefore, the goal of the LC-MS/MS peptide Map is to find every peptide of the protein digest and by this cover the complete sequence of the mAb. As a result, attributes such as glycosylation pattern, charge variants and purity could all be monitored by MS-based peptide mapping [46-48]. Thus, several conventional assays for instance IEX, HILIC or SDS-PAGE could be replaced by MAM leading to a cost reduction [49].

Recently, Bomans and co-workers (Roche Diagnostics, Basel, Switzerland) published a similar MAM workflow and demonstrated feasibility of the workflow to monitor all attributes of the therapeutic mAb trastuzumab [50].

Thus, the overall trend in quality control and release testing, as can be seen by the recent publications of Roche and Amgen, goes towards more powerful techniques that allow the simultaneous analysis of multiple quality attributes by one single method [46-51].

1.1.6 Post-translational modifications in mAbs

Modifications that occur after transcription and translation to proteins are defined as post-translational modifications (PTMs) [52]. As recombinant mAbs are produced in non-human cell lines, it bares the risk of introducing PTMs that are normally not found in humans. Furthermore, during processing and storage further types of modifications can be introduced to the molecules. In general, modifications can add or replace functional groups but also structural changes such as racemization, cleavage or folding could take place. Some of the most common modifications encountered during antibody production and storage are highlighted in Table 2. [53]

Table 2 – Common post-translational modifications and their relevance *in-vivo*

Modification	Description	Relevance *in-vivo*
N-terminal pyro-glu formation	Cyclization of the terminal amino acid (Q or E)	No impact on mAb structure and binding
Oxidation	Introduction of an oxygen atom into amino acid (mostly M, but also W and less frequently H).	In Fc-region: can impact half-life and clearance In CDR-region: can impair target binding
Glycosylation	MAbs are glycoproteins and carry different glycan structures.	Important for structure and function of the mAb High-mannose glycans have higher clearance rates
Deamidation	Loss of a primary amine (N, Q)	In CDR-region: can impair target binding
Isomerization	Dehydration and subsequent hydrolysis leading to isomer formation (D)	In CDR-region: can impair target binding
C-terminal lysine clipping	(In)complete removal of the *C*-terminal lysine residue (K)	Might influence complement activation

1.1.6.1 N-Terminal modifications

In most antibodies the first amino acid of the light and heavy chain is either glutamine (Q) or glutamic acid (E). Both amino acids can undergo spontaneous cyclization leading to the formation of pyro-glutamic acid (pyro-E) as shown in Figure 5. [54, 55]

Investigations on the effect of pyro-E modification on the mAb structure and binding properties showed that presence of this modification has likely no significant impact. Also mAb clearance rate do not change for mAbs containing pyro-E. [56-58]

However, in case of pyro-E formation from *N*-terminal Q, the reaction results in a loss of an amine group. Therefore, the molecule loses a positive charge and becomes more acidic. Due the fact that charge changes might impact the structure and folding of a molecule, this modification is routinely monitored during production and storage to ensure product quality [56].

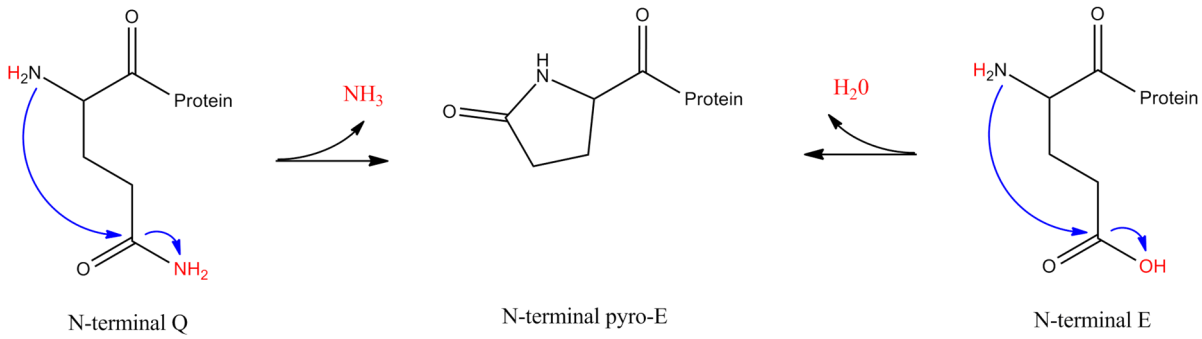

Figure 5 – Pyroglutamic acid formation

The terminal amino acids glutamine (Q) and glutamic acid (E) can result in the formation of pyro-glutamic acid formation due to a spontaneous cyclization reaction. (Cf. Liu 2011 [56])

1.1.6.2 Oxidation

Oxidation of amino acid residues is a major degradation pathway of biotherapeutics and has been observed during production, purification, formulation and storage [59-61]. Primarily, oxidation of methionine (M) and less frequently oxidation of tryptophan (W) and histidine (H) can occur. As can be seen from Figure 6, the oxidation of M leads to methionine sulfoxide (oxMet) while W oxidation can lead to single (oxTrp) and double oxidized (dioxTrp) molecules. [61]

The major factors defining the susceptibility of a particular amino acid residue to oxidation are the location of this residue in the three dimensional protein structure and its solvent exposure. It has been shown that the DTLMISR-peptide and the WQQ-peptide located in the second (C_H2) and third (C_H3) constant domain, respectively, are highly susceptible to oxidation. Investigations on the thermal and chemical stability of protein therapeutics revealed that those residues are preferentially oxidized, while other methionine residues were relatively stable. [62-64]

Several authors investigated whether the individual contribution of site-specific oxidations can affect biological properties or conformation of mAbs [64]. It has been demonstrated that methionine oxidation in the Fc-region reduces binding affinity to protein A and G, commonly used for antibody purifications [65].

In contrast to this, binding affinity of oxidized mAbs to Fcγ receptors was found to remain the same [66]. Further investigations showed that methionine oxidation significantly lowers the mAb affinity to FcRn receptor which plays an important role in antibody circulation time [62, 66, 67]. Stracke and co-

workers reported that methionine oxidation of the WQQ-peptide has only a minor impact on FcRn binding. They found that a single DTLMISR oxidation per antibody molecule (i.e. when only one HC is oxidized) also had little effect compared to the unmodified mAb. However, when the DTLMISR peptides of both HCs of one antibody molecule are oxidized, a significant faster clearance was observed. [68]

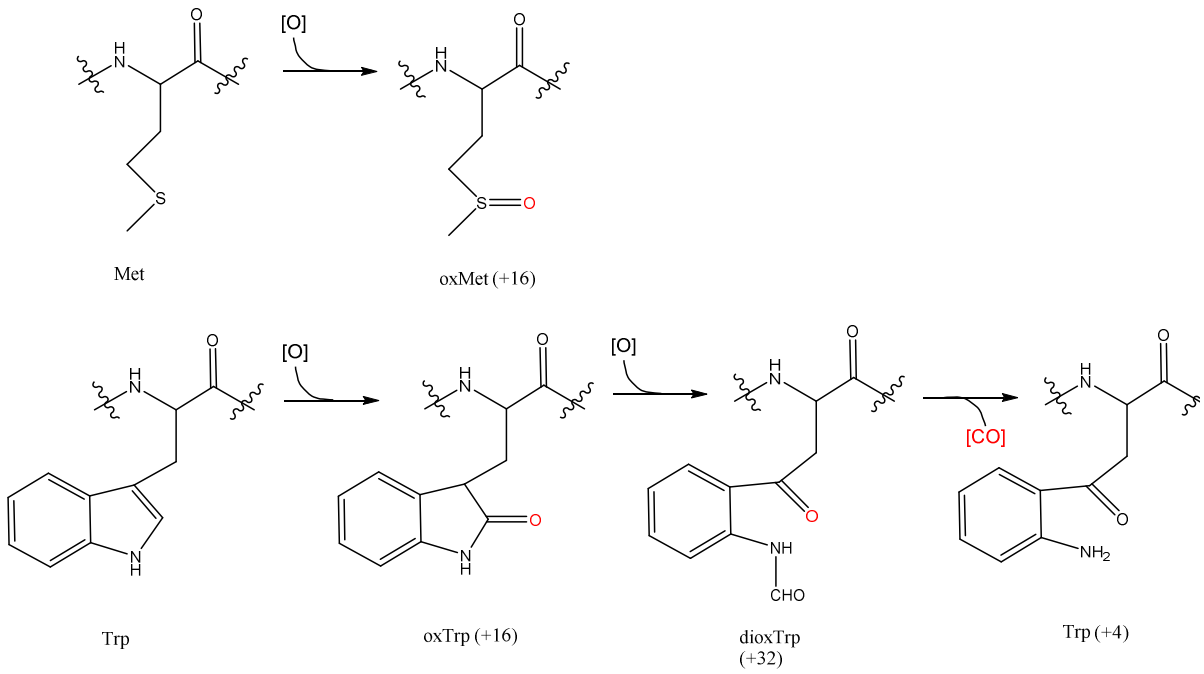

Figure 6 – Oxidation of methionine and tryptophan

Oxidation of methionine (Met) is frequently observed, leading to the methionine sulfoxide (oxMet). Tryptophan oxidation can form single oxidized (oxTrp) and double oxidized molecules. CO loss can form a species with a 4 Dalton mass shift to the unmodified Trp. (Cf Lam et al. [61])

Cymer *et al.* investigated the influence of oxidized methionine residues in human IgG1 on binding and activation of human Fc-Receptors. They demonstrated that oxidation of DTLMISR but not WQQ is responsible for decreased binding to the receptor and leads to the shortened serum half-life. Thus, it is not the modification in general that is relevant for the mAb behavior *in-vivo*, but a specific position of this modification in the protein 3D structure. [69]

In contrast to methionine oxidation, the reaction rates for tryptophan are much slower and less is known about the overall mechanism and kinetics of this reaction. However, it has been reported that increased peroxide levels of the non-ionic surfactant polysorbate 20 (PS20) leads to a site-specific oxidation of W50. As PS20 is a common excipient in protein formulations the peroxide level needs to be analyzed and kept low. [61]

Furthermore, it has been shown that oxidation of histidine is another potential modification common for an antibody molecule stressed by the light exposure [70].

1.1.6.3 Glycosylation

Therapeutic mAbs are glycoproteins, similar to their endogenous IgG counterparts. Human IgGs contain a single, highly conserved, glycosylation site in the C_H2 domain, called the "NST-motif". Depending on the antibody sequence the glycosylation site is located around the amino acid 300 (in the HC). Complex biantennary glycan structures are linked via the nitrogen molecule to the Asn residue. The core is built by two N-acetylglucosamine (GlcNAc) residues, three mannose moieties and two further GlcNAcs. As the two GlcNAcs are β-1,2 linked to α-3 and α-6 mannose, respectively the biantennary structure is built. [71]

There is a huge variety of glycoforms with a considerable heterogeneity. Figure 7 presents only the major N-linked glycoforms of mAb therapeutics.

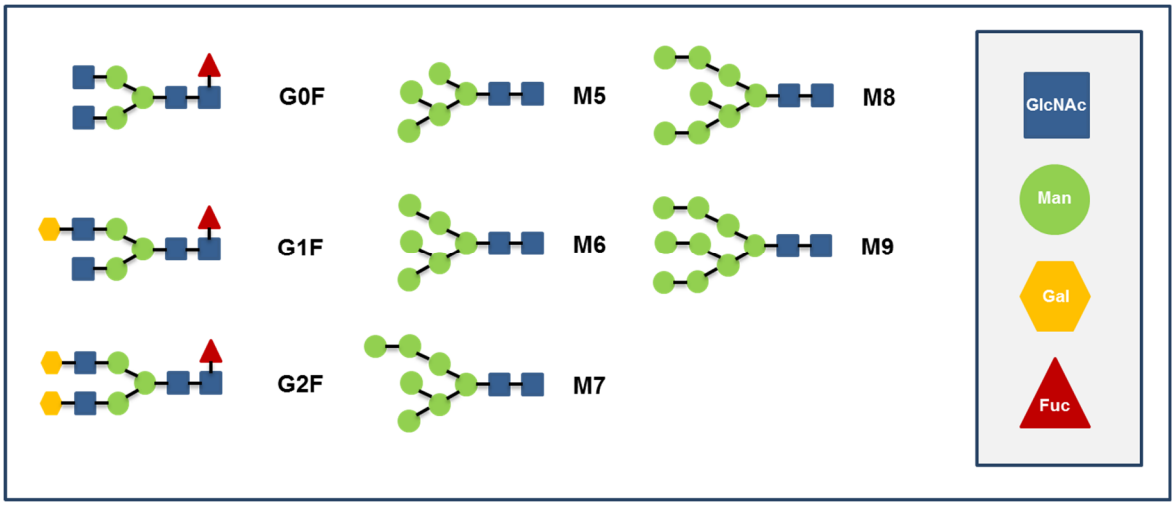

Figure 7 – Glycosylation, core structure

The core structure is built by four N-acetylglucosamine (GlcNAc) and three mannose residues forming two antennae. The main glycoforms are G0F, G1F and G2F, but also high mannose structures are present (M5 – M9).

To build the G0F an additional fucose (Fuc) residue is added to the core structure. The 0 indicates that no additional galactose (Gal) is added, whereby the F stands for the additional fucose. The G1F glycoform carries one additional galactose residue, the G2F-glycan two additional galactose residues, one on each antenna. Furthermore, a small amount of afucosylated IgGs also exists. [71]

The high-mannose glycans M5 to M9 are less mature structures. Those glycans are the precursors of the main glycoforms and can be found at lower levels. [72]

It has been shown, that glycans are very important for the structure of IgGs, as their removal leads to conformational changes of the Fc domain [71, 73, 74]. It is also well established that the glycan structures are essential for specific effector functions. However, their presence was reported to have no effect on the binding to the FcRn receptor and therefore to not influence the mAb serum half-life. [75, 76]

Endogenous human IgGs contain only trace amounts of high-mannose glycans (i.e. less than 0.1%). In contrast to this, recombinant antibody therapeutics can show levels ranging from 1 to 20% [77]. Therefore, the impact of those high mannose glycans has been investigated. Goetze and co-workers demonstrated that therapeutic mAbs containing high mannose glycans are cleared faster than the major glycoforms. As they observed a slower relative clearance rate at higher doses, they assumed that the clearance occurs via the mannose receptor that shows saturation. [78]

Thus, monitoring the glyco-pattern is of high importance to assure that the product contains correctly folded IgGs, which could affect stability and functionality of the therapeutic mAb. [71, 73, 74]

1.1.6.4 Deamidation and iso-aspartic acid formation

Deamidation of asparagine (N) is one of the most frequent modifications occurring in proteins and peptides. This spontaneous non-enzymatic reaction proceeds under physiological conditions via the nucleophilic attack of the nitrogen atom in the peptide bond on the carbonyl group of the asparagine side chain as shown in Figure 8.

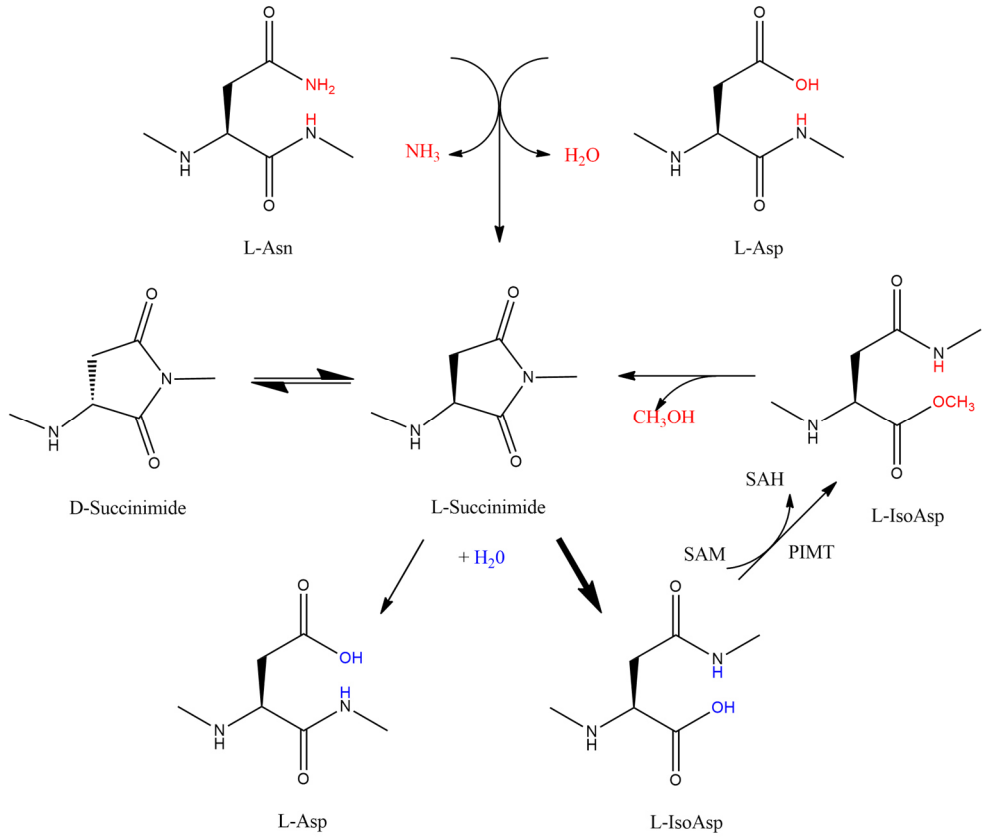

Figure 8 – Deamidation of asparagine and dehydration of aspartic acid

Deamidation of asparagine and dehydration of aspartic acid both lead to the formation of the succinimide intermediate. After hydrolysis of the intermediate aspartic acid and iso-aspartic acid are formed. Via racemization reaction also D-*aspartic and* D-*iso-aspartic acid can be formed. In-vivo the succinimide intermediate can be reformed from* L-*isoaspartic acid via the enzyme* L-*isoaspartyl O-methyltransferase (PIMT). (Cf. Yang 2010 [79])*

Thus, a five-membered succinimide ring is formed as an intermediate. Also for aspartic acid (D) a similar nucleophilic attack can lead to dehydration and the formation of the L-succinimide intermediate. The intermediate then undergoes hydrolysis at the carbonyl group. Depending whether the α- or β-carbonyl group get hydrolyzed, either L-aspartic or L-iso-aspartic acid is formed in a ratio 1:3. However, via reversible racemization of the L-intermediate also the D-succinimide can be formed, leading to the D-aspartic and D-iso aspartic acid. [79]
In contrast to deamidation of asparagine, isomerization of L-iso-Asp is a reversible process. The α-carbonyl group can be methylated via an enzymatic repair of the protein L-isoaspartyl O-methyltransferase (PIMT). This reaction requires the transformation of S-adenosylmethionine (SAM) to S-adenosylhomocysteine (SAH) as methyl donor. The following spontaneous ester hydrolysis then leads to the reformation of the succinimide intermediate, and the previously described hydrolysis. [79]

Another amino acid where deamidation is frequently observed is glutamine [80]. It has been shown that external factors, such as temperature and pH, can favor deamidation reactions leading to deamidation artifacts. Therefore, pH value of the antibody formulations as well as incubation times and temperature during the sample preparation are of high importance. Furthermore it is well known, that susceptibility to deamidation and reaction rates highly depend on the protein amino acid sequence. Stephenson and co-workers found that succinimide formation occurs predominantly when the neighboring amino acid is glycine (NG-motif) or serine (NS-motif). [81]
More recently, Kumar *et al.* reported a sequence related factor that contributes to the stabilization of the succinimide intermediate. They observed a stable succinimide present in an enzyme called Methanocaldococcus jannaschii glutaminase and identified the following n+1 residue D to stabilize the succinimide intermediate. [82]

Several approaches focusing on the investigation of deamidation *in-vivo* found some hot spots to increase over time in serum [80, 83-86]. It has been shown that deamidation occurring in the CDR region could decrease biological activity of therapeutic antibodies [83, 87, 88]. Other studies found one conserved Asn residue at position 384 to be prone to deamidation under physiological conditions. This residue is located in the peptide GFYPSDIAVEWES**NG**QPE**NN**YK (PENNYK-peptide) which is due to the NG-motif known to be preferentially deamidated [80, 81, 83-86]. However, they revealed that deamidation also occurs *in-vivo* and is a natural phenomenon as endogenous serum mAbs show deamidation values of around 20%. [86]

In any case, deamidation leads to the introduction of negative charges, which may influence protein properties and should therefore be monitored.

1.1.6.5 *C*-Terminal lysine clipping

Proteins that are expected to end with *C*-terminal lysine often lack this amino acid. Human IgG genes generally encode a lysine residue at the *C*-terminus of the heavy chains which is usually absent after isolation from serum. It has been suggested that carboxypeptidases in cultured cells cleave the terminal lysine. However, the exact cleavage mechanism of this PTM is still unknown. [89, 90]

As the removal of the *C*-terminal lysine residue leads to the loss of one positive charge unit, charge heterogeneity is introduced. It has been shown that lysine processing is sometimes incomplete leading to a mixture of differently charged mAb molecules. Each of the heavy chains could carry one terminal lysine, as shown in Figure 9. Therefore, the mAb molecules could have a maximum of two terminal lysine residues (2K), one terminal lysine on just one heavy chain (1K), or no terminal lysine (0K). [91]

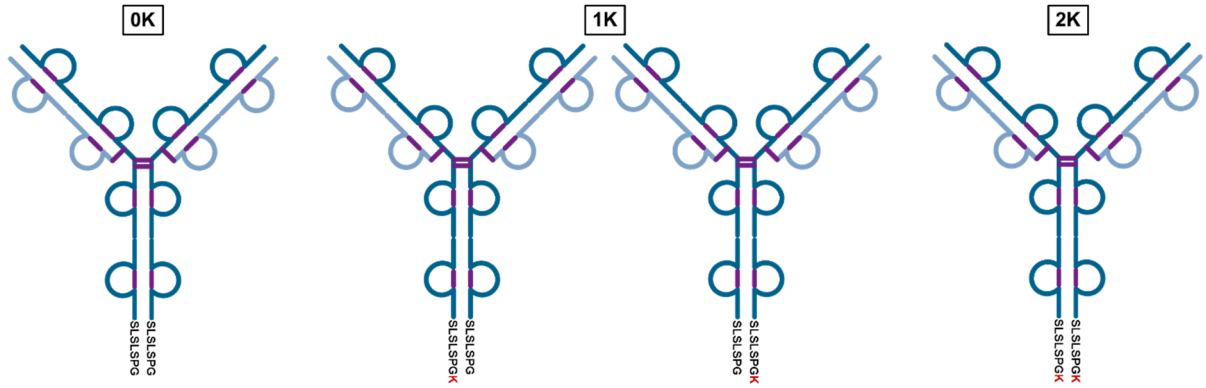

Figure 9 – Different C-terminal lysine residues

The C-terminal lysine K (red) can be completely absent forming the 0K-mAb species. If one heavy chain contains a lysine residue the mAb is described as 1K-species. MAbs with a terminal lysine on both chains are the 2K-species.

It has been reported that C-terminal lysine is rapidly lost after intravenous injection *in-vivo*, which is consistent with the finding, that endogenous IgGs show very low levels of C-terminal lysine (~0.02%) [92]. Other studies showed that the loss of C-terminal lysine has no impact on Fc-mediated effector functions and potency of mAbs [93-95].

Therefore, the C-terminal lysine heterogeneity was long regarded as important product quality attribute to verify good and consistent product process and stability, but to be less critical than other attributes. However, more recent findings suggest that C-terminal lysine's may interfere with complete activation of the complement-dependent cytotoxicity (CDC) [96]. Therefore, Jiang *et al.* presented an approach to control C-terminal modifications during mAb productions, by simply removing C-terminal lysine completely [95].

1.1.7 Relevance of *in-vivo* analyses

Although biotherapeutic molecules are extensively characterized by many *in-vitro* techniques, some information can only be provided by *in-vivo* tests. Therefore, further analyses are required to allow the assessment of pharmacological activities as bioavailability, clearance or efficacy [57]. As discussed in 1.1.5, in most cases the definition and evaluation of CQAs is based on *in-vitro* studies and prior knowledge from previous molecules [97]. However, as chemical conversion also occurs *in-vivo,* the goal is to identify those CQAs that are really critical and have a significant impact on the performance of a given biologic (see Figure 10). Therefore, the question what happens to the CQAs after administration gains more and more interest. [83, 85, 86, 92, 97].

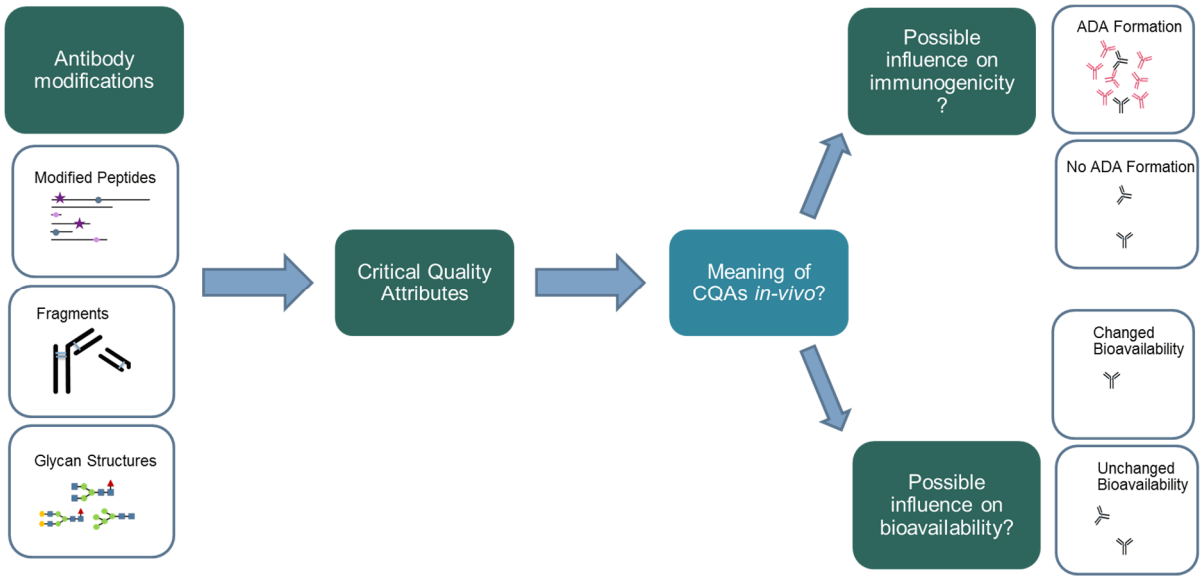

Figure 10 – Critical Quality Attributes and their meaning *in-vivo*

The different modifications and glyco forms are defined as critical quality attributes (CQAs) based on prior knowledge. However, the question what happens to those CQAs in-vivo gains more and more attention. Knowledge whether a specific modification leads to the formation of anti-drug antibodies (ADA) or changes bioavailability is of high interest.

Bioanalytical procedures are routinely used to quantify the level of therapeutic proteins, metabolites and biomarkers in urine, blood, serum, plasma and different tissues [112]. Ligand binding assays (LBA) are the traditional approach used for quantification of therapeutic proteins in pharmacokinetic, pharmacodynamic und toxicokinetic studies [113]. However, LC-MS/MS analysis has emerged as a promising supplement or alternative to the classical LBAs [114, 115].

Most commonly therapeutic proteins are quantified at peptide level using a triple-quadrupole mass spectrometer operated in selected-reaction monitoring mode (SRM). The first quadrupole serves as a mass filter and selects a specific peptide from the mixture. This peptide is then fragmented by collision induced dissociation (CID) in the second quadrupole and a specific fragment produced during CID is finally monitored in the third quadrupole. The quantification is based on a signature peptide (SP) of the

target protein and an internal standard, which is usually a stable isotope labeled surrogate of the selected SP. This targeted LC-SRM/MS quantification approach is highly sensitive and robust. However, with SRM only a few signature peptides are identified for quantification and therefore the majority of the protein sequence remains uncovered. But, in order to monitor the CQAs *in-vivo*, full sequence coverage is required.

Thus, the MAM workflow (described in 1.1.5.) used for characterization *in-vitro*, might be applied also for *in-vivo* characterization. The challenge, however, is that the absolute amount of therapeutic mAb after injection *in-vivo* is in the nanogram to microgram range. Therefore, a highly sensitive MAM workflow is required that allows the analysis of multiple attributes for *in-vivo* samples such as serum. Besides the analysis of mAbs in serum also knowledge about modifications occurring in the subcutaneous tissue are of high interest.

1.1.8 Open Flow Microperfusion

Open flow microperfusion (OFM) is a minimal invasive sampling technique similar to microdialysis that allows direct access to interstitial fluid (ISF) from different target tissues. While microdialysis can be easily applied to sample small molecules, such as metabolites and neurotransmitters from a tissue environment via a membrane, sampling of highly lipophilic or high molecular weight substances is not that simple. Clotting and fouling of the membrane are common issues [98]. In contrast to microdialysis, OFM uses probes with macroscopic openings instead of a membrane and therefore overcomes those problems (see Figure 11).

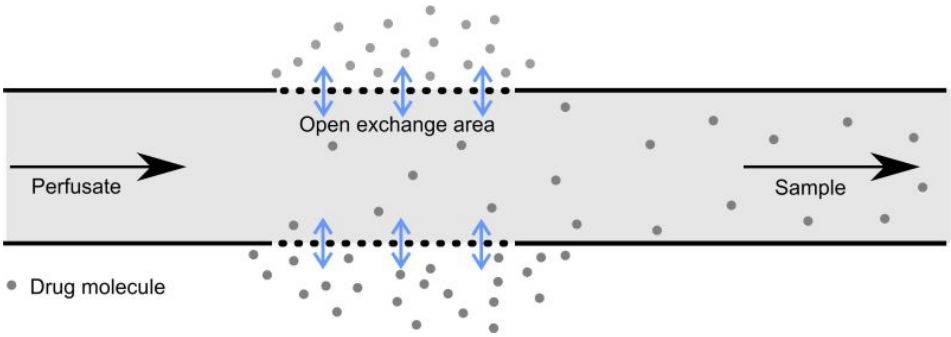

Figure 11 – Schematic figure of the Open Flow Microperfusion probe

The open flow microperfusion (OFM) probe is inserted into the target tissue and is connected to a peristaltic pump. Via push-pull tubing's perfusate is continuously pumped through the probe. At the exchange area, the macroscopic openings allow a free exchange between the probes and the surrounding tissue. (copied with permission from Pieber et. al. [99])

The probes are connected to a pump system that is operated in push/pull mode to allow the exchange of interstitial fluid with the perfusat and to avoid perfusat loss into the tissue. To ensure stable sampling volumes the pump pushes the perfusate actively into the probe and pulls the sample actively into a

sampling vial. The steel mesh of the OFM probes is inserted into the target tissue and is fully coated with polymer, except the area where the mesh openings are located, building the exchange areas (see Figure 11 and Figure 12). The inner walls of the probe are coated with teflon to minimize unspecific adsorption. For insertion of the OFM probe, a thin needle is attached to the probe and a wire is placed inside to stabilize the exchange area. After exact positioning via markings on the OFM probe the needle and the wire are removed. [99]

A

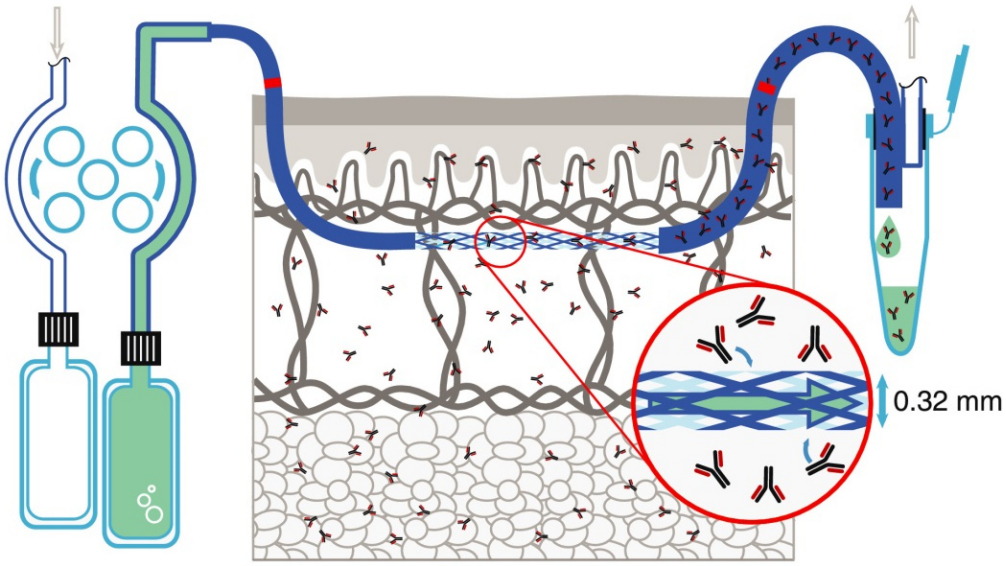

B

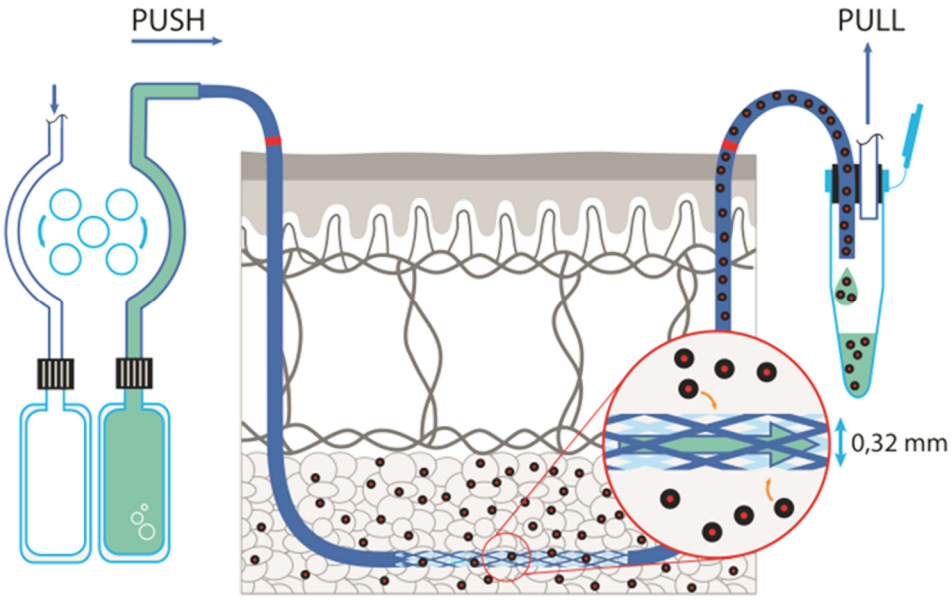

Figure 12 – Schematic figure of the Open Flow Microperfusion technique

A) For the dermal open flow microperfusion (dOFM) the OFM probe is inserted into the dermis and is connected to a peristaltic pump.(copied with permission from Dragatin et al. [100]) B) In the adipose subcutaneous tissue (aOFM) application the probe is inserted one layer below into the adipose subcutaneous tissue.(copied with permission from Tiffner et al. [101])

Thus, by using the OFM technique different types of body fluids can be extracted from the target tissue and analyzed by adequate analytical technologies. It has been applied to adipose subcutaneous tissue (aOFM) and dermal tissue (dOFM) to extract substances ranging from small ions and lipophilic topical drugs to large biomolecules such as cytokines and mAbs, as shown in Figure 12-A and B. [98] Furthermore, it has been designed for use in cerebral tissue (cOFM) to allow sampling in brain tissue [102].

Ikeoka *et al.* applied the aOFM technique to study cytokine production in sepsis patients and to investigate the correlation between tissue inflammation and blood pressure [103]. Another study performed by Bodenlenz and co-workers demonstrated suitability of OFM to sample lipophilic drugs and locally released biomarkers from the dermis of psoriatic patients. They successfully determined pharmacokinetics and pharmacodynamics of a lipophilic topical drug in psoriatic patients by the dOFM technique. [104]

In 2016, Dragatin *et al.* demonstrated by dOFM that the therapeutic mAb Secukinumab (AIN457) distributes into dermal ISF of psoriasis patient and neutralizes its target IL-17A in the skin. They applied OFM tubes into the skin of healthy subjects and psioriasis patients and injected Secukinumab subcutaneously. Afterwards, they determined the Secukinumab concentration in serum and ISF, demonstrating the feasibility to extract mAbs from the dermis after subcutaneous injection. Thus, therapeutic mAbs had been sampled from the subcutis of patients after injection using the OFM technique. [100]

However, until now no characterization of the mAb molecule has been performed yet and with this there is no knowledge about mAb modifications occurring in the subcutis.

1.2 Analytical Methods

1.2.1 Nano-High Performance Liquid Chromatography

In the last decades there was an increasing demand for instrumentation with high sensitivity that offer the ability to analyze also trace sample amounts [105-107]. Karlsson and Novotny tested packed columns with very small inner diameters in 1988, and by this first introduced the currently known nano-LC technique. The miniaturized separation technique offers a large decrease in mobile phase consumption and also waste production. [108]

Although there is no consistent classification of the microscale separations, Chervet *et al.* defined separations performed with inner diameter columns of < 100 µm and flow rates of 50 – 800 nL/min as nano-LC. Columns of 100 – 500 µm inner diameters were described as capillary-LC, and 0.5 – 1mm columns as micro-LC. However, there are no strict boundaries/classifications and no agreement about the terminology. [109]

Table 3 – Columns sizes, flow rates and various areas of application (modified from [109])

Description	Inner diameter	Typical flow rate	Predominant application area
nano-LC	20-100 µm	20-800 nL/min	Proteomics
Capillary LC	100-500 µm	0.5-10 µL/min	Protein prefractionation
Micro LC	0.5-2.1 mm	10-500 µL/min	DMPK, LC-MS, Metabolomics
Standard bore column	2.1-4.6 mm	0.5-2.5 mL/min	Small molecules, pharma, protein prefractionation
(Semi)preparative LC	≥4.6 mm	≥2.5 mL/min	Protein purification

Following injection, the analytes undergo so-called “chromatographic dilution D” (i.e. change in the analyte concentration) in the column, which can effect separation. As described by equation 1, where C_0 and C_{max} are the initial and final analyte concentration, respectively, chromatographic dilution depends on the internal column diameter d_c, the total porosity of the column ε, the column length L_c, the injected sample volume V_{inj} and the chromatographic parameters, i.e. retention factor k and plate height H.

$$D = \frac{C_0}{C_{max}} = \frac{\pi d_c^2 \varepsilon (1+k)\sqrt{2LH\pi}}{4V_{inj}} \quad (1)$$

Therefore, D decreases dramatically with a reduction of inner column diameter as it is in nano-LC columns. By this, mass detectability is increased leading to a higher sensitivity .[110]

The overall gain in sensitivity f resulting from the exchange of a column with a larger diameter d_1 to a smaller column d_2 can be estimated using the following equation

$$f = \frac{{d_1}^2}{{d_2}^2}, d_1 > d_2 \quad (2)$$

Thus, for downscaling from a 2.1 mm diameter column to a nano-column with a diameter of 75 µm the sensitivity gain should be a factor of ~800. In the pharmaceutical industry (e.g. at AbbVie) a dimension of 2.1 mm is often used for peptide separation. Therefore, the relative sensitivity increases compared to a 2.1 mm was calculated according to equation 2 and is displayed in Figure 13 [109].

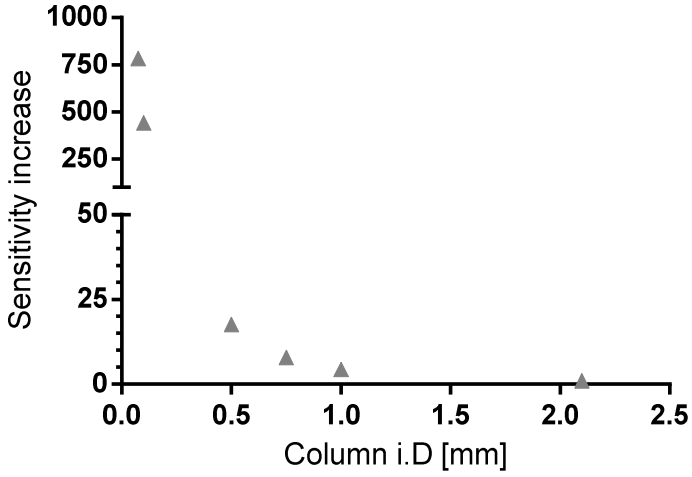

Figure 13 – Relative sensitivity increase compared to a 2.1 mm column

With decreasing inner column diameter the relative sensitivity increases. The plotted values were calculated using equation 2 and a starting diameter of 2.1 mm column was chosen.

As the reduction of a column diameter influences the entire setup, in practice such an increase is not readily reached. Another important point to consider is the effect of extracolumn peak broadening, which significantly influences separation efficiency and sensitivity. To achieve optimal performance connection tubings should be as narrow and short as possible to reduce dead volumes and thus minimize extracolumn peak broadening. [109]

Reaching accurate gradients and stable flow rates require suitable and reliable pumping systems. Originally, nano-flow separations were performed with conventional LC pumps equipped with a T union. In this simple approach, the pump flow is divided at the T union between the nano-LC column and a waste capillary, whereby the length and inner diameter of the waste capillary determines the split ratio. The split-flow approach works very well for isocratic separations but mostly fails for gradient elution, as the backpressure changes with the viscosity of different solvent compositions.
Thus, although this approach is very easy and cheap, it compromises on accuracy of gradient elution and still requires high amounts of solvent. Preferably, the flow should be delivered directly from a nano-

pump without flow splitting, which is nowadays possible with one of the different commercially available systems (e.g. UltiMate 3000 RSLCnano System). [109, 111]

Consequently, when working with nano-LC systems it should be considered, that the column volume is very low and therefore, the sample volume that can be injected on a nano-column is limited. The injected volume should be as low as possible in order to avoid band broadening effects and also column overloading. [111]
As in many biological samples the analyte concentration is very low, it is a common approach to apply either an online-prefocusing directly on the analytical column or more often a pre-concentration step on an additional trap column. For the trap columns, dimensions producing a lower backpressure are chosen to be able to load a larger amount of sample with higher flow rates. [112]

Proteomics/peptidomics is probably the research area where nano-LC is applied mostly, due to the low available amounts of sample for analysis. However, the technique finds also application in environmental, food and pharmaceutical analysis. [109]

1.2.2 Electrospray Ionization and nano-spray techniques

The basic requirement for a mass spectrometric determination is the conversion of the neutral analyte into a gas-phase ion. Motion and direction of charged particles can be easily manipulated e.g. by the application of electric and magnetic forces. This is of high importance for the subsequent separation and detection of ions in the mass spectrometer. [113]

For electrospray ionization (ESI) the analyte of interest is dissolved in a liquid and in most cases previously separated by chromatographic or electrophoretic techniques. The liquid is guided thorough a stainless steel capillary at atmospheric pressure. Between the tip of the capillary and the entrance into the MS a high voltage of 2 – 5 kV is applied, depending on polarity and flow rate. Under the influence of the resulting electric field the liquid forms a cone at the tip of the spray needle, described as Taylor cone and a fine spray of highly charged droplets is formed, as shown in Figure 14. During their passage through the source the droplets undergo desolvation resulting in smaller droplets. [114]
As a consequence of the decreasing droplet size, the charge density increases until the Rayleigh limit is reached. At this point the so-called Coulomb explosion occurs as the repulsion of charges becomes the same as the surface tension of the droplet. This event leads to the production of even smaller droplets and repeats until it is small enough to be desorbed. [115]

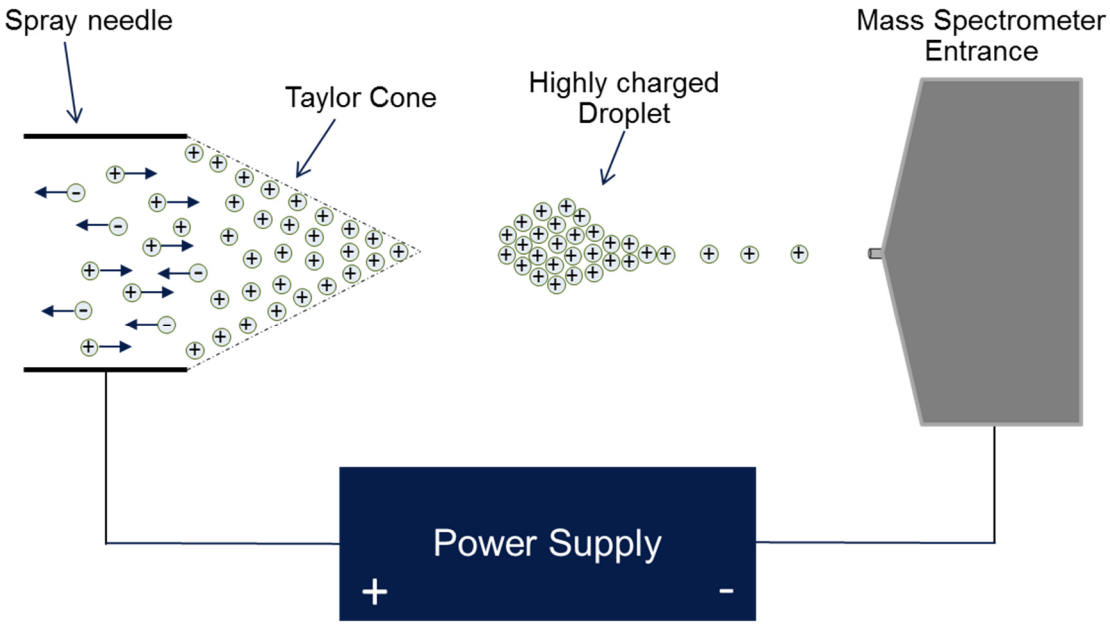

Figure 14 – ESI-Spray mechanism

Due to the electric field a taylor cone is formed at the tip of the spray needle creating a fine spray of highly charged droplets. (Cf. Cech 2001[116])

During the ionization of biomolecules using ESI, usually several protons can get attached to the molecules. The differently charged ions are described as $[M + nH]^{n+}$, whereby the molecular mass of the molecule is M, n the number of charges and H the mass of a proton. [113]

With the introduction of nano-electrospray MS analyses by Wilm and co-workers in 1996, the drawbacks of conventional flow ESI MS analyses were overcome. Compared to the conventional flow ESI the nano-ESI-MS requires lower sample volumes and therefore allows detection and analysis of low abundant proteins in complex samples, where only a limited sample volume is available. Due to the low nanoliter/min flow rates smaller droplets are created, which leads to a higher surface-to-volume ratio and therefore an improved desolvation. The overall efficiency can be described by the amount of recorded analyte ions at the detector divided by the amount of sprayed analyte ions. In nano-ESI sources all three efficiency defining factors: desolvation, ionization and transfer efficiency into the lenses system are improved [117]. Wilm *et al.* reported a 510-fold improvement using the nano-ESI source compared to a conventional source.

Despite all advantages, nano-ESI was characterized at the beginning by laborious alignments of the spray tips and also a low throughput. However, those disadvantages have been overcome by the development of an ESI-based monolithic microchip electrospray device. The ESI-Chip is produced from a monolithic silicon substrate using deep reactive ion etching (DRIE) (Figure 15-D). With this technique nozzles are etched from the planar surface of a silicon wafer building a 10 x 10 array of nozzles.

Compared to pulled capillaries, sensitivity is 1.5 – 3 times higher with the ESI-nozzles and they also offer higher spray stability. [118]

The first generation of the ESI-based microchip electrospray device was the NanoMate® 100, holding an ESI-chip, a 96-well plate and a rack of 96 disposable, conductive pipette tips. For infusion analysis, 1 – 20 µL of sample is aspirated from the well-plate with a conductive pipette tip and delivered to the inlet side of the ESI-Chip. The pipette tip seals against the chip and a spray voltage of 1.2 – 2.0 kV and a pressure of 0.1 – 2 psi are applied to the sample in the tip, to initiate the spray. After mass spectrometric analysis the disposable tip is ejected. [119]

The ESI-nozzle spray mechanism differs greatly from the conventional spray sources, as the counter electrode is incorporated into the nozzle. Hereby, the electric field is formed from the potential difference between the voltage applied to the fluid via the conductive pipette tip and the silicon substrate itself (Figure 15-C).

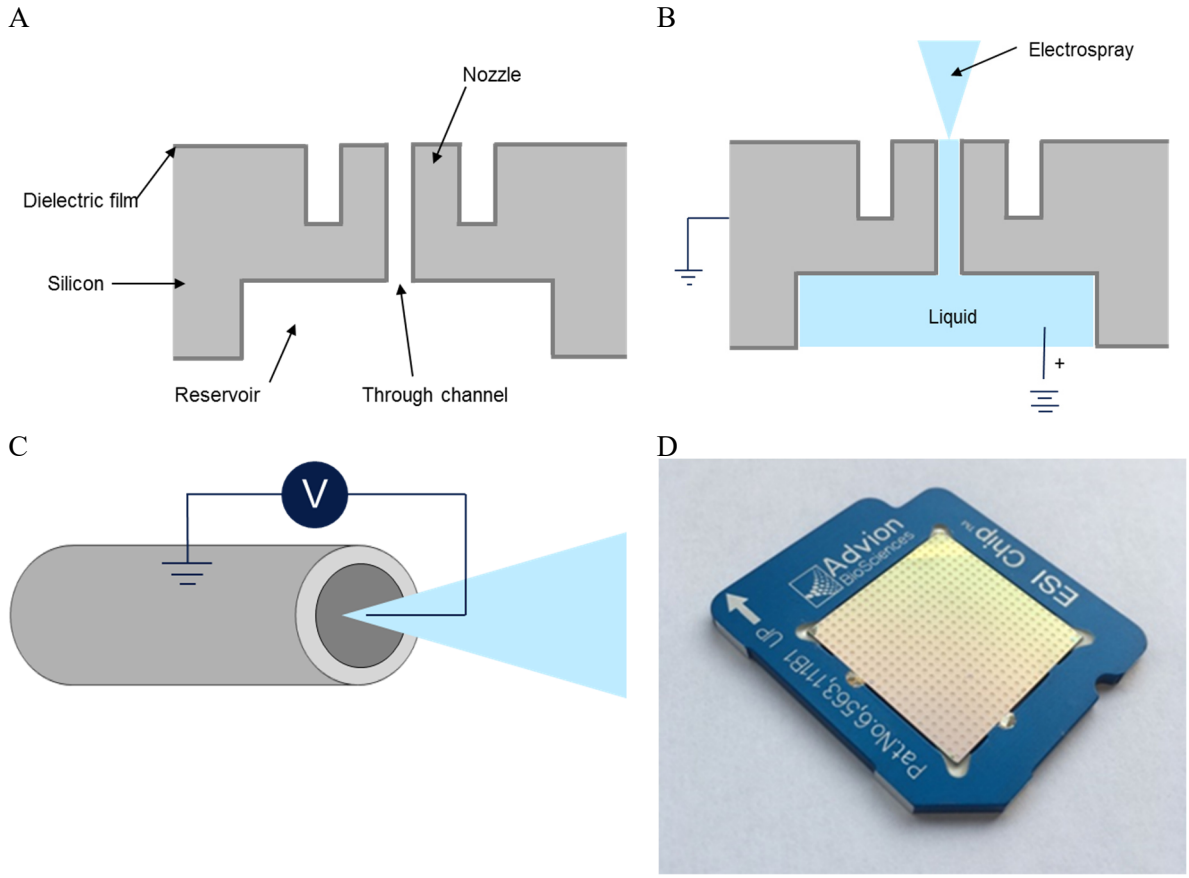

Figure 15 – ESI spray chip and nozzles

A) Graphical illustration of the cross section of an ESI nozzle. The silicon substrate is covered with a dielectric film. B) Cross section of the nozzle filled with a liquid creating a fine electrospray. C) Spraying a sample trough the ESI nozzle. (Cf. Schultz 2000 [118]) D) ESI-spray chip

With the next generation source, the TriVersa NanoMate®, two further modes of operation (the LC-coupling and the fraction collection mode) became available. In the LC-coupling mode, the outlet of a flow column is connected to an LC-coupler, consisting of a capillary with a conductive sprayer at the

end. With this mode, online analysis of LC-runs with flow rates ranging from 20 nL/min to 1 mL/min can be performed. Furthermore, individual fractions of the LC-flow can be collected by the fraction collection mode and analyzed after the LC-run using the direct infusion mode.
The spray current of the electrospray is constantly monitored, and therefore it is immediately recognized if a nozzle gets blocked, due to the increase in spray current. Thus, an automatic nozzle-to-nozzle switch can be configured resulting in a highly stable spray. [118, 119]

An alternative way to produce a nano-spray is the EASY-Spray™ technology. It consists of a nano-ESI source with a plug-in mechanism for a unique type of columns called EASY-Spray™ columns. The columns are coiled up in a circular design and are equipped with an integrated column heater (see Figure 16).

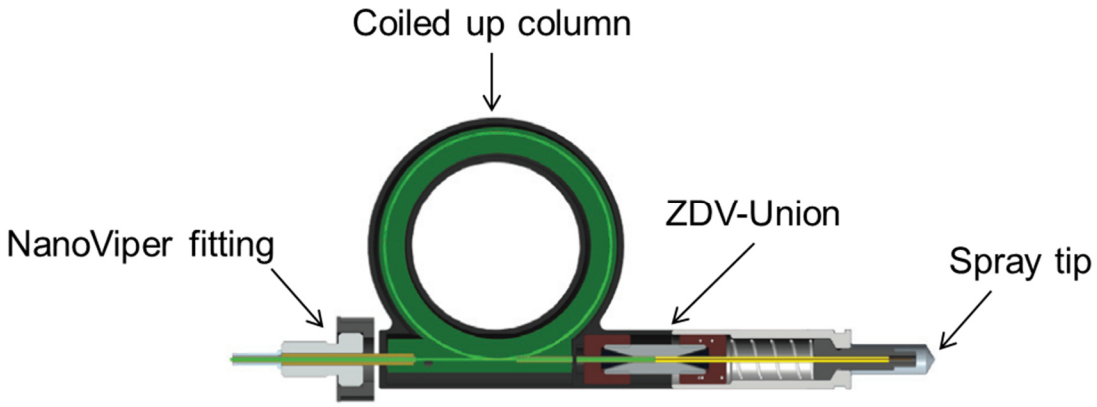

Figure 16 – EASY Spray™ column

The column material is coiled up in a circle and can be tempered by an integrated column heater. A NanoViper fitting and the integrated zero dead volume union eliminate dead volumes. (Modified from [120])

Via a zero dead volume (ZDV) union the column outlet is connected to an integrated glass emitter. At the tip of the emitter, a fine nano spray is produced. Due to the special design, only a single connection via a NanoViper™ fitting is required to connect the HPLC-pump to the column inlet. Thus, dead volumes are eliminated and narrower peaks are expected than in conventional nano-flow HPLC-MS systems. [120]

The advantage of the EASY-Spray technology is the highly user friendly plug and spray mechanism and the single NanoViper™ connection that is required. In contrast to this, the TriVersa NanoMate® requires a manual assembly of a microtight sleeves and microtight unions to connect the LC-flow to the source. This connection needs to be really tight and dead-volume free in order to achieve narrow peaks. However, the advantage of the TriVersa NanoMate ® is the integrated spray current monitoring and that it can be combined with columns from different vendors.

1.2.3 Orbitrap Mass Spectrometry

Mass Spectrometry (MS) is a specific and highly sensitive technique used for the characterization of analytes from several diverse fields, such as chemistry, physics and pharmaceutical science. The mass of atoms or molecules is determined and presented as mass-to-charge ratio (m/z). [113]

The Orbitrap mass analyzer, developed by A. Makarov, was first commercialized as part of a tandem-mass spectrometer by Thermo Electron in 2005. However, the Orbitrap has its origins in a previously developed and modified device known as the "Kingdon Trap". In 1923 K.H. Kingdon designed an ion storage device that utilizes electrostatic fields only for the storage of charged particles. The Kingdon trap was the first device that allows trapping of particles in orbit motions. Originally, the trap consisted of a central wire, an outer cylinder and two end caps enclosing the trap. [121, 122]. A radial logarithmic potential is produced when a DC voltage is applied to the central wire and the outer cylinder, whereby A and B represent constants and r the radial coordinate in equation 3.

$$\phi = A \ln r + B \tag{3}$$

Ions that enter the trap with a defined velocity will move in stable orbits around the central wire. To achieve simultaneous trapping in axial direction, a potential needs to be applied to the endcap electrodes. In 1981, R.D. Knight employed an additional axial electric field by modifying the shape of the outer electrode of the Kingdon trap. In equation 4 r and z represent the cylindrical coordinates, and A and B are constants based on the geometry of the Kingdon trap.

$$\phi = A \left(\frac{z^2 - r^2}{2 + B \ln r} \right) \tag{4}$$

The additional quadrupole term allowed harmonic oscillation of ions in the z-direction. To allow injection of ions into the trap, Knight radially split the outer electrode in the middle. The "Knight-style Kingdon Trap" could monitor trapped ions and allowed the observation of axial and radial resonances. However, the ion mass identification was still not possible as the measured resonances were considerably weaker, broadened, and shifted in frequency. [123]
Thus, the idea to use the Kingdon trap for the determination of m/z ratio resulted in poor mass resolution due to the strong dependence of rotation frequency on initial radius and velocity of ions [122].

With the invention of the Orbitrap mass spectrometer, Makarov revised the concept of orbital trapping for mass analysis application. Although the Orbitrap was a completely new type of instrument, it can be considered as a modified "Knight-style Kingdon Trap" and quadrupole ion trap. The potential

distribution of the field employs a quadrologartihmic field for ion trapping. It combines a logarithmic field of a cylindrical capacitor with a quadrupole field of the ion trap:

$$U(r,z) = \frac{k}{2}\left(z^2 - \frac{r^2}{2}\right) + \frac{k}{2}(R_m)^2 \ln\left[\frac{r}{R_m}\right] + C \tag{5}$$

with r and z being the cylindrical coordinates, k the field curvature, R_m the characteristic radius and C a constant. As is evident from equation 5 the potential in z-direction is completely independent from r, φ motion and exclusively quadratic (Figure 17). Thus, m/z can be described by the frequency of oscillation along the z-axis (see equation 6)

$$\omega = \sqrt{\left(\frac{z}{m}\right) \cdot k} \tag{6}$$

Detection of ions is performed in analogy to the FT-ICR mass spectrometer, by broadband image current detection. To convert the time-domain signal into a final mass-to-charge spectrum a fast Fourier transform (FFT) algorithm is applied.

The Orbitrap mass analyzer has a much higher mass resolution and accuracy than a linear ion trap and is less cost intensive as an FT-ICR. Furthermore, it has a larger trapping volume than both and an increased space charge capacity due to independence of trapping potential on m/z ratio. [123]

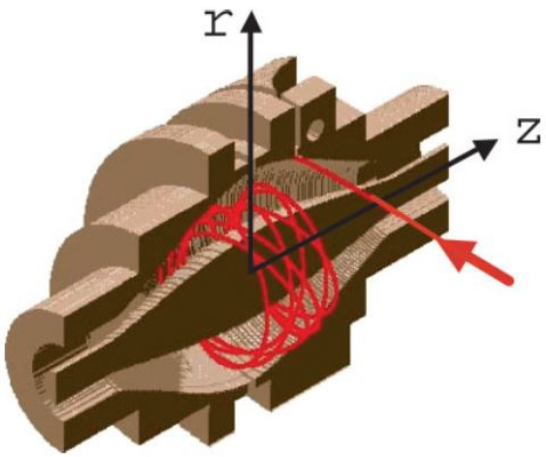

Figure 17 – Orbitrap mass analyzer

The ions are injected at the indicated point (red arrow) with a velocity perpendicular to the z-axis of the Orbitrap. (copied with permission from Hu et al. [123])

In a first step the analytes are ionized at atmospheric pressure in the ESI-source as described in chapter 1.2.2. The generated ions are then drawn into a tube and transported to the tube lens/S-lens (depending on type of Orbitrap used), where the ion beam is focused (see Figure 18). Three consecutive multipoles transmit and focus the ions into a concise beam by the application of radiofrequencies.

In addition the ion optics allows oppositely charged ions or remaining neutrals to get lost in vacuum. In the linear ion trap ions are trapped in radial and axial direction. Afterwards the ions are axially ejected via a multipole into a C-shaped RF-only quadrupole. The C-trap is filled with N_2 as a dampening gas (10^{-3} mbar) and allows storage and subsequent injection of significant ion populations into the Orbitrap (10^{-10} mbar). After short ion packages of each m/z population are formed, the RF on the rods is ramped down. Then a DC voltage is applied to create a field across the trap. The packages are ejected along lines converging to the entrance of the outer curved electrode of the Orbitrap. [124]

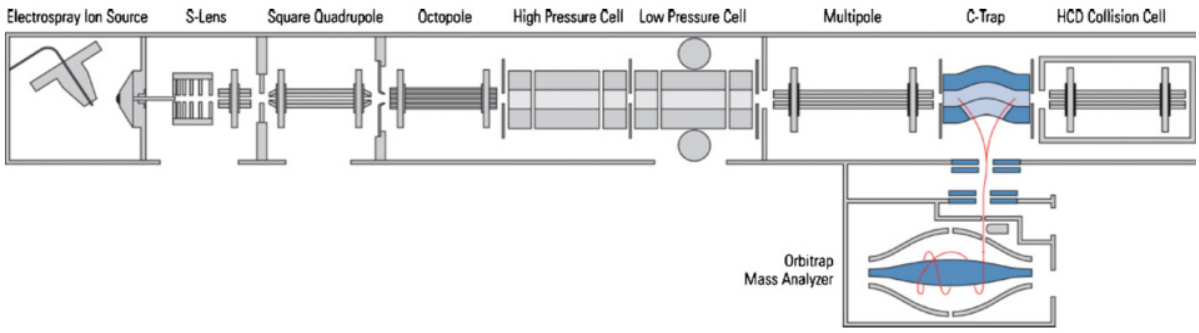

Figure 18 – Components layout of the Orbitrap Velos mass spectrometer

The Orbitrap Velos mass spectrometer consists of an ESI source for ionization. Ions are focused by the S-lens and the following ion optics and get trapped in the linear ion trap. The C-trap prepares ion-packages for the analysis in the Orbitrap mass analyzer. (copied with permission from Makarov et al. [124])

Inside the Orbitrap a strong electrical field is created by the central electrode, called spindle, and the outer electrode. Ions that enter this field are attracted towards the central electrode initiating axial oscillation without any further excitation. This phenomenon is called “excitation by injection”. To prevent the ions from hitting the outer electrode the principle of “electrodynamic squeezing” is employed. The DC voltage of the central electrode is quickly ramped leading to a compression of ion trajectories in axial and radial dimensions. As soon as the trajectories become a stable spiral and no more ions get lost on the electrodes, voltage increase stops and the ions oscillate harmonically along the axis. Then image current detection starts at the detection electrode and the recorded time-domain signal is converted into a m/z spectrum by a FFT algorithm. [122-124]

1.2.4 Design of Experiments (DoE)

The use of statistical tools in the design and optimization of experiments (DoE) was first exploited by Fisher [125] in 1958 and since then has become increasingly popular in diverse disciplines. The intuitive approach to change one separate factor of an experiment at a time can result in a huge number of experiments with incomplete information [126]. On the contrary, a DoE represents a systematic approach and leads to a comprehensive understanding of the design space offering maximal gain in

information out of a minimal amount of experiments. It connects experiments in a rational manner finally resulting in an organized experimental setup. [125]

One of the commercially available DoE packages is Minitab® from Minitab Inc. It offers different experimental designs for robustness testing, screening, response surface modeling and optimization. The simplest type of experimental design is based on *factorial design*, whereby different experimental variables serve as *factors* for the design. For instance, in a *two-level factorial design*, a low and high value for each factor is combined. In a *fractional factorial design*, fewer experiments are required than in a *full factorial design* exploiting statistical correlations. Despite less data obtained, the set-up still fulfills the requirements for the determination of significant factors with a minimum number of experiments. Basically, in all cases the desired gain of information and the number of experiments to be conducted must be compromised. [125]
By using a suitable design, DoE saves a large amount of time and is able to make predictions leading to real optimum conditions. For this reason, the use of DoE has become increasingly prevalent in scientific areas among the last decades [126-128]. As can be seen from Figure 19, the number of scientific publications including DoE approaches increased from 14 in the year 2008 up to 125 in 2018.

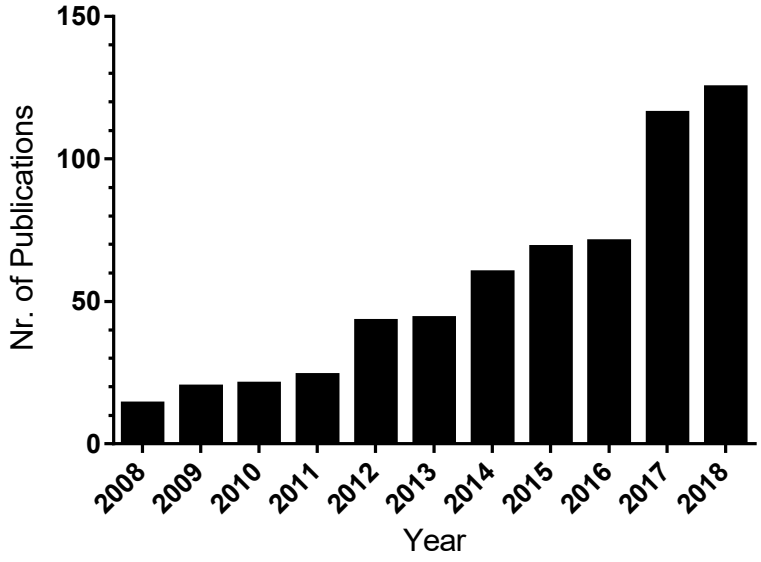

Figure 19 – Publication trends for design of experiment.

During the last ten years, the number of publications in PubMed about "design of experiment" increased from 14 to 125 publications (Search details "Design of experiment"[All Fields] AND ("2008/01/01"[PDAT] : "2018/12/31"[PDAT]).

1.3 Aims of this thesis

Over the last years, a lot of attempts have been done in the field of analysis of *in-vivo* samples. However, the previously published studies focused mostly on one type of modification at a time and therefore could not provide a full picture of the antibody modifications. Furthermore, the capture efficiency in the used protocols was often unknown and therefore a contamination by endogenous mAbs and their interference with the analysis of target mAb modifications could not be ruled out.

Thus, the main scope of this work is to shed a light upon the question what happens to therapeutic antibodies *in-vivo* after subcutaneous injection. For this purpose, the suitability of the open flow microperfusion technique to extract interstitial fluid from the subcutaneous tissue has been previously investigated. However, to analyze the obtained biological samples a specific and sensitive workflow was required.

Therefore, the first aim of the current study is the development of a suitable capture protocol that specifically isolates the target molecules from animal serum and interstitial fluid with high efficiencies. After optimizing the capture efficiency, the linear range determination is required to show suitability of the protocol for a broad concentration range. As it is of high importance that the antibody capture proceeds in the unbiased manner and does not favor a specific modification, the assessment of the performance of the capture procedure in the case of stressed samples is mandatory. Thus, feasibility to capture modified antibodies should be demonstrated.

In addition to the establishment of an efficient capture procedure, development of an optimized peptide map protocol for low sample amounts, which could use 1 µg of antibody or less, is required, as a very limited amount of antibody is available in the case of *in-vivo* samples. Also the demonstration that the workflow does not introduce any additional modifications to the captured antibody is necessary.

Then, for the final analysis a highly sensitive method that enables the quantification of peptide modifications is required. This problem should be approached by implementation of the nano-flow HPLC device coupled via a nano-spray source to a mass spectrometer. Therefore, one of the aims of this thesis is the development of the nano-flow LC-MS peptide map analysis procedure.

Finally, the developed workflow should be suitable to analyze the *in-vivo* samples from the open flow microperfusion study. By comparing the modifications found in interstitial fluid and serum, a better understanding of what happens to the antibodies in the subcutis should be achieved.

Thus, the aims can be briefly summarized as follows:

- Development of a specific and unbiased capture protocol for the isolation of therapeutic mAbs from biologic matrices with high efficiencies.
- Optimization of the peptide map protocol for *in-vivo* samples that achieves high sequence coverage also for the low sample amount of 1 µg mAb (or less).
- Implementation of a nano-flow HPLC device and the coupling to a high-resolution mass spectrometer via a nano-ESI spray source.
- Application of the developed workflow for the analysis of the *in-vivo* samples from the OFM study.

2. Experimental Section

2.1 Instruments

Equipment	Model Number	Vendor
Adjustable piston pipets	Research 2,5 µL	Eppendorf (Hamburg, Germany)
	Research 10 µL	
	Research 20 µL	
	Research 100 µL	
	Research 200 µL	
	Research 1000 µL	
	Research 5000 µL	
Vaccum rotary evaporator	RVC 2-18 CDplus	Martin Christ (Osterode am Harz, Germany)
SpeedVac Concentrator	Salvant SPD 1010	Thermo Fisher Scientific (Dreieich, Germany)
Vaccum rotary evaporator	Concentrator plus	Eppendorf (Hamburg, Germany)
Extraction Plate Manifold for Oasis 96-Well Plates	186001831	Waters (Milford, USA)
Thermomixer	Comfort	Eppendorf (Hamburg, Germany)
Thermomixer	ThermoMixer C	Eppendorf (Hamburg, Germany)
Ultrasonic bath	Ultrasonic Cleaner USC-T	VWR (Radnar, USA)
Dionex Ultimate3000 nano-LC	SRD-3400; NCS-3500RS Cap; WPS-3000TBFC analytical	Thermo Fisher Scientific (Dreieich, Germany)
Mass Sepctrometer	Orbitrap XL	Thermo Fisher Scientific (Dreieich, Germany)
Mass Sepctrometer	VelosPro	Thermo Fisher Scientific (Dreieich, Germany)
nanoESI source	TriVersa NanoMate®	Advion (Harlow, UK)
nanoESI source	EASY-Spray™ Source	Thermo Fisher Scientific (Dreieich, Germany)
Scale	AT460 Delta Range	Mettler-Toledo (Giesen, Germany)
Power Supply	POWER PAC 200	BioRad (Hercules, USA)

Mini Cell	Novex Mini-cell	Invitrogen (Thermo) (Carlsbad, USA)
Calibrated densitometer	GS800	BioRad (Hercules, USA)
Shaker	REAX control	Heidolph (Schwabach, Germany)
Centrifuge	MiniSpin plus	Eppendorf (Hamburg, Germany)
Centrifuge	C1301B-230V	Labnet International (Edison, USA)
Magentic Particle Concentrator	Dynal MPC-S	Invitrogen (Thermo) (Carlsbad, USA)
Water Supply	Milli-Q unit	Merck Millipore (Burlington, USA)
Magnetic Stirrer	MR Hei-Standard 505-200001-00	Heidolph (Schwabach, Germany)
Freezer	Premium NoFrost	Liebherr (Bulle FR, Switzerland)
Fridge	Medline	Liebherr (Bulle FR, Switzerland)
Capillary Column Cutter	Shortix	SGT (Singapore)

2.2 Material

Material	Model Number	Vendor
96-well plate	P-96-450V-C	Axygen (Reynosa, Mexico)
Total recovery vial with caps	186002805	Waters (Milford, USA)
Protein LoBind Tubes - **0.5 mL,** - **1.5 mL,** - **2.0 mL**	 525-0132, 525-0133, 525-0134	Eppendorf (Hamburg, Germany)
CellStar Tubes 50 mL	227201	Greiner bio-one (Kremsmünster, Austria)
ESI Spray Chip	HD_A_384	Advion (Harlow, UK)
Alignment carbon tip rack	1004760	Advion (Harlow, UK)
Sample tip rack	1004763	Advion (Harlow, UK)
Alignment Chip	-	Advion (Harlow, UK)
LC-Coupler (30 cm)	CS110-Coupler	Advion (Harlow, UK)
epT.I.P.S Reload PCR clean - **0.1-20 µL,** - **2-200 µL,** - **20-300µL,** - **50-1000 µL,**	 613-3561, 613-3563, 613-3564, 613-3565,	Eppendorf (Hamburg, Germany)

- **100-5000 µL**	613-3543	
Microvolume Filter Tips	4801	Corning (Reynosa, Mexico)
NAP-5 column	17-0853-02	GE Healthcare (Chicago, USA)
Amicon® Ultra 0.5mL, 50K	UFC505024	Merck Millipore (Tullagreen, Ireland)
Oasis PRiME HLB 96-well µElution plate	186008052	Waters (Milford, USA)
Zebaspin Desalting columns,		Thermo Scientific (Rockford, USA)
- **0.5 mL, 7K**	89882	
- **0.5 mL, 40K**	87766	
PhyTip Columns, 10K, 600 µL	91-60-17	PhyNexus (San Jose, USA)
Staining and Blotting Tray	345-9920	BioRad (Hercules, USA)
Gel Knife	EI9010	Invitrogen (Thermo) (Carlsbad, USA)
Union assy MicroTight PEEK	1180510	Upchurch (Oak Harbor, USA)
Microtight Sleeves		Upchurch (Oak Harbor, USA)
- **Orange 0.13x0.025**	F-184	
- **Green 0.155x0.025**	F-185X	

2.3 Chemicals

Reagent	Article/Prod.Nr.	Vendor
Ammoniumbicarbonate	151.941.600	Bernd Kraft (Duisburg, Germany)
32% Hydrochloric acid	08256-100ML-F	Honeywell (Mexico, USA)
Guanidine-Hydrochloride	50933-250g	Sigma-Aldrich (Steinheim, Germany)
Tris (hydroxymethyl)aminomethan	T1503-100g	Sigma-Aldrich (Steinheim, Germany)
Dithiothreitol	R0862	Thermo Scientific (Rockford, USA)
Iodoacetic acid sodium salt	I6125-5G	Sigma-Aldrich (Steinheim, Germany)
Trypsine	V5111	Promega (Madison, USA)
Trypsine-Lys-C-Mix	V5073	Promega (Madison, USA)
Trifluoracid acid	1.082.620.100	Merck (Darmstadt, Germany)
Formic Acid	94318-50ML-F	Honeywell (Mexico, USA)
Acetonitril MS Grade	34967-6x1L	Sigma-Aldrich (Steinheim, Germany)
Methanol	14262-1L	Sigma-Aldrich (Steinheim, Germany)
Ethanol	1.117.272.500	Merck (Darmstadt, Germany)
BupH™ Tris Buffered Saline	28379	Thermo Scientific (Rockford, USA)
Surfact-Amps 20/Tween-20	28320	Thermo Scientific (Rockford, USA)

Pierce™ IgG Elution Buffer	21028	Thermo Scientific (Rockford, USA)
NuPAGE™ LDS-Sample Buffer (4x)	NP0007	Invitrogen (Thermo) (Carlsbad, USA)
NuPAGE™ MOPS-SDS-Running Buffer (20x)	NP0001	Invitrogen (Thermo) (Carlsbad, USA)
Page Ruler Unstained Protein Ladder	26614	Invitrogen (Thermo) (Carlsbad, USA)
NuPAGE ™Antioxdiant	NP0005	Invitrogen (Thermo) (Carlsbad, USA)
NuPAGE™ Sample Reducing Agent	NP0004	Invitrogen (Thermo) (Carlsbad, USA)
NuPAGE™ 3-8% Tris-Acetate Gels	EA03752Box	Invitrogen (Thermo) (Carlsbad, USA)
SimplyBlue™ SafeStain	LC6060	Invitrogen (Thermo) (Carlsbad, USA)
Pierce Silver Stain Kit	24612	Thermo Scientific (Rockford, USA)
Pierce Sreptavidin Magnetic Beads	88817	Thermo Scientific (Rockford, USA)
MagSi protein A 600	MD42011	AMS biotechnology (Abingdon, UK)
SILu™MAb stable-Isotope labled	1002322304	Sigma-Aldrich (Steinheim, Germany)
Acetic Acid	1000631000	Merck (Darmstadt, Germany)
L-Methionine	M8439	Ajinomoto (Singapore)
Sera-Mag SpeedBeads Streptavidin-Blocked Magnetic Particles	21152104010150	GE Healthcare (Chicago, USA)
DT(L*)MISR synthetic peptide	AU-P-2443-1	PANATecs (Heilbronn, Germany)
Pierce LTQ Velos ESI positive Ion calibration solution	88323	Thermo Scientific (Rockford, USA)

2.4 Columns

Vendor	Material		ID [mm]	Lenth [mm]	Particle [µm]	Pore [Å]	Article/ Prod.Nr
Thermo	Acclaim™ PepMap™ RSLC	C18	0.075	250	2	100	164941
Thermo	Acclaim™ PepMap™ RSLC	C18	0.075	150	3	100	164534
Thermo	Acclaim™ PepMap™ EASY	C18	0.075	250	2	100	ES802
Thermo	Acclaim™ PepMap™ µ-Precolumn	C18	0.300	5	5	100	160454
Thermo	Acclaim™ PepMap™ NanoTrap	C18	0.075	20	2	100	164946
Waters	nanoEase M/Z Peptide BEH	C18	0.075	250	1.7	130	186008795
Waters	nanoEase M/Z Peptide BEH	C18	0.180	5	1.7	100	186008821

2.5 Antibodies

The experiments were performed using an AbbVie IgG1 antibody abbreviated with mAb-1. Furthermore, the NISTmAb Reference material (RM 8671) from the National Institute of Standards and Technology (NIST, Washington (DC), USA) was used for the method development. This reference material is a commercially available humanized IgG1 mAb that is well characterized and therefore intended to use for method development [129].

For the capture experiments an AbbVie internal capture antibody named in-house capture mAb, was used. This molecule is a biotinylated IgG1 antibody directed against the Fc-part of human antibodies.

2.6 Methods

2.6.1 Solvent change and calibration of the Nano-HPLC

The mobile phases were replaced every four weeks and for this, a specific procedure, which includes purging of pumps and flowmeter, pressure calibration and viscosity measurement, was performed. Firstly, the purge screw of the loading pump was opened and the pump purged for 5 minutes. After that, the purge valve was closed. In a second step, the purge screws of both channels of the nano/cap pump (NCP) module were opened and the purge syringes put on the output tubes of the channels (Figure 20).

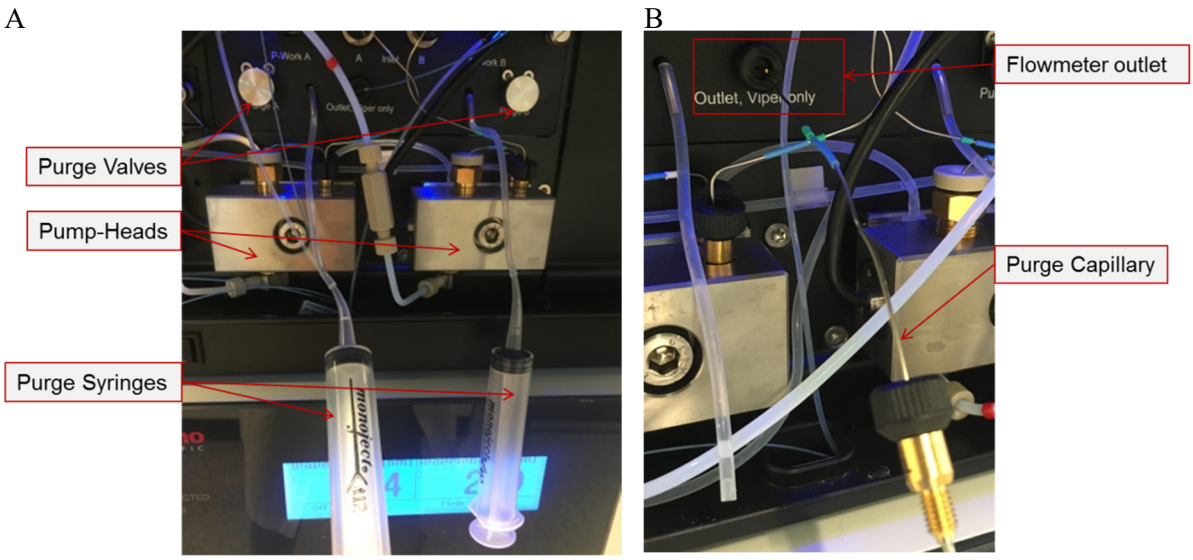

Figure 20 – Purge valves and purge syringes

A) The purge valves of the nano/cap pump (NCP) were opened and the purge syringes used to accelerate the removal of airbubbles. B) Installation of the purge capillary to purge the flowmeter.

Then purging was started and the plunger of the syringes slightly pulled back to accelerate the removal of air bubbles from the system. After two minutes purging was stopped and the fluid removed from the syringes. The empty syringes were put back on the output tubes and purging restarted for a total time of 30 minutes. After that, the purge screws of the NCP were closed and the syringes removed.

In a next step, the flowmeter was purged and for this the column was removed from the outlet of the flowmeter and the purge capillary installed. Following this, the pressure transducer test was performed to match the system to ambient pressure. For this, the purge screws of the NCP were opened and the purge capillary removed from the flowmeter outlet. After that, the viscosity measurement was performed. For this, the purge capillary was installed on the flowmeter outlet and the purge valves opened. Then, the purge capillary was removed and the viper blind nut needs to be installed. After about 15 minutes the viscosity measurement and calibration was finished. At the end, the column was reinstalled at the flowmeter inlet and pump flow was ramped up stepwise (50 nL/min, 100 nL/min, 150 nL/min, 200 nL/min, 250 nL/min, 300 nL/min with five minutes each step).

2.6.2 Calibration of the NanoMate®

Calibration of the TriVersa NanoMate® was run to align the sampling probe with the chip holder, when the system was switched from infusion to LC-coupling mode, after exchange of the LC- coupler, and when misalignment was suspected (Figure 21).

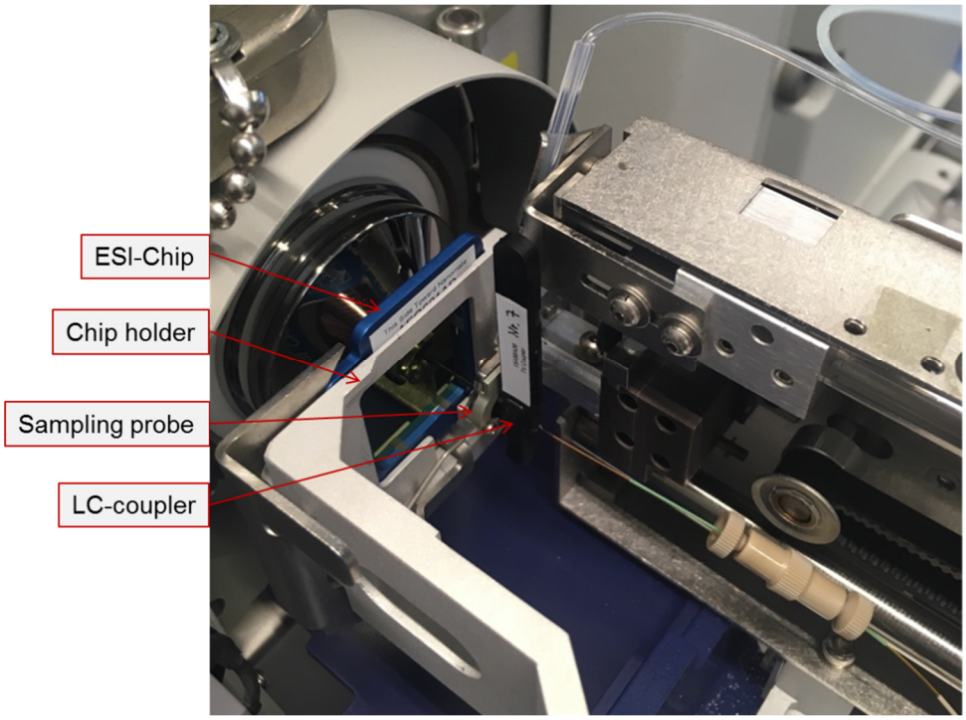

Figure 21 – TriVersa NanoMate®

To align the sampling probe with the chip holder of the TriVersa NanoMate®, the ESI-Chip was removed and a new LC-coupler was installed.

The chip alignment frame, shown in Figure 22 was inserted into the chip holder in the same orientation as the ESI Chip.

A B

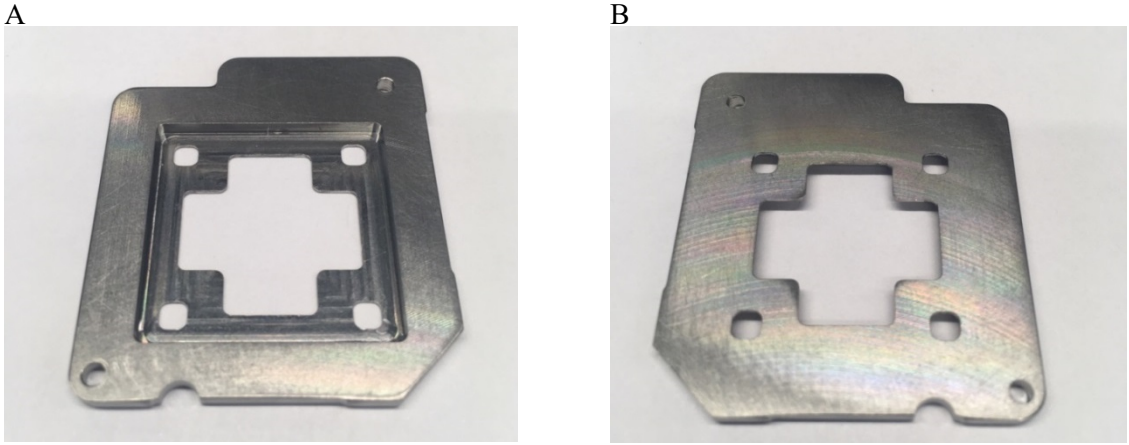

Figure 22 – Chip alignment frame

A) Front view and B) back view of the chip alignment frame.

The LC-coupler was connected to the outlet of the LC column via a microtight union and two microtight sleeves as shown in Figure 23. This connection needs to be tight and dead volume free as it is crucial for the peak shape of the chromatographic separation. Although, this connection is not required for calibration of the TriVersa NanoMate® itself, it should be prepared in advance. The reason for that is that in order to achieve optimal spray results, the LC-coupler should not be removed from the TriVersa NanoMate® once calibrated.

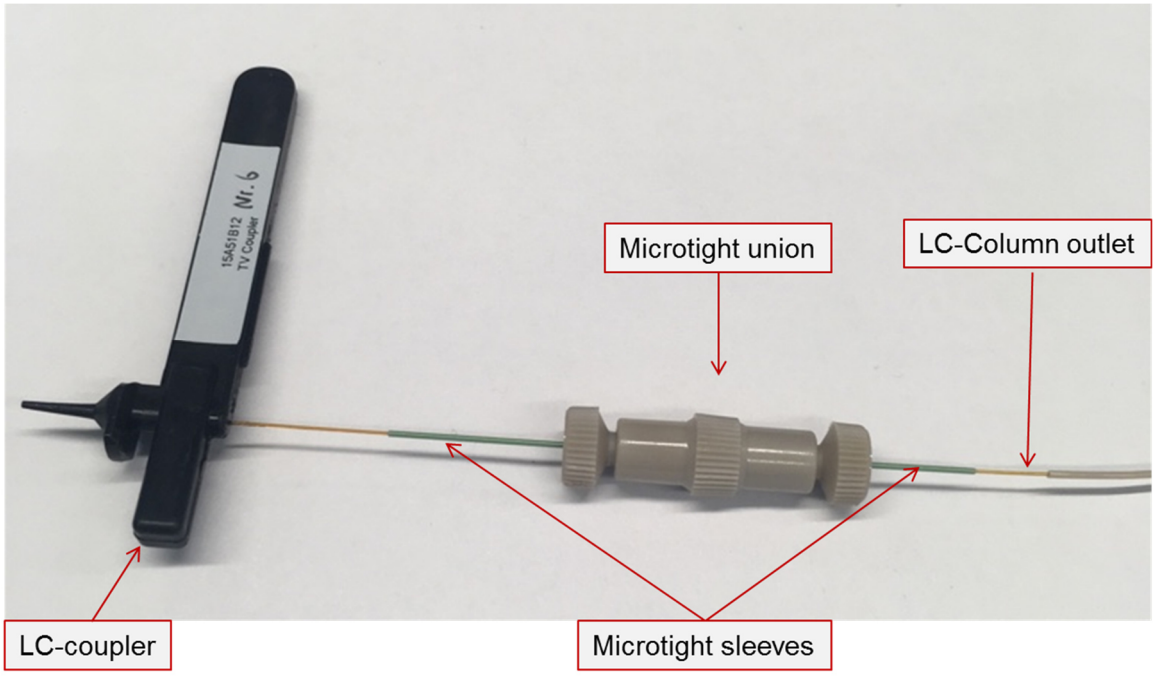

Figure 23 – LC-coupler

The LC-coupler was connected to the column outlet via a microtight union and two microtight sleeves. Then the LC-coupler was installed in the TriVersa NanoMate® and calibration was started.

After insertion of the chip alignment frame and the LC-coupler into the TriVersa NanoMate®, calibration was started. During this procedure the tip of the LC-coupler is aligned with the alignment chip. When calibration is finished the new settings were displayed (Figure 24). If the new settings matched the current ones the alignment was valid. If the new settings differ from the current ones then, the new settings were accepted but the alignment routine was repeated. After the repetition, the new settings should display the current ones.

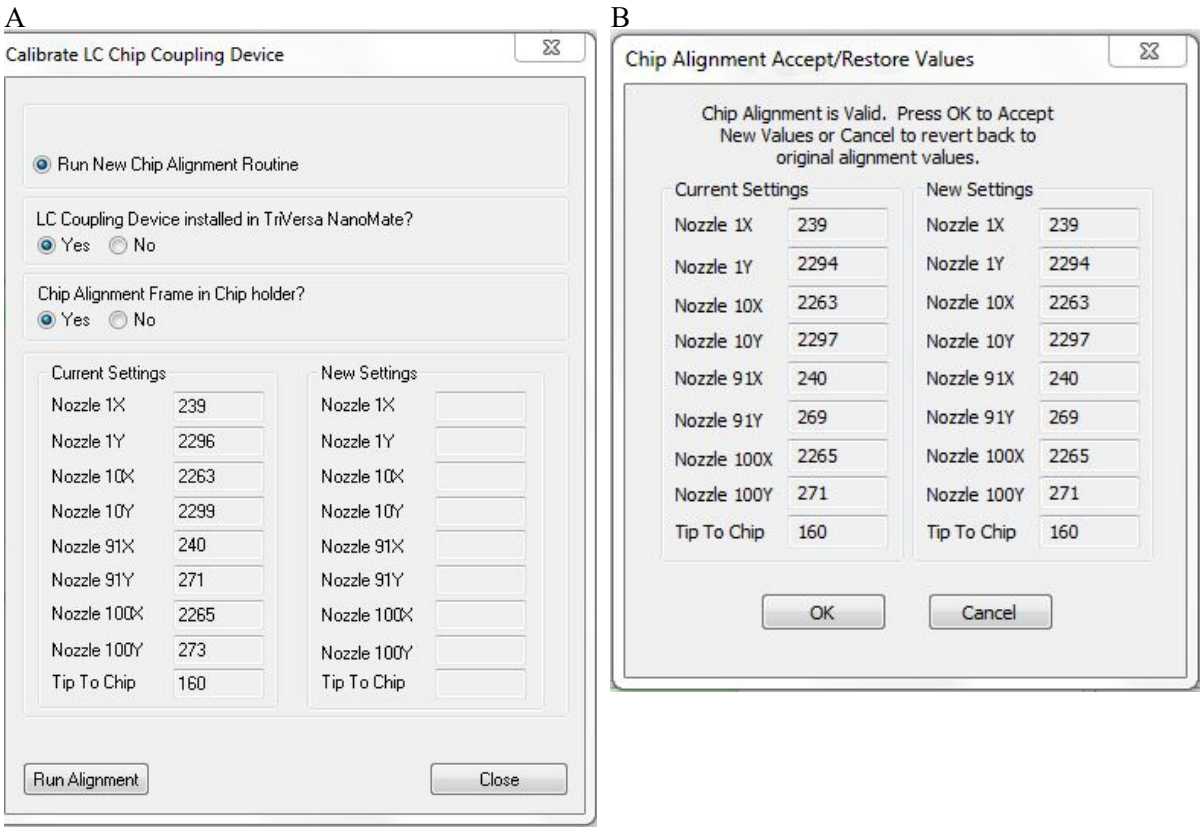

Figure 24 – Alignment routine

A) The window displays the stored alignment settings of the previous alignment routine. After the alignment the new values are displayed. If they do not match the current ones, alignment is repeated. B) If the new settings match the current ones, chip alignment is valid.

2.6.3 Calibration of the Orbitrap Velos Pro using the NanoMate®

The Orbitrap Velos Pro was calibrated using the direct infusion mode of the TriVersa NanoMate®. For this a sample well plate and a box of spray tips were installed as can be seen in Figure 25. Furthermore, an ESI-Spray-Chip was applied to the chip holder as shown in Figure 26.

Then 200 µL of the Pierce LTQ Velos ESI Positive Calibration solution was transferred into an unused well of the plate. The solution was aspirated with an ESI spray tip and directly sprayed through the next free nozzle of the spray chip. For the NSI source a spray voltage of 1.7 kV and a capillary temperature of 275°C were chosen. The calibration solution was sprayed and the signal observed until it was stable. Then an automatic tuning of m/z 524 was performed first, followed by semi-automatic calibration.

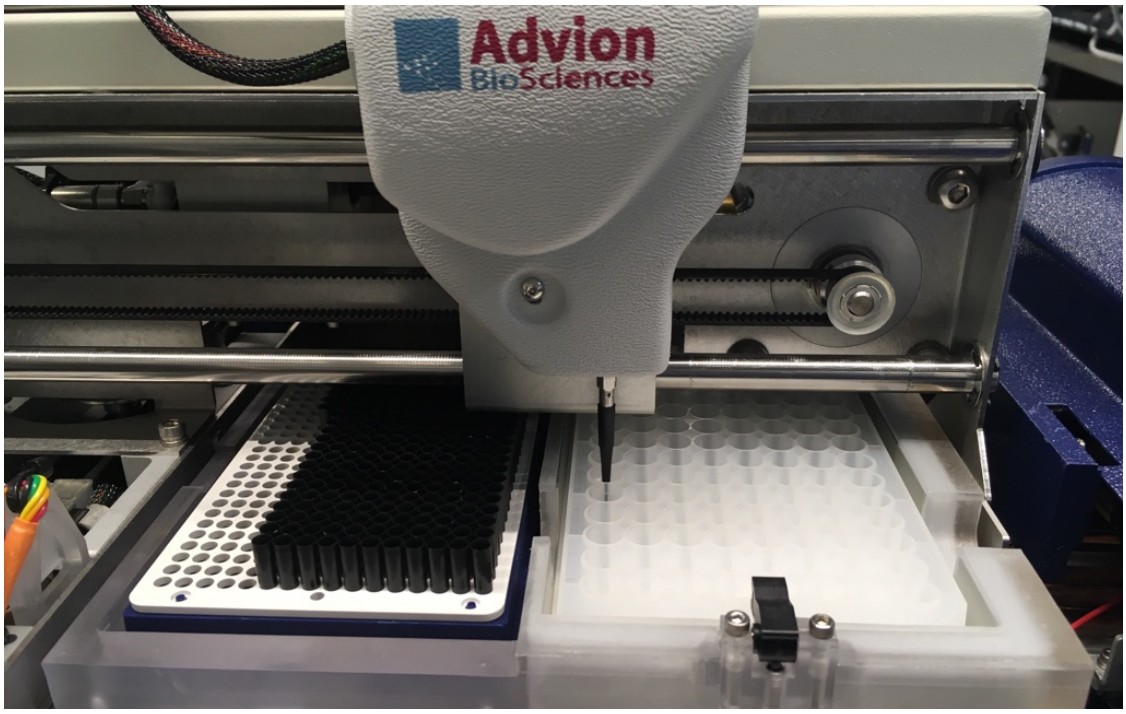

Figure 25 – Spray tips and sample well plate

The LC-coupler was connected to the column outlet via a microtight union and two microtight sleeves. Then the LC-coupler was installed in the TriVersa NanoMate® and calibration was started.

A

B

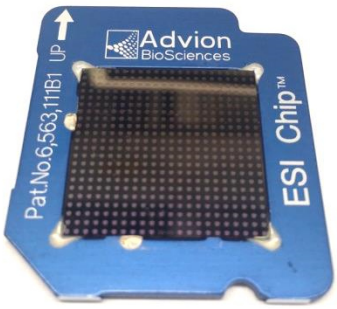

C

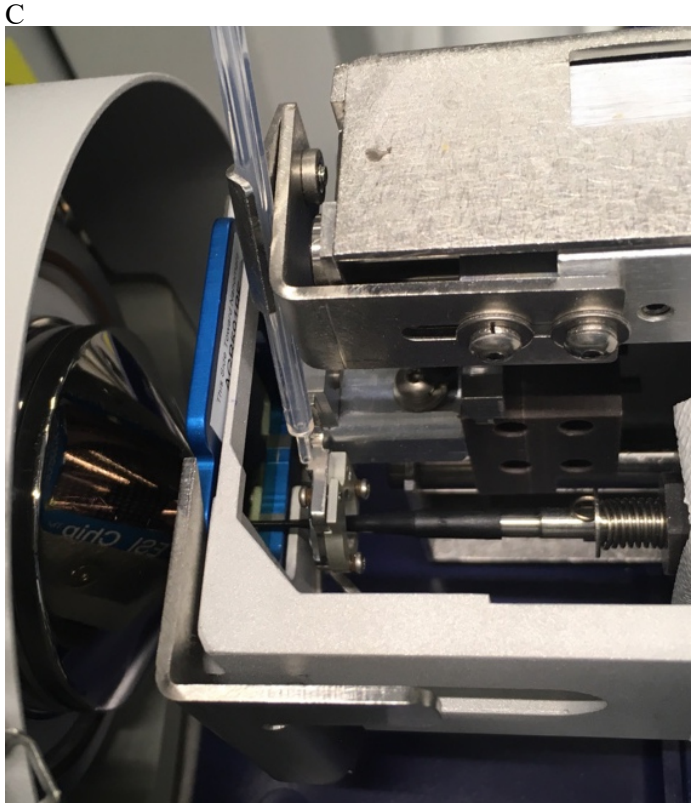

Figure 26 – ESI-Spray Chip

A) Front view and B) back view of the ESI-Spray chip. C) The ESI Spray Chip was applied to the chip holder with the back side oriented to the mass spectrometer orifice.

2.6.4 OFM sampling

In order to analyze the therapeutic antibody after subcutaneous injection, the OFM sampling technique was used. Three OFM probes (A, B and C) were inserted into the subcutaneous adipose tissue of a domestic pig in a depth of 7 mm as shown in Figure 27. Tubes A and B were 10 mm apart from each other, tube C 5 mm further from Tube B (Figure 27-B). The setup was applied at three different areas on the back of a domestic pig as shown in Figure 27-C. Thus, three times tube A (A1, A2, A3), tube B (B1, B2, B3) and tube C (C1, C2, C3) were applied for sample collection.

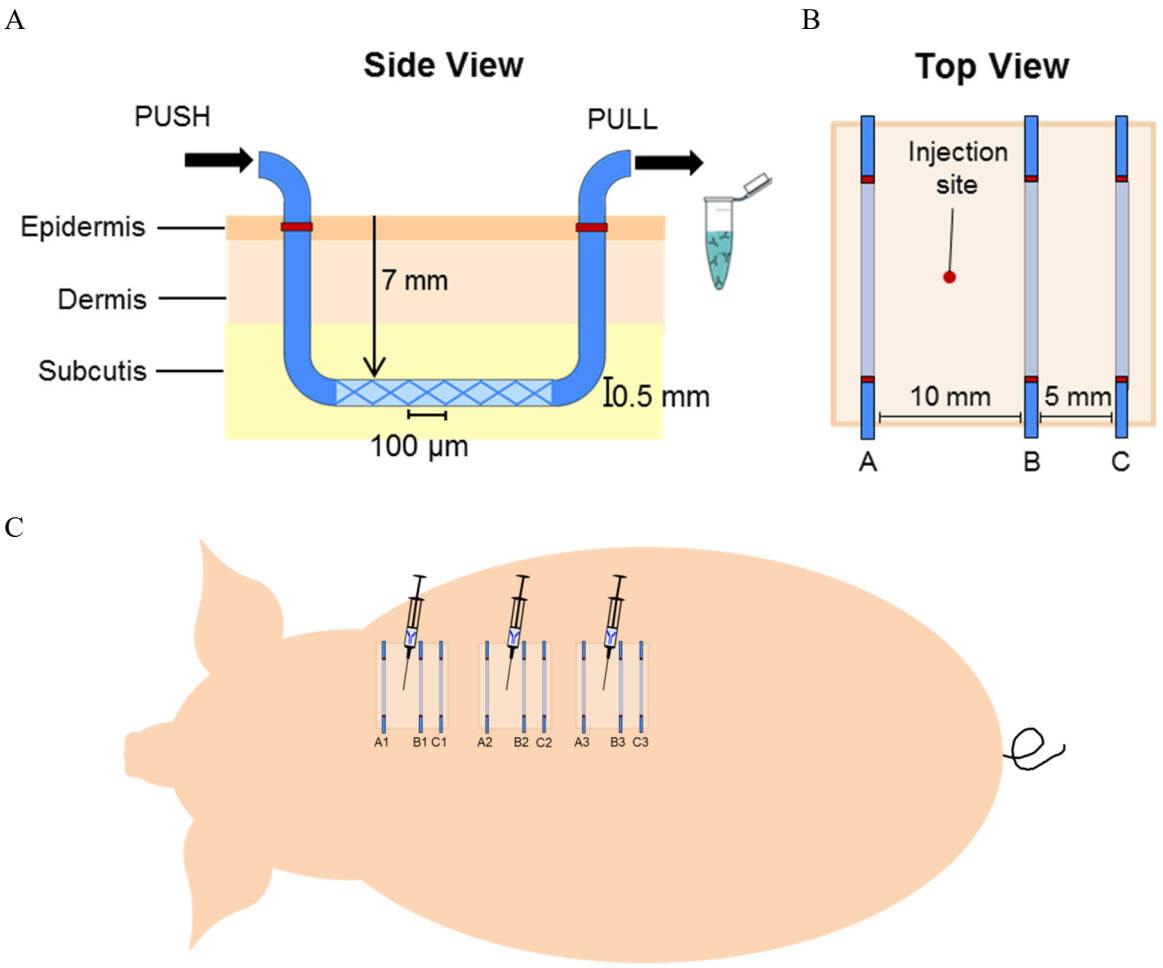

Figure 27 - Open Flow Microperfusion Principle.

Open Flow Microperfusion principle. A) Side View: The tubes are located in the subcutis and interstitial fluid is sampled via a push-pull mechanism. B) Top View: Tubes A and B were 5 mm apart from the injection site, and tube C was 5 mm apart the tube B. C) This setup was applied at three sites on the back of a domestic pig.

A bolus of 300 µL therapeutic antibody solution (100 mg/mL) was injected in between tubes A and B in a depth of 7 mm using a 30 Ga injection needle. The OFM probes were perfused with an artificial interstitial fluid, ELO-MEL isoton (Fresenius Kabi, Austria) and 1% Albunorm® 20g/L (Octapharma, Austria) at a flowrate of 1 µL/min and respective individual samples were taken over one hour for a total time of 10 hours from all tubes (one hour prior to the drug injection until 10 hours after). Thus, for

each tube 11 samples were collected, leading to a total number of 99 samples. Furthermore, serum samples were drawn hourly resulting in 11 additional samples.

The experimental protocol for this study was approved by the Federal Ministry of Science, Research and Economy (BMWFW-66.010/0204-WF/V/3b/2017) and the animal experiment was conducted by the group of Dr. Frank Sinner at the Joanneum Research institute in Graz. Sample clean up and subsequent analysis was performed at AbbVie and is described in this thesis.

2.6.5 Antibody capture using protein A Agarose

First, the filter plate run off openings were sealed with a duo sealing mat. Then 300 µL 1x Dulbecco's Phosphate-Buffered Saline (DPBS) was pipetted in each well, as can be seen in Figure 28. After that 50 µL sample was added in each well and mixed for 1 min at 550 rpm. The Pierce™ Protein A Plus Agarose was mixed with a magnetic stirrer while pipetting 50 µL into each well, to prevent sedimentation.

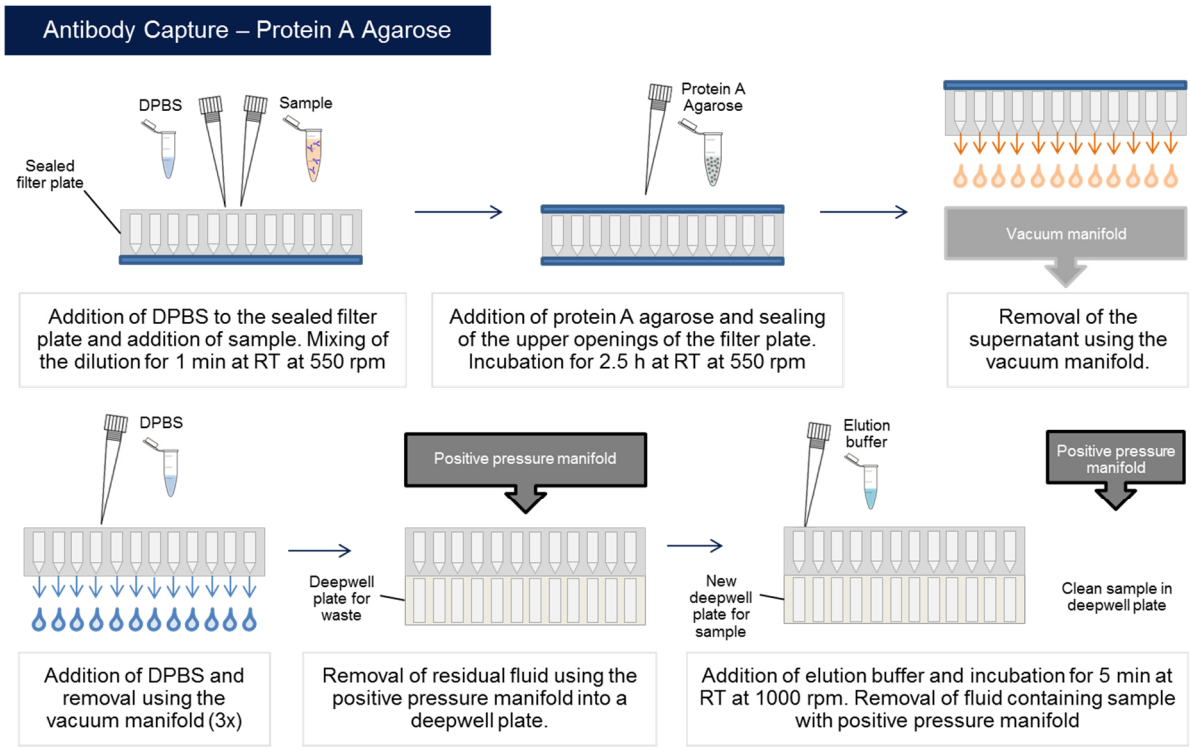

Figure 28 – Schematic illustriation of the capture protocol using protein-A Agarose

The samples were diluted in a sealed filter plate with DPBS. Protein A Agarose was added, the plate was sealed and incubation performed for 2.5 hours at 550rpm. The supernatant was removed using a vacuum manifold and afterwards DPBS was added to wash the sample bound to the agarose. The residual fluid was removed using the positive pressure manifold and collected in a deepwell plate. Elution buffer was added to the filter plate and placed on a new deepwell plate for the collection of elution.

The upper openings of the filter plate were sealed with adhesive tape and the plate incubated for 2.5 h at room temperature at 550 rpm. The adhesive tape from the discharge opening was taken off and

supernatant was removed using the vacuum manifold TurboVap® 96. Into each well 800 µL DPBS buffer was added and supernatant again removed using vacuum manifold to wash the samples. This step was repeated two times. To remove residual fluids, the filter plate was placed onto an Eppendorf Protein LoBind Deepwell plate and then both plates were placed onto Waters positive pressure-96 manifold. The regulator was turned to right side for 5 second to apply the positive pressure. Then, the filter plate was placed on a new deepwell plate and not anymore removed from the elution plate.
For the elution step the filter plate was placed onto a new deepwell plate and 150 µL of elution buffer was added into each well. Incubation was performed for five minutes at room temperature at 1000 rpm. Then, the plates were placed onto the Waters positive pressure manifold for 5 seconds. The elution step was repeated two times. The eluate containing the target molecule was collected in the deepwell plate and saved for analysis.

2.6.6 Antibody capture using Streptavidin Magnetic Beads

First, 50 µL sample was diluted with 250 µL binding/wash buffer containing Tris-buffered saline and 0.1% Tween™-20. Then the samples were combined with the biotinylated capture molecule as shown in Figure 29. For this 3 µL of CaptureSelect™ Human IgG-Fc PK Biotin Conjugate was added. The samples were then incubated for 2 h at room temperature at 550 rpm.
Pierce Streptavidin Magnetic Beads were thoroughly mixed before use. Afterwards, 50 µL (0.5 mg) of magnetic beads were added into a 1.5 mL microcentrifuge tube. The beads were collected with a magnetic stand MagnaBind™ and the supernatant was removed and discarded. Then 1 mL of binding/wash buffer was added to the tubes, and the tubes were several times inverted (gently vortexed) to achieve mixing. Again, the beads were collected with a magnetic stand and the supernatant was removed and discarded.
The sample/ CaptureSelect™ mixture was added to the pre-washed magnetic beads and incubated for 1 h at room temperature at 550 rpm. The beads were then collected and the supernatant was saved for analysis. Then the beads were washed with 300 µL binding/wash buffer and gently mixed. The beads were then collected and the supernatant was removed and discarded. The washing procedure was repeated two times. Then the beads were pre-rinsed with 300 µL of 0.1% Tween-20 solution in H_2O. The beads were then collected and the supernatant was removed and discarded. To elute the target, 100 µL of IgG elution buffer was added to the collected beads and incubated for 5 min at room temperature with mixing. Then the beads were collected and the supernatant containing the target was collected and saved for analysis.

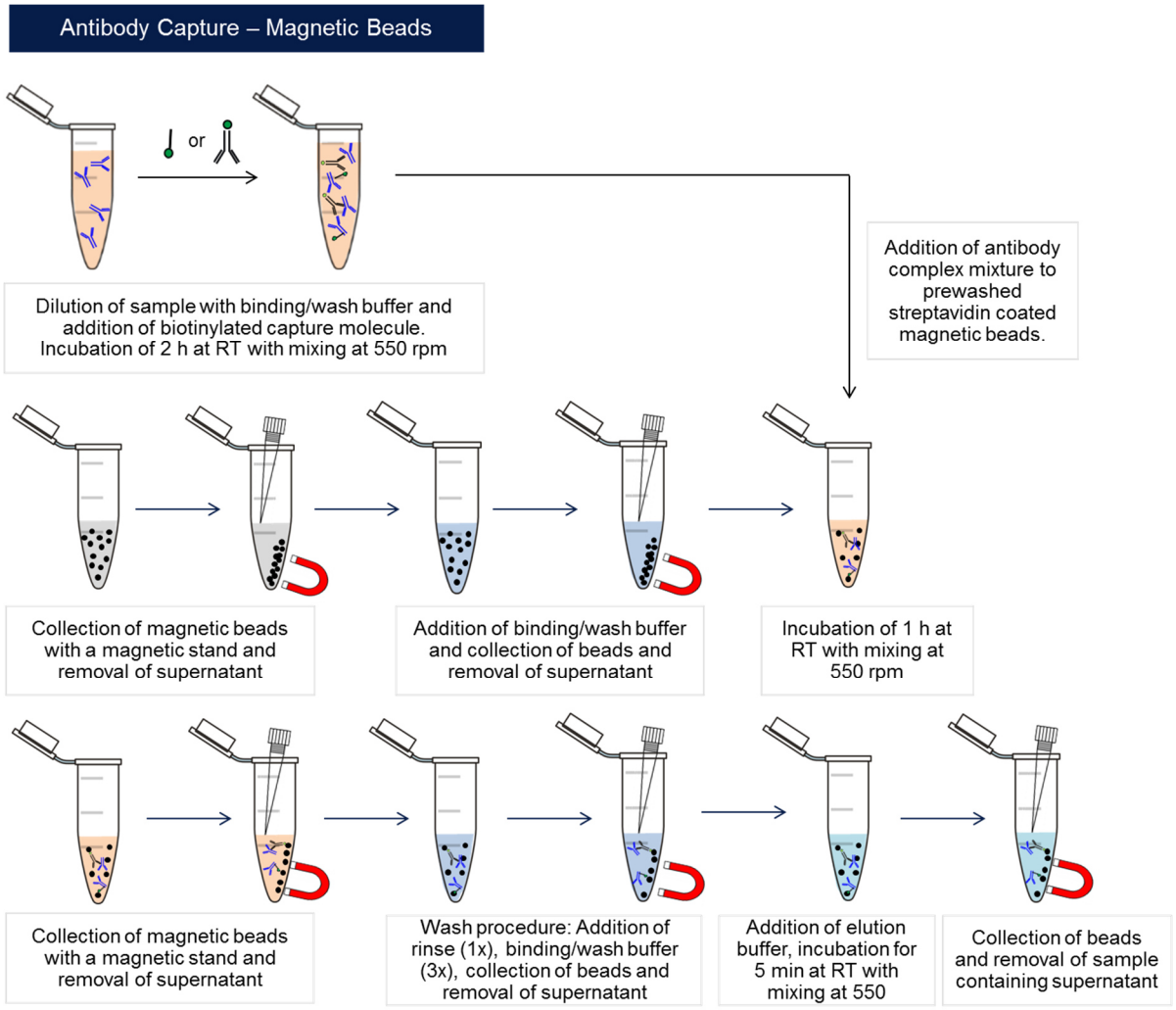

Figure 29 – Schematic illustration of the capture protocol using streptavidin magnetic beads

The biotinylated capture molecule was added to the diluted sample and incubated for 2 hours at room temperature with mixing at 550 rpm. Meanwhile, the magnetic beads were collected with a magnetic stand and the supernatant removed. The beads were washed with binding/wash buffer and the wash solution removed. Then the mixture containing sample bound to the capture molecule was added to the pre-washed magnetic beads and incubation performed. Afterwards, beads were collected and supernatant removed. As wash procedure first pre-rinse buffer and then binding/wash buffer (3x) were used. Finally, elution butter was added and after 5 min incubation the beads collected and the supernatant containing the target mAb was removed and used for analysis.

2.6.7 Gelelectrophoresis

The electrophoresis running buffer (1x) was prepared by dilution of the (20x) NuPAGE™ MOPS SDS Stock solution with water. Afterwards, the Page Ruler unstained protein ladder was diluted 1:10 with NuPAGE™ LDS-Sample Buffer (4x). For this 90 µL LDS Sample Buffer (4x) was pipetted in an Eppendorf tube and 10 µL of the protein ladder added. Then, 15 µL sample were transferred in a separate Eppendorf tube and 5 µL LDS Sample buffer (4x) added. The samples (NOT protein ladder) were heat shocked for 10 min at 70°C under shaking at 650 rpm.

The comb of NuPAGE™ Novex 4-12% Bis-Tris-Gel was carefully removed from gels. Each well was rinsed with running buffer. For this, gel loader tips were used to load buffer into the pockets. To remove the buffer from the wells, gels were shaken overhead. Then, the white tape from the bottom of the gel cassettes was peeled off. The gels were oriented in the Mini-cell such that the "well" side of the cassette faced inwards toward the buffer core. Then the upper gel chamber was filled with 1x SDS Buffer, so that the gels were completely covered with liquid. Ladder and samples were shortly spinned down and afterwards loaded on gels. At first the sample was loaded (15 µL per well) and then the protein ladder was loaded (5 µL/well). Finally the lower gel chamber was filled with running buffer. The lid was put on the chamber and connected with the power station. Then the device was turned on and electrophoresis was performed at a constant potential of 200 V, 120 mA, 25.0 W. Electrophoresis was complete when the color front of the sample buffer reached the lower edge of the gel (approx. 40 – 50 minutes).
The gel was taken out of the chamber and laid with comb side facing upwards on a clean surface. A gel knife was inserted into the groove between the cassette covers and opened carefully on all three closed sides. The upper cover was carefully removed and the gel transferred into the staining tray.

2.6.7.1 Silver staining

Staining was performed using the Pierce® Silver Stain Kit from Thermo containing Silver Stain Sensitizer, Silver stain Enhancer, Silver Stain and Silver Stain Developer solutions.
First, the gel was rinsed two times with 25 mL ultrapure water for five minutes. Then the gel was fixed two times with 25 mL fixing solution (30% ethanol, 10% acetic acid) for 15 minutes. Afterwards, the gel was rinsed two times with 25 mL wash solution (10% ethanol) for five minutes, followed by two wash steps with 25 mL ultrapure water for five minutes. During the last wash step, the sensitizer working solution was prepared. For this 50 µL sensitizer was added to 25 mL ultrapure water and the gel sensitized for exactly 1 minute. Meanwhile the stain working solution was prepared by adding 500 µL Enhancer to 25 mL Stain solution. The sensitizer working solution was removed and the stain working solution was added. The gel was stained for 30 minutes and the developer working solution was prepared at the end of the staining time. For this 500 µL Enhancer was added to 25 mL Developer solution. Stain solution was removed and the gel quickly washed two times with 25 mL ultrapure water for 20 seconds. Immediately after washing, the developer working solution was added and incubated until protein bands appeared. Depending on the amount of protein this step takes between 2 and 3 minutes. The developing step was stopped by the addition of 25 mL Stop solution (5% acetic acid).

2.6.7.2 Coomassie staining

The gel was stained with SimplyBlue SafeStain. First, the gel was rinsed three times with 100 mL Milli-Q H_2O for 5 min and the wash rinse discarded. Then the gel was stained with simply Blue safe stain (approx. 40 mL for one midi-gel) so that the gel was fully covered with solution. Staining was performed

for 1.5 hours at room temperature with gentle shaking. Stain solution was discarded afterwards. Then the gel was washed with 100 mL of Milli-Q water for 1.5 h and scanned at BioRad GS800 gel scanner.

2.6.8 Miniaturized peptide map

The antibody was denatured and reduced in the presence of 100 µL 8 M guanidine-HCl, 400 mM tris solution and 1.5 µL 1 M dithiotreitol (DTT) for 1 h at 37°C. Then 5 µL 600 mM iodacetic acid (IAA) was added and incubated for 15 min at room temperature in the dark (Figure 30).

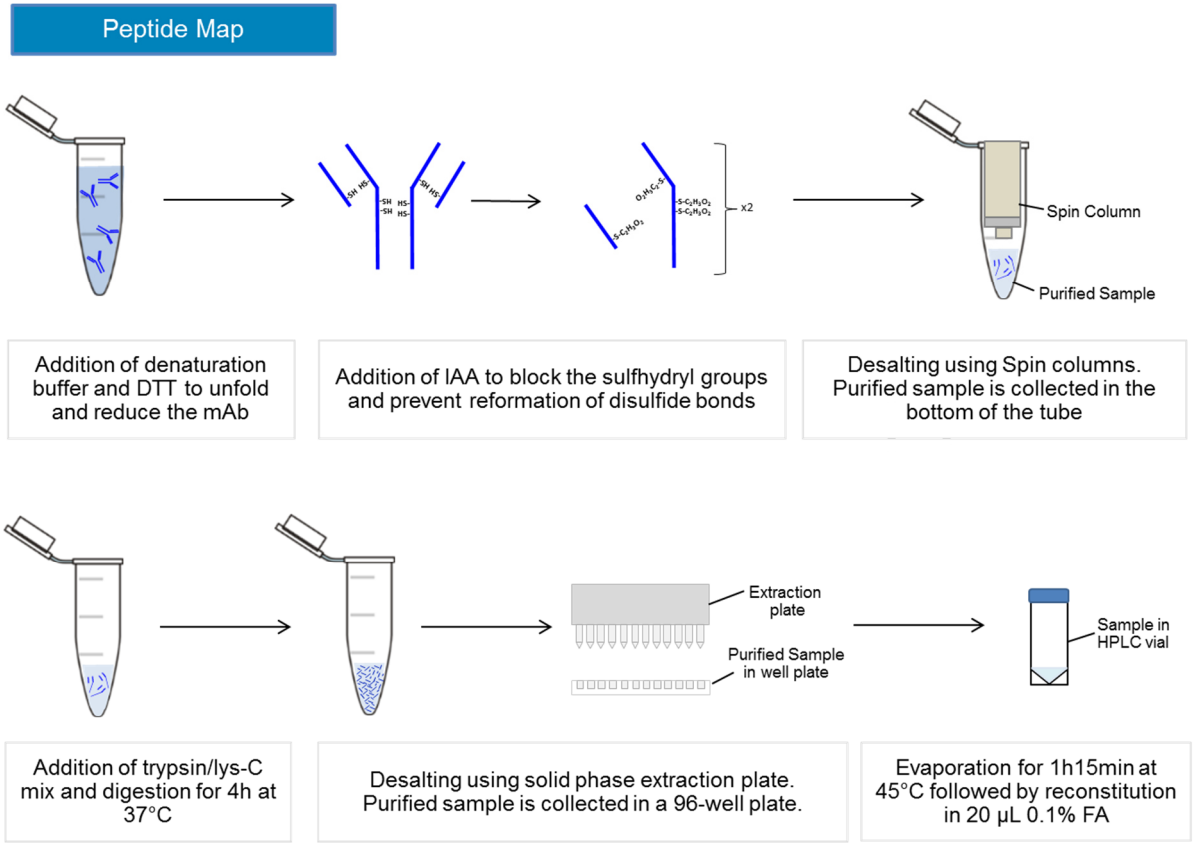

Figure 30 –Schematic illustration of peptide map for low sample amounts

The antibody is denaturated and reduced by the addition of denaturation buffer and dithiotreitol (DTT). Then iodacetic acid (IAA) is added to the sample to alkylate the sulfhydryl groups. In a next step the sample is desalted using Zebaspin desalting columns and the purified sample is collected in the bottom of the tube. Trypsin/Lys-C mix is added and digestion performed for 4h at 37°C. The peptide mix is then desalted using the Oasis-Prime µelution SPE plate. After evaporation of the organic solvent, the peptides are reconstituted on 20 µL 0.1% FA.

The reaction was stopped by adding 1.5 µL 1 M DTT. Afterwards the samples were desalted using Zeba™ Spin Desalting Columns, 40K MWCO, 0.5 mL as described in the instruction manual. For digestion 0.1 µg Trypsin/Lys-C-Mix was added to each sample and incubated for 4 h at 37°C at 550 rpm. The reaction was stopped by adding 2 µL of 10% formic acid (FA).

Prior LC-MS analysis the samples were desalted and concentrated using Oasis PRiME HLB 96-well µElution Plate. For this, the Oasis plate was placed on the vacuum manifold and 200 µL of solution

containing 80% acetonitrile and 0.05% formic acid (FA) was added to the wells. The vacuum was switched on at the lowest possible setting and was gradually increased as required. Afterwards 200 µL 0.05% FA was added and the vacuum was switched on to 5" Hg for 30 to 60 seconds. Then the samples were added and the vacuum was switched on at the lowest possible setting and was gradually increased as required.

Afterwards 200 µL 0.05% FA was added and the vacuum switched on to 5" Hg for 30-60 s to eliminate the wash solvent. The vacuum was released and the waste fluid discarded. A new collection device was inserted and 100 µL of 80% ACN, 0.05% FA was applied for elution. The vacuum was set on at the lowest possible setting for another 30 to 60 s to collect the rest of the elution solvent. Solvent evaporation was performed for 1 h and 15 min at 45°C using the SPD1010 vacuum concentrator.

2.6.9 In-gel digestion

In a first step, the gel was washed with water and put on a glass plate. Then, as shown in Figure 31 the bands of interest were excised with a scalpel as precisely as possible.

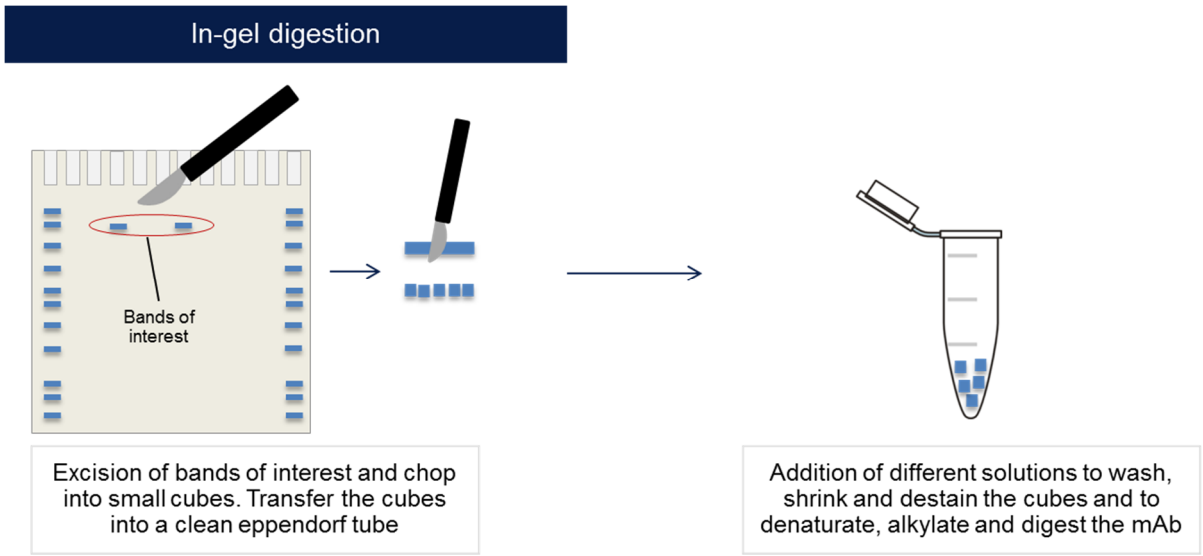

Figure 31 –Schematic illustration of the in-gel digestion protocol

The band of interest is excised from the gel and chopped into small cubes. The cubes are transferred into a clean eppendorf tube.

The band was then chopped into 1x1mm cubes and transferred into a clean 0.5 mL Eppendorf tube. The gel cubes where washed and shrunk as described in Table 4. In order to reduce the disulfide linkages of the mAb, a denaturation step was performed, followed by a destaining of the bands.

Table 4 – Different steps of the in-gel digestion protocol

Step	Volume	Solution added/removed	Incubation for/at
Wash	200 µL	Water	10 min, RT, 650 rpm
Shrink	200 µL	ACN	15 min, RT, 650 rpm
Denaturation	200 µL	1.5 mg/mL DTT in 100 mM NH_4HCO_3	15 min, 56°C, 650 rpm
Destain **- if incomplete**	200 µL 200 µL +200 µL	ACN ACN + 100 mM NH_4HCO_3)	20 min, RT, 650 rpm
Alkylation (in the dark)	200 µL	10 mg/mL IAA in 100 mM NH_4HCO_3	20 min, RT, 650 rpm
Shrink	200 µL	ACN	15 min, RT, 650 rpm
Digestion	30 µL	6.25 ng/µL Trypsin in 50 mM NH_4HCO_3	30 min, on ice
	30 µL	50 mM NH_4HCO_3	Overnight, 37°C, 650 rpm
Digestion stop	15 µL	5% FA in 50% ACN	Sonication, 15 min, Save supernatant
	30 µL	ACN	Sonication, 15 min, Save supernatant
Evaporation	45 µL	Combine supernatants	10 min, RT
Reconstitution	10 µL	0.1% TFA	

In case of incomplete destaining, the liquid was removed and refilled with 200 µL acetonitrile and 200 µL ammonium bicarbonate solution. After successful destaining, the liquid was removed and alkylation performed. Then, antibody digestion was achieved by overnight incubation with trypsin solution. For this, the samples were first incubated for 30 min on ice to let the trypsin enter the gel pieces. Then, the remaining digestion buffer was removed and 30 µL of 50 mM ammonium bicarbonate was added. Digestion was performed at 37°C overnight at 650 rpm.

The samples were spinned down in a benchtop centrifuge and digestion stopped. Sonication was performed and then the sample was spinned down to collect the supernatant into a separate Eppendorf tube. After that acetonitrile was added to the gel pieces and the samples sonicated again. Then the samples were spinned down and the supernatant removed and combined with the supernatant of the first

extraction step. Finally, the combined supernatants of extraction one and two were evaporated in a vacuum centrifuge to remove the liquid.

In a next step the dried samples were reconstituted in 10 µL 0.1% TFA solution and afterwards desalted using ZipTips®. The different steps of the protocol are shown in Figure 32.

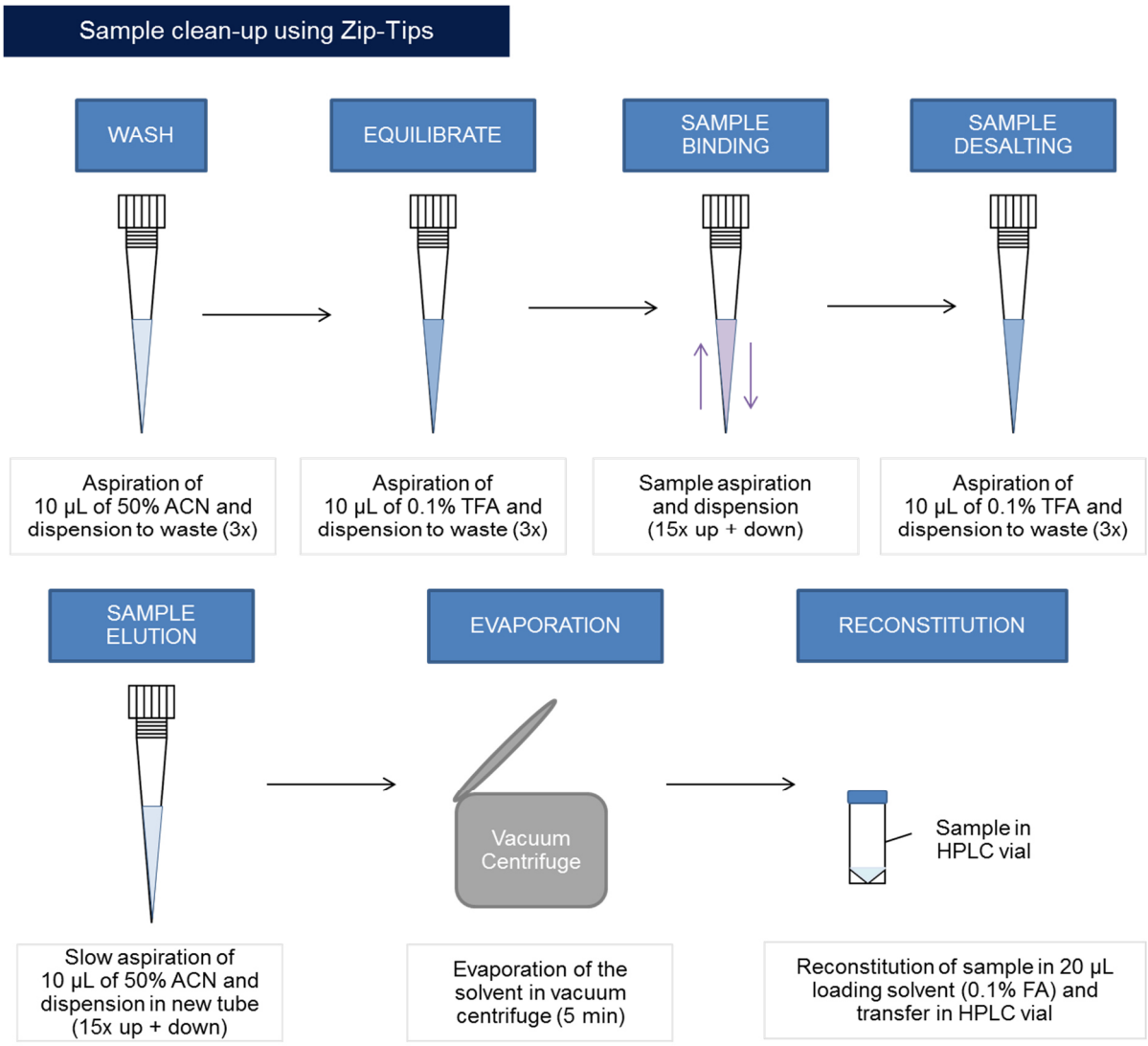

Figure 32 –Schematic illustration of the ZipTip® desalting protocol

The ZipTips® are washed three times with acetonitrile (ACN) by aspirating the solution up and dispensing into waste. Equilibration is performed by aspiration of trifluoracetic acid (TFA) and dispension (3x). After that the sample is aspirated into the Tip and pipetted 15-times up and down, to bind the peptides to the ZipTip® material. Then the sample is desalted by aspiration and dispension of 0.1% TFA. For sample elution, 50% ACN is aspirated and dispensed into a new tube. This solution is reaspirated and redispensed in the new tube 15 times. The solution is evaporated in a vacuum centrifuge (5 min) and afterwards reconstituted and transferred into a HPLC-vial.

2.6.10 LC-MS measurement

For all experiments the peptide separations were performed on an Ultimate 3000 RSLCnano system. Prior analysis the samples were reconstituted with 20 µL of 0.05% (*v/v*) FA. The mobile phases for sample loading and separation were 0.1% (*v/v*) FA in MS grade water (A) and 0.1% (*v/v*) formic acid in acetonitrile (B). The samples were loaded onto a NanoEase M/Z Symmetry trap column, C18, 5 µM, 0.3 x 20 mm, with a flow rate of 15 µL/min. After three minutes the trap column was put on-line with the analytical NanoEase M/Z column C18, 0.075 x 250 mm. For this a flow rate of 300 nL/min was applied for 120 min at 35°C. Samples were eluted using the gradient listed in Table 5.

Table 5 – Final gradient

Time [min]	B [%]
0.0	2
3.0	2
10.5	8
30.0	18
52.5	25
75.0	30
84.0	40
90.0	90
100.0	90
100.1	2
120.0	2

The peptides were ionized by the TriVersa NanoMate® and analyzed in data dependent acquisition mode by the LTQ Velos Pro mass spectrometer. In nESI positive mode a spray voltage of 1.7 kV and a capillary temperature of 275°C was applied. Acquisition was performed in the mass range of 250 – 2,000 m/z at a resolution of 30,000. Precursors were accumulated with a maximum injection time of 500 ms, dynamic exclusion of 30 s and an AGC target value of 1E6 in a top-5 method. The MS settings were developed and optimized in previous experiments at AbbVie.

2.6.11 Analysis of LC-MS/MS data

All raw data were acquired by Thermo Xcalibur software and subsequently processed with PMI Suite (Protein Metrics, Cupertino, USA). First, the quality of MS1 and MS2 spectra were evaluated by PMI-Preview. This software lists possible modifications that can then be used for identification. Identification of ions was performed by PMI-Byonic using the following parameters: arginine (R) and lysine (K) as C-terminal cleavage sites, maximum number of two missed cleavages, precursor mass tolerance 5 ppm, and fragment mass tolerance 0.4 Da. Carboxymethylation was set as fixed modification on cysteine. The following dynamic modifications were selected: deamidation on asparagine and glutamine; oxidation on methionine and tryptophane, methylation on histidine, lysine, arginine and asparagine; dioxidation on tryptophane; pyroglutamic acid formation on N-terminal glutamine and glutamic acid. For final inspection and quantification of modifications PMI-Byologic was used. The label-free quantification of peptide modifications in this software is based on equation 7, whereby XIC Area represents the combined extracted ion chromatogram (XIC) of all charge states.

$$\%_{modified} = \frac{XIC\ Area_{modified}}{XIC\ Area_{modified} + XIC\ Area_{unmodified}} \times 100 \quad (7)$$

Thus, the method is based on a relative quantification.

2.7 Software

Software type	Software Name	Vendor
Computer software	Office 2010	Microsoft
HPLC software	Chromeleon 7.2	Thermo Fisher Scientific
Mass Spectrometer software	LTQ Tune	Thermo Fisher Scientific
LC-MS software	Xcalibur	Thermo Fisher Scientific
NanoMate® software	Chipsoft 8.3.1	Advion
NanoMate® software	Chipsoft Spray Sensing Viewer	Advion
Gel Aquisition software	Image Lab	Bio-Rad
Gel Analysis software	Image Lab	Bio-Rad
Drawing software	ChemDraw Professional 15.0	CambridgeSoft
Analysis and graphic software	Prism 6	GraphPad
Statistics software	Minitab 18	Minitab
Citation software	Endnote X7	Clarivate Analytics
Graphic software	PyMOL	DeLano Scientific LLC, Schrödinger
General Protein/Mass analysis software	GPMAW 10.31	Lighthouse data
MS Data Analysis software	Proteome Discoverer 2.0	Thermo Fisher Scientific
MS Data Analysis software	PMI Suite: - PMI Byonic - Byonic Viewer - PMI Byologic - PMI Batcher	Proteinmetrics

3. Results and Discussion

3.1 Antibody capture

For the analysis of therapeutic antibodies after injection *in-vivo*, a suitable capture protocol was required, that purifies the target mAb from the complex biological matrices. This step is crucial in order to remove matrix proteins and other components from the sample that may interfere with the further MS analysis [130]. One example of the interfering proteins are endogenous IgGs that are very abundant in plasma and share many sequence homologies to the therapeutic target mAb [131]. Furthermore, it needs to be considered, that the concentration of the endogenous IgGs is 1000 to 10000-fold higher than that of the therapeutic mAb in the *in-vivo* samples. [131]

Therefore, with the antibody capture step, enrichment and clean-up of the target mAb should be achieved. Several experiments, including protein A Agarose and magnetic beads in combination with different capture molecules, were carried out to find the most suitable capture approach.

3.1.1 Protein A Agarose

The use of bacterial proteins such as staphylococcal protein A crosslinked to beaded Agarose, is a classical approach in antibody purification [132, 133]. However, it shows affinities for the Fc portion of IgGs from several species and is thus not exclusively specific to human antibodies. Nevertheless, it is a fast and common method for purifying antibodies and was therefore used as a starting point for the development of the capture procedure [51, 134].

	A	B	C	D
c(mAb)	10 ng/µL	5 ng/µL	1 ng/µL	0.5 ng/µL

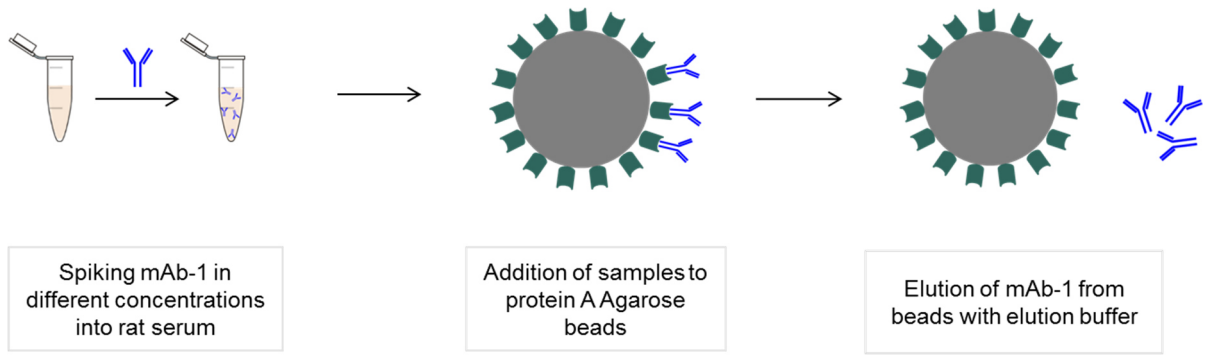

Figure 33 – Concentrations tested using the protein A Agarose approach

Different concentrations of mAb-1(blue) were spiked in serum and afterwards cleaned up using protein A (green) agarose beads (grey). The target was eluted by addition of elution buffer.

Different amounts of mAb-1 were spiked in rat serum (concentrations A-D) and captured via the Fc-part with the protein A Agarose beads, as shown in Figure 33 and explained in detail in 2.6.5. The captured samples were diluted 1:10 with water as diluent and then separated by gel electrophoresis followed by silver staining (see 2.6.7 and 2.6.7.1). As can be seen from Figure 34 the protein bands in the SDS-PAGE were extremely intense which was not expected for such low mAb-1 concentrations.

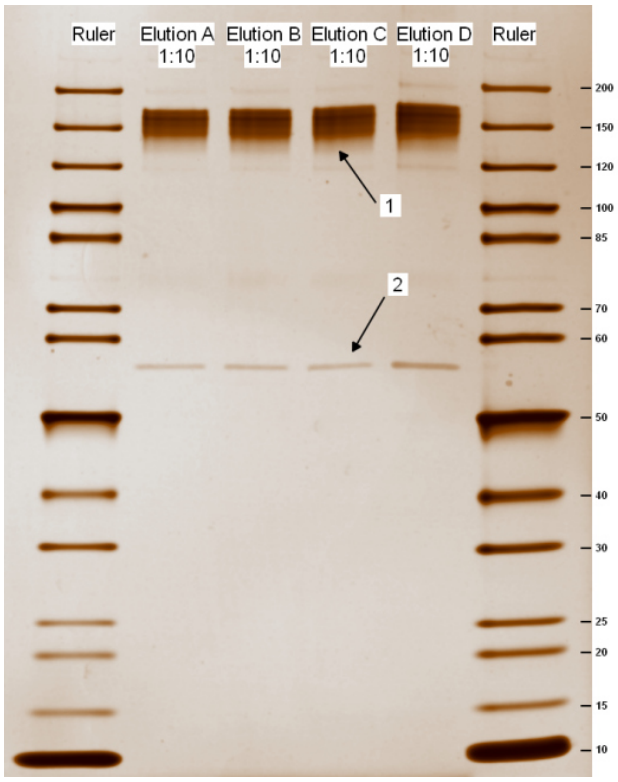

Figure 34 – SDS-gel of samples captured using protein A agarose beads

The captured samples A-D were diluted 1:10 and then separated on the SDS-gel. For all concentrations a very broad band at 150 kDa was observed, indicating a cross-contamination with rat IgGs (band 1). Furthermore, an additional band at 56 kDa was observed, which is assumed to be either Protein A or any unknown contamination (band 2).

In contradiction to an article that reported the binding of protein A to rat IgGs to be weak [135], it was apparent that the high intensity of the SDS-PAGE protein bands could be attributed to cross contamination of the target mAb with endogenous IgGs from the rat serum. Other sources reported, a strong binding of protein A to rat IgG1 and a weak binding to rat IgG2 [130], which could explain the observed cross contamination results.

Furthermore, for every sample one additional band at approximately 56 kDa was apparent. This band could be attributed to a protein fragment, protein A (46 kDa) or any other non-specifically captured protein (Figure 34).

In a recently published study, Schmid *et al.* applied protein A chromatography for the purification of the therapeutic mAb trastuzumAb from mouse serum [51]. Although, they used a severe combined

immune deficient (SCID) mouse model, they found minor levels of endogenous serum IgGs after their capture with protein A. Due to a mutation, the SCID mice are almost fully deficient in the production of functional B and T lymphocytes. Therefore, no or only low levels of endogeneous IgGs can be produced by those mice. [136] However, Schmid and co-workers reported minor impurities during the capture using protein A chromatography with endogenous IgGs from the SCID-mouse [51].

Those results are consistent with the cross contamination observed in this work and confirmed the initial assumption that the traditional immuno purification using protein A is not sufficiently specific. Therefore, alternative approaches have been investigated.

3.1.2 Streptavidin Magnetic Beads using an in-house capture mAb

Another approach that is widely used for IgG capture from serum, is the use of magnetic beads covered with streptavidin in combination with a biotinylated capture molecule directed against the target. An AbbVie in-house produced and biotinylated anti-human antibody was used as a capturing agent. Different amounts of mAb-1 (concentrations C1-C4) were spiked in rat serum and interstitial fluid. Then the mAb-1 was captured with the in-house capture mAb and streptavidin coated magnetic beads, as shown in Figure 35 (see also 2.6.6).

	Neg.Contrl	C1	C2	C3	C4
c(mAb)	No mAb	40 ng/µL	10 ng/µL	1 ng/µL	0.1 ng/µL

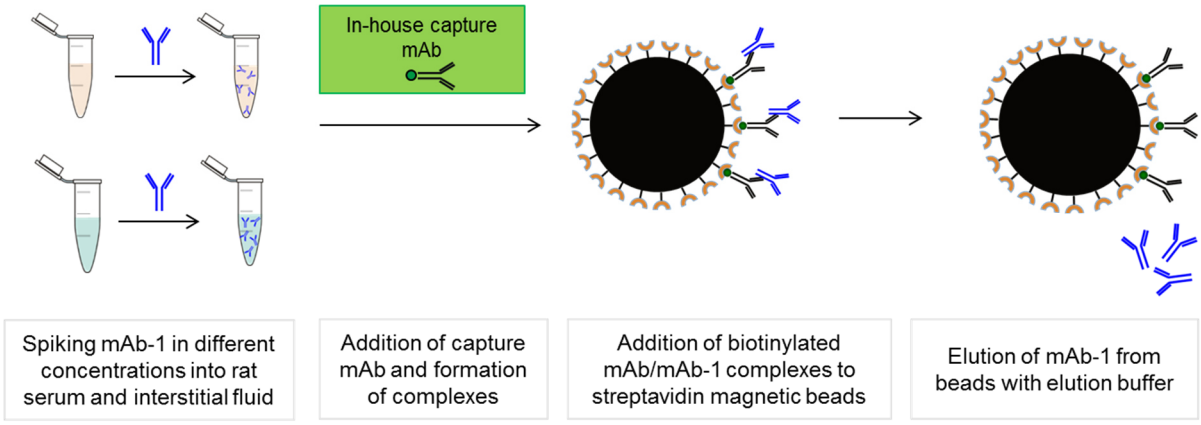

Figure 35 – Streptavidin Magnetic Beads using a biotinylated capture mAb

Different concentrations of mAb-1 were spiked into serum and interstitial fluid. The in-house capture mAb was added to the samples to form complexes. The capture mAb is directed against the Fc-part of human mAbs and therefore binds to mAb-1. The mixture was added to the magnetic beads to collect the complexes via the interaction of streptavidin and the biotinylated capture mAb. The target mAb-1 was eluted by addition of elution buffer.

The in-house capture mAb binds to the Fc-region of human antibodies and thus observation of binding only to the target mAb-1 but not the endogenous mAbs in the rat serum was expected. The approach contained the following workflow: the mixture was added to the streptavidin-coated magnetic beads and the target mAb pulled out of the biological matrix. After four wash steps, mAb-1 was eluted from the beads. As the binding between the capture-mAb and the human target mAb-1 is pH dependent, elution is performed by the addition of a low pH elution buffer.

The different elution fractions were separated undiluted by an SDS-gel and stained using coomassie staining (see 2.6.7.2). For both matrices two bands at 150 kDa were observed. While band 1 showed concentration dependent intensities, the intensity of band 2 remained the same for all concentrations. Furthermore, band 2 was also observed in both negative controls (no mAb serum, and no mAb ISF) where no antibody has been present (Figure 36-A/B). For all serum samples two additional bands at 10 and 15 kDa were detected, which was assumed to be caused by serum-related contamination.

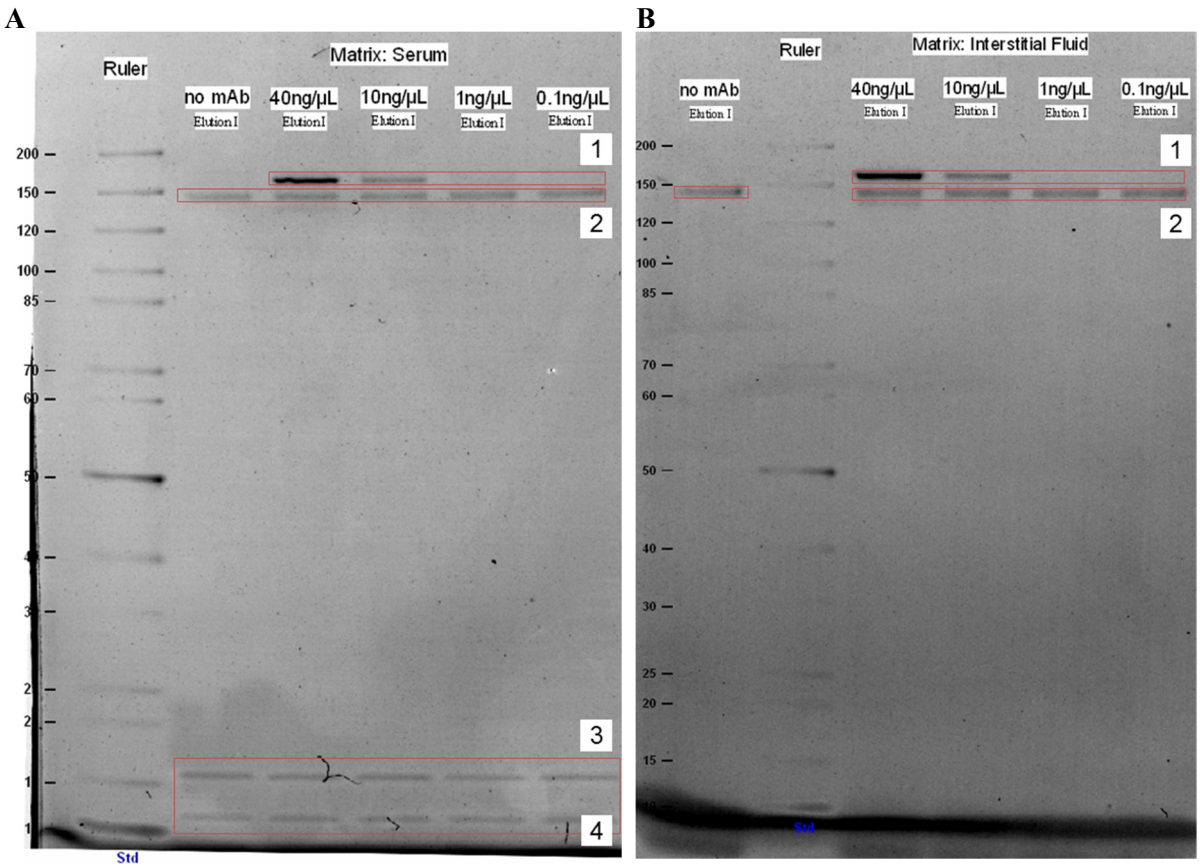

Figure 36 – Results of capture from serum and interstitial fluid

The SDS-gel of the serum (A) and interstitial fluid (B) samples revealed two bands (band 1 and 2) at 150 kDa. Band 2 was suggested to be produced by the capture-mAb as intensity was the same for all tested mAb-1 concentrations, whereas band 1 was assumed to be the target mAb-1. For the serum samples two additional bands at 10 and 15 kDa (bands 3 and 4) were detected. Those are probably contaminations from serum (A).

As the concentration dependence of band 1 was consistent with the expected intensities, this band was assigned to the target mAb-1. In contrast to this, band 2 showed equal intensities for all mAb-1

concentrations and was also present in the negative control without mAb-1. Therefore, band 2 was assumed to be originated by the in-house capture mAb.

In order to prove this assumption, an in-gel digestion was performed. For this, the capture experiment was repeated with sample C1 (40 ng/µL mAb-1 spiked in water) and, therefore, with the highest concentration of mAb-1, in order to obtain enough material. The eluate was loaded ten times onto the gel, and the bands of the different lanes were excised and pooled together. As shown in Figure 37 the band pattern was slightly different, as three instead of two bands were visible.

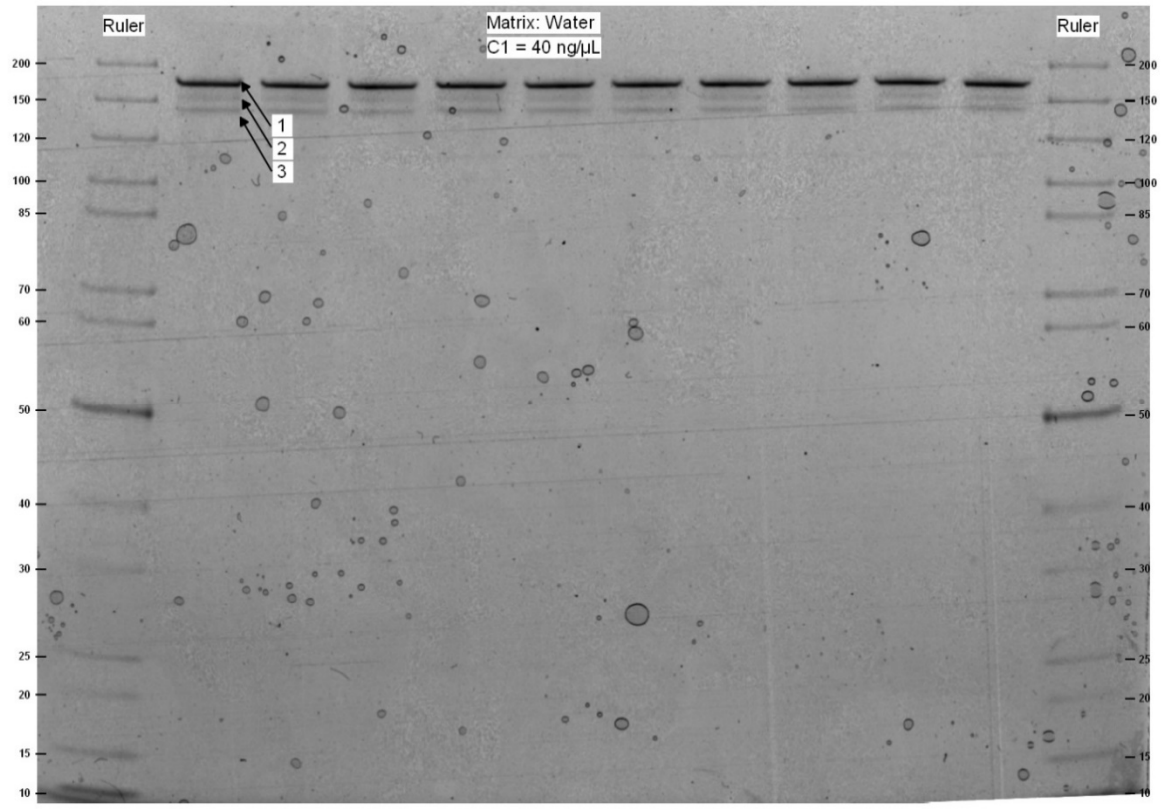

Figure 37 – Gel for in-gel digestion

The eluate of the capture was loaded in ten lanes and showed three bands. Band 1 of each lane was excised and pooled in one tube. The same was done for bands 2 and 3.

The mass spectrometric analysis of the in-gel digested bands 1, 2 and 3 revealed that all three bands were originated by mAb-1, as at least one of the CDR-regions in LC and HC were found. The CDR-regions determine the binding properties, and thus define the specificity of an mAb to bind its target [137]. Therefore, they provide clear evidence that the peptides identified in all three bands belong to mAb-1. Thus, the expectation that the second band shown in Figure 36 was originated by the capture mAb, could not be confirmed. A possible explanation could be that for the second gel used for the in-gel digestion (Figure 37) the capture experiment was repeated and a new capture-mAb lot was used. The capture molecule is biotinylated in house and the biotinylation efficiency is unknown. It was assumed, that the capture mAb lot used in the first approach was not efficiently biotinylated and therefore found also in the control sample.

To investigate this further, the experiment was repeated a third time for the sample C1 using the new capture-mAb lot. This time also a negative control without mAb-1 was included to prove whether a band is visible in the antibody free control sample. As shown in Figure 38, no band is visible in the negative control sample using the new in-house capture-mAb lot. The absence of a band in the control sample strengthens the assumption that the 150 kDa band in the control lane of Figure 35 was likely produced by the old lot of the in-house capture-mAb. Probably, the biotinylation process of the previous charge was not efficient enough, leading to a leaching of the capture-mAb during the elution step of the capture.

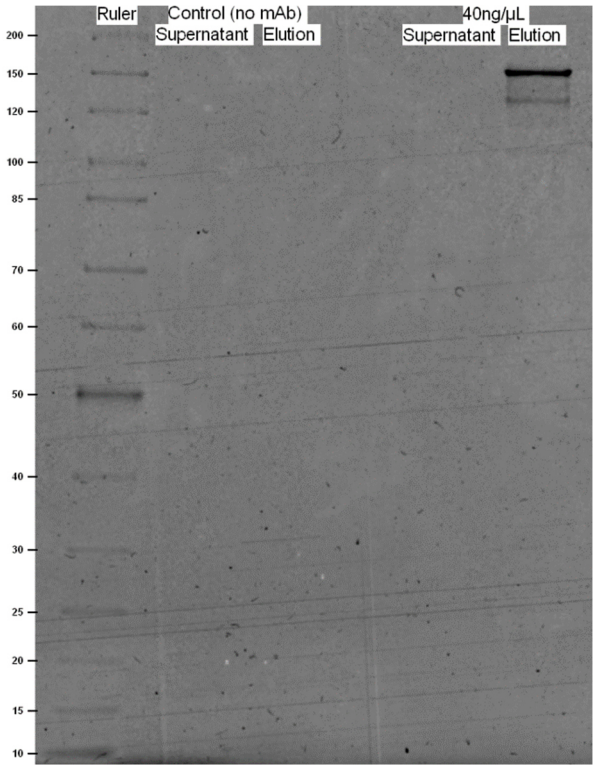

Figure 38 – Repetition using new capture-mAb lot

For the new lot of capture-mAb no band is visible in the negative control. This result is in agreement with the assumption that the previously detected band was probably produced by the leaching of the capture-mAb during elution.

Although band 2 observed in the first experiment (Figure 36-A/B) could be assigned, using the new capture-mAb lot, an unexpected double band pattern was observed as can be seen in Figure 38. Consistent with a recently published study, these bands likely correspond to mAb size heterogeneity due to different states of unfolding during the heat denaturation prior SDS-PAGE [138].

Kirley and co-workers found that the heating conditions critically influence the resulting band pattern in non-reducing SDS-PAGE. After heat denaturation at 50°C they observed four different bands at 150 kDa as shown in Figure 39-A. Band D at highest molecular weight was assigned to the totally unfolded mAb, whereas band C was assigned to partially unfolded mAb with folded C_H3 domain. Band

B was assigned to mAbs containing folded C_H3 domain and one folded Fab region and band A only contained unfolded C_H2 domain.

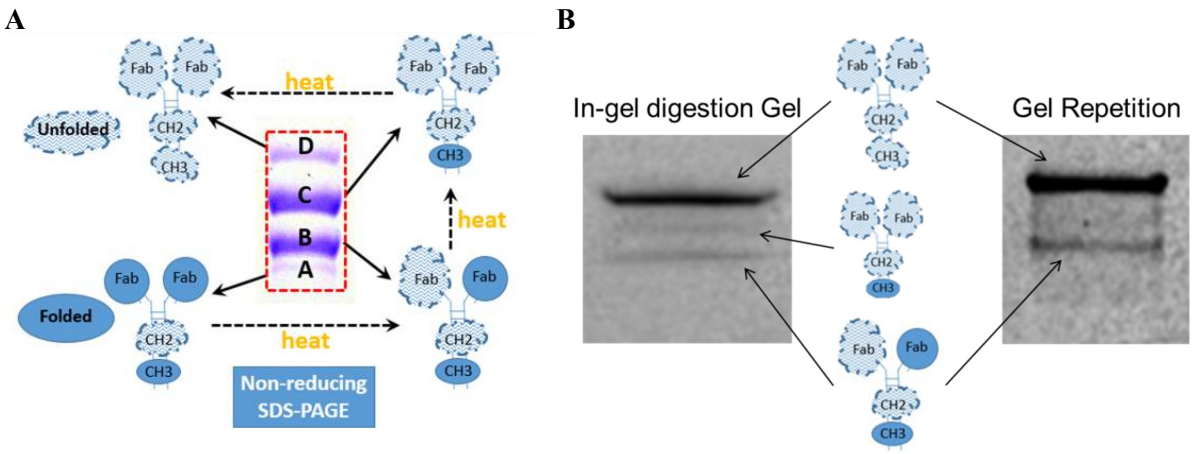

Figure 39 – Band Assignment

A) Domain unfolding of mAbs during heat denaturation prior SDS-PAGE [139] (copied with permission from Kirley et al.) B) Based on the results from Kirely et al. the bands observed after the capture using the new lot of capture mAb were assigned to the fully unfolded mAb-1, mAb-1 containing folded C_H3 domain, and mAb-1 containing folded Fab and C_H3 domain, respectively.

As described in 2.6.7 mAb-1 was heat denatured for 10 min at 70°C prior SDS-PAGE. Based on the recent findings of Kirley *et al.* the denaturation step is assumed to produce partially unfolded mAbs and therefore three bands in the SDS-PAGE. The most intense band is expected to be the totally unfolded mAb (see Figure 39-B), whereas the second band is probably the mAb containing folded C_H3 domain. The lowest band could be the partially unfolded mAb-1 containing folded Fab and C_H3 domain.
However, as the SDS-PAGE in this workflow is only the proof of a successful capture process, a clear assignment of the individual bands to the different states of unfolded mAb-1 was not required.
Overall, the results show that using the new capture-mAb lot a successful capture without contamination of the capture mAb was achieved. However, taking into account that a lot-to-lot variability was observed, also alternative molecules were tested.

3.1.3 Streptavidin Magnetic Beads using CaptureSelect™

In the next step a commercially available biotinylated capture molecule CaptureSelect™ Biotin Anti-IgG-Fc (Hu) Conjugate 13 kDa Llama antibody fragment was tested. Similar to the previously described in-house capture-mAb, CaptureSelect™ binds specifically to the Fc part (C_H3 domain) of all four human IgG subclasses. The basic workflow (Figure 40) is identical to the previously described protocol using the in-house capture mAb.

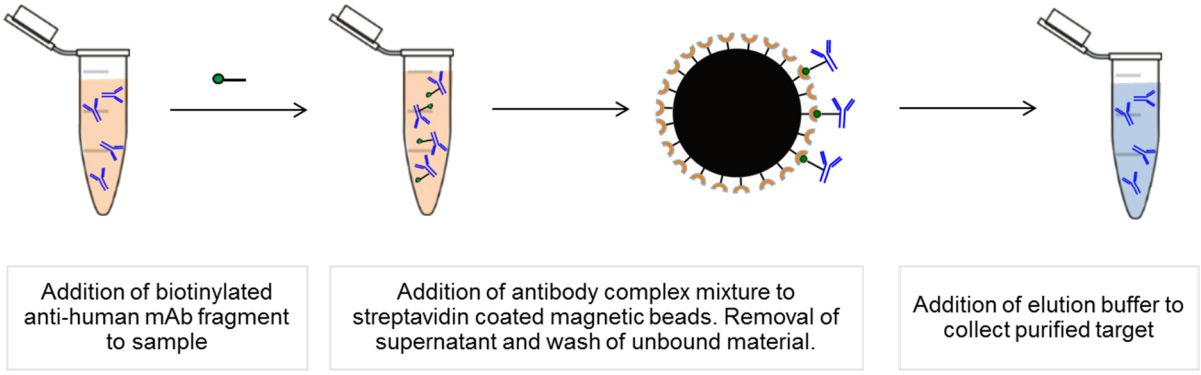

Figure 40 – Capture process using CaptureSelect™ and streptavidin coated magnetic beads

The commercial available molecule CaptureSelect™ binds to the Fc part of mAb-1, forms complexes and is then added to streptavidin coated magnetic beads. After four wash steps mAb-1 is eluted by the addition of a low pH elution buffer.

As shown in Figure 41, the reference material NISTmAb was spiked into pig serum and into water with final concentrations of 10 ng/µL. To investigate the capture efficiency of the commercial capture mAb fragment and the in-house capture mAb, six replicates of NISTmAb in serum and six replicates of NISTmAb in water, were captured using both capture molecules. After the capture process, 500 ng of the stable isotope labeled antibody SilumAb was spiked into every sample

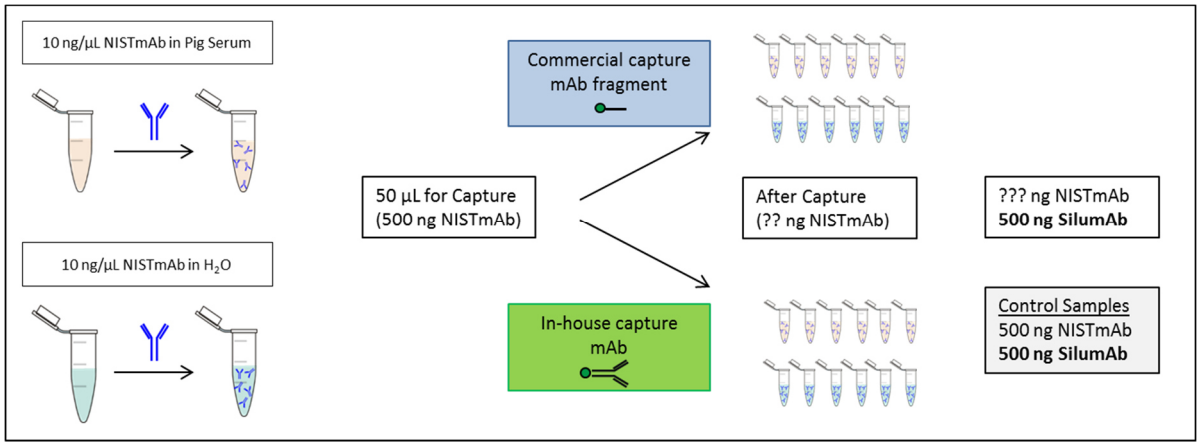

Figure 41 – Determination of capture efficiency for both capture molecules

The NISTmAb was spiked in pig serum and water with a final concentration of 10 ng/µL. Six replicates of each sample type were captured using the commercial capture mAb fragment and the in-house capture mAb. After the capture 500 ng of stable isotope labeled SilumAb were spiked in to determine the capture efficiency. In addition, six control samples containing 500 ng NISTmAb and 500 ng SilumAb without capture were prepared.

The SilumAb molecule contains heavy labeled arginine (R), $^{13}C_6$ $^{15}N_4$ leading to a mass shift of +10.008 Da, and heavy labeled lysine (K) $^{13}C_6$ $^{15}N_2$ leading to a mass shift + 8.014 Da. Also 6 control samples containing 500 ng NISTmAb and 500 ng SilumAb were prepared.

NISTmAb and SilumAb share two identical peptides FNWYVDGVEVHNAK and VVSVLTVLHQDWLNGK. The heavy labeled SilumAb peptides elute at the same retention time as its non-labeled NISTmAb counterparts as they are chemically identical. Furthermore, they show same

ionization efficiencies and can therefore be used for quantification of the captured amount of NISTmAb due to the known amount of SilumAb in all samples.

As shown in Figure 42, FNWYVDGVEVHNAK elutes at 54 minutes and gives rise to the triply charged NISTmAb peptide m/z 559.939 and the heavy SilumAb peptide m/z 562.610. Both peptides are present at a relative abundance of 100% in the control sample, showing that the quantification strategy is valid.

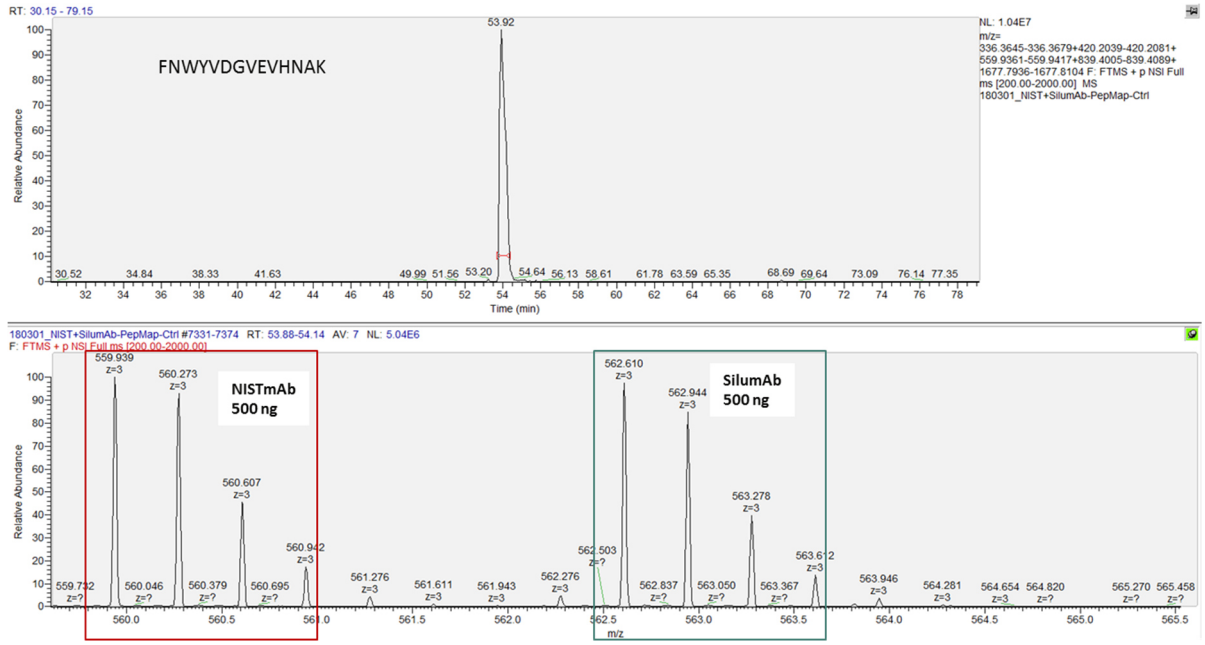

Figure 42 – Extracted ion chromatogram of FNWYVDGVEVHNAK of one control sample

The quantification peptide FNWYVDGVEVHNAK elutes at 54 minutes and shows equal relative abundances for NISTmAb and SilumAb in the control sample.

The six control samples containing equal amounts of both mAbs showed a capture efficiency of 104.5 ± 5.4% (Figure 43-A). In addition, two negative controls were included, to see whether any nonspecific molecules are captured. For this, blank water and blank pig serum without NISTmAb were subjected to the capture procedure using both capture molecules. All four negative controls revealed no nonspecific binding of the capture molecules, as no peptides were found for those samples. For the NISTmAb in water and NISTmAb in serum samples, the commercial capture molecule provided capture efficiencies of 95.7% ± 3.0% and 103.4 ± 6.7%, respectively. The in-house capture mAb showed lower capture efficiencies of 36.3% ± 5.6% and 1.3% ± 1.6%, respectively (Figure 43-A).

A

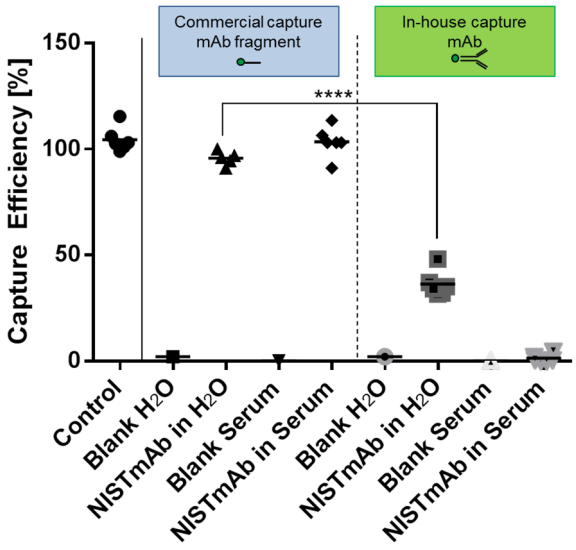

B

Unpaired t-test – "NISTmAb in H_2O" CaptureSelect™ vs. In-house mAb	
P value	< 0,0001
P value summary	****
(P < 0.05)	Yes
One- or two-tailed P value?	Two-tailed
t, df	t=19.43 df=9
Mean ± SEM (CaptureSelect)	95.7 ± 1.5, n=5
Mean ± SEM (in-house mAb)	36.3 ± 2.5, n=6
Difference between means	-59. 5 ± 3.1
95% confidence interval	-66.4 to -52.5
R squared	0.9767
F,DFn, Dfd	3.395, 5, 4
P value	0.2598
P value summary	ns
(P < 0.05)	No

Figure 43 – Capture efficiency

A) The control samples show capture efficiencies of 104.5 ± 5.4%, whereas the blank H_2O and blank serum samples where both negative for the two capture molecules. The commercial capture fragment showed much higher capture efficiencies for both sample types, compared to the in-house capture mAb. B) Statistical comparison of the NISTmAb in H_2O revealed a significant difference between the efficiency of CaptureSelect™ and the in-house capture mAb. With a p-value of 0.0001 the commercial capture fragment is significantly more efficient.

For statistical comparison of the NISTmAb in water sample captured with both molecules, a two-tailed t-test was performed. A confidence interval of 95% was chosen and therefore statistical significance defined to be $p < 0.05$. The commercial capture molecule showed a significantly higher efficiency than the in-house mAb (p-value < 0.0001) as shown in Figure 43-B. Furthermore, an F-test was performed to compare variances of the two sample sets. With a p-value of 0.2598 the variances are found to be not significantly different, which is a prerequisite for the application of the t-test.

Over the last years, a lot of work has been done on the analysis of *in-vivo* samples including immune-purification steps. However, the capture efficiency of those protocols is most of the time unknown and, therefore, a contamination by endogenous mAbs that could interfere with the analysis cannot be ruled out. [51, 131, 140]

The capture efficiencies of 95.0 – 100% achieved with CaptureSelect™, are much higher than expected. Furthermore, they are superior to the recovery rate of ~70% for a mAb drug captured from serum reported by Liu *et al.* [141].

Based on these results, the commercial capture mAb fragment, CaptureSelect™, was chosen as capture molecule for all future experiments.

3.1.4 Capture efficiency using two different types of magnetic beads

After selection of the capture molecule, a different type of magnetic beads was tested and compared to the previously used Pierce™Beads. The new Sera-Mag™ SpeedBeads offer a double magnetic layer, which could enable faster capture and improved efficiencies.

For this, the NISTmAb was spiked into pig serum or water to a final concentration of 10 ng/µL, as described previously (3.1.3). CaptureSelect™ was used as a capture molecule and three samples of each sample type were subjected to the capture procedure using either the standard Pierce™Beads or the new Sera-Mag™ SpeedBeads. For quantification 500 ng SilumAb were spiked into the samples after the capture. Furthermore, three control samples containing 500 ng NISTmAb and 500 ng SilumAb were prepared without subjecting them to the capture procedure (see Figure 44).

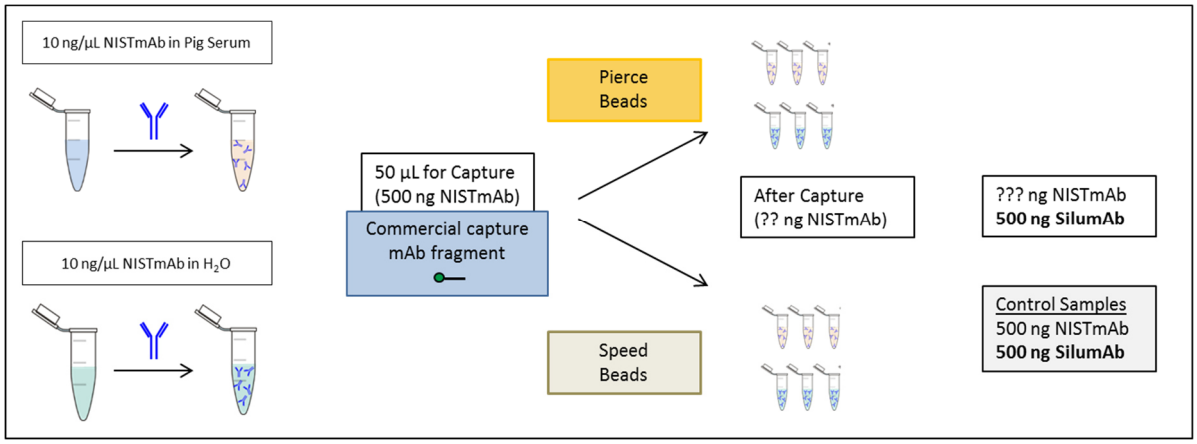

Figure 44 – Determination of capture efficiency of two types of magnetic beads

A) The NISTmAb was spiked in pig serum and water with a final concentration of 10 ng/µL. Three replicates of each sample type were captured using the previously used Pierce™Beads and the new SpeedBeads. After the capture 500 ng of stable isotope labeled SilumAb were spiked in to determine the capture efficiency. In addition, three control samples containing 500 ng NISTmAb and 500 ng SilumAb without capture were prepared.

The Pierce™Beads showed high capture efficiencies for both the NISTmAb in H_2O and the NISTmAb in serum samples (96.5 ± 1.3% and 99.0 ± 1.0%, respectively) and by this verified the previously obtained results. For the Sera-Mag™ SpeedBeads, also high efficiencies of 92.9 ± 3.5% and 95.7 ± 8.4% were achieved for NISTmAb in H_2O and the NISTmAb in serum (see Figure 45).

Based on these results it can be concluded that the Sera-Mag™ SpeedBeads did not lead to a further improvement of the capture efficiency. Furthermore, the initial hypothesis of a faster capture using the new beads due to the double magnetite layer, could not be confirmed.

However, the high capture efficiencies achieved with the Pierce™Beads and the commercial capture molecule CaptureSelect™ are very reproducible. Furthermore, the results obtained by the developed capture protocol are highly superior to the results published in literature, as mentioned previously [51, 131, 140, 141].

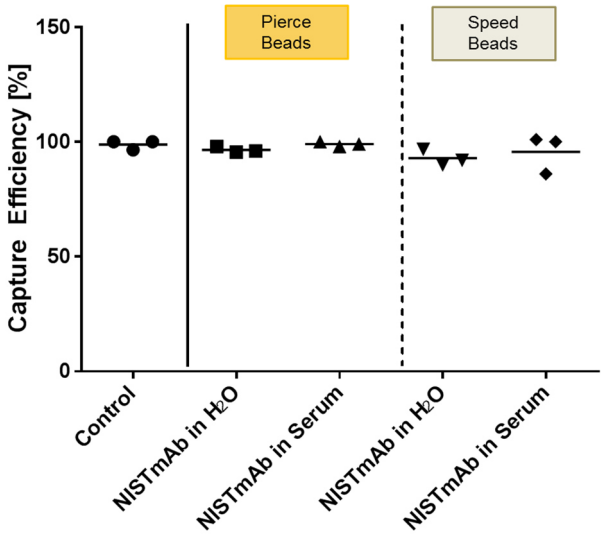

Figure 45 – Capture efficiency of two types of magnetic beads

The capture efficiency for the control samples was 98.8 ± 2.0%. Both types of magnetic beads revealed very high sequence coverages.

Therefore, the commercial capture mAb fragment CaptureSelect™ and the Pierce™Beads were selected for future experiments (see Figure 46 for the final capture protocol)

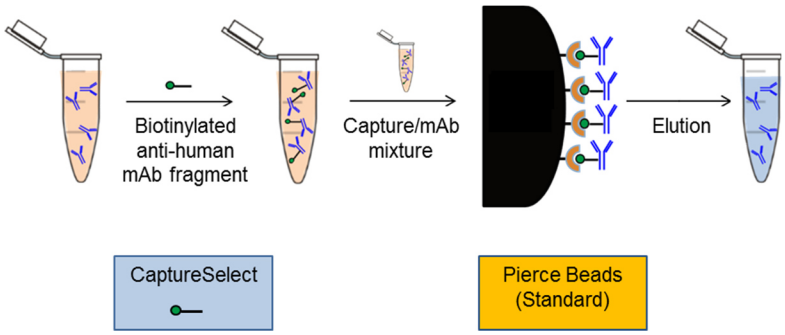

Figure 46 – Final capture protocol

As the SpeedBeads did not show an improved efficiency, the standard Pierce™Beads were selected. Therefore, the final protocol uses CaptureSelect™ and Pierce™Beads.

3.1.5 Determination of the linear range of the final capture protocol

After successful optimization of the capture procedure, the linear range of the final protocol was determined. Ten different NISTmAb samples in water were prepared, with concentrations ranging from 0.1 ng/µL to 0.1 µg/µL. Then, the NISTmAb was captured using the final protocol and SilumAb was spiked in for antibody quantification. The captured versus total amount of NISTmAb is plotted in Figure 47-A. The tested concentration range reveals a very good correlation with a correlation coefficient of 0.9988.

Li and co-workers used a CaptureSelect™ affinity reagent to purify a human mAb from monkey serum [97]. They determined the linearity of their parallel reaction monitoring quantitation coupled to affinity purification to be 0.9950, which is consisted with the results presented in Figure 47-A.

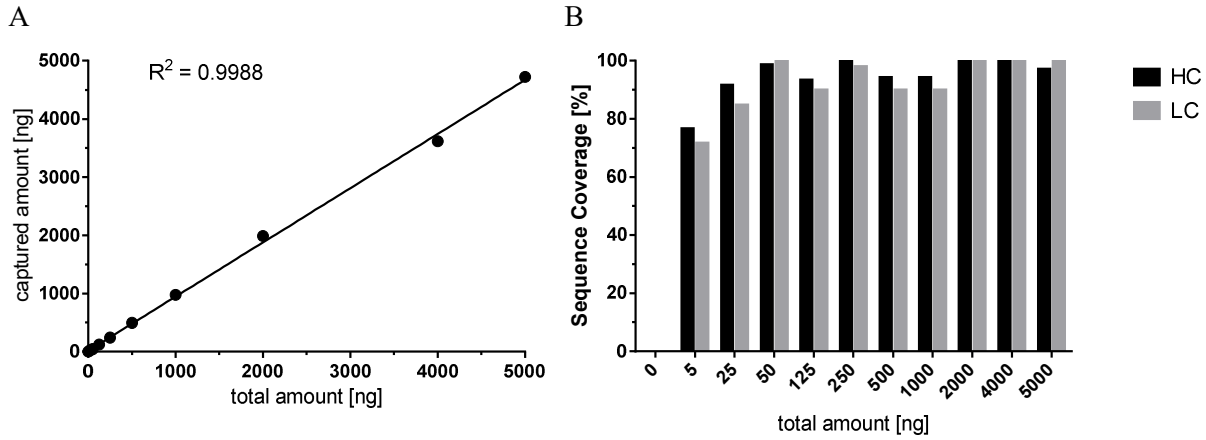

Figure 47 – Linear range and sequence coverage

A) Determination of the linear range revealed a high correlation between captured versus total amount of NISTmAb. The final protocol shows a good linearity with a correlation coefficient of R2 = 0.9988. B) For all tested concentrations high sequence coverages were achieved. Already for the lowest tested amount of 5 ng sequence coverages of more than 70% were observed.

As can be seen in Figure 47-B, even for the lowest tested antibody amounts (i.e. 5 ng), sequence coverages of 76.4 and 71.4% for HC and LC were achieved. For absolute amounts greater than 50 ng very high sequence coverages could be achieved. This indicates that the before mentioned workflow is perfectly applicable for the tested concentration range.

3.1.6 Testing whether the capture protocol is unbiased

As final step of the development of the capture protocol, a stress study was conducted to demonstrate feasibility to capture also modified antibodies. Based on the results obtained in 3.1.3 and 3.1.4 that revealed equal capture efficiency for the NISTmAb in water and NISTmAb in serum samples, water was chosen as incubation medium for the stress study. The use of water instead of serum has the advantage that the capture step is not required, and thus the sample could be digested directly. To investigate the existence of a capture protocol bias, a comparison between stressed sample with and without capture can be made to see whether the same types of modifications are found.

Thus, the NISTmAb was spiked in water with final concentrations of 10 ng/µL and stressed for 5 days at 50°C at 550 rpm. Six replicates of the stressed material were captured using the optimized capture protocol (Stress-Capture). Six further replicates of the stressed material were digested without prior capture procedure to see whether the same amount of modifications is found (Stress-NoCapture). In

addition to the stressed samples, six control samples were prepared freshly before the peptide map (Control). 500 ng SilumAb was spiked into every sample group and afterwards the peptide map using the optimized workflow was performed with all samples (See Figure 48).

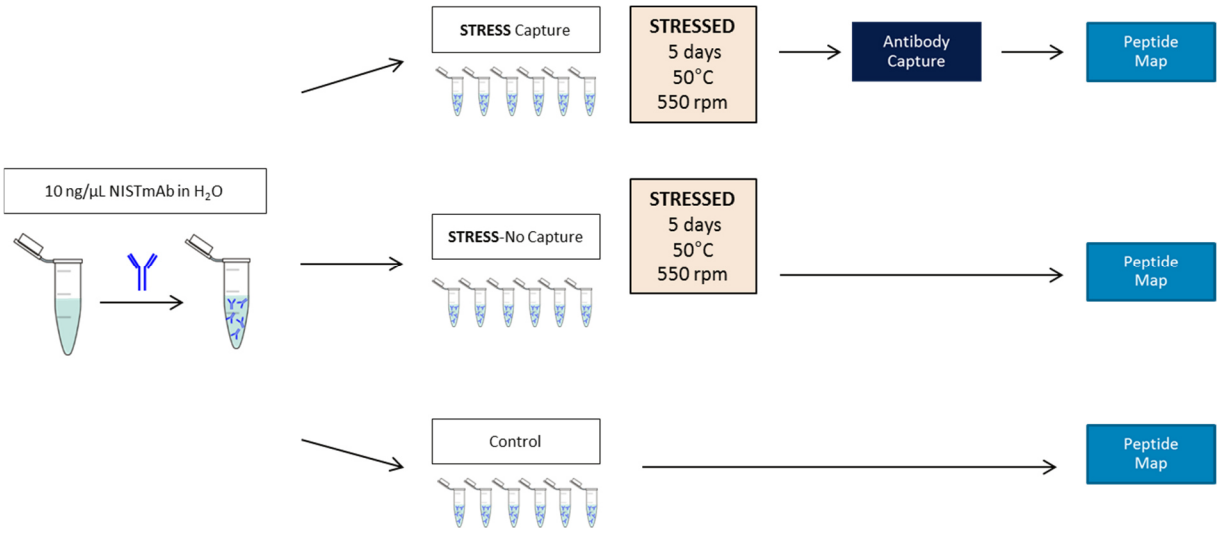

Figure 48 – Stress study to show unbiasedness

The NISTmAb was spiked into water to a final concentration of 10 ng/µL and stressed for 5 days at 50°C and 550 rpm. Six stressed samples were captured and digested, whereas six further samples were only digested. Furthermore, six control samples were prepared freshly and digested directly without being stressed or captured.

The sequence coverage was very high for all sample types as shown in Figure 49-B. For the control samples the capture efficiency was determined to be 104.8% ± 7.8%. Reduced capture efficiencies of 83.6 ± 4.5% and 85.0 ± 3.8% were observed for the stressed samples without and with capture, respectively (See Figure 49-A).

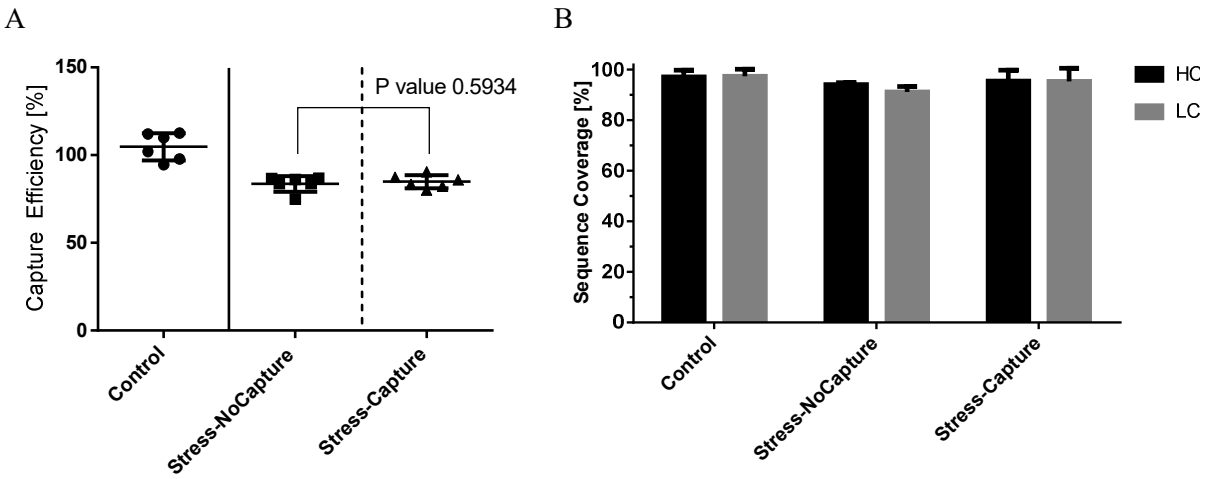

Figure 49 – Capture efficiency and sequence coverage of stressed samples

A) For stressed samples the capture efficiency was reduced compared to the control samples. However, no significant differences for captured and non-captured samples was observed (p = 0.593). B) The sequence coverages were equally high for all tested sample types.

A two tailed t-test of the capture efficiency of Stress-NoCapture and StressCapture was performed showing a p-value of 0.5934. With a confidence interval of 95% and a level of significance of 0.05, the test revealed, that the two sample types show statistically no significant difference.

The lower capture efficiency of the stressed samples can be explained by the fact that quantification is based on the comparison of the absolute amount of unmodified NISTmAb to SilumAb peptide. For the stressed samples the amount of native peptides is reduced, as the incubation at 50°C for 5 days and 550 rpm led to the introduction of modifications. As can be seen from Figure 50, the stressed samples (Stress-NoCapture und Stress-Capture) showed reduced amounts of the native peptides that are used for quantification.

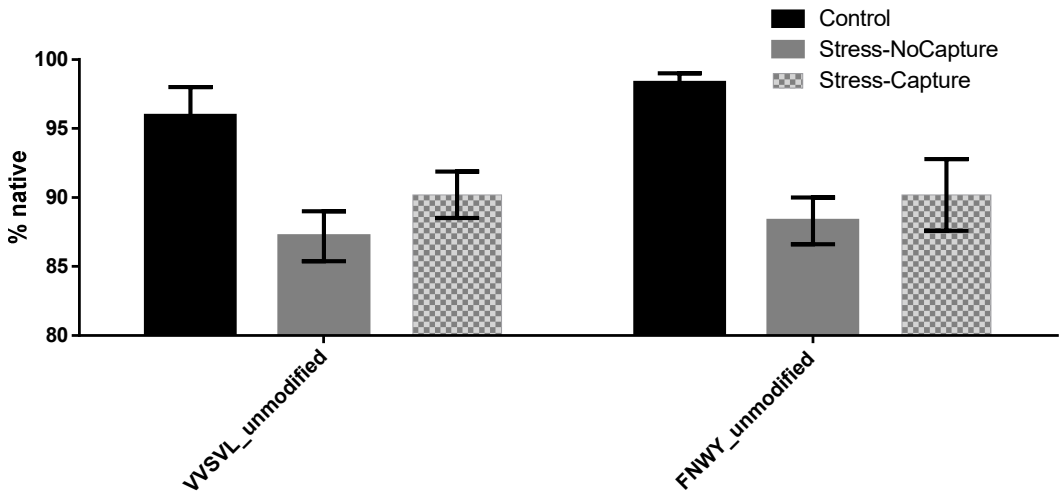

Figure 50 – Relative amount of native quantification peptides

The amount of native, unmodified quantification peptides in the control samples is around 95 – 98%. For both stressed sample types, the amount of native VVSL and FNWY peptides is reduced to 85 – 90%.

Interestingly, the extracted ion chromatogram of the FNWY-peptide resulted in a double peak for all stressed samples as shown in Figure 51-A. The relative abundance of the triply charged NISTmAb peptide (m/z 559.939) was approximately 90% for the main peak, while the SilumAb peptide (m/z 562.610) was 100%. In contrast to this, the pre-peak only contains the NISTmAb peptide (Figure 51-B).

As shown in Figure 51-C, the MS2 spectra of the m/z 559.939 from pre- and main-peak resulted in the same fragment pattern, indicating that the double peak is a result of NISTmAb peptide isomerization.

Based on the amino acid sequence of the peptide FNWYV**D**GVEVHNAK the formation of iso-D was found to be the only possible explanation for a second peak with exactly the same m/z and fragment spectrum pattern.

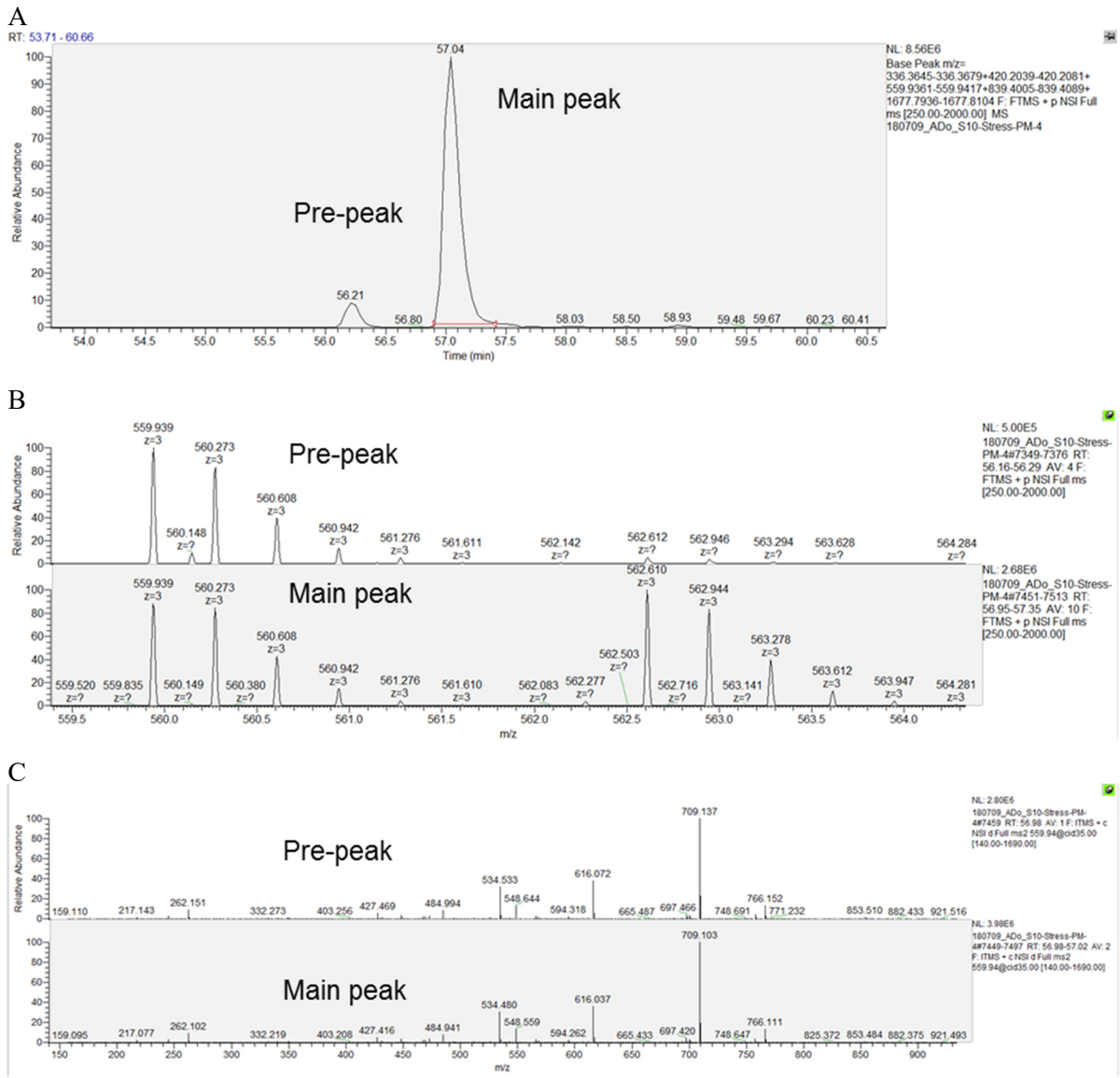

Figure 51 – Double peak observation in stressed samples

A) For the stressed samples a double peak was observed in the extracted ion chromatogram of the FNWY-quantification peptide. B) The main peak contained the unmodified FNWY-peptide of NISTmAb and SilumAb with relative abundances of 90% and 100%, respectively. In the pre-peak only the m/z of the NISTmAb peptide was found. C) The MS2 spectra of m/z 559.939 result in exactly the same fragment pattern for pre- and main peak. Thus, the peptide observed in the pre- and main peak are stereo-isomers.

In Figure 52 the chemical structure of the peptide is drawn. There are three positions that can result in the formation of a succinimide intermediate. However, in case of the two asparagines a deamidation would lead to a loss of -17 Da and subsequent hydrolysis to the addition of +18 Da. The final iso-D peptide would therefore show a mass shift of +1 Da. As the observed double peak has the exact same mass, the formation of the iso-D is a result of dehydration [-18 Da] of the aspartic acid, followed by hydrolysis [+18 Da].

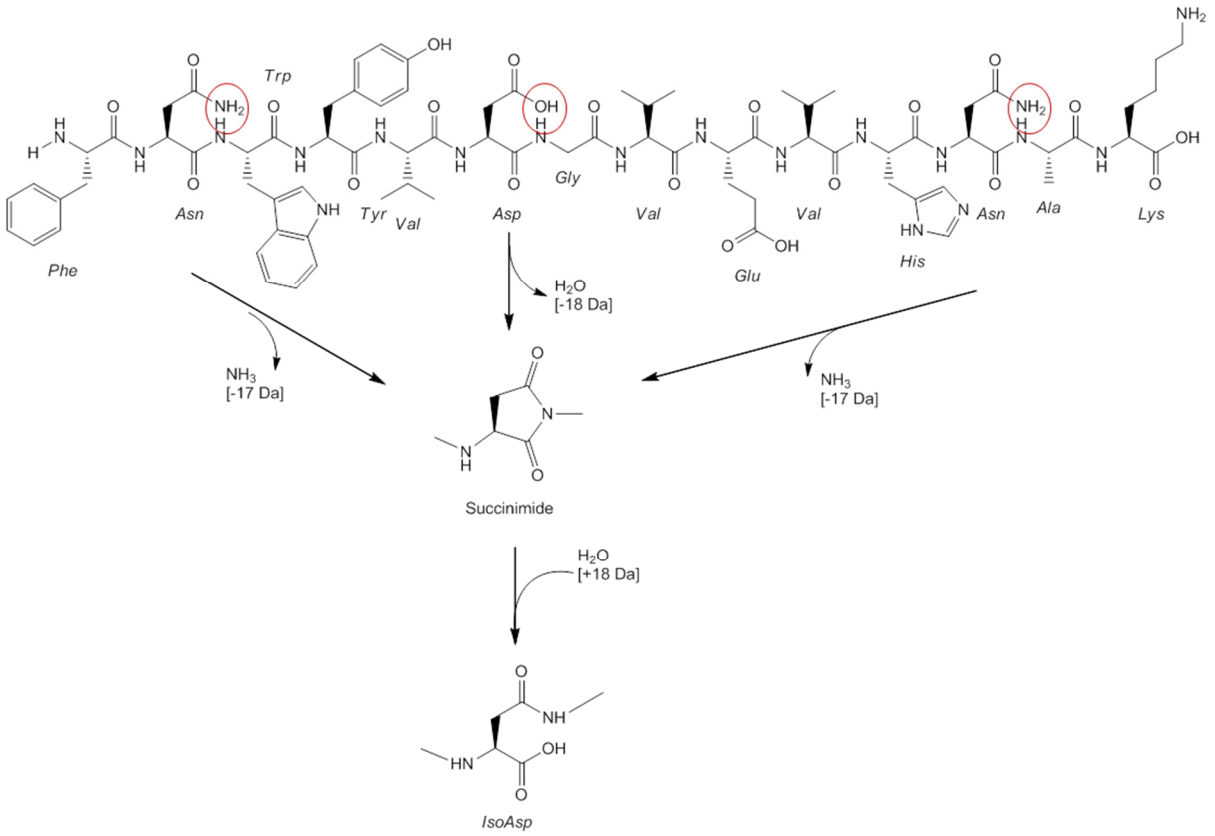

Figure 52 – Formation of isoAsp in FNWYVDGVEVHNAK

Isomerization of the aspartate residue leads to the loss of water and the formation of the succinimide intermediate. Subsequent hydrolysis reaction leads to the formation of the isoAsp residue, and therefore the formation of the stereoisomer.

Therefore, it can be concluded that the stress conditions led to the formation of iso-Asp in the FNWYVD**G**VEVHNAK-peptide. This finding is consistent with reported studies on isomerization rates, where the formation of iso-Asp was reported to be increased and favored, when the C-terminal amino acid is a glycine or serine (DG-motif) [81, 87, 142].

For the detailed analysis of peptide modifications three of six samples from the Stress-Capture setup were excluded, as significant spray issues were observed for those samples. Therefore, six control samples were compared to six Stress-NoCapture and three StressCapture samples. In case of the six Stress-NoCapture samples, replicate 5 showed increased oxidation values compared to the other replicates and was assumed to be an outlier. To proof this, the so called ROUT method was applied, which combines robust non-linear regression and the removal of outliers. It is based on the false discovery rate (FDR) and specified by the maximum desired FDR value Q. For statistical identification of outliers a Q-value of 1% was chosen, meaning that 99% of the identified outliers are actual outliers. [143]

In summary, three outliers were removed for the later analysis which came all from the same sample. The values of replicate sample 5 were identified as statistic outlier for M255, M32 and W384 but not for M87 and M431.

In Figure 53 all replicates of the differently modified peptides of the Stress-NoCapture setup were plotted. Statistically identified outliers are marked with red circles and were excluded from subsequent t-test analysis.

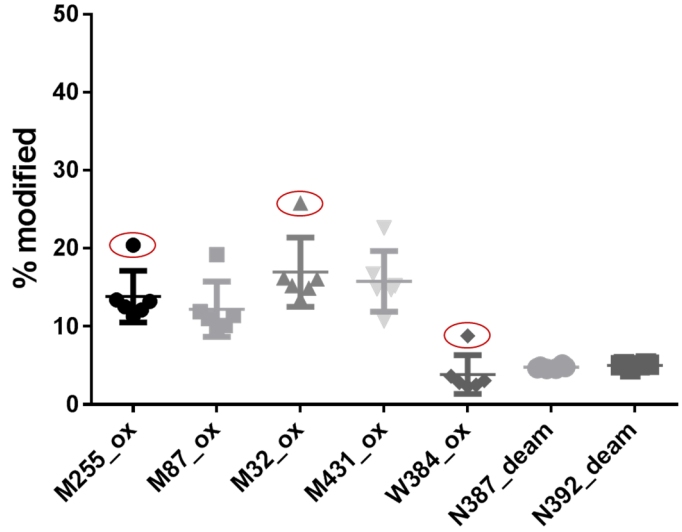

Figure 53 – Modified peptides of the Stress-NoCapture setup

Statistical analysis using the ROUT method identified three data points as outliers in the replicate 5 of the setup Stress-NoCapture. Identified outliers are marked with red circles and were excluded from subsequent analyses.

As can be seen from Figure 54 the level of methionine oxidation for the M255 in the DTLMISR peptide increased from 6.1 ± 0.8 in the control, to 12.5 ± 0.9 and 12.3 ± 1.9 for the Stress-NoCapture and Stress-Capture samples, respectively.

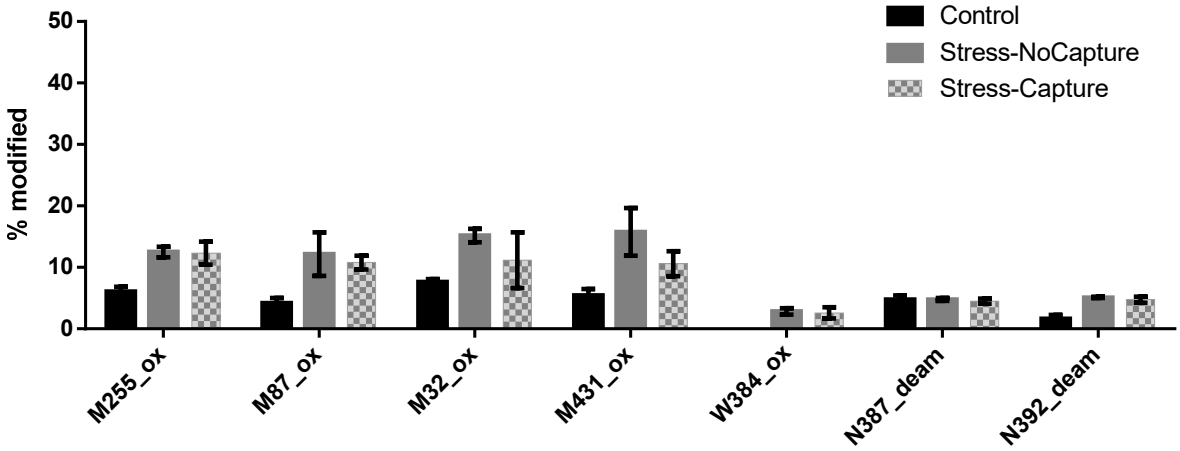

Figure 54 – Comparison of modification levels in differently treated samples

The oxidation values for M255 and M87 increased for the stressed samples compared to the control samples. However, no difference between the captured (StressCapture) and non-captured (Stress-NoCapture) were observed. Also deamidation rates at N387 and N392 were not different before and after capture. For captured and non-captured samples the modification levels were analyzed using an unpaired t-test and found to be not statistically different, demonstrating that the workflow is unbiased.

Also, an increase in N387 deamidation in the PENNYK-peptide was observed for the stressed samples. However, the values are not different for the Stress-NoCapture and StressCapture sample, with 4.8 ± 0.2 and 4.5 ± 0.4, respectively.

For all peptides shown in Figure 54 an unpaired t-test between the Stress-Capture and the Stress-NoCapture samples was performed. The results summarized in Table 6 did not found a statistical significant difference between the two tested sample groups, which clearly demonstrates that the capture workflow is unbiased.

Table 6 – Statistical analysis using an unpaired t-test

	Unpaired t-test (two-tailed)						F-test	
Peptide	P value	t, df	Mean ± SEM		95% confidence interval	R squared	F, DFn, Dfd	P value
			Stress-Capture	Stress-NoCapture				
M255_ox	0.8381	t=0.2134 df=6	12.5 ± 0.4, n=5	12.3 ± 1.1, n=3	-2.5 to 2.1	0.007534	4.814, 2, 4	0.1723
M87_ox	0.5411	t=0.6424 df=7	12.2 ± 1.4, n=6	10.8 ± 0.7, n=3	-6.5 to 3.7	0.05566	9.657, 5, 2	0.193
M32_ox	0.0955	t=1.976 df=6	15.2 ± 0.5, n=5	11.2 ± 2.6, n=3	-9.0 to 1.0	0.3942	17.29, 2, 4	0.0215*
M431_ox	0.072	t=2.118 df=7	15. 8 ± 1.6, n=6	10.6 ± 1.2, n=3	-11.0 to 0.6	0.3905	3.671, 5, 2	0.4556
W384_ox	0.6285	t=0.5096 df=6	2.9 ± 0.2, n=5	2.6 ± 0.5, n=3	-1.5 to 0.9	0.04149	2.902, 2, 4	0.3329
N387_deam	0.1282	t=1.725 df=7	4.8 ± 0.09, n=6	4.4 ± 0.3, n=3	-0.9 to 0.1	0.2983	5.108, 2, 5	0.1238
N392_deam	0.3245	t=1.060 df=7	5.0 ± 0.1, n=6	4.8 ± 0.3, n=3	-0.8 to 0.3	0.1382	3.430, 2, 5	0.2308

Only for peptide M32_ox the comparison of variances in the F-test revealed a statistical significant difference, with p = 0.0215. This result indicates that the variances between the two sample groups (Stress-Capture and Stress-NoCapture) are statistically different, which can also be seen in Figure 54. However, the unpaired t-test assumes that variances are the same for the two sample groups, which is not the case for M32_ox. This discrepancy in the result could arise from the fact that for the Stress-Capture setup, only three samples could be analyzed due to the spray issues. Furthermore, M32 is located in the Fab region as shown in Figure 55 and thus, relatively far away from the site of binding between the capture molecule and the NISTmAb. Thus, an increased oxidation at this residue unlikely contributes to reduced capture efficiency, and is therefore of minor interest. Interestingly however, for all other tested peptides same variances were observed and the differences between modifications found to be non-significant.

Special focus was given to the DTLMISR peptide as it is located in the C_H2 domain of the Fc region where the binding occurs (see Figure 55). Therefore, modification of the M255 in the DTLMISR peptide might influence the binding to the CaptureSelect™ molecule and with this, impairs capture efficiency. However, as can be seen in Table 6, the values for methionine oxidation at position 255 are statistically not different. Thus, the same amount of oxidized M255 is found for the stressed samples with and without capture.

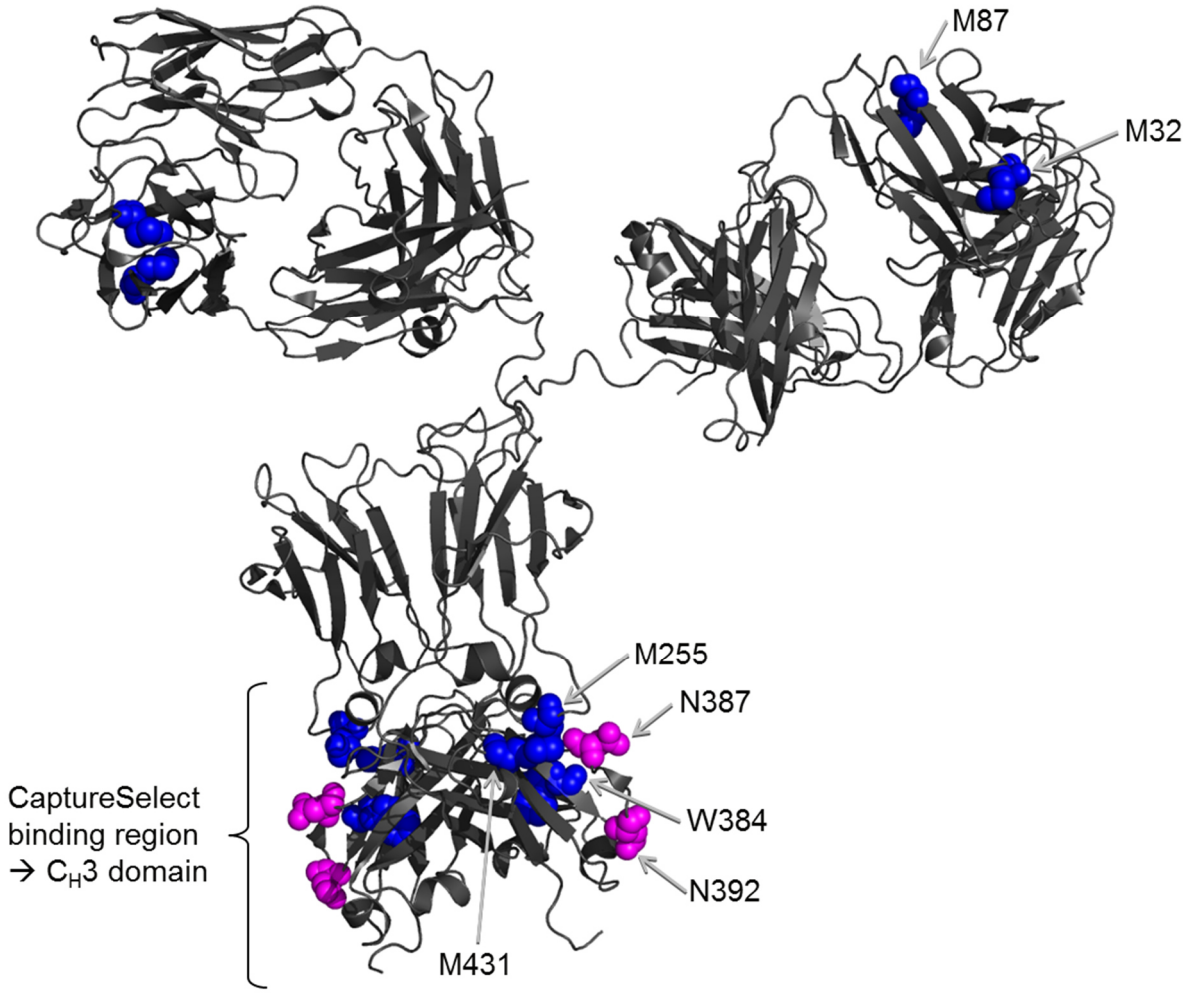

Figure 55 – Location of modified amino acids in the 3D structure of the mAb

The location of the modified residues is indicated by arrows on one HC and one LC. Oxidized residues are shown in blue, deamidated residues are displayed in magenta. M32 and M87 are located in the Fab region of the mAb, whereas M255, W387, M431, N387 and N392 are located in the Fc-region. The CaptureSelect binds in the C_H3 domain of the mAb.

Thus, given the data obtained in this study the capture workflow is unbiased and also able to capture stressed and modified antibodies.

3.2 Development of an optimized peptide map protocol for low sample amounts

In order to localize the sites of particular modifications, it is a common approach to apply enzymatic digestion followed by LC-MS analysis (peptide mapping). This peptide map procedure is routinely performed using several hundred nanogram mAb for digestion. However, due to the low concentration of the target antibody in the *in-vivo* samples, development of an optimized sample preparation workflow was required. The first steps of the peptide mapping procedure include antibody denaturation and alkylation, followed by the enzymatic digestion. However, the removal of denaturation and alkylation agents by a desalting step prior digestion significantly increases the activity of the enzyme [40]. Thus, the particular focus was given to the desalting step due to its importance for the efficiency of further trypsin digestion step (Figure 56).

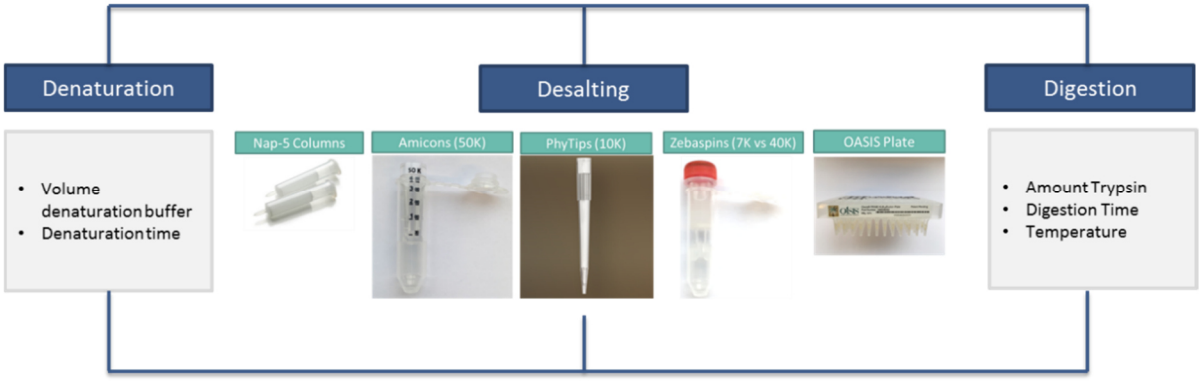

Figure 56 – Overview of the tested desalting procedures

Several desalting techniques were tested in order to find optimal conditions to allow an efficient tryptic digestion. NAP™-5 columns, Amicons®, PhyTips, and Zebaspin columns in combination with the Oasis µElution plate were investigated.

Therefore, in the following section different desalting techniques were investigated starting with the default used NAP™ columns. In the second experiment Amicon® centrifugal filters and in the third approach PhyTip gel filtration columns were tested. Lastly, a design of experiment setup was chosen to test and optimize the combination of Zebaspin desalting columns and Oasis Prime µelution plate.

3.2.1 Desalting using the NAP™-5 columns

NAP™ gelfiltration columns are prepacked with Sephadex® G-25 DNA grade and commonly used for desalting and buffer exchange in protein and peptide purification [144-147]. Thus, in a first approach, it was investigated whether the columns are suitable for the low sample amount of only 1 µg mAb. For this, a 10 ng/µL NISTmAb sample was prepared and 100 µL of this solution was used per sample. The antibody was denatured and reduced in the presence of 100 µL 8 M Gua-HCl, 400 mM tris solution and

1.5 µL 1 M DTT for 1 h at 37°C. Then 5 µL 600 mM IAA was added and incubated for 15 min at room temperature in the dark. The reaction was stopped by adding 1.5 µL 1 M DTT. Afterwards the samples were desalted using the NAP^{TM}-5 columns as described by manufacturer's protocol. For digestion 0.1 µg Trypsin/Lys-C-Mix was added to each sample and incubated for 4 h at 37°C at 550 rpm. The reaction was stopped by adding 2 µL of 10% formic acid.

As can be seen from Figure 57 one dominant peak was detected in every NAP^{TM}-5 sample.

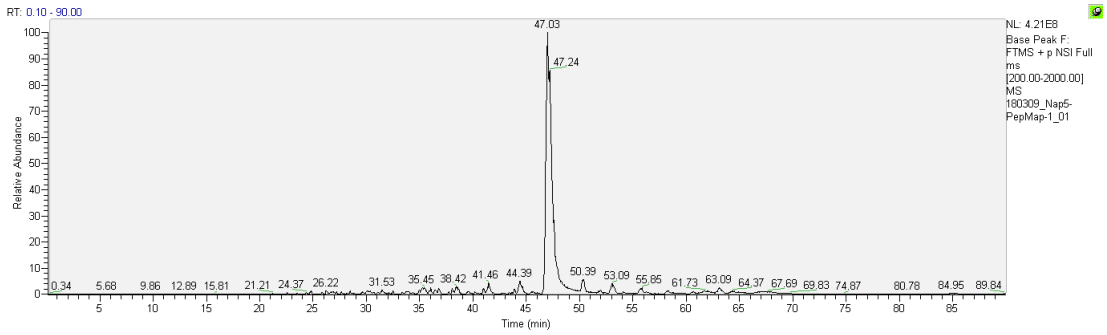

Figure 57 – Base peak chromatogram of NAP^{TM}-5 peptide map

For every sample one dominating peak was observed with very high intensity.

The intense peak was produced by an m/z value of 453.342. Using the software Xcalibur a theoretical spectrum of $C_{24}H_{44}N_4O_4$ was generated with an m/z value of 453.344 (Figure 58).

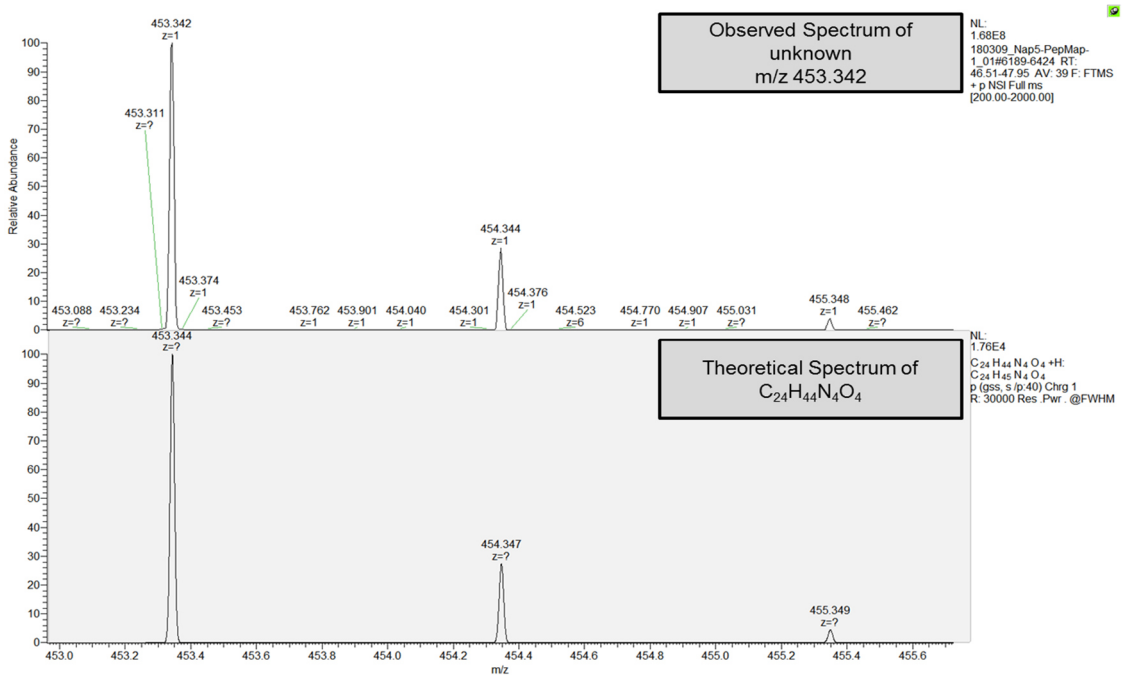

Figure 58 – Observed spectrum of unknown m/z value and theoretical spectrum

The m/z value of 453.342 produced the intense peak and was unknown. Using XCalibur a theoretical spectrum was generated for the formula $C_{24}H_{44}N_4O_4$ which shows similar m/z value 453.344 and isotopic pattern as the unknown m/z.

This theoretical spectrum revealed a highly similar isotopic peak pattern compared to the unknown m/z value. The fragment spectrum of the unknown m/z is shown in Figure 59. Tran *et al.* identified the m/z value of 453.344 to be a contamination from nylon membranes. They investigated cyclic polyamide oligomers from nylon membrane to be a source of contamination in LC-MS [148]. The fragment spectrum of Tran *et al.* revealed the same fragments as the pattern for the unknown mass observed with the NAP™-5 columns.

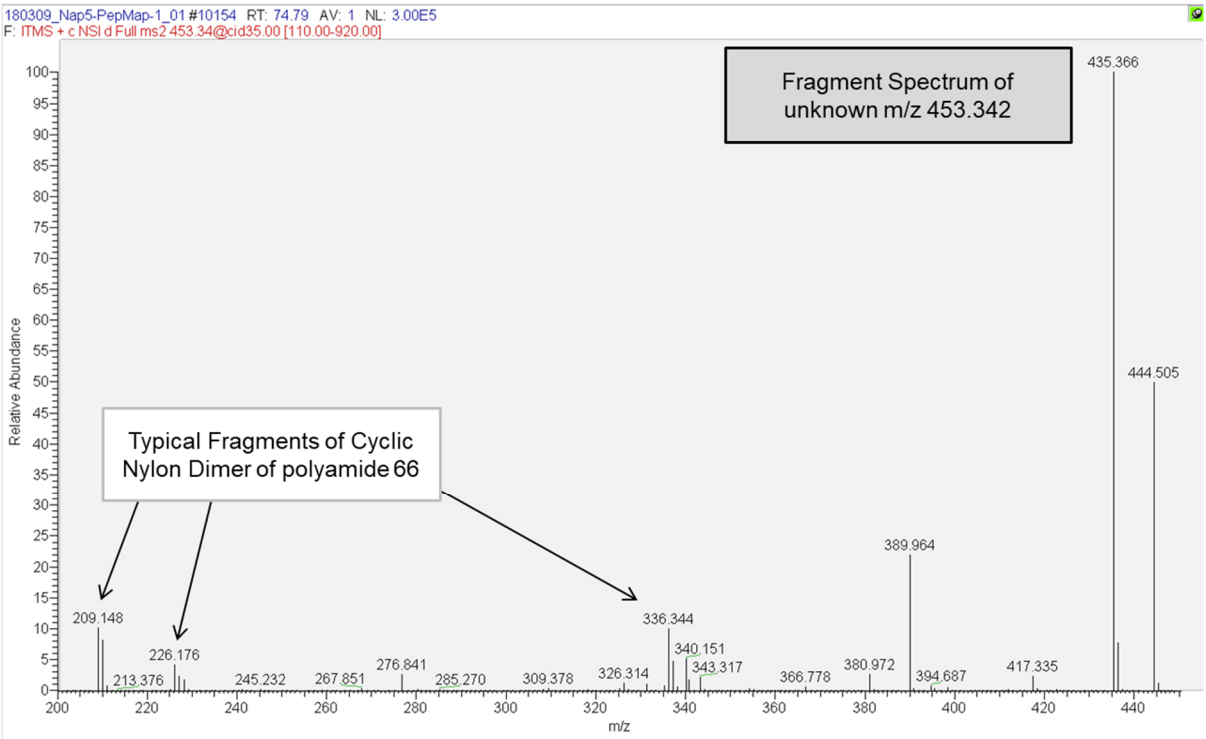

Figure 59 – Fragment spectrum of unknown m/z 453.432

The fragment spectrum of the unknown m/z 453.432 was compared to a fragment spectrum of a publication from Tran et al. They found a similar fragment pattern for a compound with an $[M+H]^+$ of 453.4 and defined the fragment masses 209, 226 and 336 to be typical fragments of cyclic nylon dimer of polyamide 66.

Taking into account that other studies used 500 to 1000-fold higher amounts of mAb for digestion, these results indicate that the contamination may not be as disturbing as it is the case for 1 µg absolute protein amount [144-147]. Based on these observations the NAP™-5 columns are concluded to be not suitable for the low sample amounts. Therefore, alternative desalting procedures were investigated.

3.2.2 Desalting using Amicon® centrifugal filters

Amicon® centrifugal filters are widely used in the purification and concentration of antibody solutions. A big advantage of the centrifugal-filter devices is the possibility to also concentrate the sample after buffer exchange [149]. Most studies applied the Amicon® centrifugal filters with a Cutoff of 10 kDa and with much higher amounts of antibody [150, 151]. However, previous experiments revealed that

desalting using Amicons® with a 10K cut off is not applicable to the extended handling time of several hours. Therefore, it was investigated, whether a 50K cutoff might be an alternative, or whether LC and HC are washed out. For this, in total 4 different samples were prepared in duplicates (see Table 7). The Amicons® were washed prior use either three or six times using 500 µL Milli-Q water. Furthermore, two different amounts (200 µL and 300 µL) of denaturation buffer (8 M Guanidine-HCl, 400 mM Tris) were tested to improve denaturation.

Table 7 – The different combinations for the Amicon® optimization experiment

Sample	Wash steps	Denaturation buffer [µL]
200µL-denat_3wash	3	200
200µL-denat_6wash	6	200
300µL-denat_3wash	3	300
300µL-denat_6wash	6	300

As shown in Figure 60 the different tested combinations revealed low sequence coverages and bad overall reproducibility. This finding is consistent with the manufacturer's specification, that molecular weights (MWs) of 45 kDa are retained for approximately 40%, and lower MWs for around 20% or less. Thus, the 50K cutoff of the Amicon® filters are no alternative, as HC and LC are washed out to a great extent.

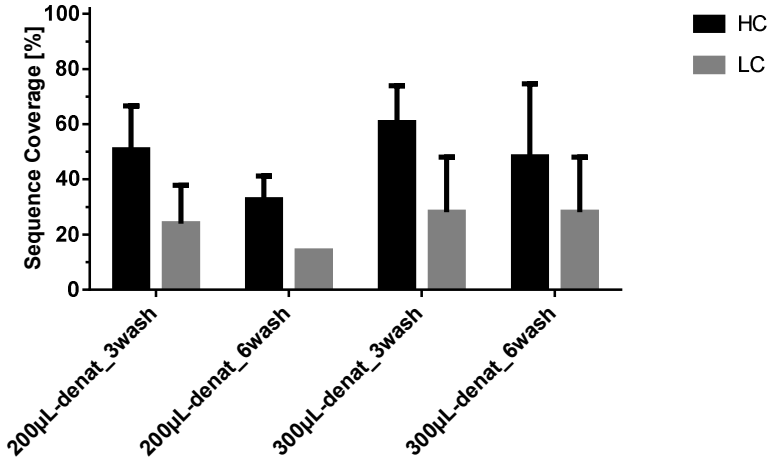

Figure 60 – Sequence coverage of different Amicon® combinations

For the Amicon® protocol different combinations of denaturation buffer volume and the number of wash steps prior use were tested in duplicates. All combinations resulted in low sequence coverages and did not show sufficient reproducibility.

3.2.3 Desalting using PhyTip gelfiltration columns

Next, PhyTip gelfiltration columns with a 10K desalting resin in a tip volume of 1000 µL were tested in triplicates. As can be seen from Figure 61-A, the PhyTips showed high variations in their performance. It was observed, that the first tip eluted well, and also showed very high sequence coverages (PhyTip-1). However, for the other two tips sample elution was incomplete as the solution did not flow through completely. This could arise from the fact that the PhyTip columns may partially ran dry during shipment, which could lead to the formation air bubbles in the resin bed.

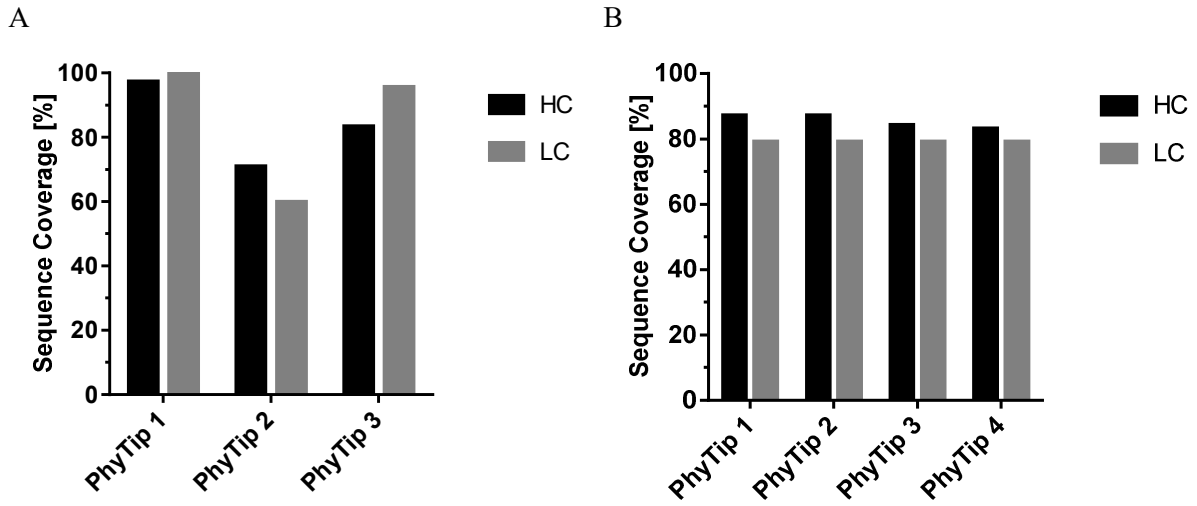

Figure 61 – Sequence coverage of PhyTips

A) In a first experiment the PhyTip gelfiltration columns had high variations in their performance and showed sequence coverages ranging from 60% up to 100%. B) With an overnight preparation step, the Phytips were pre-equilibrated and the whole experiment was repeated. Using the preparation protocol a very high reproducibility was achieved

To investigate this assumption, in a next experiment the PhyTips were prepared prior usage. For this, the PhyTips were transferred into 50 mL hydrolysis buffer (50 mM Tris, pH 7.5) so that the whole Tip was in solution and the bed completely wet overnight. Then the solution was eluted through by gravity (approximately 17 min) and again 1 mL fresh hydrolysis buffer was added on top. After further 17 minutes, the samples were added and waited for 5 minutes. After this hydrolysis buffer was added for elution and the sample was collected in an Eppendorf tube. As can be seen from Figure 61-B, this improved preparation protocol led to highly reproducible results of the sequence coverage for all four replicates.

In order to further optimize the protocol and maximize the sequence coverage, three factors influencing the elution and desalting efficiency were varied. Therefore, different volumes of denaturation buffer, elution buffer and the amount of Trypsin/Lys-C mix were tested, which resulted in eight different combinations (see Table 8).

Table 8 – The different combinations for the PhyTip optimization experiment

Sample	Denaturation buffer [µL]	Elution buffer [µL]	Trypsin/LysC [µg]
S1-lowD_highE_lowT	180	200	0,06
S2-lowD_highE_highT	180	200	0,12
S3-lowD_lowE_lowT	180	100	0,06
S4-lowD_lowE_highT	180	100	0,12
S5-highD_highE_lowT	275	100	0,06
S6-highD_highE_highT	275	100	0,12
S7-highD_lowE_lowT	275	50	0,06
S8-highD_lowE_highT	275	50	0,12

The experiment was performed on two independent days but the results did not show sufficient reproducibility of the abovementioned parameters (Figure 62).

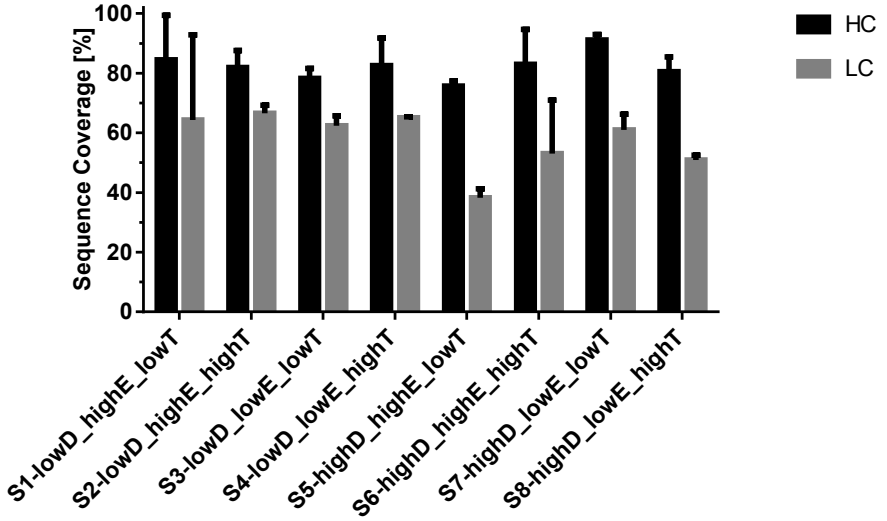

Figure 62 – Sequence Coverage of different PhyTip combinations

For the PhyTip protocol different combinations of the amount of denaturation buffer, elution buffer and the amount of enzyme were tested in duplicates (samples S1 to S8). However, the tested combinations did not show sufficient reproducibility of the sequence coverage of LC and HC.

Based on these results it is suggested that PhyTip columns did not represent the optimal solution for the desalting procedure of the low amount peptide map.

3.2.4 DoE Desalting using Zeba™ Spins and Oasis PRiME µElution plate

Lastly, Zeba™ spin desalting columns with mass cut off values of 7K and 40K were compared and the influence of a pre-equilibration step prior usage was investigated. Thus, the Zeba™ spins were either used directly after the removal of the storage solution or washed three times with 300 µL hydrolysis buffer.

Previous experiments showed that Zeba™ spins alone does not provide sufficiently clean samples for analysis on a Nano-flow HPLC. Therefore, a solid phase extraction plate was included as additional clean-up and concentration step after enzymatic digestion. According to the manufacturer specification, the Oasis PRiME µElution plate is ready to use and requires no priming with organic solvent and subsequent equilibration with wash solvent. However, it was investigated whether the priming of the plate brings any benefit to sample quality and reproducibility. The plate was therefore, either used directly, or primed with 200 µL 80% ACN, 0.1% FA followed by equilibration using 200 µL 0.1% FA. After digestion, the samples were applied to the plate and the peptides washed with 200 µL 0.1% FA. To investigate, whether a second wash step leads to a cleaner sample, the peptides were either washed once or twice. After that samples were eluted using 100 µL 80% ACN.

In order to test all mentioned factors in one experimental approach, a Design of Experiment (DoE) setup was planned using the statistical software Minitab 18. A full-factorial setup with four factors (Table 9) and two blocks was chosen, ending up with a total number of 32 experiments (Table 10). In order to test day-to-day reproducibility, the two blocks were prepared on individual days.

Table 9 – DoE factors and levels

Factor	Low	High
A: Cut Off	7K	40K
B: Spin Wash	Yes	No
C: Oasis Prime	Yes	No
D: Oasis Wash	1	2

The sequence coverage of each sample was determined and is presented in Figure 63. DoE-Samples-21 and -22 stick out, as they show significantly lower sequence coverages. Both used the 7K columns and were considered to be outliers. To proof this, the ROUT method was applied, and a Q-value of 1% was chosen. By this, the two data points of DoE-Sample-21 and -22 were statistically identified as outliers and therefore, excluded from subsequent analyses (see Figure 63).

Table 10 – DoE Setup: Overview of different combinations

Sample Name	Cut Off	Spin Wash	Oasis Prime	Oasis Wash steps
DoE_1	40K	Yes	Yes	1
DoE_2	40K	Yes	Yes	2
DoE_3	40K	No	Yes	1
DoE_4	7K	Yes	Yes	1
DoE_5	7K	No	No	2
DoE_6	40K	Yes	No	2
DoE_7	7K	No	Yes	2
DoE_8	7K	Yes	No	2
DoE_9	40K	Yes	No	1
DoE_10	7K	No	Yes	1
DoE_11	7K	Yes	No	1
DoE_12	40K	No	No	2
DoE_13	7K	Yes	Yes	2
DoE_14	40K	No	No	1
DoE_15	7K	No	No	1
DoE_16	40K	No	Yes	2
DoE_17	7K	No	Yes	1
DoE_18	7K	Yes	No	2
DoE_19	40K	No	No	1
DoE_20	7K	Yes	Yes	2
DoE_21	7K	No	No	1
DoE_22	7K	Yes	Yes	1
DoE_23	40K	No	Yes	2
DoE_24	40K	Yes	No	1
DoE_25	7K	No	Yes	2
DoE_26	7K	No	No	2
DoE_27	40K	Yes	No	2
DoE_28	40K	No	Yes	1
DoE_29	7K	Yes	No	1
DoE_30	40K	Yes	Yes	2
DoE_31	40K	Yes	Yes	1
DoE_32	40K	No	No	2

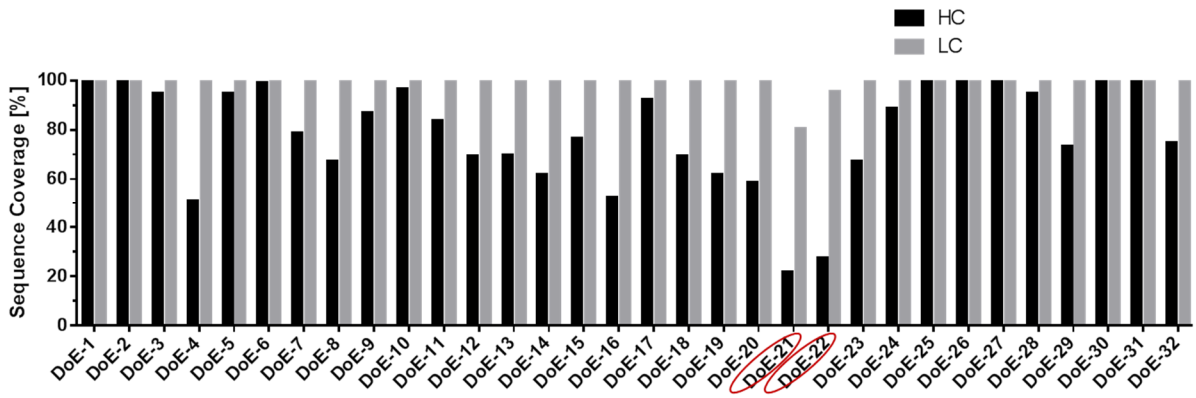

Figure 63 – Sequence coverage for all DoE-Samples

The sequence coverage of the LC was very high for all samples. For the HC higher variations were observed. Statistical analysis identified samples DoE-21 and DoE-22 to be outliers (marked in with red circles).

For every tested combination the sequence coverage of the LC was 100% and only the HC coverage varied. To simplify the graphs, the mean was built between sequence coverage of HC and LC (see equation 8).

$$\text{Mean(Seq. Cov)} = \frac{Seq.Cov_{HC} + Seq.Cov_{LC}}{2} \tag{8}$$

In Figure 64 the results from each combination of block 1 and 2 were compared and the mean and standard deviation plotted. Only for combination“7-no-no-1” and “7-yes-yes-2” the results of block two were excluded, as they were previously identified as outliers. Thus, for those samples no standard deviation was calculated.

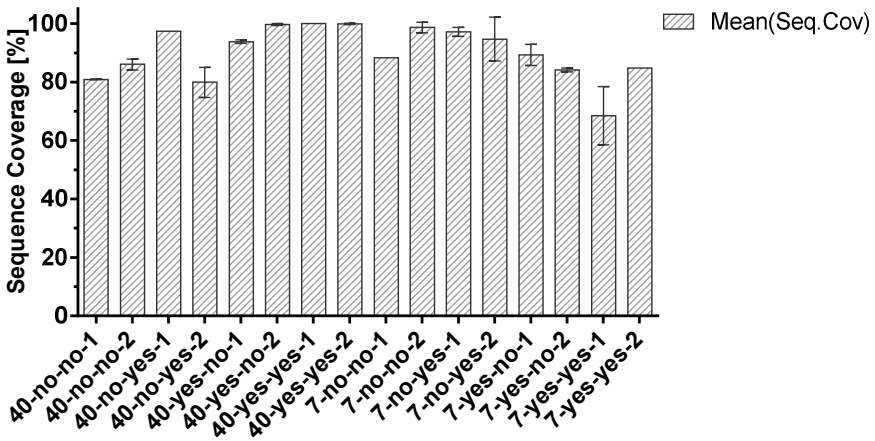

Figure 64 – Mean Sequence coverage of different combinations

For all combinations the mean sequence coverage of block one and two were compared and the standard deviation plotted. Only for samples“7-no-no-1” and “7-yes-yes-2” the results of block two were excluded, as they were previously identified as outliers.

The DoE was analyzed for the response sequence coverage including all main effects, A:Cut off, B:Spin Wash, C:Oasis Prime and D:Oasis Wash. The second level interactions AC, AD, BC and BD were not considered, as the Zeba™ spin factors A and B probably do not influence the Oasis factors C and D. Therefore, only AB and CD were included in the model.

Non-significant terms were removed by backwards elimination. The blocks were found to be not significant, as no statistical significant difference was observed between the two days. As can be seen from Figure 65-A the second level interaction between Cut Off and Spin Wash was determined to be highly significant (p-value = 0.000). Also the interaction between Oasis Prime and Oasis Wash showed a significance (p-value = 0.042).

The factor A:CutOff shows the highest slope for the main effects plot, which means that this factor has the greatest influence on the model (Figure 65-B). The interaction plot reveals a high interaction between CutOff and SpinWash. For 40K columns, it is best to wash the columns prior use. However, for the 7K columns the interaction plot shows better sequence coverage when no wash step was included (Figure 65-C). Overall, the results revealed that the highest sequence coverage is observed using a CutOff of 40K, SpinWash, priming of the Oasis Plate and one wash step prior elution.

Therefore, as final protocol the setup listed in Table 11 was chosen.

Table 11 – Final Peptide Map protocol

Step	Description
Denaturation	100 µL Denaturation Buffer
Desalting	Zeba™ spin 40K (Wash 3 times before use)
Digestion	Trypsin/mAb (1/10)
Desalting	Oasis Plate (Prime, 1 Wash step)
Evaporation	1 h 15 min at 45°C
Reconstitution	20 µL 0.1% FA

A

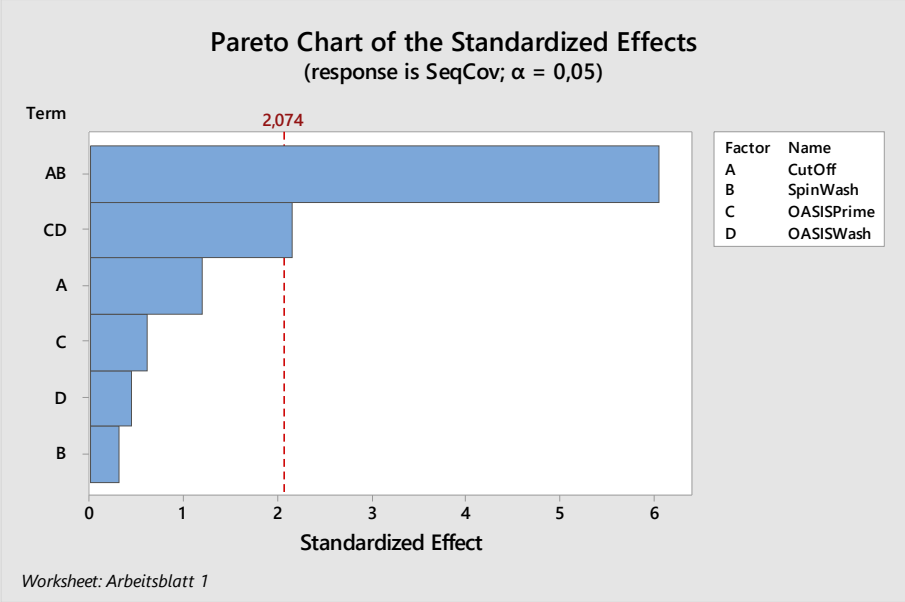

B

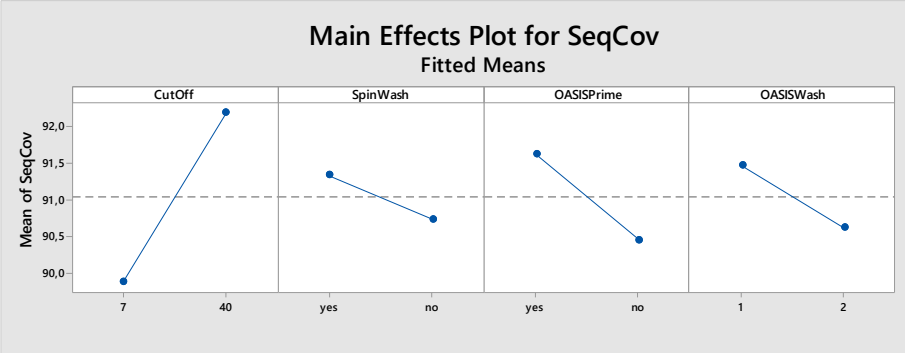

C

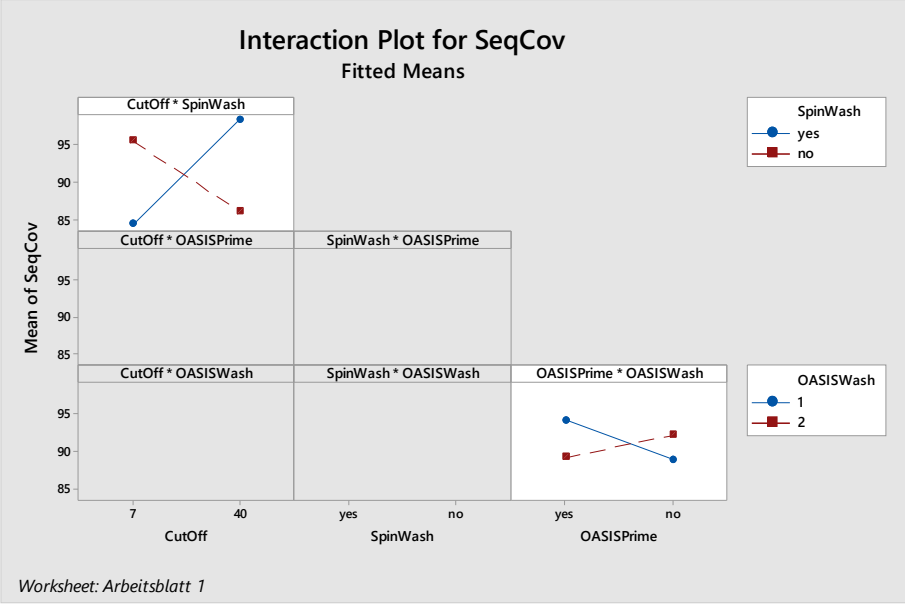

Figure 65 – Pareto Chart, main effect and interaction plots

(A) The second level interaction AB was found to have the greatest effect on the result. (B) The main effect plot shows that factor A:CutOff has the greatest influence. C) The interaction plot found that there is a high interaction between A:CutOff and B:SpinWash. Grey fields were found to be non-significant.

3.3 Nano-HPLC-MS implementation and development

In order to achieve the required improved sensitivity to be able to measure *in-vivo* samples, the standard chromatographic conditions routinely used for peptide map separations at AbbVie needed to be adopted to nano flow conditions. Using the Thermo UltiMate™ 3000 RSCLnano System and Thermo Orbitrap Velos Pro, column dimensions were changed from 2.1 x150 mm to nano scale (0.075 x150 mm or 250 mm). In theory this downscaling should result in a 784-fold improved sensitivity (see equation 9).

$$f = \frac{2.1mm^2}{0.075mm^2} = 784 \tag{9}$$

A comparison between different trap columns, analytical columns and two types of nESI sources was made, as shown in Figure 66. With the TriVersa NanoMate® the peptides are ionized by a conductive sprayer at the end of the capillary of the LC-coupler and sprayed through an ESI-nozzle. This source offers a high flexibility, as it can be combined with columns from different suppliers. The EASY-Spray™ technology is limted to columns manufactured by Thermo, but has the advantage of an easy plug in mechanism.

The standard Acclaim™ PepMap™ columns using the TriVersa NanoMate® as nESI-source were compared to the EASY columns packed with Acclaim™ PepMap™ using the EASY spray source. Furthermore, the BEH-columns manufactured by Waters were tested in combination with the TriVersa NanoMate®. As trap columns the cartridge based µ-precolumns were used, as well as the Nanotrap columns, both with Acclaim™ PepMap™ material. Furthermore, the Waters BEH-Nanotrap columns were tested.

Figure 66 – Overview of trap columns, analytical columns and nESI sources

As trap columns the Acclaim™ PepMap™ trap cartridges and the Acclaim™ PepMap™ nanotrap columns were compared to the peptide BEH nanotrap column. The Acclaim™ PepMap™ material was further tested as standard analytical nano column and in the EASY-spray format. As third analytical column the peptide BEH columns were tested. For ionization the TriVersa NanoMate® or the EASY-Spray™ source were used

3.3.1 Acclaim™ PepMap™ column and TriVersa NanoMate®

The starting platform consisted of an Acclaim™ PepMap™ column fitted with a TriVersa NanoMate® ESI source and the conditions listed in Table 12 were used.

Table 12 – Starting column dimensions

	Starting conditions
Column Diameter	0.075 mm
Column length	150 mm
Particle Size	2 µm
Column	45°C
Solvent A	H_2O + 0.1% FA
Solvent B	ACN + 0.1% FA
Loading solvent	98% H_2O + 2% ACN + 0.05% TFA
Loading Flow rate	10 µL/min
Trap Column	µ-precolumn (Cartridge)

The column base material is spherical silica with pores of 100 Å and chemically modified with C18-endcapped tails. A gradient of 90 min that was developed in previous experiments at AbbVie, was used as a starting point for separation of peptides (Table 13).

Table 13 – Starting gradient

Time [min]	B [%]
0	2
3	2
7	8
20	18
35	25
50	30
56	40
60	90
70	90
74	2
90	2

As can be seen from Figure 67 the used method provided sufficient separation of the peptides from the mAb-1 digest.

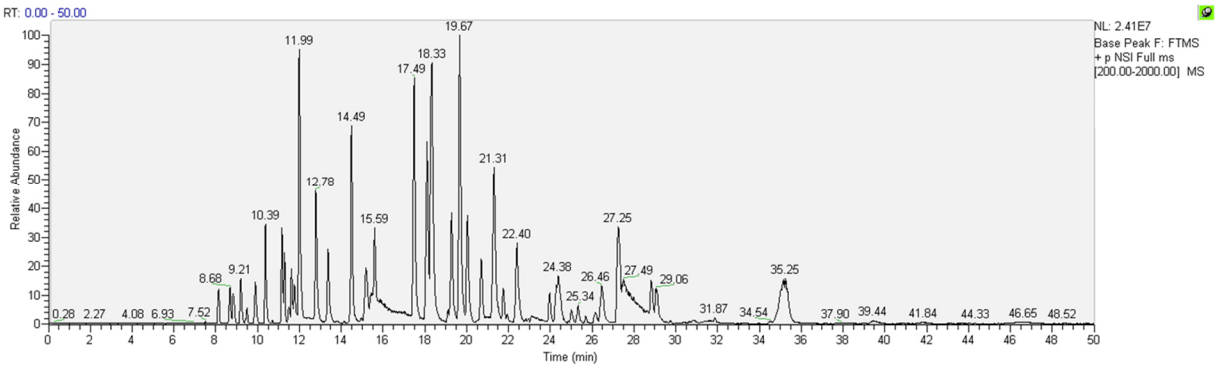

Figure 67 – Base peak chromatogram of mAb-1 digest on standard column

The base peak chromatogram of mAb-1 digest revealed a good separation on the Acclaim™ PepMap™ columns. However, several issues were observed due to the prefixed sleeves.

However, the outlet of the nano columns is fitted with a nano connector that offers pressure stability up to 300 bars. This connection is prefixed by the manufacturer and consists of a special sleeve, two black nuts and a transparent union as shown in Figure 68.

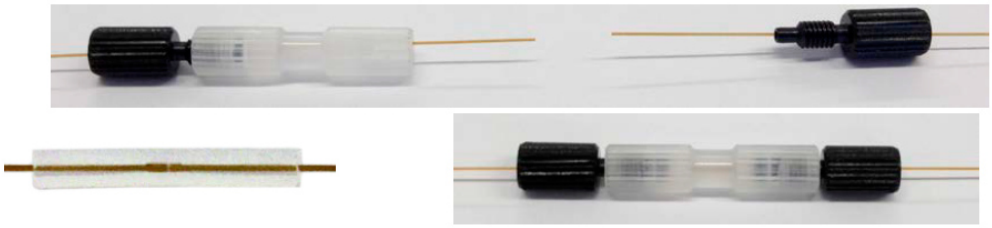

Figure 68 – Nano-Connector

The Nano connector consists of a sleeve, two black nuts and a transparent union and shows pressure stability of 300 bar.

After a few injections on the column peak tailing was observed, which could be explained by a possible leak at the nano connector. Attempts to eliminate the problem by fixing the nano connector did not result in any improvement. Also the assembly of a new nano connector tubing proved to be rather instable, which resulted in the observation of a leak already after relatively short times of use (a few separation runs). As the same issue was observed for several different column lots, the gradient development for this column type was not further investigated.
To prevent possible leakage sites in the used setup, the further attempts were focused on the reduction of the number of connections. Thus, possible application of other column types was investigated (i.e. EASY columns).

3.3.2 EASY-spray™ column and EASY-spray™ source

As the general peptide separation achieved with the Acclaim™ PepMap™ material proved to be sufficient, it was investigated whether the material packed in an EASY-spray format could provide equally good results. The EASY columns contain a precisely positioned fused-silica emitter at the column outlet which thereby enables a dead volume-free spray of the eluate [120]. Due to the direct combination of column and sprayer, a better chromatographic resolution was expected. The EASY-Spray™ technology has been used by several groups in the field of proteomics due to the simplification compared to standard nano-flow HPLC [152-154].

Thus, in the second platform a 250 mm column was used in the EASY-Spray™ format with the conditions listed in Table 14 and the gradient used in 3.3.1. Furthermore, the loading flow was changed to 20 µL/min and a loading solvent without ACN selected [155-157].

Table 14 – Column dimensions – EASY-spray

	Column and solvents
Column Diameter	0.075 mm
Column length	250 mm
Particle Size	2 µm
Column	45°C
Solvent A	H_2O + 0.1% FA
Solvent B	ACN + 0.1% FA
Loading solvent	H_2O + 0.1% TFA
Loading Flow rate	20 µL/min
Trap Column	µ-precolumn (Cartridge)

The separation of peptides of the digested mAb-1 sample under the new conditions (Figure 69) proved to be sufficient. However, unexpectedly high peptide oxidation levels were observed. The reason for this observation was not immediately apparent and therefore further investigation was required.

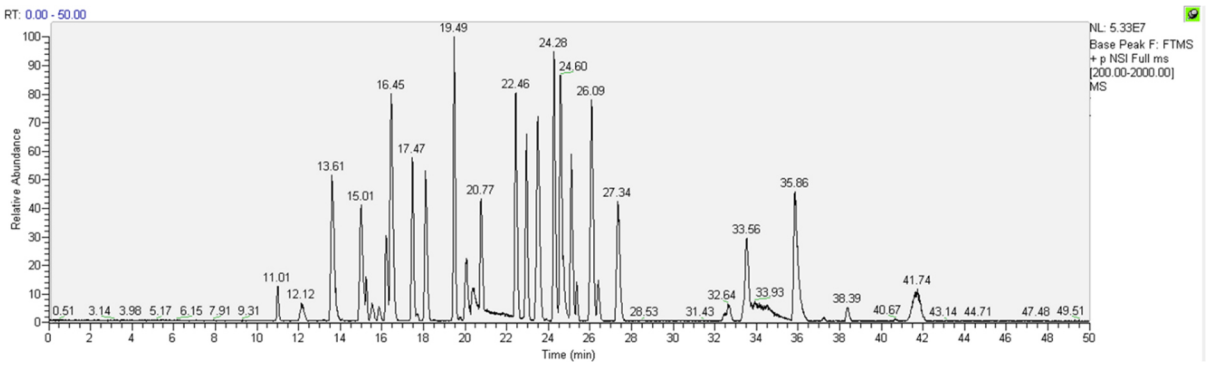

Figure 69 – Base peak chromatogram of mAb-1 digest on EASY column

The peptide separation showed good results on the EASY-spray column. However, high values of oxidation were observed for the digest.

3.3.3 Oxidation troubleshooting – Oasis-Plate

During the development of the optimized sample preparation workflow, high levels of peptide oxidation were observed. It has been reported that one methionine residue in the C_H2 domain (HC M252, DTLMISR peptide) and another (HC M428, WQQ peptide) in the C_H3 domain are the most susceptible residues for oxidation and can be treated as oxidation marker peptides [64, 65, 158]. As an indicator, the amount of oxidation on the DTLMISR peptide was further monitored.

To investigate, whether the high oxidation values are introduced during the sample preparation workflow, a comparison between a routine peptide map protocol with known modification values and the optimized protocol for low sample amounts (miniaturized peptide map) was made (Table 15).

Table 15 – Comparison between starting protocol and final protocol

	Routine protocol	Final protocol for low sample amounts
Amount of mAb	250 µg	1 µg
Desalting	NAP-5 columns	Zebaspin columns
	Direct measurement, no further desalting/concentration	Additional desalting using Oasis plate, followed by evaporation and reconstitution

Despite the different absolute amounts of mAb used for the protocol, the main difference of the low-sample amount protocol from the standard procedure is the additional desalting step in the low-sample amount protocol. It was therefore investigated, whether the desalting using the Oasis plate might be the critical factor, which results in high levels of peptide/mAb oxidation.

As can be seen from Figure 70 the expected value for DTLMISR oxidation of a mAb-1 digest prepared by the standard protocol and measured on a standard-flow HPLC-MS device is around 3% (black). The same sample was diluted 1:10 with water and then desalted using the Oasis PRiME µElution plate, as described previously. Evaporation of organic solvent was either performed at 45°C or at room temperature (RT, shown in blue).
Measurement of those samples on the nano-LC/MS device showed high oxidation values of 70% for both evaporation temperatures. Thus, it was possible, that the high oxidation values could be introduced due to the use of the Oasis plate, followed by evaporation. Therefore, in a next step the sample was desalted with the Oasis plate without dilution and then measured on the standard-LC/MS device. As can be seen from Figure 70-B, the oxidation values were between 4-5% meaning that the oxidation was probably not introduced during the desalting procedure. However, the desalted samples shown in Figure 70-A were diluted prior clean-up using the Oasis-plate, whereas the samples for the standard flow LC-MS device were desalted without dilution (Figure 70-B).
Therefore, in a next step it was tested, whether the concentration of sample used for the desalting on the Oasis plate might have an influence for the mAb oxidation. The undiluted sample was desalted using the Oasis plate and diluted prior measurement on the nano-LC/MS device. As shown in Figure 70-C the values were still high, leading to the conclusion, that the Oasis Plate unlikely contributed to the observed protein oxidation.

Thus, these results suggest, that the sample preparation procedure does not contribute to the observed increased oxidation levels. In other words, as the same sample measured on two different HPLC-MS instruments resulted in completely different results, it was assumed that the modifications are probably induced by the contact with the nano-HPLC/MS device.

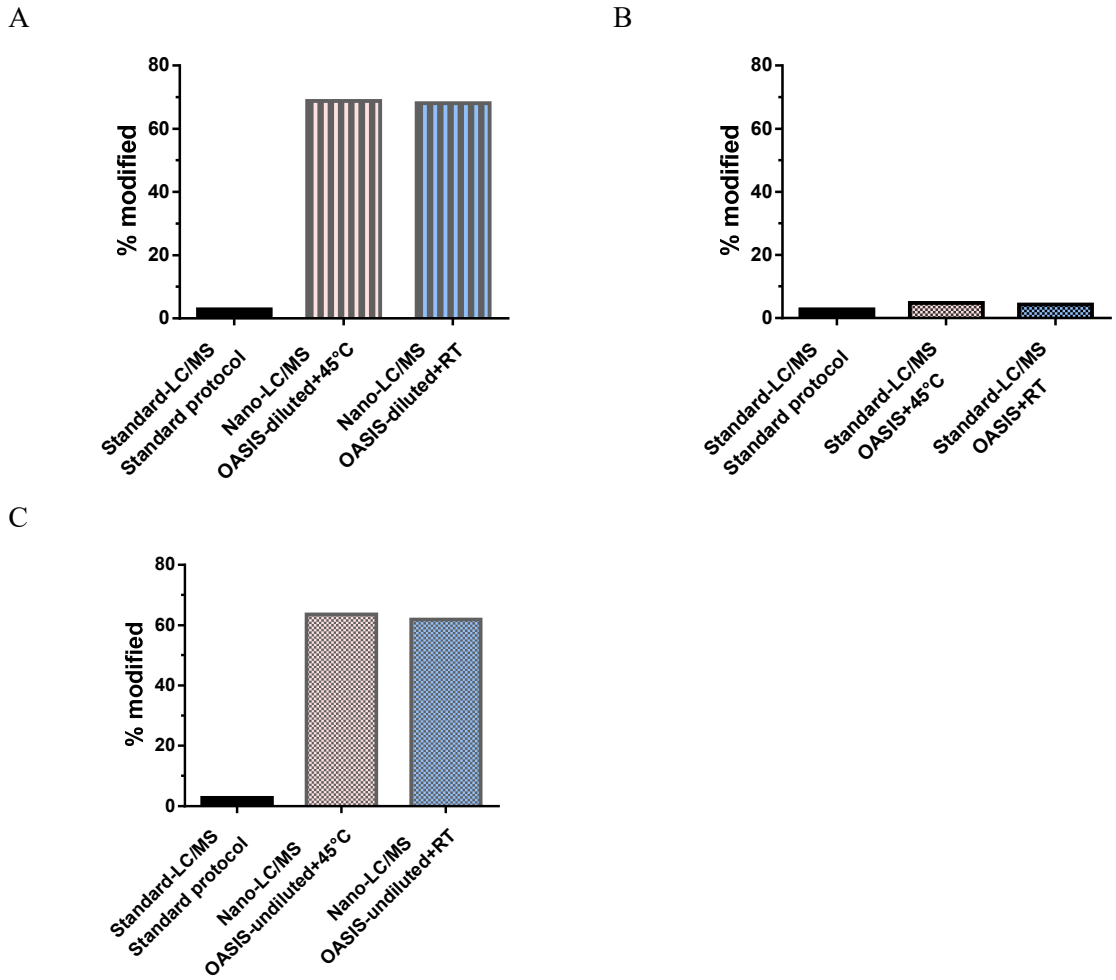

Figure 70 – Oasis -plate experiments

A) The non-treated mAb-1 measured on a standard-flow device revealed 3% DTLMISR-oxidation (black). The same sample diluted 1:10 and desalted using the Oasis -plate followed by evaporation of organic solvent at either 45°C (rose) or RT (blue) showed 70% oxidation on the nano-LC/MS device. B) Desalting of the undiluted mAb-1 digest on Oasis -plate and subsequent measurement on the standard-LC/MS device revealed low oxidations around 4-5%. C) Desalting of the undiluted mAb-1 digest on Oasis-plate and subsequent dilution for measurement on the nano-LC/MS device showed again very high oxidation values of around 60%.

3.3.4 Oxidation troubleshooting – EASY-Spray™ Source

To prove this assumption, it was investigated how the nano-HPLC/MS device could affect the mAb digest oxidation levels. As the native DTLMISR and the oxidized DTLmISR peptide are chromatographically separated, the oxidation cannot be introduced in the ESI-source (Figure 71).

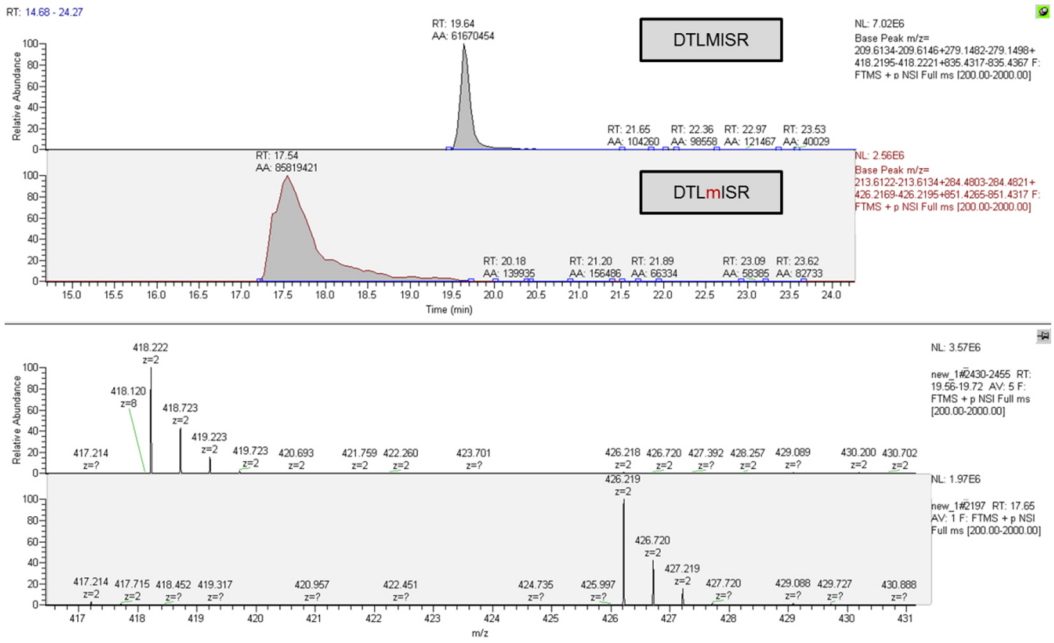

Figure 71 – Chromatographic separation of modified and native peptide

The unmodified DTLMISR and the oxidized DTLmISR peptide are chromatographically separated. Therefore, the oxidation is introduced prior separation on the column and no in-source oxidation.

Thus, the possibility of the in-source oxidation can be excluded, meaning that the EASY-Spray™ source is not the reason for the observed high oxidation levels. In the LC-MS setup using the EASY-Spray™ column, the trap is located in the column oven and connected to the analytical column via a capillary-to-column connector (Figure 72).

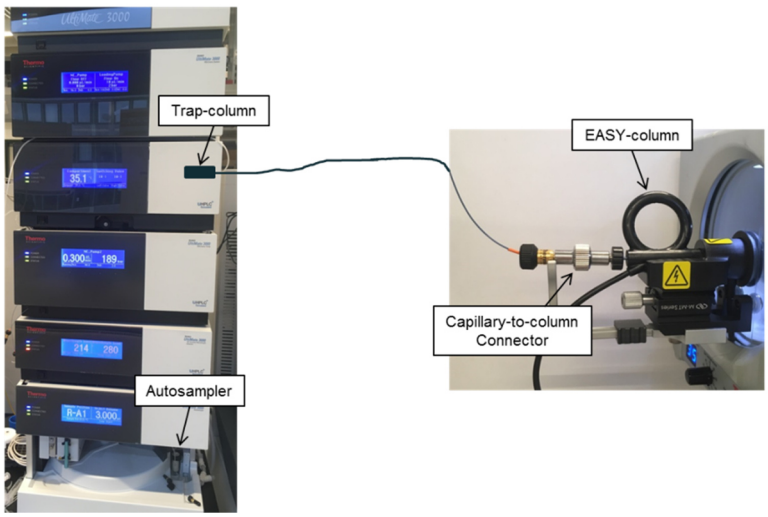

Figure 72 – Nano-HPLC/MS setup with EASY-Spray™ column

The trap column is located in the column oven and connected to the EASY-Spray™ column via a connector.

After a visual inspection, deposits of unknown material and incrustations were observed at the outlet of the capillary as shown in Figure 73-A. The origin of the observed deposits was unclear; however,

comparison with the new connector showed that the material is supposed to be deposit free (Figure 73-B).

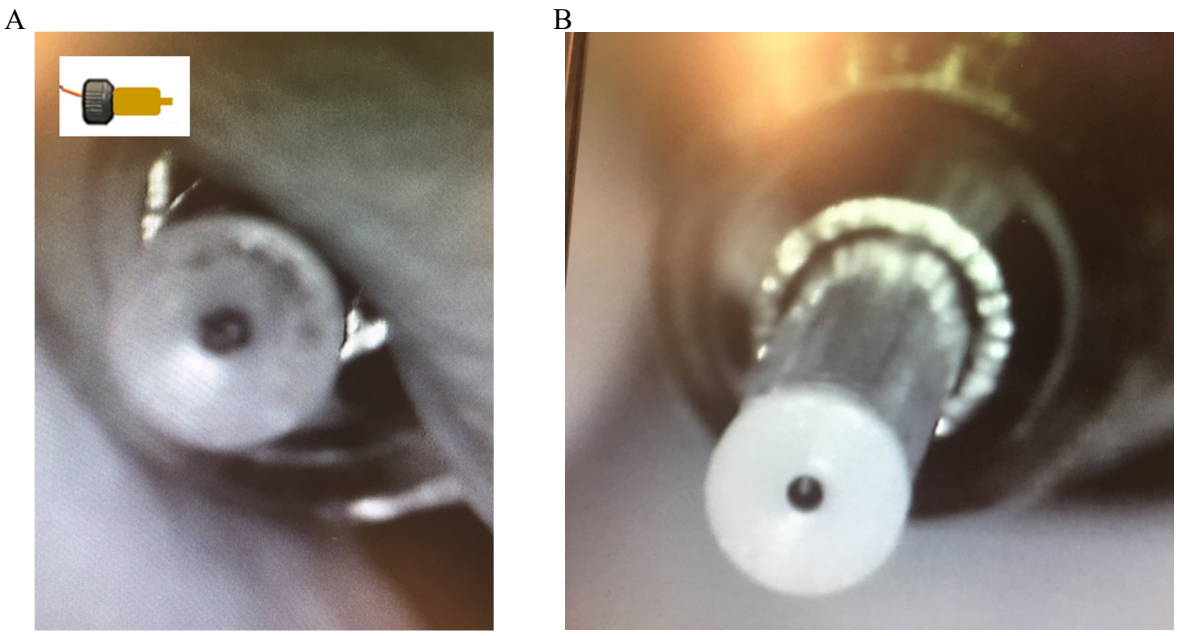

Figure 73 – Deposits on the capillary

A) The capillary showed precipitations at the outlet. B) A new capillary did not show any precipitates.

The similar deposits were found in the capillary to column connector (Figure 74).

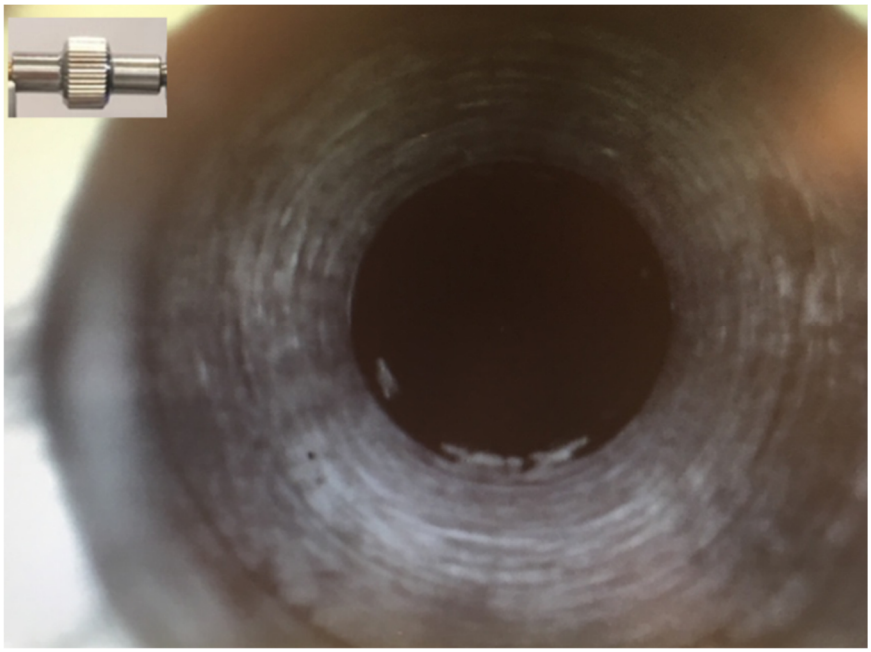

Figure 74 – Capillary and capillary-to-column connector

Visual inspection revealed that the capillary-to-column connector showed similar precipitates.

Based on these observations, one could hypothesize that the high levels of oxidation are related to the described deposits on the capillary-to-column connector. Therefore, the decision has been made to switch back to the platform using the TriVersa NanoMate® as ion source and normal nano-flow columns, as no metal connector was there required.

3.3.5 Oxidation troubleshooting – NanoMate®

A new Acclaim™ PepMap™ column was used and the NanoMate® was reinstalled as an ion source. The previously described issues of leaking connections were not observed for the newly installed column. However, measurements of the NISTmAb digest prepared by the standard workflow still revealed high oxidation values of 60 to 80% as assessed by oxidation of DTLMISR peptide. These results indicate that the capillary-to-column connector was unlikely responsible for the high oxidation values.

In a next step, a synthetic DT(L*)MISR-peptide containing a heavy labeled lysine (L*), $^{13}C_6$ $^{15}N_1$ leading to a mass shift of +7.017 Da, was measured on the nano-LC/MS device and oxidation levels of 14% were observed. The synthetic peptide was then spiked into the NISTmAb-digest in the same molar ratio as it is present in the sample. As can be seen from Figure 75 the oxidation of the NISTmAb DTLMISR peptide (shown in black) was reduced to 40%, whereas the synthetic DT(L*)MISR peptide oxidation was increased to 40% (shown in grey).

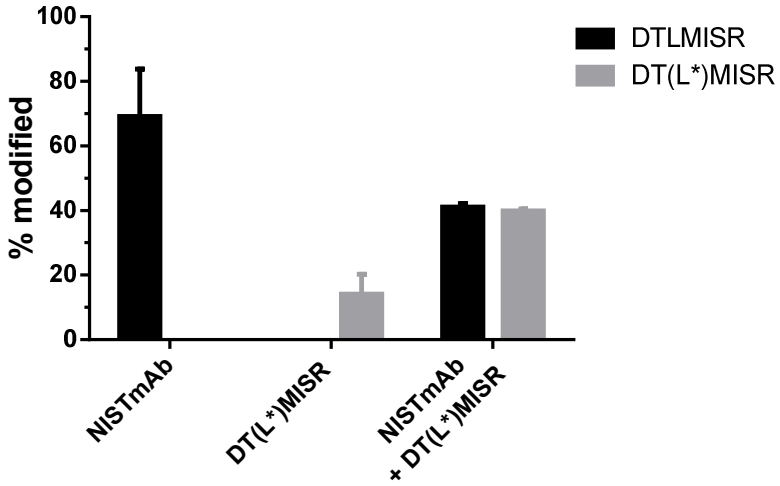

Figure 75 – Oxidation values of heavy labeled DTLMISR spiked in NISTmAb samples

Also using the standard Acclaim™ PepMap™ columns and the NanoMate® as ion source, the digest of NISTmAb revealed oxidation values of 60-80% (black). Measurement of the synthetic peptide DT(L)MISR showed oxidation values of 14%. When the synthetic DT(L*)MISR was spiked into the NISTmAb digest prior measurement, the oxidation of DTLMISR was reduced to 40% and the DT(L*)MISR was increased to 40%.*

These observations are of interest, as they suggest that the oxidation process likely reaches particular saturation level and depends on the initial peptide concentration leading to competition between labeled and unlabeled peptides. The levels of Met oxidation also imply that there is a limited availability of the oxidative agent in the reaction or limited access of the peptide to the surface that could potentially catalyzes the reaction, if such catalysis events indeed occur. In other words, the results revealed that the synthetic DT(L*)MISR peptide can partially prevent the NISTmAb peptide from oxidation and act as an oxidation scavenger.

This finding is consistent with the fact that free methionine, but also tryptophan has been described as protective components in formulations of protein therapeutics due to their potential to act as an antioxidant [159]. Ji *et al.* reported that free methionine protected methionine residues in the protein from oxidations, whereas free tryptophan was described to protect tryptophan residues [160].

Thus, to investigate this phenomenon further, the spiking experiments were performed in more details. This time the experimental setup included different ratios of NISTmAb digest/synthetic peptides with or without addition of free Met (Figure 76).

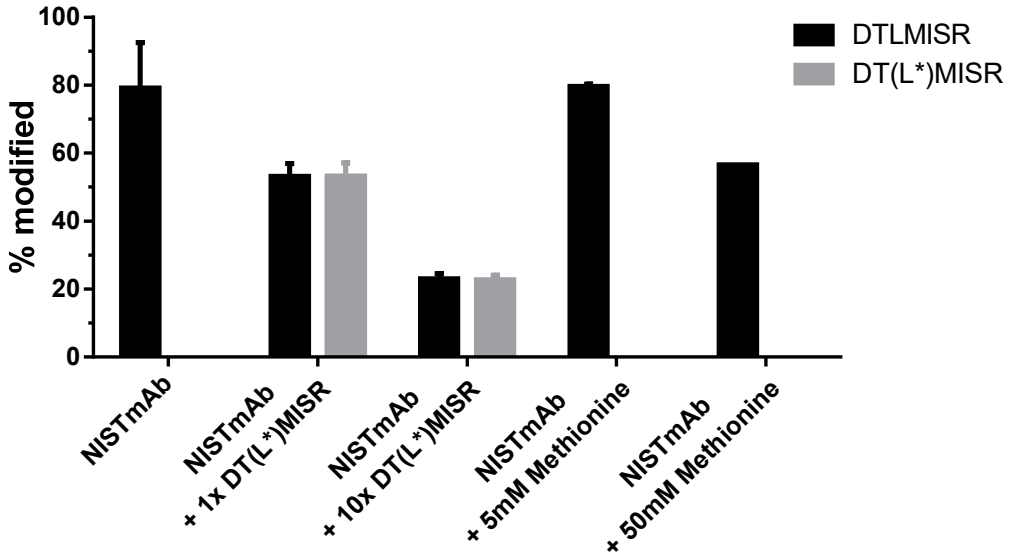

Figure 76 – Spiking in heavy labeled DT(L*)MISR and methionine as scavengers

The heavy labeled DT(L)MISR lead to a reduction in DTLMISR oxidation to 50 and 20% when spiked into the NISTmAb sample in the same molar ratio and a 10-fold higher ratio, respectively. A methionine concentration of 5 mM did not prevent the DTLMISR peptide from oxidation, whereas a 10-fold higher concentration had the same effect as the 1x DT(L*)MISR peptide.*

As can be seen from Figure 76, the oxidation levels of the NISTmAb digest remained unchanged in the range of 70-90%, reproducing the values obtained in the previous experiment. It was shown, that with a 10-fold higher amount of DT(L*)MISR spiked into the NISTmAb digest, the oxidation value was decreased further to 20%. However, a concentration of 5 mM free methionine did not reduce the amount

of DTLMISR oxidation in the NISTmAb sample. A concentration of 50 mM methionine achieved a similar effect as spiking in DT(L*)MISR in a 1x amount (Figure 76).
Interestingly, the levels of the synthetic peptide oxidation were always totally equal to the oxidation level of the NISTmAb peptide. Although the heavy labeled DT(L*)MISR shows a mass shift of +7.017 Da, the chemistry of the peptide is not changed and no distinction is made between the two chemically identical peptides. The observation that they get modified in the same amount suggests that the oxidation effect is related to the instrument.

Overall, the spiking experiments showed that free methionine [161] but also the DT(L*)MISR peptide scavenges oxidizing molecules and by this partially prevents the NISTmAb peptide from oxidation. This led to the assumption that the protein digest either encounters reaction with oxidative species or may get oxidized on a reactive surface in the Nano-HPLC instrument

Furthermore, it has been frequently described that biomolecules can get oxidized by metal catalyzed reactions [160, 162, 163]. Therefore, it was investigated, where in the Nano-HPLC device the protein digest can encounter contact with metal or other reactive surfaces.

3.3.6 Oxidation troubleshooting – Exchange of metal containing parts

In a next step, all metal containing parts in the Nano-HPLC configuration were exchanged. First, the 10-port switching valve in the column oven consisting of titan/stainless steel was replaced by a PEEK valve. Second, the 6-port PEEK valve of the autosampler was removed and a new PEEK valve was implemented.
Furthermore, the trap cartridge was removed, as the cartridge contains a frit of unknown material. Instead of the cartridge an Acclaim™ PepMap™ nanotrap column was installed into the column oven. Also the installed analytical Acclaim™ PepMap™ column (Nr. 1) was replaced by a new column with the same material an dimensions (Nr. 2). With the new configuration reduced oxidation values of approximately 15% were found compared to the previously measured 65% for the old configuration. Although, the new results manifested significant improvement of the method, the determined oxidation values were still far from the value of 3-5% Met oxidation reported for NISTmAb. [164]
Furthermore, an on-column oxidation was observed with the Acclaim™ PepMap™ column which has been published recently by Dong *et al.* [165].

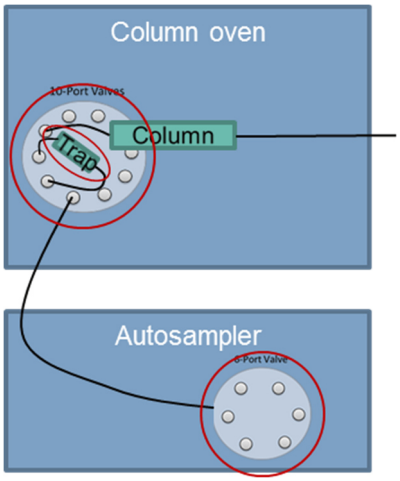

Exchange of several parts in configuration

	Before	Changed to
10-port valve column oven	titan/ stainless steel	PEEK
Column	Nr. 1 (Acclaim™ PepMap™)	Nr. 2 (Acclaim™ PepMap™)
Trap	Acclaim™ PepMap™ Cartridge	Acclaim™ PepMap™ Nanotrap column
6-port valve autosampler	PEEK valve	New PEEK valve

Figure 77 – Exchange of different parts in the nano-LC configuration

The titan/stainless steel 10-port valve of the column oven was removed and instead of this a PEEK valve installed. The 6-port valve of the autosampler was exchanged by a new PEEK valve. Furthermore, the trap cartridge was removed and a nano-trap column installed instead.

On-column oxidations can be distinguished from in-source oxidations and in-sample oxidations based on their retention times as shown in Figure 78. Thus, peptide oxidations that are present in the sample prior chromatographic separation elute in a defined peak 1 separated from the non-modified peptides (peak 2). Oxidations that co-elute with the non-modified peptide (peak 2), are produced after chromatography and therefore called in-source oxidation. As in this case the oxidation is introduced in the source, and thus, after the column, no separation is observed. However, oxidations observed in-between the peak 1 and the non-modified peak 2 are assumed to be oxidation artifacts of non-modified peptides produced during their passage through the column (on-column oxidation).

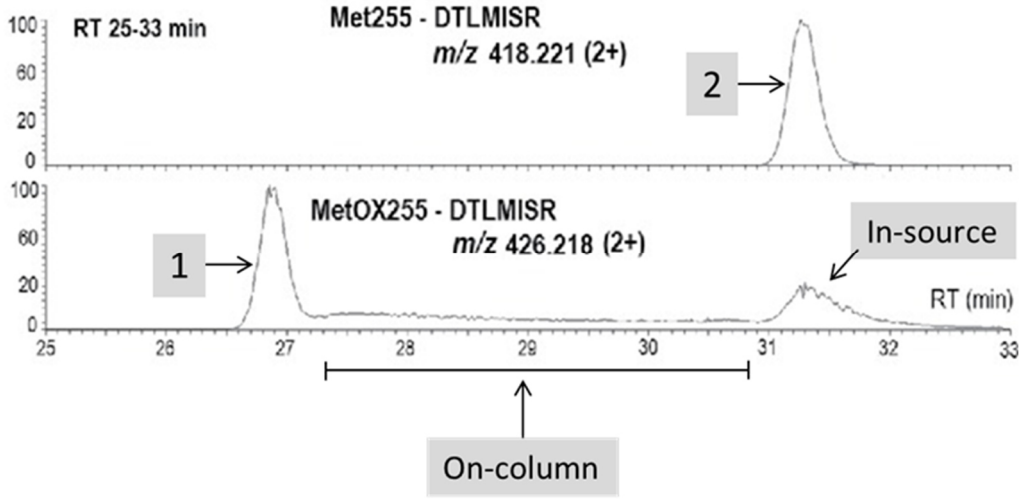

Figure 78 – Differentiation between in-source, on-column and real sample oxidation

Peak 1 represents the oxidized DTLmISR peptide, which is chromatographically separated from the native DTLMISR peptide in peak 2. The oxidized DTLmISR that co-elutes with the native peptide is produced in the source and thus, not separated from the unmodified peptide. The oxidized peptide that elutes in between peak 1 and 2 is produced during the passage of the non-modified peptide through the column (modified from Dong et al. [165]).

Thus, as for the newly installed column Nr. 2 on-column oxidations was observed, it was tested whether the oxidation levels can be reduced with another new Acclaim™ PepMap™ column (Nr. 3). As can be seen from Figure 79 the opposite was the case.

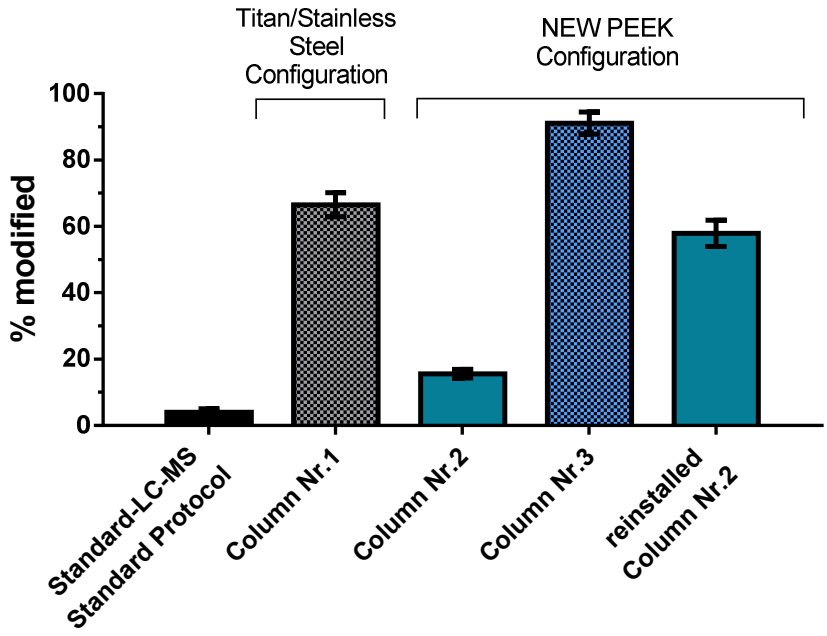

Figure 79 – Comparison of old and new configuration and comparison of different columns

Using the new configuration and column-2 reduced oxidation values of 15% were observed compared to the stainless/steel configuration (65%). However, as the value was still much higher than the expected 3 – 4% from the standard LC-MS device another column was tested. For column-3 extremely high values of 90% were observed. Reinstallation of column-2 also revealed high values of 60%.

For unknown reasons, the oxidation values were extremely high again after the insertion of column Nr.3. Therefore, column Nr. 2 was reinstalled. However, also for this column the oxidation value was again in the range of 60%.

A preventative maintenance was performed including the exchange of capillaries, seals and frits for the whole nano-LC device. After this, the oxidation value was again in the range of 18%, as shown in Figure 80. With the reduction of the column temperature from 45°C to 35° the oxidation levels were reduced to 13%.

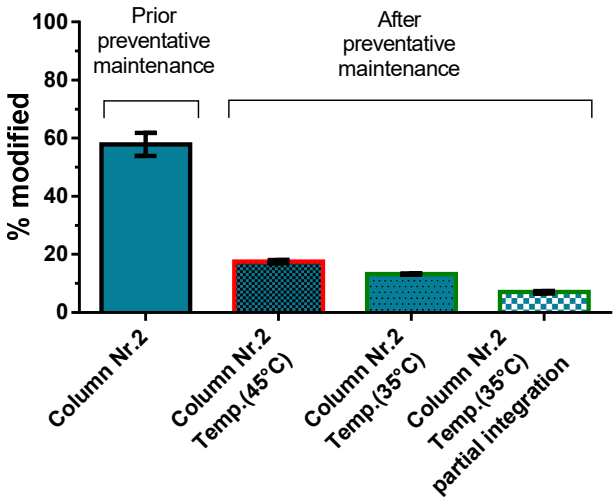

Figure 80 – Oxidation values prior and after preventative maintenance

After the preventative maintenance the oxidation value was at 18% for a column temperature of 45°C and 13% for 35°C. By assuming the peak shape of the oxidized peptide by a partial integration an oxidation of 7% was observed.

As can be seen from Figure 81, still a high amount of on-column oxidation was observed. In case of a partial integration of the peak without the on-column oxidation, level of oxidation was at 7%.

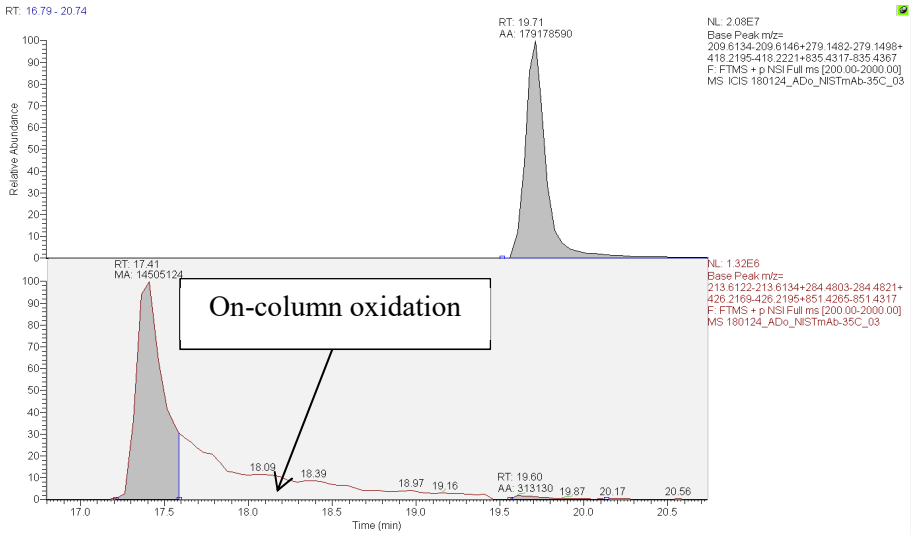

Figure 81 – Partial integration of oxidized peak

For the oxidized peptide a large portion of on-column oxidation occurs. Therefore, a partial integration of the modified peak was performed by assuming the "real" peak shape.

Thus, it is assumed, that the column material might be responsible for the partial oxidation. The Acclaim™ PepMap™ columns are widely used in the field of proteomics, where the level of modifications is of minor interest. The focus in proteomics is more on the identification of peptides and proteins than on the characterization. Thus, this might be no problem for Proteomics researches but it is the case for full characterization of antibodies and quantification of amino acid modifications.
Therefore, alternative column materials were investigated.

3.3.7 Oxidation troubleshooting – Waters BEH-columns

Thermo was the only supplier, delivering special Nano-fittings with a low dead volume called NanoViper™ (Figure 82). However, recently Waters developed a similar type of connection and brought on the market its widely used peptide BEH columns in Nano-scale format with suitable Nano-fittings [166].

A B

Figure 82 – NanoViper™ and ZenFit connections

A) NanoViper™ fittings from Thermo. B) ZenFit fittings from Waters

With this, it became possible to test different column materials than the previously used Acclaim™ PepMap™ material from Thermo. The BEH columns from Waters are used for the LC-MS analysis in the peptide map reference protocol described in Table 15, where no on-column oxidation is observed. Thus, it was expected that with the new column material, the issue of on-column oxidations might be solved. Therefore, the column dimensions listed in Table 16 and a gradient of 120 min (see Table 5 in section 2.6.10) was used for separation of peptides.

Table 16 – BEH-column dimensions

	Starting conditions
Column Diameter	0.075 mm
Column length	250 mm
Particle Size	1.7 µm
Column	35°C
Solvent A	H_2O + 0.1% FA
Solvent B	ACN + 0.1% FA
Loading solvent	H_2O + 0.1% TFA
Loading Flow rate	15 µL/min
Trap Column	BEH-NanoTrap

Using the new Waters BEH columns no on-column oxidation was observed (Figure 83) and the measured values of DTLMISR oxidation for a NISTmAb digest were 8-10%. Although, the oxidation values were reduced compared to the Acclaim™ PepMap™ columns, they were still slightly higher than the reported Met oxidation values of 3-5% for NISTmAb [164].

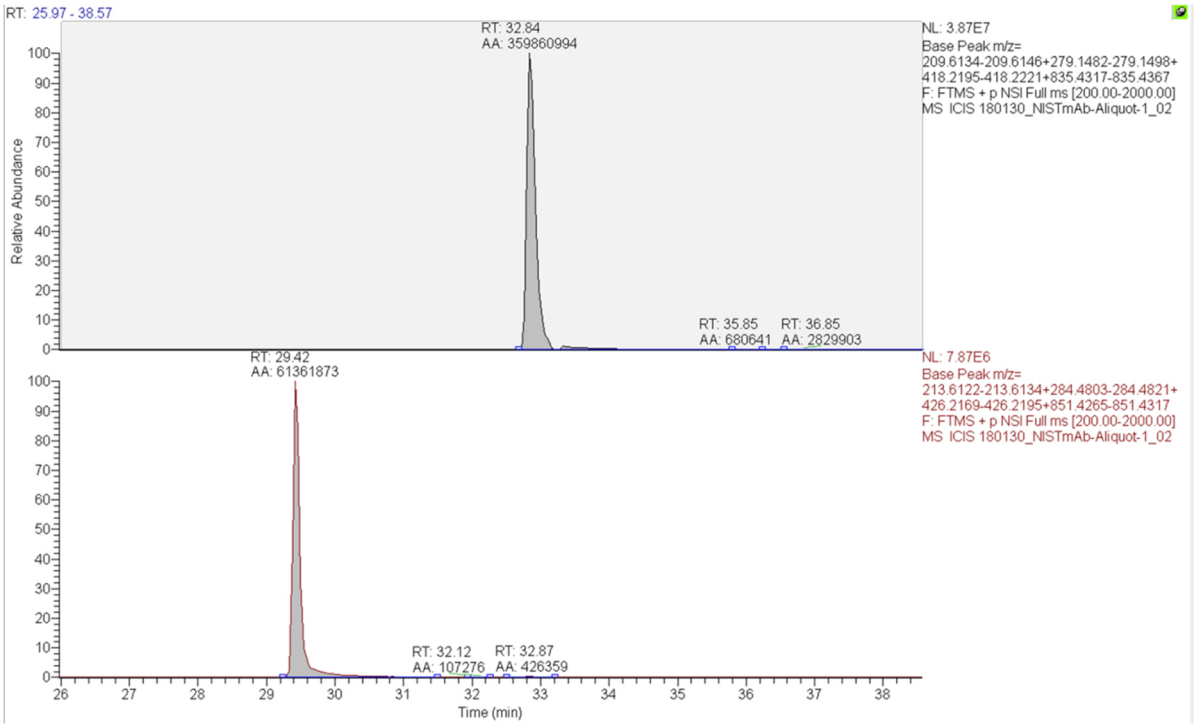

Figure 83 – Oxidation results on Waters column

Using the new Waters BEH column no on-column oxidation was observed.

Furthermore, a relatively high variability in the measured oxidation, independent of the chronological measuring order was observed (Figure 84).

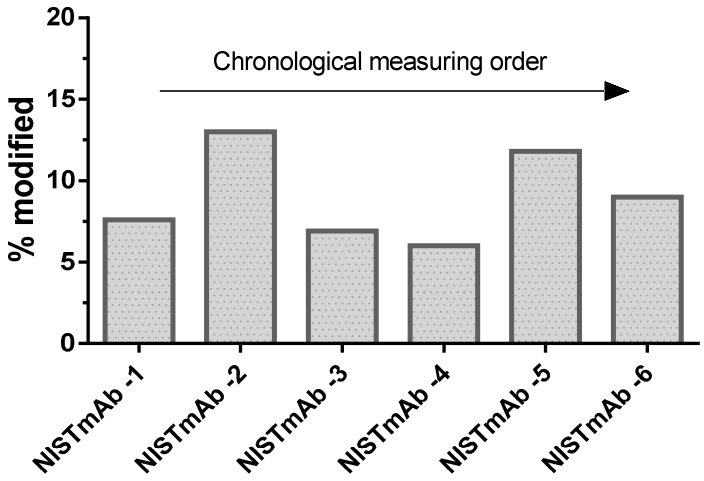

Figure 84 – High variability of oxidation values on the Waters BEH column

Although the oxidation levels were reduced compared to the previously used Acclaim™ PepMap™ columns, independent on the chronological measuring order still a high variation in the oxidation values was measured.

It was investigated whether the absolute amount of injected sample might influence the oxidation and whether the composition of the loading solvent influences the results. Therefore, it was tested whether

the addition of methionine to the loading solvent might scavenge oxidative species and by this leads to more reproducible values. Each concentration described in Table 17 was measured in duplicates.

Table 17 – Overview of different tested sample concentrations and loading solvents

Concentration	Injection volume	Injected amount
C1 = 0.5 µg/µL	V(inj.) = 0.5 µL	m(inj.) = 250 ng
C2 = 0.05 µg/µL	V(inj.) = 2.0 µL	m(inj.) = 100 ng
C2 = 0.005 µg/µL	V(inj.) = 6.0 µL	m(inj.) = 30 ng
Different loading solvents tested:		
A: H_2O + 0.1% **TFA**	**B:** 50 mM Methionine + 0.1% **TFA**	**C:** 50 mM Methionine + 0.1% **FA**

As can be seen from Figure 85 the observed modification levels were all in the range of 2 – 5%, independent on the loading solvent, which is consistent with the reported values for the NISTmAb [164]. However, the addition of 50 mM methionine to the loading solvent was not required, as low oxidation values were observed also in the case of the loading solvent A, which contained no methionine.

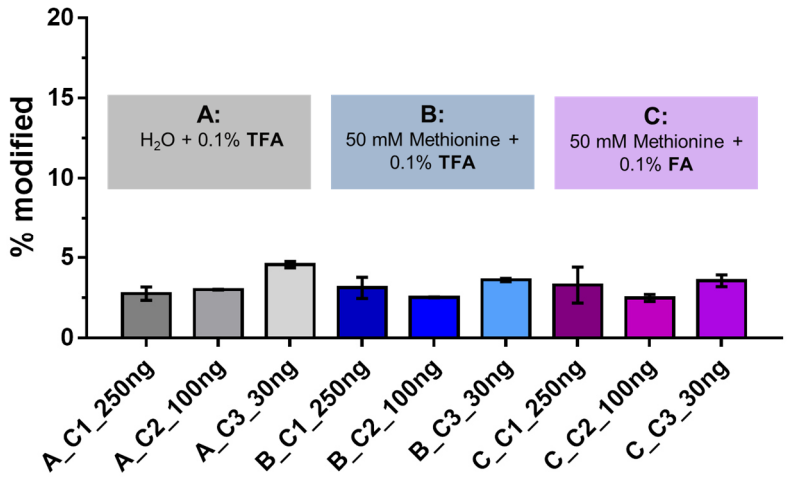

Figure 85 – Different absolute amounts and loading solvents

For all tested absolute amounts very low oxidation values were observed independent on the loading solvent used.

Furthermore, no difference between the loading solvent containing TFA and FA was observed. TFA is well-known to improve the peak shape but has the side effect of ion suppression in the mass spectrometer and therefore reduces intensity [167, 168]. Thus, it was decided to use 0.1% FA in order to prevent ion suppression effects (the analysis of low sample amounts would require significant intensity of the signal, therefore the agents reducing the intensity should be avoided).

Interestingly, no dependency of the oxidation value on the absolute amount of mAb injected onto the column was observed. However, it can be concluded based on the experiments prior the preventative maintenance that a saturation level of the injected sample was already reached, as spiking in scavenger molecules reduced the levels of DTLMISR oxidation in NISTmAb digest. These results suggest, that the previously observed oxidation effect have likely been resolved by the exchange of frits, seals and capillaries.

3.3.8 Reinstallation of titan/stainless steel valve and conclusion

However, the described results were contradictory to some extent. In the beginning the assumption that the titan/stainless steel valve might be responsible for the high oxidation values was confirmed, as the oxidation values were dramatically decreased from 65 to 15%. Conversely, this assumption was then invalidated by the fact that, after the column exchanges again high oxidation values were observed.

In order to isolate the factors responsible for the high levels of oxidation, in the next step the default 10-port titan/stainless steel valve was reinstalled.
Using the titan/stainless steel valve oxidation values were still low manifesting the fact that the valve was not responsible for the high oxidation values. As after the preventative maintenance the oxidation values were reduced to 15 to 17% on the Acclaim™ PepMap™ columns, it was assumed that one of the frits, capillaries or seals might have caused the high oxidation values. However, for the Acclaim™ PepMap™ material still a considerable amount of on-column oxidation was observed and the oxidation value could not be reduced further than 15%. With the installation of the Waters BEH-columns the measured oxidation values were finally consistent with those reported for NISTmAb.

Overall, the results show that the exchange of frits, capillaries and seals in combination with the new column material resolved the observed problem. The discrepancy in the results could arise from the fact that probably not a single factor, but a combination of several factors was responsible for the observed high oxidation values.

As final platform the conditions listed in Table 18 and a gradient of 120 min (see Table 5 in section 2.6.10) was used for separation of peptides.

Table 18 – Final column dimensions and solvent conditions

	Starting conditions
Column Diameter	0.075 mm
Column length	250 mm
Particle Size	1.7 µm
Column	35°C
Solvent A	H_2O + 0.1% FA
Solvent B	ACN + 0.1% FA
Loading solvent	H_2O + 0.1% FA
Loading Flow rate	15 µL/min
Trap Column	Waters NanoTrap

Overall, with the Nano-flow device and the final settings a 300-fold increase in sensitivity was achieved as can be seen in Figure 86.

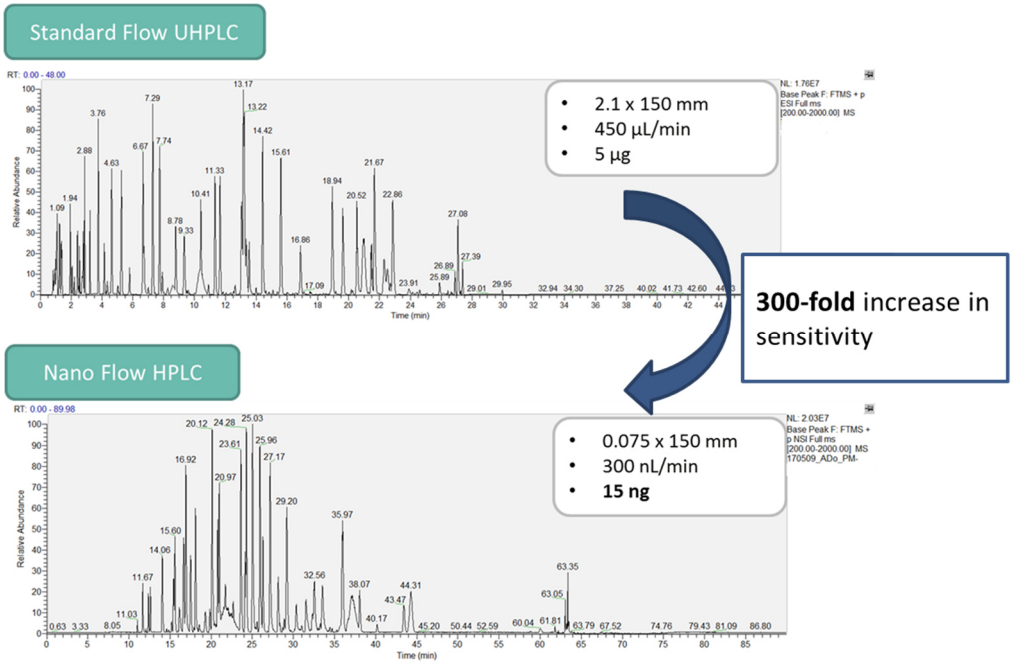

Figure 86 – Comparison between standard flow UHPLC and nano flow HPLC

There is a high increase in sensitivity when switching from a standard flow HPLC to a nano-LC device. Changing the column inner diameter from 2.1 mm to 0.075 mm yields a reduction in sample consumption from 5 µg to 15 ng.

This is lower, than the theoretically calculated one of 784, but the difference can be explained by the fact, that the equation only considers the column diameter (equation 10). However, to enable the change

to nano-flow conditions, separation is performed on a special instrument (Thermo UltiMate™ 3000 RSCLnano System and Thermo Orbitrap Velos Pro) and with this the whole setup is changed.

$$f = \frac{2.1mm^2}{0.075mm^2} = 784 \tag{10}$$

Many factors such as connections, tubings, capillary length, pumping system and many more are changed with the switch to a different instrument. However, those factors are not considered in the equation. Nevertheless, it can give an overall estimation of the potential increase that could be achieved.

3.4 Evaluation of the *in-vivo* characterization workflow

As demonstrated in chapter 3.1.6, the antibody capture proceeds in an unbiased way and does not favor a specific modification. However, in order to show that the previously developed workflow, including antibody capture, sample preparation and final LC-MS analysis does not introduce any artificial modifications a validation strategy was established. For this, two differently treated sample types, shown in Figure 87, were prepared and analyzed for peptide modifications. The NISTmAb was spiked in water to a final concentration of 10 ng/µL and each sample type includes five replicates of the analysis.

Sample type	Performed Analysis			To Proove
Capture + PepMap	**Capture**	**Sample Preparation**	**LC/MS-Analysis**	Efficency of capture protocol using defined amount of NISTmAb.
PepMap only		**Sample Preparation**	**LC/MS-Analysis**	That the capture process is native by comparing captured to non-captured NISTmAb. That the sample preparation is native as NISTmAb is fully characterized.
	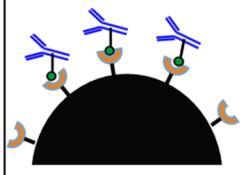 SPECIFIC IMMUNO CAPTURE	 PEPTIDE MIXTURE	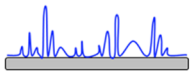 LC SEPARATION 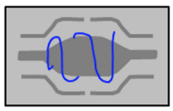 MS/MS ANALYSIS	

Figure 87 – Workflow validation strategy

To demonstrate that the individual steps of the workflow are native, two sample types were compared to each other. The "Capture + PepMap" map samples were captured and digested, whereas the "PepMap only" samples were not captured. A comparison of the modification levels of both sample types should reveal the same values.

The "Capture + PepMap" samples undergone the whole workflow including capture, digestion and LC-MS analysis and were prepared on five individual days. In contrast to this, the "PepMap only" samples were not captured, and therefore digested and analyzed directly and all prepared on one day. To investigate whether the capture protocol is native, the modification levels for sample type 1 (Capture + PepMap) and 2 (PepMap only) should be the same.

Thus, for each peptide modification – listed in Table 19 – an unpaired t-test between the "Capture+PepMap" and the "Pep-Map only" samples was performed and a confidence interval of 95% and a level of significance of 0.05 were chosen.

As can be seen in Table 19, the comparison of variances in the F-test revealed no statistical difference for most of the modifications, except for W280_ox (p = 0.0037). Notably, the standard error of mean (SEM) of the "PepMap only" samples for this modification is much lower (SEM = 0.04%) than for all other peptide measurements, which could explain this outlier result of the F-test. Thus, although the SEM of the "Capture + PepMap" with 0.2% is significantly different from the one for the "PepMap only" sample, this result is likely an artefact and and its interpretation should be taken with care. In contrast to the five replicates of "Capture + PepMap" that were all prepared and measured on different days, the replicates of the "PepMap only" samples were prepared and measured on the same day. Thus, for the "PepMap only" samples no interday variability is included, which likely resulted in the observation of the low error. However, for all other peptides the F-test revealed no statistically significant difference between the two sample groups.

Table 19 – Statistical analysis using an unpaired t-test

	Unpaired t-test (two-tailed)						F-test	
Peptide	P value	t, df	Mean ± SEM		95% confidence interval	R squared	F, DFn, Dfd	P value
			PepMap Only	Capture + PepMap				
M87_ox	0.2345	t=1.286 df=8	4.2 ± 0.4 n=5	3.2 ± 0.6, n=5	-2.6 to 0.7	0.1713	3.073, 4, 4	0.3024
M255_ox	0.0002*	t=6.701 df=8	6.2 ± 0.1, n=5	4.8 ± 0.1, n=5	-1.9 to -0.9	0.8488	1.063, 4, 4	0.9539
M431_ox	0.295	t=1.120 df=8	5.9 ± 0.5, n=5	5 ± 2, n=5	-3.8 to 1.3	0.1356	3.964, 4, 4	0.2108
W280_ox	0.6336	t=0.4955 df=8	1.60 ± 0.04, n=5	1.5 ± 0.2, n=5	-0.6 to 0.4	0.02977	39.06, 4, 4	0.0037*
W316_ox	0.9771	t=0.0295 6 df=8	1.6 ± 0.2, n=5	1.5 ± 0.3, n=5	-0.9 to 0.9	0.0001092	3.104, 4, 4	0.2983
N136_deam	0.0937	t=1.902 df=8	0.60 ± 0.03, n=5	0.49 ± 0.05, n=5	-0.2 to 0.02	0.3114	2.469, 4, 4	0.4027
N318_deam	0.1275	t=1.700 df=8	3.6 ± 0.4, n=5	2.7 ± 0.3, n=5	-2.0 to 0.3	0.2655	2.855, 4, 4	0.3339
N387_deam	0.0006*	t=5.489 df=8	4.1 ± 0.3, n=5	2.4 ± 0.1, n=5	-2.3 to -0.9	0.7902	3.089, 4, 4	0.3003
N392_deam	0.3151	t=1.072 df=8	2.2 ± 0.2, n=5	2.6 ± 0.3, n=5	-0.5 to 1.3	0.1256	3.189, 4, 4	0.2875

For the t-test no statistically significant difference between the two sample groups was found for the oxidations (on M87, M431, W280 and W316) and deamidations (on N136, N318 and N392). This means that the samples that went through the whole workflow revealed the same levels as the samples that were digested without prior capture procedure. In other words, the results demonstrate that the capture process does not introduce additional modifications.

Only for the oxidation on M255 (DTLMISR) and the deamidation on N387 the t-test revealed statistical significant differences, with p = 0.0002 and p = 0.0006. However, in both cases, the level of modification was higher for the samples that were digested only. If the sample preparation workflow itself would be responsible for the increased modification values, they should be also observed in the samples that were captured prior the digestion. This inconsistency in the results can be explained by the fact that the five replicates of the "PepMap only" sample were prepared from different NISTmAb starting material than those that were captured and digested. Thus, it is highly likely that the NISTmAb aliquot used for the "PepMap only" samples initially showed slightly elevated modification probably due to the freeze-thaw cycles that the aliquot went through. However, these observations do not influence the conclusion that the workflow does not introduce any artificial modifications.

To further demonstrate that the whole workflow is native, the values were then compared to the modification levels reported by Li *et al.* from an interlaboratory NISTmAb PTM characterization study [53]. In this study, three different laboratories, named Lab-1, Lab-2 and Lab-3, analyzed the PTMs of the NISTmAb reference material by their individual peptide mapping procedures and the results are displayed in Figure 88.

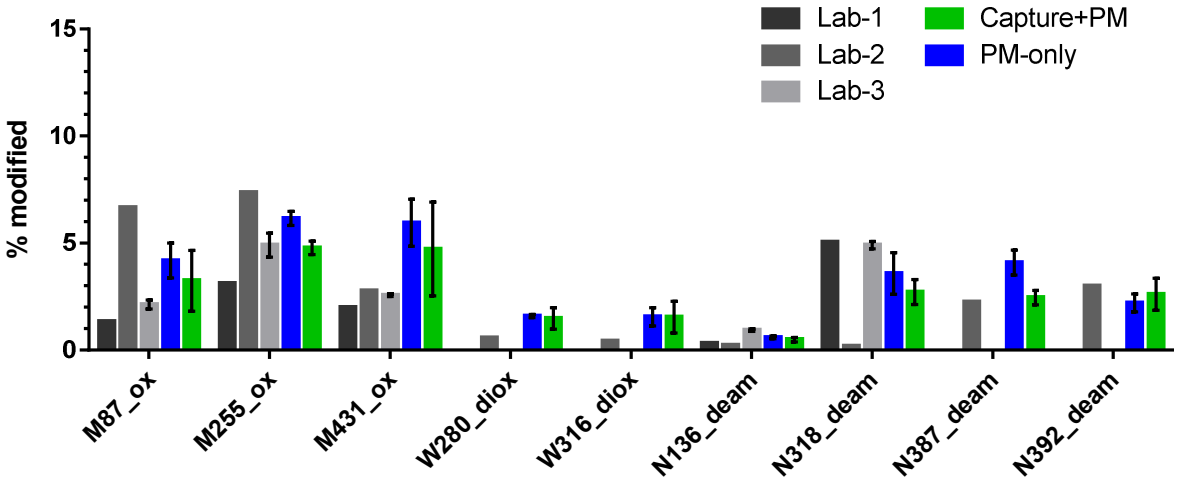

Figure 88 – Comparison of the two sample types with the interlaboratory study

The NISTmAb modification levels of the "Capture+PepMap" (green) and the "PepMap only" (blue) samples are consistent with the values reported by Lab-1, -2 and -3 from the interlaboratory study reported by Li et al. [53]

Laboratory 1 and 2 generated their results based on a single analysis, whereas Lab-3 performed triplicate analyses from separate digests, with the same protocol and thus includes error bars. Overall, it should be highlighted that the reported values of the three labs show inherent fluctuations due to the differences in sample preparation and evaluation conditions.

As can be seen from Figure 88, the modification levels of both sample types “Capture+PepMap” (green) and “PepMap only” (blue) are in good agreement with the values reported by the different laboratories of the interlaboratory study (grey).
Methionine oxidation at the position 87 (M87_ox) of the “PepMap only” and the “Capture+PepMap” samples was found to be in between the values of Lab-2 and 3. The highest oxidation values were observed for the DTLMISR (M255_ox) and the WQQ-peptide (M431_ox), which are known to be the most susceptible oxidation sites [62, 64]. For the DTLMISR peptide of both sample types (“blue” and “green”), the oxidation values were consistent with the ones reported by Lab-2 and Lab3.

The oxidation at the WQQ-peptide (M431_ox) was significantly higher for both sample types compared to the results from the study. This difference in the results may arise from the fact, that quantification of methionine oxidation is not that trivial. Several studies reported a complex elution behavior of peptides containing methionine oxidation [165]. Furthermore, it should be considered, that in this thesis a 100-fold (for Labs 1 and 3) to 500-fold (Lab 2) lower amount of NISTmAb was used and therefore a significantly lower concentrated sample. This might have contributed to the slightly higher values for some modifications. Regarding the tryptophane dioxidations at W280 and W316 it should be pointed out, that Lab-1 and 3 did not include dioxidations in their search parameters.

The highest deamidation values were observed for N318 and N387 which is consistent with literature as for both peptides the amino acid following the asparagine is a glycine. The NG-motif is known to deamidate readily due to minimal steric hindrance by the small amino acid glycine [53, 81].
As can be seen from Figure 88 for N318_deam the values of the “PepMap only” and the “Capture+PepMap” samples are in agreement with the values generated by Lab-1 and -2. In contrast to this, the values of the N387_deam are not consistent with the ones reported by the three labs. Lab-1 and Lab-3 were not able to discriminate between the deamidation on N387 and N392 and thus reported a summed deamidation value for the PENNYK-peptide (containing both deamidation sites). Lab 1 calculated 2.62% and lab-3 0.67% PENNYK deamidation.
Overall, accurate quantification of deamidation is challenging, as a clear separation from the main peak is required to be able to discriminate between the modified and non-modified peptide. Due to the low mass difference of only 0.989 Da for deamidated to non-deamidated peptides, the first isotopic peak of the deamidated peptide interferes with the second isotopic peak of the non-modified peptide as can be seen in Figure 89. [80]

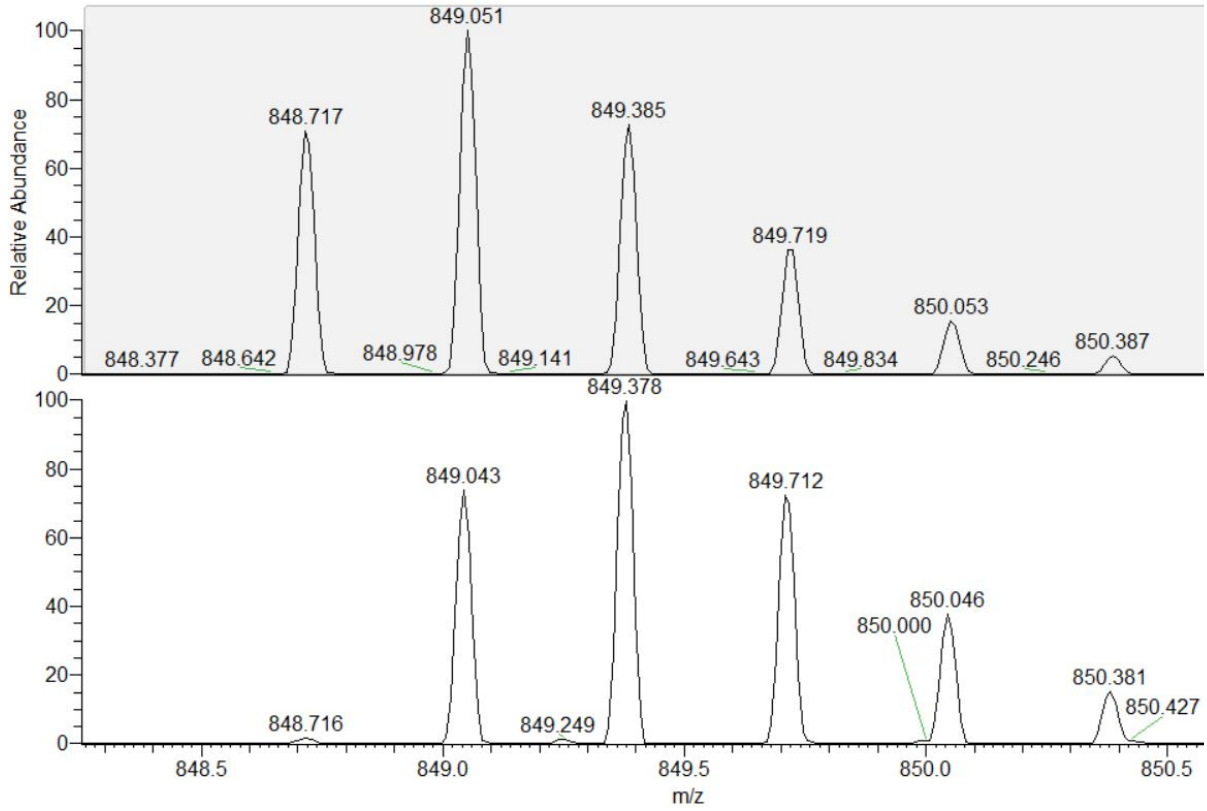

Figure 89 – Isotopic peak interference between native and deamidated PENNYK-peptide

The second isotopic peak of the non-modified PENNYK-peptide (upper XIC) interferes with the first isotopic peak of the deamidated PENNYK-peptide (lower XIC). The observed m/z difference of the two peaks is only 0.0048 with a z of 3.

The exact mass m of the non-modified ^{13}C isotope of the triply charged PENNYK-peptide (849.0498) has a mass difference Δm of 0.0048 to the ^{12}C isotope of the deamidated PENNYK-peptide (849.0450). According to equation 11 a high mass accuracy with an error of less than 5.6 ppm is required to discriminate between the modified and non-modified PENNYK-peptide in case of coelution of the peptides.

$$mass\ error = \frac{\Delta m}{m} \cdot 10^6 = \frac{0.0048}{849.0498} \cdot 10^6 = 5.6\ ppm \tag{11}$$

Generally, it is important to consider that all three labs used different quantification strategies which may account for substantial variances in the identified PTMs. Nevertheless, the results reported by the interlaboratory study provide an overall impression on the values generated by different labs.
In summary, the validation strategy revealed no significant difference between the two sample types and thus demonstrates that the workflow does not introduce artificial modifications.

3.5 Open Flow Microperfusion study

With the successful method development described in the previous chapters, the analysis of low concentrated *in-vivo* samples became possible. In the OFM study a therapeutic antibody was administered subcutaneously and extracted from the subcutis using the OFM technique (see also 2.6.4). Furthermore, serum samples were taken hourly.

Both types of biological samples, serum and ISF, were cleaned up using the developed capture protocol described in 2.6.6. In the next step the samples were digested using the optimized workflow developed for low sample amounts (2.6.8). Finally, separation of peptides and mass spectrometric analysis was performed using the final Nano-HPLC-MS/MS setup (see 2.6.10). An overview of the whole workflow is shown in Figure 90.

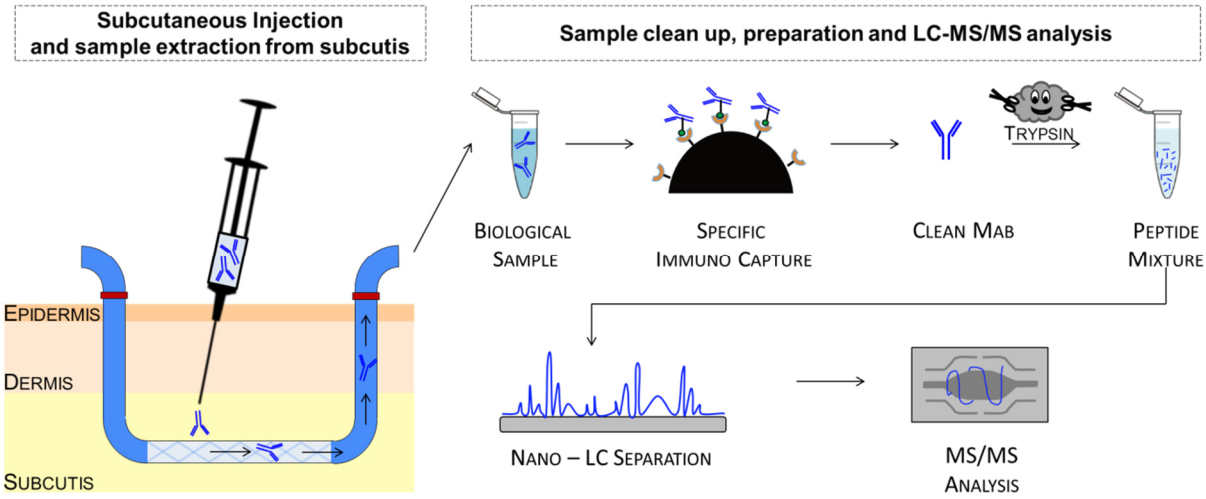

Figure 90 – From subcutaneous injection over sample clean up, preparation and final analysis

A therapeutic antibody was injected subcutaneously to a domestic pig and extracted from the subcutis by the application of the open flow microperfusion technique. Biological samples were cleaned up by immuno capture and prepared for nano-LC-MS/MS analysis using an optimized peptide map workflow.

Thus, the results presented in this chapter show whether it is possible to apply the OFM technique to extract therapeutic antibodies after subcutaneous injection from the subcutis. The goal is to obtain a better understanding of bioavailability of therapeutic mAbs by investigation of their biotransformation *in-vivo*.

3.5.1 Analysis of serum samples

First, the serum samples of the OFM study were analyzed by the developed workflow. As can be seen from Figure 91, for the first two hours the concentration of mAb-1 was below the limit of quantification (LOQ) of 6 ng/µL (The determination of mAb-1 concentration in serum and ISF samples was performed by Shirin Haas in the Bioanalytics group at AbbVie GmbH & Co. KG).

However, due to the increased sensitivity of the nano-LC-MS system even for those time points a few peptides were identified, displayed by the sequence coverage in Figure 91-B. After three hours, a quantifiable amount of the therapeutic antibody reached the circulation with the determined concentration of 8 to 10 ng/µL. LC-MS analyses revealed high sequence coverages for both LC (91.5-100%) and HC (94.5-100%), which means that the majority of the mAb sequence was identified (Figure 91-B).

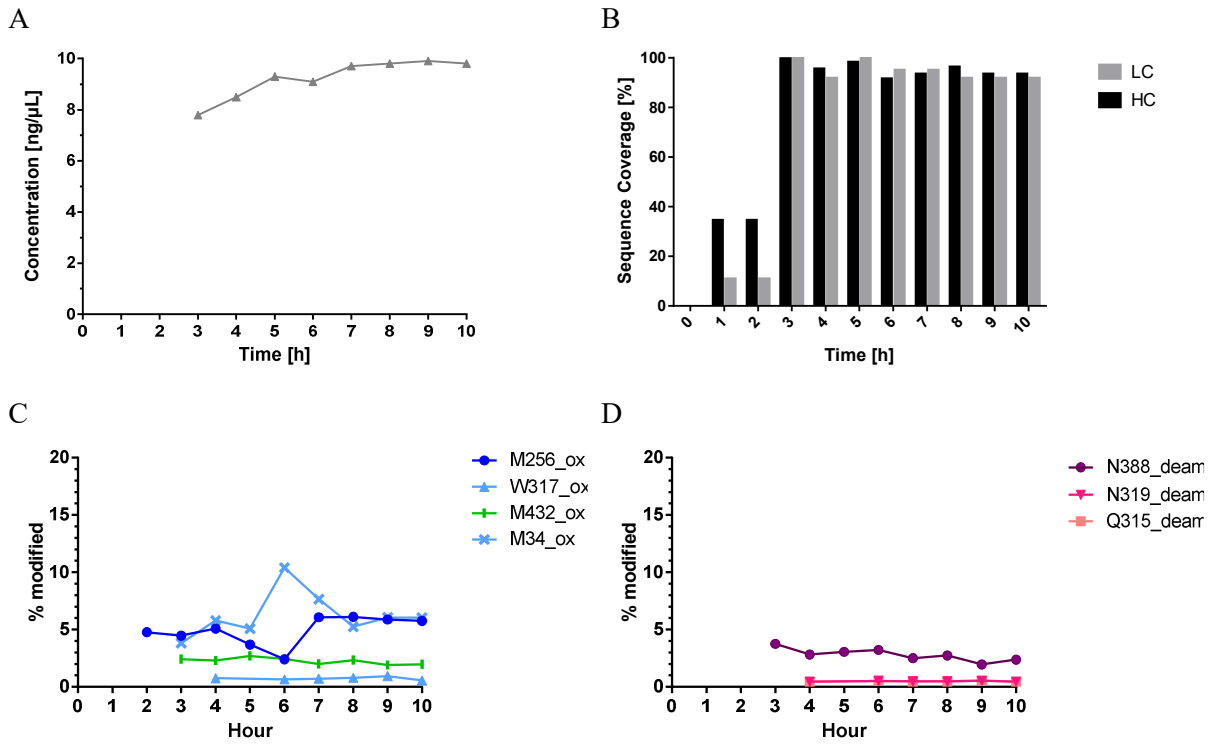

Figure 91 – Results of the serum samples

A) The concentrations in serum were in the range between 7 and 10 ng/µL. For time points T1h and T2h the concentration was below the level of quantification (6 ng/µL). B) For time points T3h-T10h very high sequence coverages for LC and HC were observed. C) Low abundant oxidations on tryptophanes and methionines were detected but remained unchanged over time. D) Three deamidated peptides were detected and found to remain stable for the 10h sample collection.

The level of modification for eg. M256_ox was quantified based on the equation 12.

$$\%_{M256\_ox} = \frac{XIC\ Area_{M256-oxidized}}{XIC\ Area_{M256-oxidized} + XIC\ Area_{M256-native}} \times 100 \quad (12)$$

Low abundant oxidations in the range of 0.5 – 1% and 2.5 -5.6% were detected for tryptophan (W317) and methionine (M256, M432, M34), respectively. According to the EU numbering, M256 and M432 correspond to the DTLMISR and WQQ-peptide. Thus, the observed oxidation sites are consistent with results published in literature as those residues are known to be preferentially oxidized [62-64]. Recently, Li and co-workers studied sequence-related modifications of a therapeutic mAb in human studies after intravenous injection and reported Fc methionine oxidation levels of 6 – 8.5% [140]. Also the observation that the levels of oxidation remain constant over the investigated time of 10 hours is consistent with recently published *in-vivo* studies [97].

Deamidation has been described to increase rapidly *in-vivo* from 5% to 35% during a time span of six weeks. As can be seen from Figure 91-D, the observed deamidations on N388, N319 and Q315 were in the range of 0.5 – 4% and remained constant over the 10 hours in serum. The initial value of 5% deamidation is consistent with the value observed in the serum samples.

Overall, the results show, that the developed workflow is suitable to capture and analyze therapeutic mAbs from serum samples after subcutaneous injections. In contrast to intravenous injections where the therapeutic mAbs are immediately present at high levels, the initial serum concentrations after subcutaneous injections significantly lower. Therefore, the implementation of a nano-flow HPLC device and a nano-spray source was essential to offer the required sensitivity. As nano-HPLC setups are usually less robust than standard flow systems, like the one used by Li et al. for the investigaton of modifications after intravenous injection [97, 140] a huge amount of work was invested to ensure that no artificial modifications are introduced by the setup (see chapter 3.4).

In summary, the observed levels of modification are consistent with published literature and did not reveal any unexpected results. However, it must be considered that the absorption process of antibodies after subcutaneous injection proceeds relatively slow. Thus, it normally takes 2 – 8 days until the maximal serum concentration is reached. [169] Therefore, serum sampling for several days or weeks would be necessary to investigate the transformation of mAbs in serum further.

3.5.2 Analysis of interstitial fluid samples

Lastly, the interstitial fluid samples from the OFM study were investigated. As can be seen from Figure 92 the ISF samples showed a different concentration/time-profile compared to the serum samples. The profiles of tubes A1, A2 and A3 are very similar and reveal a high concentration for the first time point (Figure 92-A). This can be explained by the fact that in case of tubes A and B the mAb is directly extracted 5 mm apart from the injection site and therefore immediately available in high concentrations after injection (Figure 92-D). However, as can be seen from Figure 92-B the concentration of the first time point for tubes B is much lower than for tubes A. It was expected, that the profile looks identical for tubes A and B, as both tube groups are located at the same distance from the injection site. In contrast to tubes A and B, tubes C were located 10 mm apart from the site of injection and thus showed much lower concentrations (Figure 92-C/D).

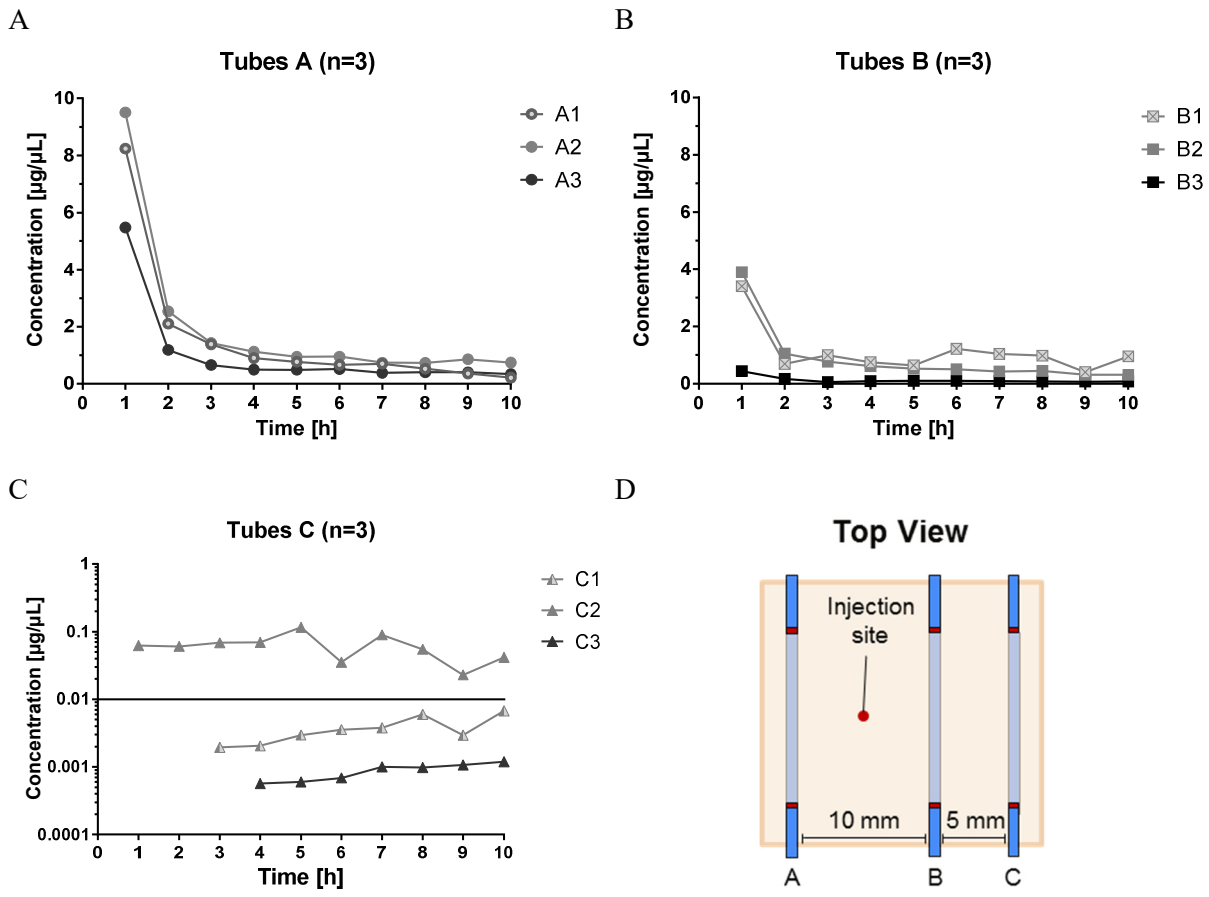

Figure 92 – Antibody concentration/time profiles for the different tubes

A) The concentration of tubes A was in the range between 6-10 ng/µL for the first time point, decreased after two hours to 1-2 ng/µL and remained nearly constant for the following time points. B) Tubes B showed a similar profile, but revealed lower concentrations for the first time point. The concentration of B3 was much lower than the concentrations of B1 and B2. C) Tubes C showed concentrations in the range between 0.5 ng/µL and 0.1 µg/µL, which was significantly lower than the concentrations of tubes A and B. D) Top View: Tubes A and B were 5 mm apart from the injection site, and tube C was 5 mm apart the tube B.

It needs to be considered, that the positioning of the individual tubes in the subcutis is performed manually. Slight variations in the distance of the tubes to each other, but also variations of the insertion depth might be a reason for the observed differences in the concentration profile. After two hours the concentration dropped down to 1 – 2 µg/µL for tubes A and B suggesting that the mAb has been distributed in the tissue. From the time point 3 to 10 hours the concentration remained nearly unchanged, which is consistent with the previously mentioned slow process of mAb absorption after subcutaneous injection. In order to eliminate concentration effects of the different time points, the samples of tubes A and B were diluted to a final concentration of 0.02 µg/µL prior antibody capture.
In contrast to tubes A and B, the mAb needs to migrate twice the distance to reach the tubes C which were located 10 mm apart from the site of injection. Furthermore, the mAb molecules have to cross tubes B to finally reach the third tube. However, as can be seen from Figure 92-C, it was possible to extract therapeutic mAbs from the subcutaneous tissue that migrated 10 mm through the subcutis.

For tubes A, tubes B and tube C2 high sequence coverages of LC (91.5 – 100%) and HC (94.5 – 100%) were detected for all time points, except time point 10 of tube A2 and B2 (Figure 93). The observed low sequence coverage for the point 10 was consistent with the low quality of the LC-MS/MS data. This could be explained by the incomplete desalting during the sample preparation procedure in this particular case, which would consequently reduce the efficiency of the trypsin digestion step. Due to the low sequence coverage, for the time point 10 samples a quantification of modifications was unfortunately not possible. Furthermore, for two samples of tube B3 (8 and 10 hours) the data could not be acquired due to the significant spray failure.
Nevertheless, all other samples revealed high sequence coverages. However, for tubes C, where the concentration of the peptides was significantly lower, compared to the other tubes, the majority of the antibody sequence was covered.

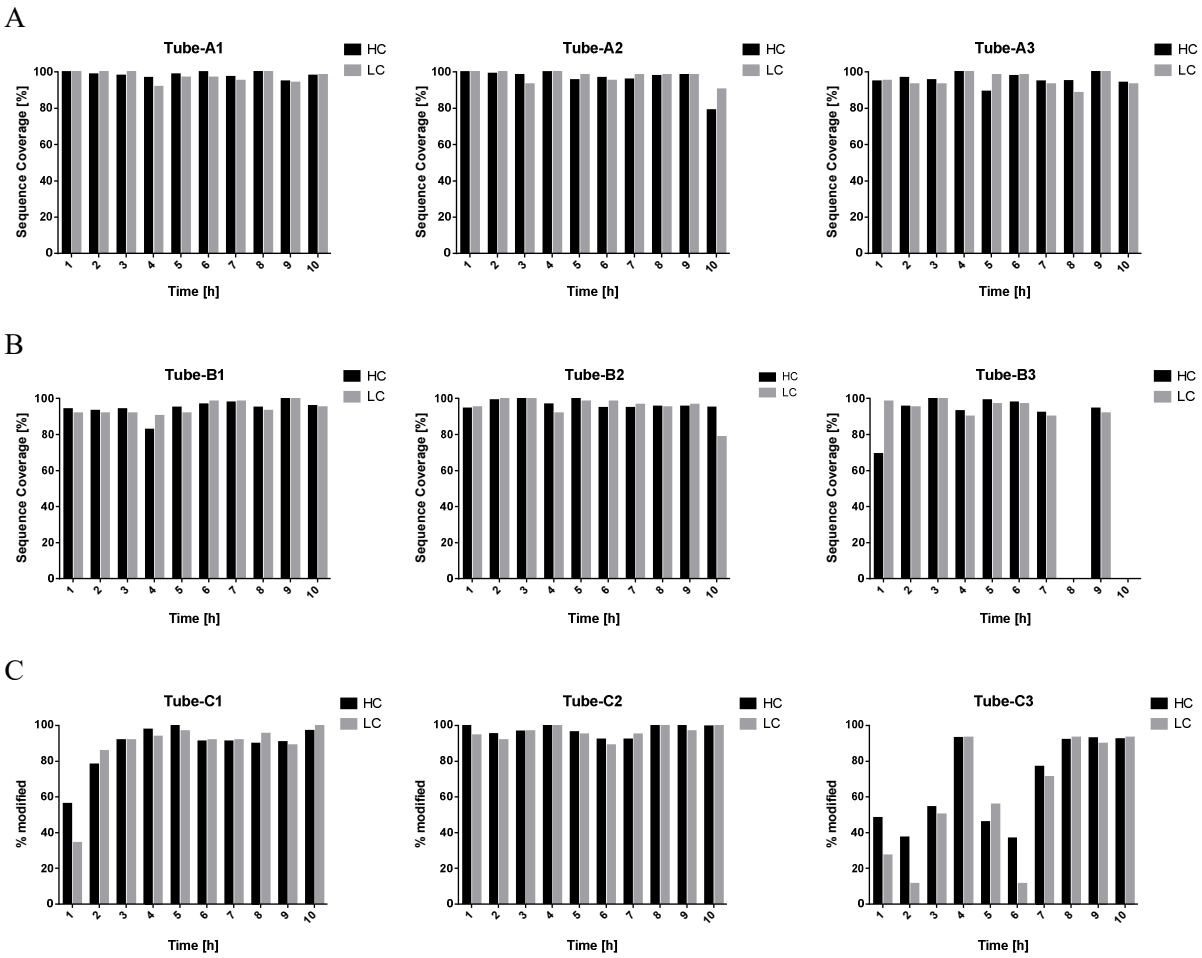

Figure 93 – Sequence coverage of all samples

A) The sequence coverage of all samples from Tube A1, A2 and A3 was in the range between 90-100%, except for the 10h time point of tube A2. B) For tubes B1, B2 and B3 also high coverages were detected. However, here time point 10 of Tube B2 and 1 of B3 showed lower values. In case of tube B3 time point 8 and 10 the acquisition of MS-spectra did not work due to a failure of the spray. C) Tube C1 and C2 revealed very good sequence coverages, although they were much lower concentrated. For the lowest concentrations of tube C3 it was also possible to find peptides.

The analysis of the peptide modifications revealed a high repeatability between tubes A1, A2 and A3. In Figure 94 the modification of selected peptides for the three tubes A were compared. The most susceptible peptide for oxidation, M256 (DTLMISR), revealed modification levels of 5% for all time points of tubes A1, A2 and A3.

Also the deamidation marker peptide PENNYK with the N388 showed highly similar results of 2 – 4% for all tubes A. Thus, as can be seen from Figure 94 a high repeatability of peptide modifications was observed for tubes A1, A2, and A3.

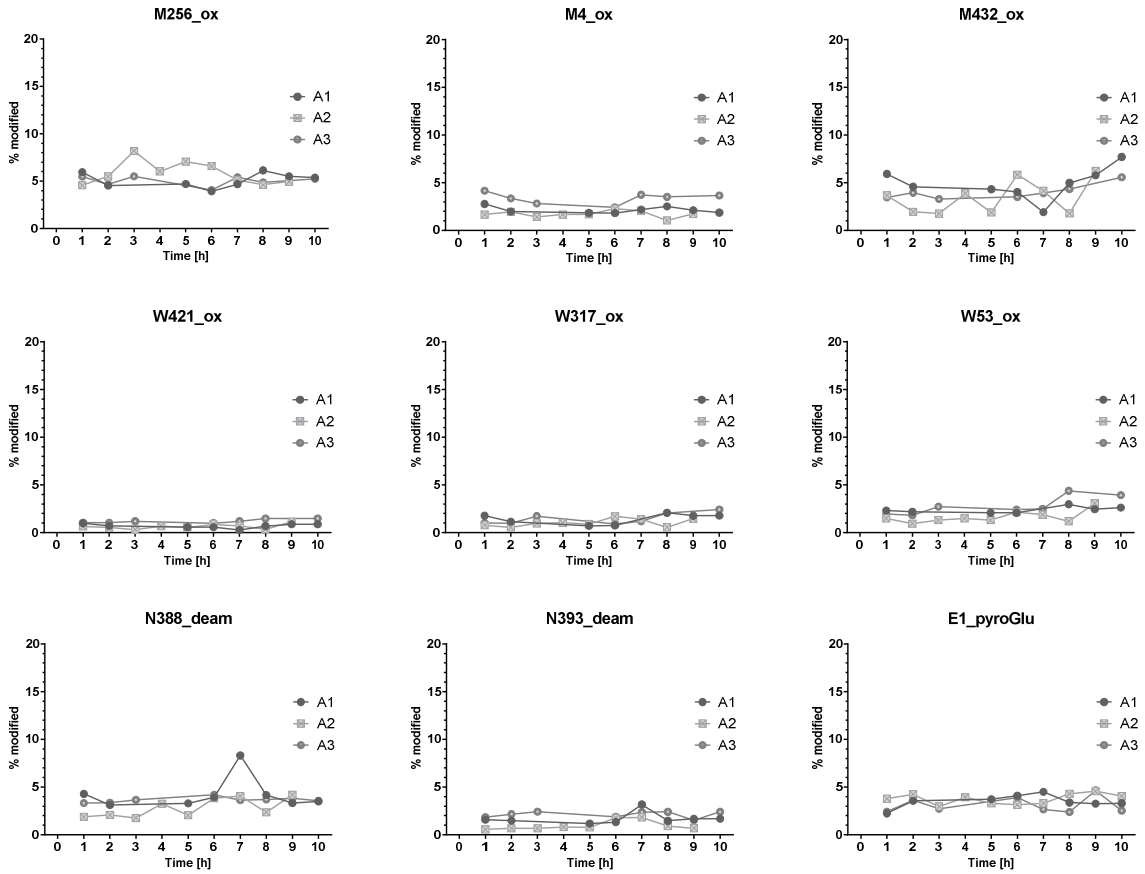

Figure 94 – Repeatability of peptide modifications for tubes A1, A2 and A3

The level of modification for selected peptides was highly similar for all three tubes A.

Therefore, the mean values and standard deviations of all tubes A are displayed in Figure 95. Similarly to the serum samples, the oxidations were in the range between 1 to 8% and remained constant (Figure 95-A). Consistent with this, also the observed deamidations did not show any trends and remained in the range of 0.1 to 5% and (Figure 95-B).

However, the concentrations were much higher for the samples from tubes A and B than the concentration for the serum samples and therefore, they were all diluted to a final concentration of 0.02 µg/µL. As a volume of 50 µL was used for the capture a total amount of 1 µg mAb was available for the OFM tubes A and B. In contrast to this, the absolute amount available for the serum samples was only 0.4 – 0.5 µg mAb. With the higher mAb amount from tubes A and B available for the analysis identification of the peptide modifications was easier due to the higher overall signal intensity. Thus, a higher number of oxidized and deamidated peptides could be identified for tubes A, than for the serum samples. However, the modification levels remained all constant and did not show any trends. Furthermore, it was possible to identify the glycosylation pattern by analysis of the glyco-peptides (Figure 95-C).

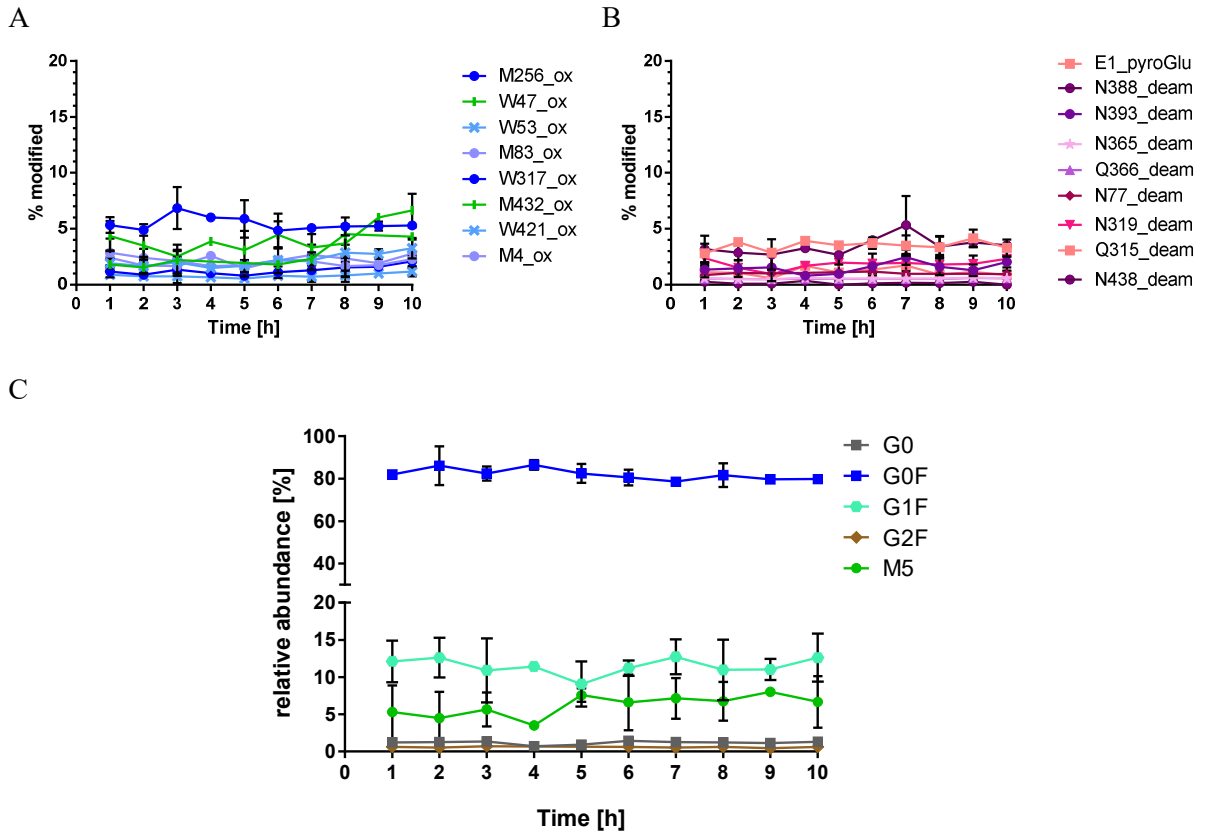

Figure 95 – Oxidation, deamidation and glycosylation pattern for tubes A

A) Several different methionine and tryptophan oxidations including the oxidation marker site M256 were detected and found to remain constant for tubes A. B) Asparagine and glutamine deamidations as well as the pyro-glutamic acid formation were found to stay constant for the first ten hours. C) Further, the analysis revealed five glycan species G0, G0F, G1F, G2F and M5. The level of the individual species did not change over time.

The relative abundance of the different glycan species was quantified manually. An extracted ion chromatogram was made for the different glycan species and the area of each species was used for the quantification by the following equation:

$$\%_{G0F} = \frac{XIC\ Area_{G0F}}{XIC\ Area_{G0F} + XIC\ Area_{G1F} + XIC\ Area_{G2F} + XIC\ Area_{G0} + XIC\ Area_{M5}} \times 100 \quad (13)$$

The main species G0F was found to be at 80% whereas the second most abundant glyco-form G1F was in the range between 10 – 15%. Also the high mannose species M5 and trace amounts of G0 and G2F could be identified.

Goetze *et al.* investigated a faster serum clearance for mAbs containing high mannose glycans (such as M5) compared to other species after 10 and 20 days [78]. As they presumed that mannose receptors contribute to the increased clearance rate of M5 glycans, it was interesting to investigate whether this phenomenon might be observed in the subcutaneous tissue directly after injection. However, as can be

seen from Figure 95-C the relative abundance of the M5-glycan species did not change over the first ten hours.

As can be seen from, Figure 96-A slightly higher variations were observed for the oxidized peptides of tubes B in contrast to the results of tubes A. However, the same peptide oxidation sites were found and remained constant over the first ten hours after injection. The results of peptide deamidation for tubes B showed the same reproducibility and are consistent with the previously described values for tubes A (Figure 96-B).

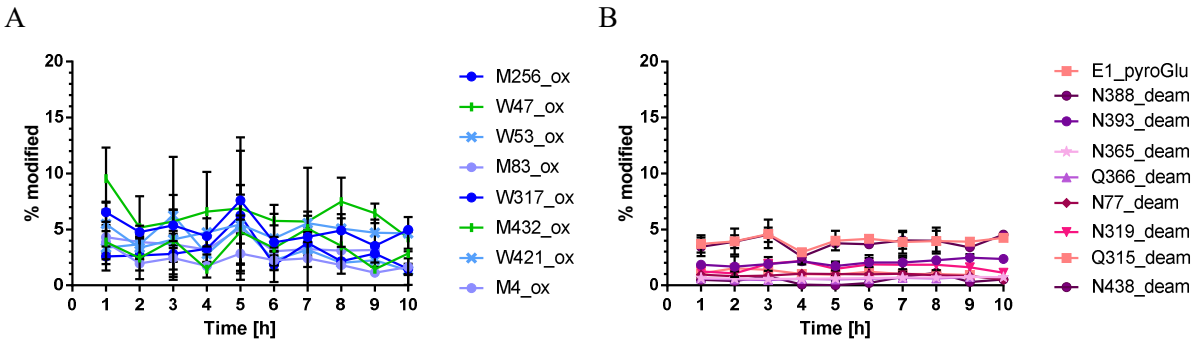

Figure 96 – Oxidation and deamidation levels for tubes B

A) For tubes B the same methionine and tryptophan oxidations were detected and found to remain constant as for tubes A. B) Also asparagine and glutamine deamidations as well as the pyro-glutamic acid formation were found to stay constant for the first ten hours.

Furthermore, the relative abundance of the glycoforms over time was in agreement with the values observed for tubes A, as can be seen in Figure 97.

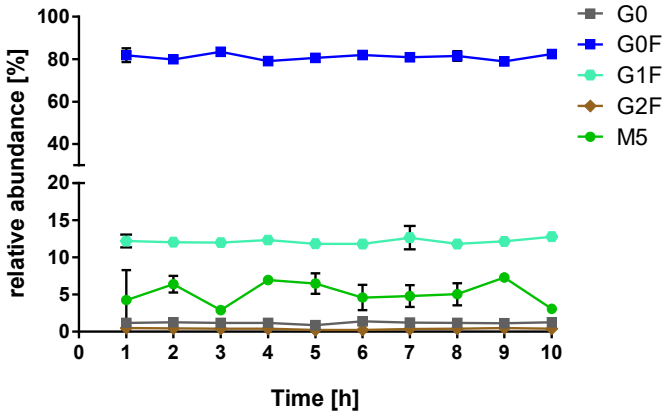

Figure 97 – Glycosylaton pattern for tubes B

The analysis revealed the same glycan species G0, G0F, G1F, G2F and M5 as for tubes A. The level of the individual species did not change over time.

Overall, the results met the expectations that the modification levels were similar for tubes A and B, as both tube groups are located at the same distance from the injection site. The values for oxidation, deamidation and the glycosylation pattern were highly reproducible for all tubes A and B.

For tubes C similar results were obtained as shown in Figure 98. The oxidation levels as well as the deamidation values remained constant for the first ten hours. This implies that the mAb molecule does not get modified during his 10 mm pathway through the subcutis and that the migration pathlength does not make any difference.

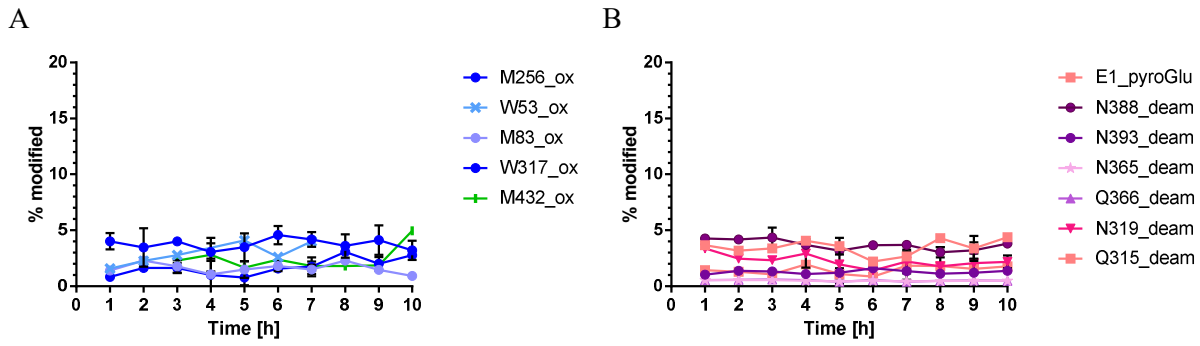

Figure 98 – Oxidation and deamidation levels for tubes C

A) Also for tubes C some methionine and tryptophan oxidations were detected and found to remain constant. B) Deamidations as well as the pyro-glutamic acid formation were below 5% and found to stay constant for the first ten hours.

Also for tubes C the different glycans species were detected and found to remain constant over time (see Figure 99).

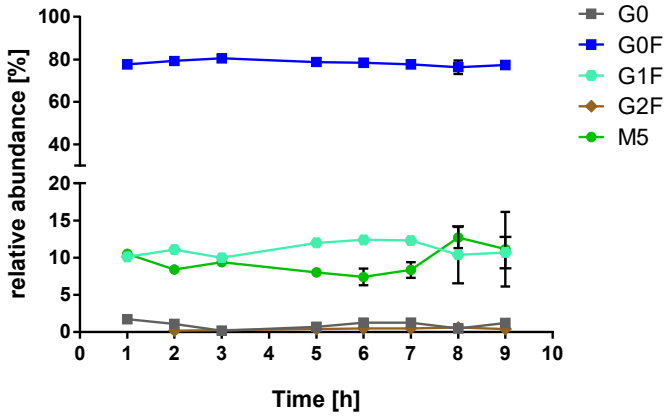

Figure 99 – Glycosylation pattern for tubes C

For tubes C, were the concentration was significantly lower, the same levels of the different glycan species G0, G0F, G1F, G2F and M5were identified and did not change over time.

So far, biotransformation of therapeutic mAbs has been studied several times in blood [83-85, 92, 97]. However, no published study has focused yet on the mAb modifications that are observed in the subcutaneous area. Thus, this is the first time, that a therapeutic mAb has been extracted from the

subcutis of a pig followed by a full mass spectrometric characterization. Due to the anatomical and physiological similarities of pig and human skin [170, 171], the application of the OFM technique to pig skin can be regarded as an excellent model to study biotransformation effects after subcutaneous injection of therapeutic mAbs.

Although, there are several approaches focusing on the investigation of deamidation *in-vivo* [80, 83-86] and other studies that evaluated the influence of oxidation on antigen binding and antibody half-life [60, 68, 69, 172], those studies focused mostly on one type of modification. In contrast to this, the workflow developed in this thesis, covers the whole mAb sequence and does not only focus on one modification at a time. It pictures several sequence related modifications and CQAs by one multiple attribute peptide mapping approach.

As can be seen by the results of the triplicates of tubes A (A1, A2, A3) and B (B1, B2, B3), the *in-vivo* protocol is highly repeatable. Furthermore, it provides the sensitivity required to assess modifications of therapeutic mAbs that are observed 10 mm apart from the site of injection in the subcutis (Tubes C1, C2, C3) and in serum.

In particular, the results of the OFM study revealed the same type and level of mAb modifications in serum and interstitial fluid. Thus, taking both sample types into account, it can be concluded, that the mAb is not modified in the subcutaneous tissue after injection within the first ten hours. The initial idea was that a modification might be less critical if it is observed after a short time course *in-vivo*, or present in high amounts in endogenous mAbs [63]. However, in this study no fast increase of a distinct modification was observed. This means, that no statement about a modification that might be less critical to monitor during production and storage due to its fast increase, can be made. Furthermore, no fast decrease of a special modification was observed in the ISF samples, leading to the assumption that none of the modifications is absorbed faster by the subcutaneous tissue. This in turn means, that no specific modification was found to be preferentially absorbed by the subcutis.

However, the results reveal that the therapeutic mAb used in this study is highly stable *in-vivo*. Based on this, it is possible to conclude that during the subcutaneous injection no modifications are introduced into the mAb and that the molecule does not get modified on its migration through the subcutis within a time span of 10 hours. As already mentioned previously, the adsorption of mAbs is a slow process. Thus, it might be investigated how long the antibody is detectable in the ISF and whether the level of modifications increases after several days.

Overall, the OFM study clearly demonstrated the feasibility of the OFM technique to be applied to the subcutaneous tissue of a pig and to successfully extract mAbs after injection into the subcutis. Furthermore, it verified the suitability of the developed antibody capture method, followed by the optimized sample preparation protocol for the low-sample amounts and the final analysis by the established Nano-HPLC-MS/MS approach for real *in-vivo* samples.

4. Conclusion and Outlook

The scope of this thesis was to investigate biotransformation of a therapeutic antibody after subcutaneous injection *in-vivo,* in both serum and the subcutis, and the development of the required workflow. Regarding the method development it could be demonstrated, that the herein established workflow is highly sensitive and specific. Human antibodies can be captured from animal serum and interstitial fluid with capture efficiencies of more than 95%. The final capture protocol offers a broad linear range and can be applied for absolute sample amounts of 5 ng up to 5 µg. Furthermore, it has been shown that also stressed and modified material can be captured using the workflow, demonstrating its unbiasedness. The optimized peptide map protocol for low sample amounts provides high sequence coverages of 90 – 100%. With the successful implementation of the nano-HPLC device coupled to a high resolution mass spectrometer, the required sensitivity for sample analysis was achieved.
Thus, the herein developed workflow provides the required specificity and sensitivity that enables a full characterization of human therapeutic antibodies after injection *in-vivo*. In contrast to other multiple attribute methods (MAM), where 100 µg mAb or more is required per sample, the herein presented workflow is capable to use only 1 µg or even less, as shown by the serum samples of the OFM study [46, 50].

It has been shown, that the Open Flow Microperfusion (OFM) technique is a useful method for the extraction of antibodies from the subcutaneous tissue. The interstitial fluid (ISF) samples from the OFM study revealed low abundant modifications, such as oxidation and deamidation, but did not show any trends. It was also possible to identify the glycosylation pattern of the ISF samples. The determined glyco-forms G0F, G1F or M5 remained constant over the measured time range. Consistent with these results also the serum samples showed low abundant oxidations and deamidations that remained constant over time. Based on the results from both sample types it can be concluded that the therapeutic antibody is not modified in the subcutis within the first 10 hours after injection.

However, it needs to be considered that the antibody absorption proceeds slow. Thus, it would be interesting, whether the level of modifications might change after one or two days in the subcutis and in serum, but also whether the molecule is still detectable in the subcutis. Furthermore, this study could be expanded to other antibody formats such as antibody-drug conjugates (ADCs) or antibody molecules containing an additional variable domain, so-called dual variable domain (DVDs) mAbs. As ADCs are an emerging drug format in the therapy and treatment of cancer, it would be of high interest whether the mAb itself, but also the drug and its linker gets modified in the subcutis. Overall, this inspires for further investigations in the field of antibody characterization *in-vivo*, which is unfortunately beyond the scope of this thesis.

Overall, the workflow described here lays the foundation for future experiments to answer the question of what happens to antibodies after injection *in-vivo*. The ability to specifically capture and fully characterize therapeutic antibodies from biologic matrices is a major improvement and of high importance for the development of biotherapeutics in future. It enables the assessment of the real criticality of quality attributes *in-vivo* by one single technique. Therefore, it might be very useful for the investigation of less stable therapeutic mAbs that are more prone to modifications.

A deeper knowledge on modifications that occur in the subcutis and in serum could furthermore build the bridge between modifications and bioavailability. Thus, this could be also a valuable approach to investigate the influence of different antibody formulations on bioavailability.

5. Appendix

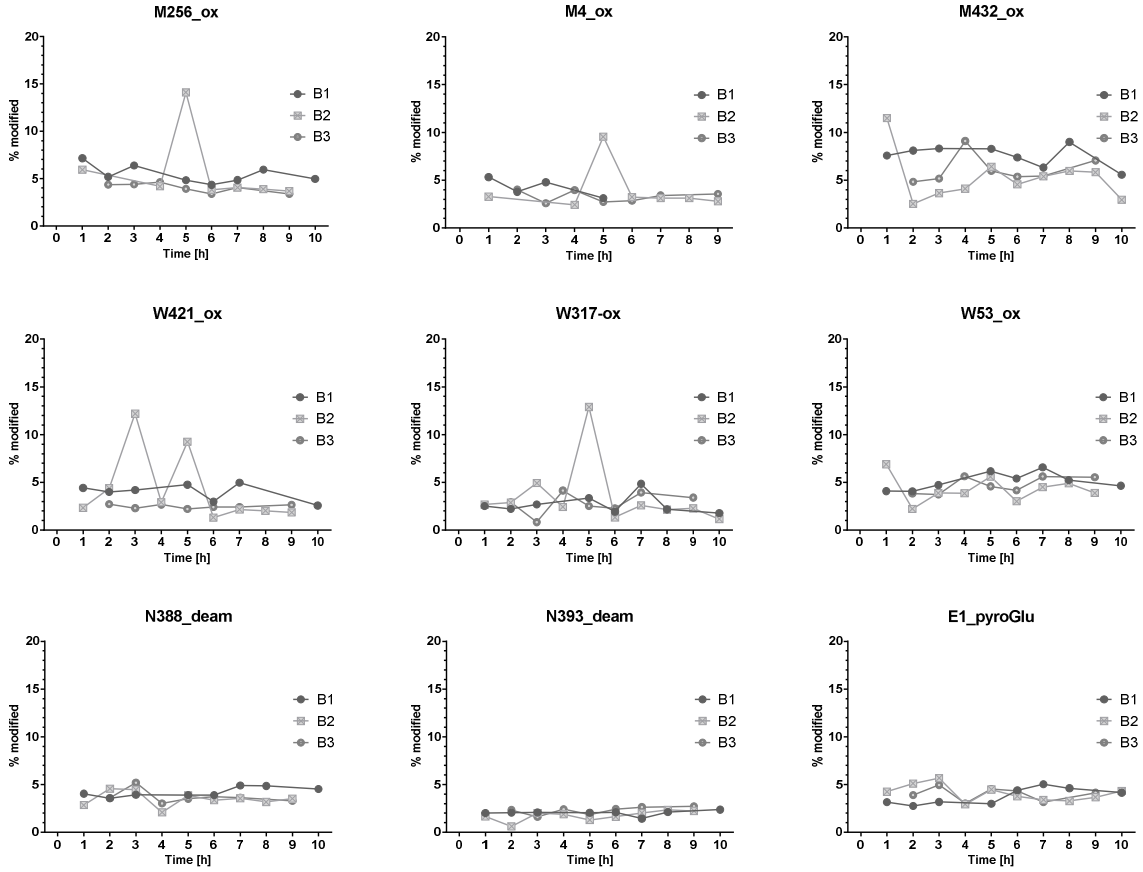

Figure 100 – Repeatability of peptide modifications for tubes B1, B2 and B3

The level of modification for selected peptides was highly repeatable for all three tubes B. The 5 hour time point of tube B2 can be regarded as outlier, as it sticks out from all the other values and is likely an in-process artifact.

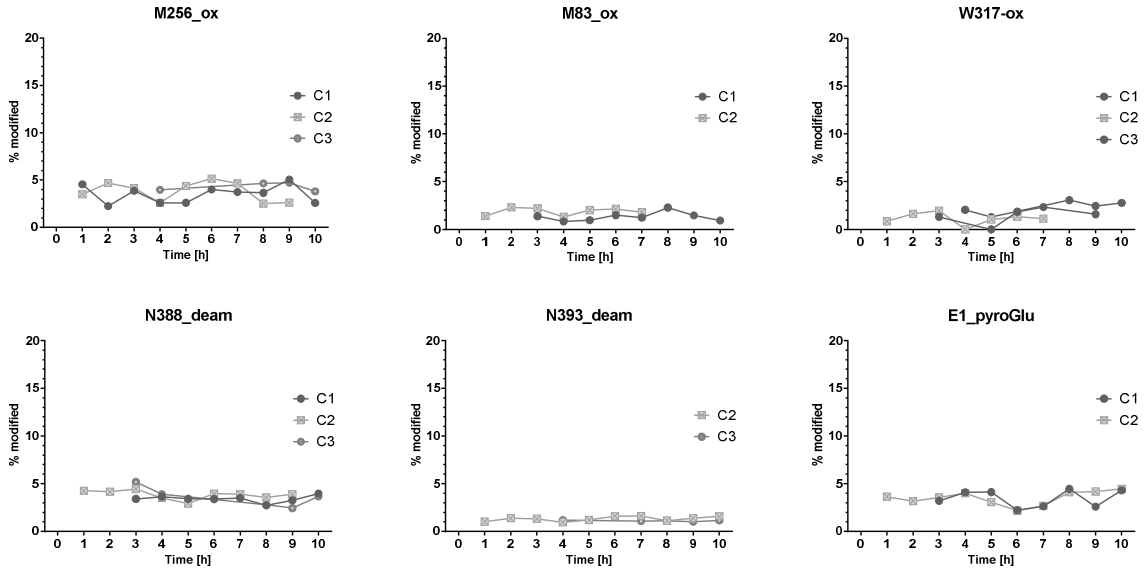

Figure 101 – Repeatability of peptide modifications for tubes C1, C2 and C3

The level of modification for selected peptides was highly reproducible for all three tubes C. Although the concentration of tubes C was significantly lower, similar modification levels could be identified.

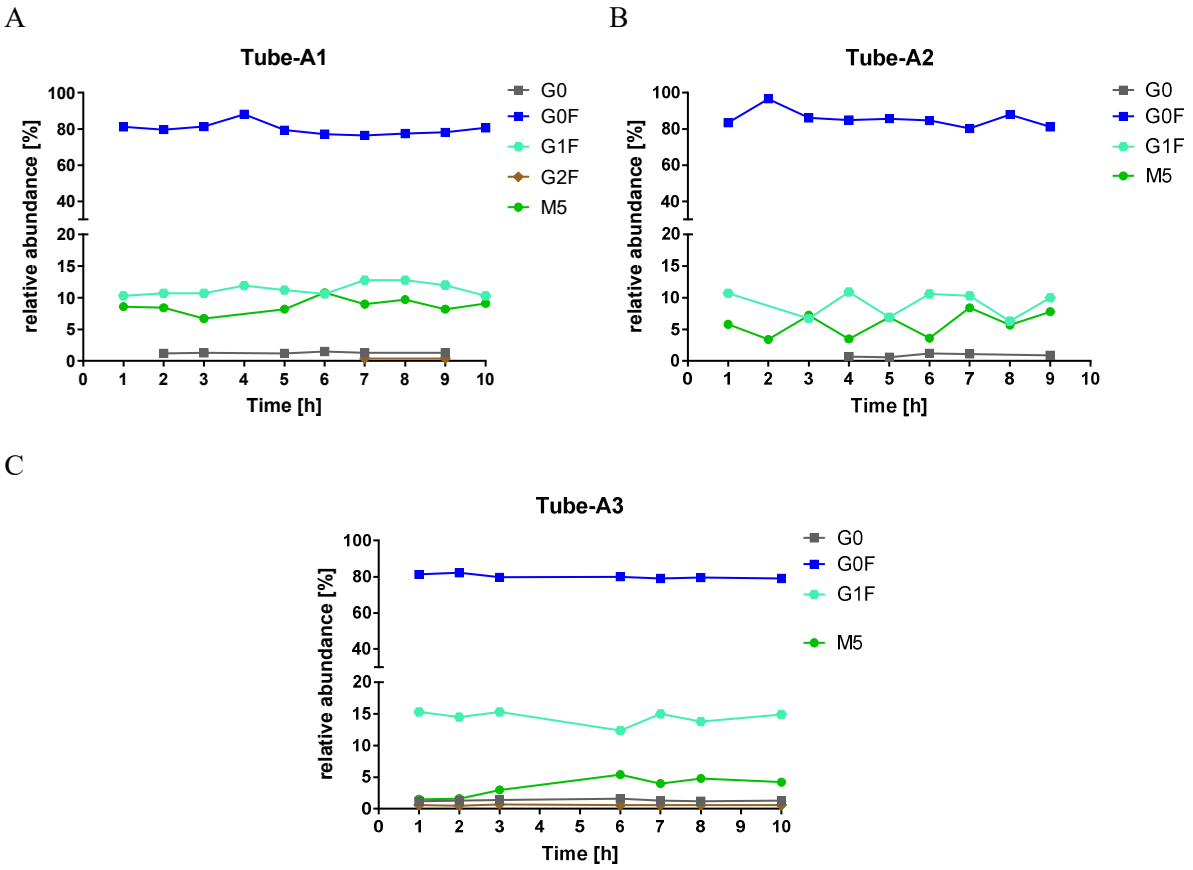

Figure 102 – Glycosylation pattern for tubes A1, A2 and A3

A) Glycosylation pattern A1. B) Glycosylation pattern A2. C) Glycosylation pattern A3.

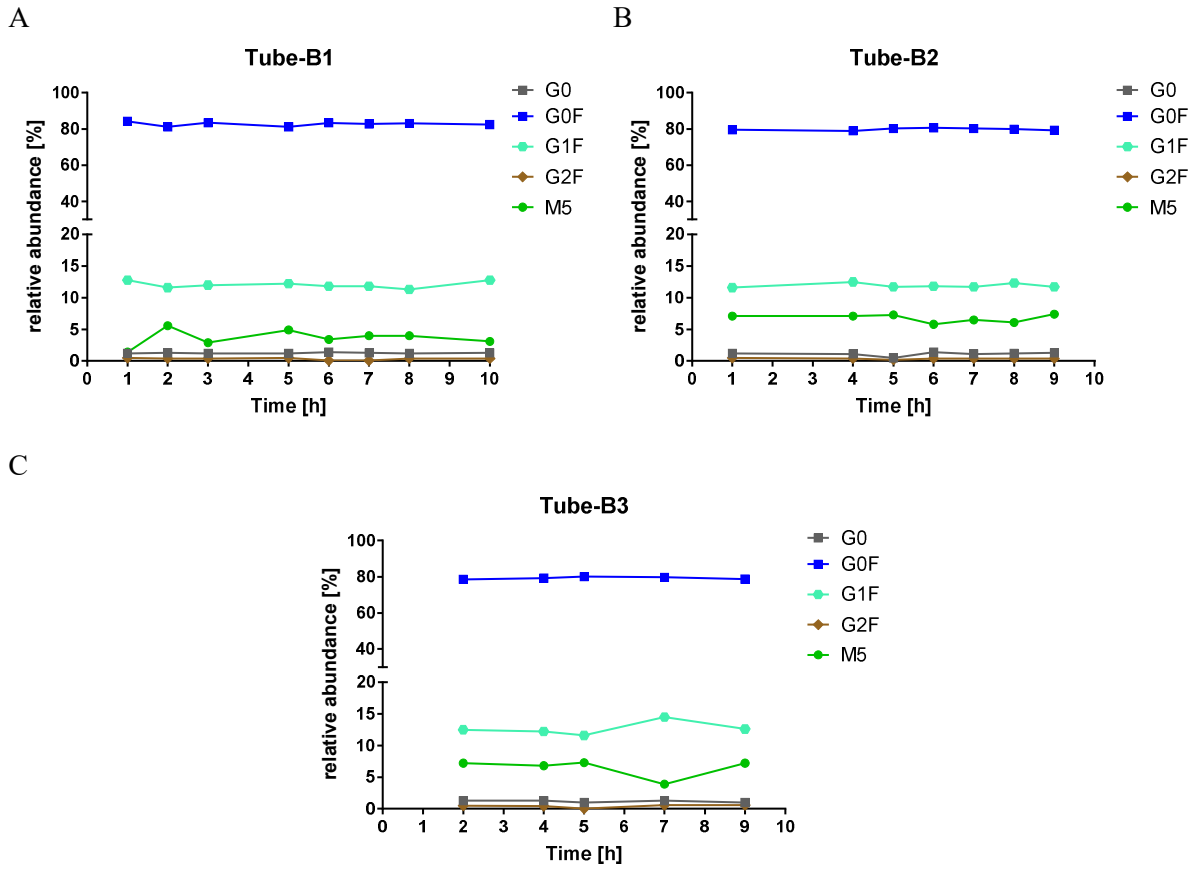

Figure 103 – Glycosylation pattern for tubes B1, B2 and B3

A) Glycosylation pattern B1. B) Glycosylation pattern B2. C) Glycosylation pattern B3.

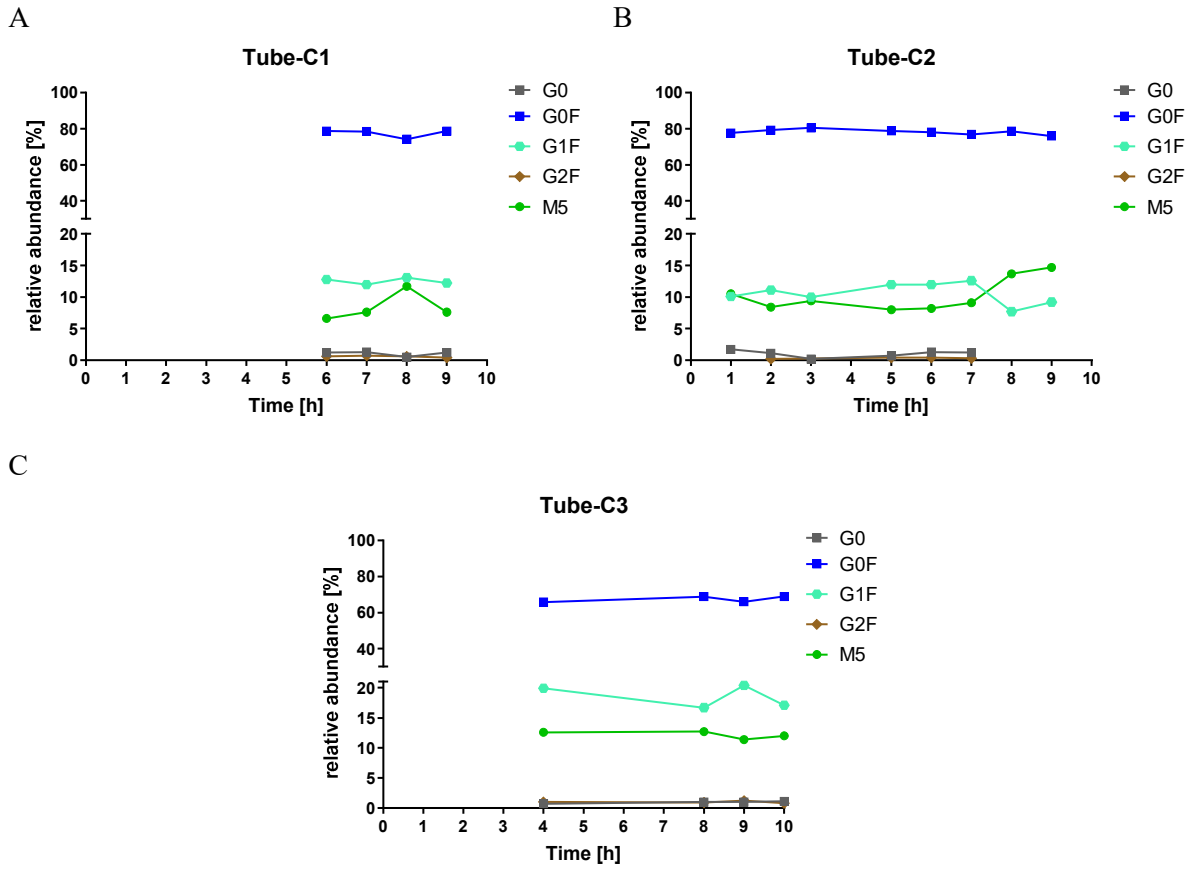

Figure 104 – Glycosylation pattern for tubes C1, C2 and C3

Although the concentration of tubes C was significantly lower, reproducible glycosylation patterns could be identified for tube C1 A), C2 B) and C3 C).

5.1 List of abbreviations

Δ2	Square difference
°C	Degree centigrade
µ	Micro
Å	Angstrom
A	Constant
ACN	Acetonitrile
ADA	Anti-drug antibody
ADC	Antibody drug conjugate
ADCC	Antibody-dependent cell cytotoxicity
aOFM	Adipose subcutaneous tissue Open Flow microperfusion
B	Constant
BG	Background
BCR	B-cell Receptor
BSA	Bovine serum albumin
C	Constant part
c	Concentration
C_0	Initial concentration
C_H1 (2,3)	Constant domain one (two, three) of the heavy chain
C_{max}	Final analyte concentration
CD	Circular dichroism
CDC	Complement-dependent cytotoxicity
CDR	Complementary-determining region
CE	Capillary electrophoresis
Cf.	confer
CID	Collision induced dissociation
cOFM	Cerebral tissue Open Flow microperfusion
CQA	Critical Quality Attribute
Cys	Cysteine
D	Chromatographic dilution
d_c	Inner column diameter
DC	Direct current
df	Degrees of freedom
DoE	Design of experiment
dOFM	Dermal Open Flow microperfusion

DMPK	Drug metabolism pharmacokinetic
DNA	Desoxiribonucleic acid
DPBS	Dulbecco's Phosphate-Buffered Saline
DSC	Differential scanning calorimetry
DRIE	Deep reactive ion etching
DTT	Dithithreitol
ε	Total porosity of the column
ESI	Electrospray ionisation
FA	Formic Acid
Fab	Fragment antigen binding
Fc	Fragment crystallizable
FcRn	Neonatal Fc-receptor
FDA	American Food and Drug Administration
FDR	False discovery rate
FFT	Fast Fourier transform
G	Gram
GlcNAc	N-acetylglucosamine
GuaHCl-	Guanidin-hydrochloride
H	Plate height
h	Hours
HAMA	Human anti mouse antibody
HAT	Hypoxanthine-aminopterine-thymidine
HC	Heavy chain
HCl	Hydrochloric acid
HESI	Heated electrospray ionization source
HILIC	Hydrophilic interaction liquid chromatography
HPLC or LC	High Performance Liquid Chromatography or Liquid Chromatography
IAA	Iodoacetic acid sodium salt
ICH	International Council for Harmonisation of Technical Requirements for Pharmaceuticals for Human Use
IEF	Isoelectric focusing
IEX	Ion exchange chromatography
Ig	Immunoglobulin
ISF	Interstitial fluid
k	Retention factor
k	Field curvature
kDa	Kilodalton

kV	Kilovolt
L	Liter
L_c	Column length
LBA	Ligand binding assay
LC	Light chain
LOQ	Limit of quantification
m	Meter
M	Molar
mA	Milli ampere
mAb	Monoclonal antibody
MAM	Multiple attribute method
min	Minutes
mL	Milliliter
mm	Millimeter
MMAE	Monomethyl auristatin E
MS	Mass spectrometry
MWCO	Molecular weight cut off
m/z	Mass-to-charge ratio
n	Number
N	Number of theoretical plates
NIST	National institute of standards and technology
nm	Nanometer
OFM	Open flow microperfusion
pAb	Polyclonal antibody
PIMT	Protein L-isoaspartyl O-methyltransferase
PS20	Polysorbate 20
psi	Pounds per square inch
PTM	Post-translational modification
r	Radial coordinate
R	Resolution
R^2	Coefficient of determination
R_m	Radius
RF	Radiofrequency
ROUT	Robust non-linear regression and removal of outliers
RP	Reversed Phase
rpm	Rounds per minute
RT	Room temperature

SAH	S-adenosylhomocysteine
SAM	S-adenosylmethionine
SDS-PAGE	Sodium dodecyl sulfate polyacrylamide gel electrophoresis
SEC	Size exclusion chromatography
SEM	Standard error of mean
SP	Signature peptide
SRM	Selected reaction monitoring
STD	Standard
TFA	Trifluoracidic acid
UV	Ultra violett
V	Volt
V	Varible part
V_{inj}	Injection volume
Vis	Visible
W	Watt
XIC	Extracted ion chromatogram
z	Cylindrical coordinate
ZDV	Zero dead volume

5.2 List of Figures

5.3 List of Tables

5.4 List of publications

Publications

Doell A., Schmitz O. J.; Hollmann M., *Shedding light into the subcutis – A mass spec based immunocapture assay enables full characterization of therapeutic antibodies after injection in-vivo,* Analytical Chemistry, 2019

Poster and Oral Presentations

45. International Symposium on High Performance Liquid Phase Separations and related techniques (HPLC), June 2017, Prague, Participation with poster presentation "Development of a sensitive nano-LC-MS approach for the *in-vivo* analysis of antibodies on peptide level".

28. Doktorandenseminar des Arbeitskreises Separation Science der GDCh-Fachgruppe Analytische Chemie, January 2018, Hohenroda, Participation with oral presentation „*In-vivo* characterization of antibodies using a sensitive nano-HPLC-MS/MS approach".

15. Symposium on the Practical Applications of Mass Spectrometry in the Biotechnology Industry, September 2018, San Francisco, Participation with oral presentation "*In-vivo* characterization of antibodies using a nano-HPLC-MS/MS approach".

Analytica China, October-November 2018, Shanghai, Participation with oral presentation "*In-vivo* characterization of antibodies using a nano-HPLC-MS/MS approach".

5.5 Curriculum Vitae

Der Lebenslauf ist in der Online-Version aus Gründen des Datenschutzes nicht enthalten**.**

5.6 Danksagung

Zunächst möchte ich meinem Doktorvater Prof. Dr. Oliver J. Schmitz ganz herzlich für die Betreuung dieser Arbeit danken. Danke, für die tolle Unterstützung und die aufschlussreichen Gespräche in stets lockerer und angenehmer Atmosphäre. Außerdem danke ich Prof. Dr. Thorsten Schmidt für die Übernahme des Koreferats.

Mein besonderer Dank gilt Markus Hollmann, der mir die Promotion in seiner Arbeitsgruppe ermöglicht hat. Vielen Dank für die wirklich tolle Betreuung der letzten drei Jahre, für alle Gespräche, Diskussionen und Tipps und natürlich für die regelmäßige Versorgung mit sauren Gurken. Ebenso möchte ich meinen Kollegen danken: Kristina, die meine Einarbeitung und somit meine ersten Schritte in der Mass-Spec Welt begleitet hat. Michael und Niko, die immer ein offenes Ohr bei Fragen oder Problemen haben und stets positive Laune verbreiten. Vielen lieben Dank an Hanna, vor allem für das Korrekturlesen meiner Arbeit, jedoch auch für die Einführung der DD-Tage und die EOB. Besonders möchte ich auch Evelyn und Kamil danken, die mich vom ersten Tag meiner Promotion begleitet haben. Danke für die tollen Gespräche, jede (un)freiwillige Essens-Einladung und eure Unterstützung und Motivation, besonders in der heißen Phase. Ich hätte mir keine besseren Kollegen vorstellen können.

Des Weiteren möchte ich dem OFM Team bei AbbVie, Preethne Böser, Sabine Eichling, Michael Siedler und Andreas Popp, für die Zusammenarbeit an diesem spannenden Projekt danken. Danke auch an das Joanneum Institut für die tolle Technik und die gute Zusammenarbeit.

Ganz herzlich möchte ich auch meiner Familie danken und ganz besonders meinem Opa Harry, der mich immer unterstützt und großes Interesse an meiner Arbeit gezeigt hat, obwohl ich mich gegen ein Geologie- oder Geschichts-Studium entschieden habe, und es leider auch nicht zum Bier brauen geschafft habe.

Abschließend möchte ich meinem Partner Dominik danken, der immer für mich da ist und hinter mir steht, mir bei Rückschlägen neue Kraft und Motivation gibt und jeden noch so kleinen Erfolg mit mir feiert.

Danke.

6. Literature

1. Wang, W., et al., *Antibody structure, instability, and formulation.* J Pharm Sci, 2007. **96**(1): p. 1-26.
2. Schmid, R.D., *Taschenatlas der Biotechnologie und Gentechnik*. 2006.
3. Chiu, M.L. and G.L. Gilliland, *Engineering antibody therapeutics.* Current Opinion in Structural Biology, 2016. **38**: p. 163-173.
4. Leusen, J.H.W. and F. Nimmerjahn, *The Role of IgG in Immune Responses*, in *Molecular and Cellular Mechanisms of Antibody Activity*, F. Nimmerjahn, Editor. 2013, Springer New York: New York, NY. p. 85-112.
5. Baker, K., T. Rath, and R.S. Blumberg, *Regulation of Immunological Responses by the Neonatal Fc Receptor for IgG, FcRn*, in *Molecular and Cellular Mechanisms of Antibody Activity*, F. Nimmerjahn, Editor. 2013, Springer New York: New York, NY. p. 189-219.
6. Lipman, N.S., et al., *Monoclonal versus polyclonal Antibodies: Distinguishing Characteristics, Applications and information resources.* ILAR Journal, 2005. **46**(3): p. 258-268.
7. Ravetch, J.V., *Fc receptors.* Current Opinion in Immunology, 1997. **9**(1): p. 121-125.
8. Martin, W.L., et al., *Crystal Structure at 2.8 Å of an FcRn/Heterodimeric Fc Complex: Mechanism of pH-Dependent Binding.* Molecular Cell, 2001. **7**(4): p. 867-877.
9. Rodewald, R. and J.P. Kraehenbuhl, *Receptor-mediated transport of IgG.* The Journal of Cell Biology, 1984. **99**(1): p. 159s-164s.
10. Brambell, F.W.R., *The transmission of immunity from mother to young and the catabolism of immunoglobulins.* The Lancet, 1966. **288**(7473): p. 1087-1093.
11. Spiegelberg, H.L. and W.O. Weigle, *The catabolism of homologous and heterologous 7S gamma globulin fragments.* The Journal of Experimental Medicine, 1965. **121**(3): p. 323-338.
12. Jones, E.A. and T.A. Waldmann, *The mechanism of intestinal uptake and transcellular transport of IgG in the neonatal rat.* The Journal of Clinical Investigation, 1972. **51**(11): p. 2916-2927.
13. Rodewald, R., *pH-dependent binding of immunoglobulins to intestinal cells of the neonatal rat.* The Journal of Cell Biology, 1976. **71**(2): p. 666-669.
14. Roopenian, D.C. and S. Akilesh, *FcRn: the neonatal Fc receptor comes of age.* Nature Reviews Immunology, 2007. **7**: p. 715.
15. Rodgers, K.R. and R.C. Chou, *Therapeutic monoclonal antibodies and derivatives: Historical perspectives and future directions.* Biotechnology Advances, 2016. **34**(6): p. 1149-1158.
16. Köhler, G. and C. Milstein, *Continuous cultures of fused cells secreting antibody of predefined specificity.* Nature, 1975. **256**(5517): p. 495-497.
17. nobelprize.org. *The Nobel Prize in Physiology or Medicine 1984*. 1984 [cited 2018 10. Oct. 2018]; Available from: https://www.nobelprize.org/prizes/medicine/1984/summary/.
18. Roque, A.C.A., C.R. Lowe, and M.Â. Taipa, *Antibodies and Genetically Engineered Related Molecules: Production and Purification.* Biotechnology Progress, 2004. **20**(3): p. 639-654.
19. Boulianne, G.L., N. Hozumi, and M.J. Shulman, *Production of functional chimaeric mouse/human antibody.* Nature, 1984. **312**(5995): p. 643-646.
20. Jones, P.T., et al., *Replacing the complementarity-determining regions in a human antibody with those from a mouse.* Nature, 1986. **321**(6069): p. 522-525.
21. McCafferty, J. and D.R. Glover, *Engineering therapeutic proteins.* Current Opinion in Structural Biology, 2000. **10**(4): p. 417-420.
22. Smith, G., *Filamentous fusion phage: novel expression vectors that display cloned antigens on the virion surface.* Science, 1985. **228**(4705): p. 1315-1317.
23. McCafferty, J., et al., *Phage antibodies: filamentous phage displaying antibody variable domains.* Nature, 1990. **348**(6301): p. 552-554.
24. NobelPrize.org, *The Nobel Prize in Chemistry 2018*. 2018: Nobel Media AB 2018.
25. Scott, C.T., *Mice with a human touch.* Nat Biotech, 2007. **25**(10): p. 1075-1077.
26. Yoon, S., et al., *Current perspectives on therapeutic antibodies.* Biotechnology and Bioprocess Engineering, 2010. **15**(5): p. 709-715.
27. Elgundi, Z., et al., *The state-of-play and future of antibody therapeutics.* Advanced Drug Delivery Reviews, 2016.

28. Jakobovits, A., et al., *From XenoMouse technology to panitumumab, the first fully human antibody product from transgenic mice.* Nature Biotechnology, 2007. **25**: p. 1134.
29. Niwa, R. and M. Satoh, *The Current Status and Prospects of Antibody Engineering for Therapeutic Use: Focus on Glycoengineering Technology.* Journal of Pharmaceutical Sciences, 2015. **104**(3): p. 930-941.
30. Chalouni, C. and S. Doll, *Fate of Antibody-Drug Conjugates in Cancer Cells.* Journal of Experimental & Clinical Cancer Research, 2018. **37**(1): p. 20.
31. Harmonisation, I.C.f. *ICH Official Website*. Available from: http://www.ich.org/home.html.
32. Medicines Agency, E., *ICH Q6B Specifications*, in *Test procedures and acceptance criteria for biotechnological/biological products*. 1999: ICH Harmonised Tripartite Guideline.
33. *ICH Harmonizes Tripartite Guideline*, in *Q8*, I.I.C.f. Harmonization, Editor. 2005, Pharmaceutical Development. p. 1-28.
34. Chirino, A.J. and A. Mire-Sluis, *Characterizing biological products and assessing comparability following manufacturing changes.* Nature biotechnology, 2004. **22**(11): p. 1383.
35. Quianzon, C.C. and I. Cheikh, *History of insulin.* Journal of community hospital internal medicine perspectives, 2012. **2**(2): p. 10.3402/jchimp.v2i2.18701.
36. Hoff, E.R. and R.C. Chloupek, *Analytical peptide mapping of recombinant DNA-derived proteins by reversed-phase high-performance liquid chromatography*, in *Methods in Enzymology*. 1996, Academic Press. p. 51-68.
37. Kannan, K., et al., *Rapid analytical tryptic mapping of a recombinant chimeric monoclonal antibody and method validation challenges1Presented at the Well Characterized Biotechnology Pharmaceuticals Meeting in San Francisco, 6–8 January, 1997.1.* Journal of Pharmaceutical and Biomedical Analysis, 1997. **16**(4): p. 631-640.
38. Dong, M.W. and A.D. Tran, *Factors influencing the performance of peptide mapping by reversed-phase high-performance liquid chromatography.* Journal of Chromatography A, 1990. **499**: p. 125-139.
39. Borman, S., *Analytical biotechnology of recombinant products.* Analytical chemistry, 1987. **59**(15): p. 969A-973A.
40. Dick, L.W., et al., *Peptide mapping of therapeutic monoclonal antibodies: Improvements for increased speed and fewer artifacts.* Journal of Chromatography B, 2009. **877**(3): p. 230-236.
41. Skrlin, A., et al., *Comparison of the physicochemical properties of a biosimilar filgrastim with those of reference filgrastim.* Biologicals, 2010. **38**(5): p. 557-566.
42. Nunnally, B., et al., *A Series of Collaborations between Various Pharmaceutical Companies and Regulatory Authorities Concerning the Analysis of Biomolecules Using Capillary Electrophoresis: Additional Instruments/Buffer.* Chromatographia, 2007. **66**(11): p. 955-961.
43. Mauko, L., et al., *Glycan profiling of monoclonal antibodies using zwitterionic-type hydrophilic interaction chromatography coupled with electrospray ionization mass spectrometry detection.* Analytical Biochemistry, 2011. **408**(2): p. 235-241.
44. Fekete, S., et al., *Analytical strategies for the characterization of therapeutic monoclonal antibodies.* TrAC Trends in Analytical Chemistry, 2013. **42**: p. 74-83.
45. den Engelsman, J., et al., *Strategies for the Assessment of Protein Aggregates in Pharmaceutical Biotech Product Development.* Pharmaceutical Research, 2011. **28**(4): p. 920-933.
46. Rogers, R.S., et al., *Development of a quantitative mass spectrometry multi-attribute method for characterization, quality control testing and disposition of biologics.* mAbs, 2015. **7**(5): p. 881-890.
47. Rogers, R.S., et al., *A View on the Importance of "Multi-Attribute Method" for Measuring Purity of Biopharmaceuticals and Improving Overall Control Strategy.* The AAPS Journal, 2017. **20**(1): p. 7.
48. Wang, T., et al., *Application of a Quantitative LC–MS Multiattribute Method for Monitoring Site-Specific Glycan Heterogeneity on a Monoclonal Antibody Containing Two N-Linked Glycosylation Sites.* Analytical Chemistry, 2017. **89**(6): p. 3562-3567.
49. Zhang, Y. and J. Guo, *Characterization and QC of biopharmaceuticals by MS-based 'multi-attribute method': advantages and challenges.* Bioanalysis, 2017. **9**(6): p. 499-502.
50. Bomans, K., et al., *Multi-attribute monitoring of antibody modifications by semi-automated liquid chromatography mass spectrometry peptide mapping.* American Pharmaceutical Review, 2016.

51. Schmid, I., et al., *Assessment of susceptible chemical modification sites of trastuzumab and endogenous human immunoglobulins at physiological conditions.* Communications Biology, 2018. **1**(1): p. 28.
52. Walsh, C.T., S. Garneau-Tsodikova, and G.J. Gatto, *Protein Posttranslational Modifications: The Chemistry of Proteome Diversifications.* Angewandte Chemie International Edition, 2005. **44**(45): p. 7342-7372.
53. Li, W., et al., *Structural Elucidation of Post-Translational Modifications in Monoclonal Antibodies.* 2015. **1201**: p. 119-183.
54. Chelius, D., et al., *Formation of pyroglutamic acid from N-terminal glutamic acid in IgG antibodies.pdf.* Anal Chem, 2006. **78**: p. 2370-2376.
55. Dick, L.W., et al., *Determination of the origin of the N-terminal pyro-glutamate variation in monoclonal antibodies using model peptides.* Biotechnology and Bioengineering, 2007. **97**(3): p. 544-553.
56. Liu, Y.D., et al., *N-terminal glutamate to pyroglutamate conversion in vivo for human IgG2 antibodies.* Journal of Biological Chemistry, 2011.
57. Lyubarskaya, Y., et al., *Analysis of recombinant monoclonal antibody isoforms by electrospray ionization mass spectrometry as a strategy for streamlining characterization of recombinant monoclonal antibody charge heterogeneity.* Analytical Biochemistry, 2006. **348**(1): p. 24-39.
58. Yu, L., et al., *Investigation of N-terminal glutamate cyclization of recombinant monoclonal antibody in formulation development.* Journal of Pharmaceutical and Biomedical Analysis, 2006. **42**(4): p. 455-463.
59. Mohammadian-Mosaabadi, J., et al., *Effect of oxidative stress on the production of recombinant human interferon-γ in Escherichia coli.* Biotechnology and Applied Biochemistry, 2005. **41**(1): p. 37-42.
60. Torosantucci, R., C. Schöneich, and W. Jiskoot, *Oxidation of Therapeutic Proteins and Peptides: Structural and Biological Consequences.* Pharmaceutical Research, 2014. **31**(3): p. 541-553.
61. Lam, X.M., et al., *Site-Specific Tryptophan Oxidation Induced by Autocatalytic Reaction of Polysorbate 20 in Protein Formulation.* Pharmaceutical Research, 2011. **28**(10): p. 2543-2555.
62. Gao, X., et al., *Effect of Individual Fc Methionine Oxidation on FcRn Binding: Met252 Oxidation Impairs FcRn Binding More Profoundly than Met428 Oxidation.* Journal of Pharmaceutical Sciences, 2015. **104**(2): p. 368-377.
63. Liu, H., et al., *In vitro and in vivo modifications of recombinant and human IgG antibodies.* MAbs, 2014. **6**(5): p. 1145-54.
64. Chumsae, C., et al., *Comparison of methionine oxidation in thermal stability and chemically stressed samples of a fully human monoclonal antibody.* Journal of Chromatography B, 2007. **850**(1): p. 285-294.
65. Gaza-Bulseco, G., et al., *Effect of methionine oxidation of a recombinant monoclonal antibody on the binding affinity to protein A and protein G.* Journal of Chromatography B, 2008. **870**(1): p. 55-62.
66. Bertolotti-Ciarlet, A., et al., *Impact of methionine oxidation on the binding of human IgG1 to FcRn and Fcγ receptors.* Molecular Immunology, 2009. **46**(8): p. 1878-1882.
67. Wang, W., et al., *Impact of methionine oxidation in human IgG1 Fc on serum half-life of monoclonal antibodies.* Molecular Immunology, 2011. **48**(6): p. 860-866.
68. Stracke, J., et al., *A novel approach to investigate the effect of methionine oxidation on pharmacokinetic properties of therapeutic antibodies.* MAbs, 2014. **6**(5): p. 1229-42.
69. Cymer, F., et al., *Oxidation of M252 but not M428 in hu-IgG1 is responsible for decreased binding to and activation of hu-FcgammaRIIa (His131).* Biologicals, 2017. **50**: p. 125-128.
70. Amano, M., et al., *Detection of Histidine Oxidation in a Monoclonal Immunoglobulin Gamma (IgG) 1 Antibody.* Analytical Chemistry, 2014. **86**(15): p. 7536-7543.
71. Liu, L., *Antibody Glycosylation and Its Impact on the Pharmacokinetics and Pharmacodynamics of Monoclonal Antibodies and Fc-Fusion Proteins.* Journal of Pharmaceutical Sciences, 2015. **104**(6): p. 1866-1884.
72. Chen, X. and G.C. Flynn, *Analysis of N-glycans from recombinant immunoglobulin G by on-line reversed-phase high-performance liquid chromatography/mass spectrometry.* Analytical Biochemistry, 2007. **370**(2): p. 147-161.

73. Krapp, S., et al., *Structural Analysis of Human IgG-Fc Glycoforms Reveals a Correlation Between Glycosylation and Structural Integrity.* Journal of Molecular Biology, 2003. **325**(5): p. 979-989.
74. Alsenaidy, M.A., et al., *Physical Stability Comparisons of IgG1-Fc Variants: Effects of N-Glycosylation Site Occupancy and Asp/Gln Residues at Site Asn 297.* Journal of Pharmaceutical Sciences, 2014. **103**(6): p. 1613-1627.
75. Johnson, J.L., et al., *The regulatory power of glycans and their binding partners in immunity.* Trends Immunol, 2013. **34**(6): p. 290-8.
76. Pawlowski, J.W., et al., *Influence of glycan modification on IgG1 biochemical and biophysical properties.* Journal of Pharmaceutical and Biomedical Analysis, 2018. **151**: p. 133-144.
77. Flynn, G.C., et al., *Naturally occurring glycan forms of human immunoglobulins G1 and G2.* Molecular Immunology, 2010. **47**(11): p. 2074-2082.
78. Goetze, A.M., et al., *High-mannose glycans on the Fc region of therapeutic IgG antibodies increase serum clearance in humans.* Glycobiology, 2011. **21**(7): p. 949-59.
79. Yang, H. and R.A. Zubarev, *Mass spectrometric analysis of asparagine deamidation and aspartate isomerization in polypeptides.* Electrophoresis, 2010. **31**(11): p. 1764-72.
80. Wang, W., et al., *Quantification and characterization of antibody deamidation by peptide mapping with mass spectrometry.* International Journal of Mass Spectrometry, 2012. **312**: p. 107-113.
81. Stephenson, R.C. and S. Clarke, *Succinimide formation from aspartyl and asparaginyl peptides as a model for the spontaneous degradation of proteins.* Journal of Biological Chemistry, 1989. **264**(11): p. 6164-6170.
82. Kumar, S., et al., *Unexpected functional implication of a stable succinimide in the structural stability of Methanocaldococcus jannaschii glutaminase.* Nature communications, 2016. **7**: p. 12798-12798.
83. Lihua Huang, et al., *In Vivo Deamidation Characterization of mAb by LC-MS/MS.pdf.* Anal Chem, 2005. **77**: p. 1432-1439.
84. Bults, P., et al., *LC-MS/MS-Based Monitoring of In Vivo Protein Biotransformation: Quantitative Determination of Trastuzumab and Its Deamidation Products in Human Plasma.* Analytical Chemistry, 2016. **88**(3): p. 1871-1877.
85. Mehl, J.T., et al., *Quantification of in vivo site-specific Asp isomerization and Asn deamidation of mAbs in animal serum using IP-LC–MS.* Bioanalysis, 2016. **8**(15): p. 1611-1622.
86. Liu, Y.D., J.Z. van Enk, and G.C. Flynn, *Human antibody Fc deamidation in vivo.* Biologicals, 2009. **37**(5): p. 313-322.
87. Harris, R.J., et al., *Identification of multiple sources of charge heterogeneity in a recombinant antibody.* Journal of Chromatography B: Biomedical Sciences and Applications, 2001. **752**(2): p. 233-245.
88. Vlasak, J., et al., *Identification and characterization of asparagine deamidation in the light chain CDR1 of a humanized IgG1 antibody.* Analytical Biochemistry, 2009. **392**(2): p. 145-154.
89. Edelman, G.M., et al., *The covalent structure of an entire γG immunoglobulin molecule.* Proceedings of the National Academy of Sciences, 1969. **63**(1): p. 78-85.
90. Harris, R.J., *Processing of C-terminal lysine and arginine residues of proteins isolated from mammalian cell culture.* Journal of Chromatography A, 1995. **705**(1): p. 129-134.
91. Tsubaki, M., et al., *C-terminal modification of monoclonal antibody drugs: Amidated species as a general product-related substance.* International Journal of Biological Macromolecules, 2013. **52**: p. 139-147.
92. Bing, C., P. Hai, and F.G. C., *C-terminal lysine processing of human immunoglobulin G2 heavy chain in vivo.* Biotechnology and Bioengineering, 2011. **108**(2): p. 404-412.
93. Antes, B., et al., *Analysis of lysine clipping of a humanized Lewis-Y specific IgG antibody and its relation to Fc-mediated effector function.* Journal of Chromatography B, 2007. **852**(1): p. 250-256.
94. Brorson, K. and A.Y. Jia, *Therapeutic monoclonal antibodies and consistent ends: terminal heterogeneity, detection, and impact on quality.* Current Opinion in Biotechnology, 2014. **30**: p. 140-146.

95. Jiang, G., et al., *Evaluation of Heavy-Chain C-Terminal Deletion on Product Quality and Pharmacokinetics of Monoclonal Antibodies.* Journal of Pharmaceutical Sciences, 2016. **105**(7): p. 2066-2072.
96. van den Bremer, E.T.J., et al., *Human IgG is produced in a pro-form that requires clipping of C-terminal lysines for maximal complement activation.* mAbs, 2015. **7**(4): p. 672-680.
97. Li, Y., et al., *Assessing in vivo dynamics of multiple quality attributes from a therapeutic IgG4 monoclonal antibody circulating in cynomolgus monkey.* mAbs, 2016. **8**(5): p. 961-968.
98. Rosenbloom, A.J., D.M. Sipe, and V.W. Weedn, *Microdialysis of proteins: Performance of the CMA/20 probe.* Journal of Neuroscience Methods, 2005. **148**(2): p. 147-153.
99. Pieber, T., et al., *Open Flow Microperfusion: An Alternative Method to Microdialysis?*, in *Microdialysis in Drug Development*, M. Müller, Editor. 2013, Springer New York: New York, NY. p. 283-302.
100. Dragatin, C., et al., *Secukinumab distributes into dermal interstitial fluid of psoriasis patients as demonstrated by open flow microperfusion.* Experimental Dermatology, 2016. **25**(2): p. 157-159.
101. Tiffner, K., et al., *Quantification of Basal Insulin Peglispro and Human Insulin in Adipose Tissue Interstitial Fluid by Open-Flow Microperfusion.* Diabetes Technology & Therapeutics, 2017. **19**(5): p. 305-314.
102. Birngruber, T. and F. Sinner, *Cerebral open flow microperfusion (cOFM) an innovative interface to brain tissue.* Drug Discovery Today: Technologies, 2016. **20**: p. 19-25.
103. Ikeoka, D., et al., *Interleukin-6 produced in subcutaneous adipose tissue is linked to blood pressure control in septic patients.* Cytokine, 2010. **50**(3): p. 284-291.
104. Bodenlenz, M., et al., *Dermal PK/PD of a lipophilic topical drug in psoriatic patients by continuous intradermal membrane-free sampling.* European Journal of Pharmaceutics and Biopharmaceutics, 2012. **81**(3): p. 635-641.
105. Zhang, S. and C.K. Van Pelt, *Chip-based nanoelectrospray mass spectrometry for protein characterization.* Expert Review of Proteomics, 2004. **1**(4): p. 449-468.
106. Shen, Y., et al., *High-Efficiency Nanoscale Liquid Chromatography Coupled On-Line with Mass Spectrometry Using Nanoelectrospray Ionization for Proteomics.* Analytical Chemistry, 2002. **74**(16): p. 4235-4249.
107. Shen, Y., et al., *Ultrasensitive Proteomics Using High-Efficiency On-Line Micro-SPE-NanoLC-NanoESI MS and MS/MS.* Analytical Chemistry, 2004. **76**(1): p. 144-154.
108. Karlsson, K.E. and M. Novotny, *Separation efficiency of slurry-packed liquid chromatography microcolumns with very small inner diameters.* Analytical Chemistry, 1988. **60**(17): p. 1662-1665.
109. Rieux, L., E.-J. Sneekes, and S. Remco, *Nano LC: Principles, Evolution, and State-of-the-Art of the Technique.* LCGC North America, 2011. **29**(10): p. 926-934.
110. Gama, M.R., C.H. Collins, and C.B.G. Bottoli, *Nano-Liquid Chromatography in Pharmaceutical and Biomedical Research.* Journal of Chromatographic Science, 2013. **51**(7): p. 694-703.
111. Byrdwell, W.C. and M. Holčapek, *Nano-Liquid Chromaographic Separation*, in *Extreme Chromatography - Faster, Hotter, Smaller*. 2011, AOCS Press.
112. María, S.J. and M.M. Luisa, *Application of micro- and nano-HPLC to the determination and characterization of bioactive and biomarker peptides.* Journal of Separation Science, 2008. **31**(3): p. 446-458.
113. Dass, C., *Fundamentals of contemporary mass spectrometry*, N.M.N. Dominic M. Desidero, Editor. 2007, John Wiley & Sons, Inc.: New Jersey.
114. Ardrey, R.E., *Liquid Chromatography - Mass Spectrometry An Introduction.pdf*. 2003: John Wiley & Sons, Ltd. 288.
115. Fenn, J., et al., *Electrospray ionization for mass spectrometry of large biomolecules.* Science, 1989. **246**(4926): p. 64-71.
116. Cech, N.B. and C.G. Enke, *Practical implications of some recent studies in electrospray ionization fundamentals.* Mass Spectrometry Reviews, 2001. **20**(6): p. 362-387.
117. Wilm, M. and M. Mann, *Analytical Properties of the Nanoelectrospray Ion Source.* Analytical Chemistry, 1996. **68**(1): p. 1-8.

118. Schultz, G.A., et al., *A Fully Integrated Monolithic Microchip Electrospray Device for Mass Spectrometry.* Analytical Chemistry, 2000. **72**(17): p. 4058-4063.
119. Van Pelt, C., S. Zhang, and J. Henion, *Characterization of a fully automated nanoelectrospray system with mass spectrometric detection for proteomic analyses.* Journal of Biomolecular Techniques : JBT, 2002. **13**(2): p. 72-84.
120. Kiyonami, R., et al., *Easy-to-use, plug-and-spray ion source for robust and reproducible ultra high pressure nanoflow LC/MS.* Thermo Fisher Scientific, CA, USA, Technical Note, 2012. **63546**.
121. Lewis, R.R., *Motions of ion in the kingdon trap.* Journal of Applied Physics, 1982. **53**(6): p. 3975-3980.
122. Makarov, A., *Electrostatic Axially Harmonic Orbital Trapping: A High-Performance Technique of Mass Analysis.* Analytical Chemistry, 2000. **72**(6): p. 1156-1162.
123. Hu, Q., et al., *The Orbitrap: a new mass spectrometer.* J Mass Spectrom, 2005. **40**(4): p. 430-43.
124. Makarov, A. and M. Scigelova, *Coupling liquid chromatography to Orbitrap mass spectrometry.* Journal of Chromatography A, 2010. **1217**(25): p. 3938-3945.
125. Tye, H., *Application of statistical 'design of experiments' methods in drug discovery.* Drug Discovery Today, 2004. **9**(11): p. 485-491.
126. Owen, M.R., et al., *Efficiency by Design: Optimisation in Process Research.* Organic Process Research & Development, 2001. **5**(3): p. 308-323.
127. Gotti, R., et al., *Design of experiments for capillary electrophoretic enantioresolution of salbutamol using dermatan sulfate.* Journal of Chromatography A, 2000. **875**(1): p. 411-422.
128. Kirchhoff, E.W., et al., *Automated Process Research and the Optimization of the Synthesis of 4(5)-(3-Pyridyl)imidazole.* Organic Process Research & Development, 2001. **5**(1): p. 50-53.
129. National Institute of Standards and Technology, N. *Report of Investigation RM 8671 - NISTmAb, Humanized IgG1κ Monoclonal Antibody*. 2018 [cited 2018 09. Dec]; Available from: https://www-s.nist.gov/srmors/view_cert.cfm?srm=8671.
130. Kruger, N.J. and J.B.W. Hammond, *Purification of Immunoglobulins Using Protein A-Sepharose*, in *New Protein Techniques*, J.M. Walker, Editor. 1988, Humana Press: Totowa, NJ. p. 363-371.
131. Dubois, M., et al., *Immunopurification and Mass Spectrometric Quantification of the Active Form of a Chimeric Therapeutic Antibody in Human Serum.* Analytical Chemistry, 2008. **80**(5): p. 1737-1745.
132. Ayyar, B.V., et al., *Affinity chromatography as a tool for antibody purification.* Methods, 2012. **56**(2): p. 116-29.
133. Marchalonis, J.J., J.L. Atwell, and J.W. Goding, *7S immunoglobulins of a monotreme, the Echidna Tachyglossus aculeatus: two distinct isotypes which bind A protein of Staphylococcus aureus.* Immunology, 1978. **34**(1): p. 97-103.
134. Grodzki, A.C. and E. Berenstein, *Antibody Purification: Affinity Chromatography – Protein A and Protein G Sepharose*, in *Immunocytochemical Methods and Protocols*, C. Oliver and M.C. Jamur, Editors. 2010, Humana Press: Totowa, NJ. p. 33-41.
135. Huse, K., *Purification of antibodies by affinity chromatography.* Journal of Biochemical and Biophysical Methods, 2002. **51**(3): p. 217-231.
136. Bosma, M.J. and A.M. Carroll, *The SCID Mouse Mutant: Definition, Characterization, and Potential Uses.* Annual Review of Immunology, 1991. **9**(1): p. 323-350.
137. Nowak, J., et al., *Length-independent structural similarities enrich the antibody CDR canonical class model.* mAbs, 2016. **8**(4): p. 751-760.
138. Kirley, T.L. and A.B. Norman, *Unfolding of IgG domains detected by non-reducing SDS-PAGE.* Biochemical and Biophysical Research Communications, 2018. **503**(2): p. 944-949.
139. Kirley, T.L., K.D. Greis, and A.B. Norman, *Domain unfolding of monoclonal antibody fragments revealed by non-reducing SDS-PAGE.* Biochemistry and biophysics reports, 2018. **16**: p. 138-144.
140. Li, Y., et al., *Quantitation and pharmacokinetic modeling of therapeutic antibody quality attributes in human studies.* mAbs, 2016. **8**(6): p. 1079-1087.
141. Liu, Y.D., et al., *Human IgG2 Antibody Disulfide Rearrangement in Vivo.* Journal of Biological Chemistry, 2008. **283**(43): p. 29266-29272.

142. Geiger, T. and S. Clarke, *Deamidation, isomerization, and racemization at asparaginyl and aspartyl residues in peptides. Succinimide-linked reactions that contribute to protein degradation.* Journal of Biological Chemistry, 1987. **262**(2): p. 785-794.
143. Motulsky, H.J. and R.E. Brown, *Detecting outliers when fitting data with nonlinear regression – a new method based on robust nonlinear regression and the false discovery rate.* BMC Bioinformatics, 2006. **7**(1): p. 123.
144. Gevaert, K., et al., *Exploring proteomes and analyzing protein processing by mass spectrometric identification of sorted N-terminal peptides.* Nature Biotechnology, 2003. **21**: p. 566.
145. Ren, D., et al., *An improved trypsin digestion method minimizes digestion-induced modifications on proteins.* Analytical Biochemistry, 2009. **392**(1): p. 12-21.
146. Rehder, D.S., et al., *Reversed-phase liquid chromatography/mass spectrometry analysis of reduced monoclonal antibodies in pharmaceutics.* Journal of Chromatography A, 2006. **1102**(1): p. 164-175.
147. Liu, H., G. Gaza-Bulseco, and L. Zhou, *Mass spectrometry analysis of photo-induced methionine oxidation of a recombinant human monoclonal antibody.* Journal of the American Society for Mass Spectrometry, 2009. **20**(3): p. 525-528.
148. Tran, J.C. and A.A. Doucette, *Cyclic polyamide oligomers extracted from nylon 66 membrane filter disks as a source of contamination in liquid chromatography/mass spectrometry.* Journal of The American Society for Mass Spectrometry, 2006. **17**(5): p. 652-656.
149. Rosati, S., et al., *Detailed mass analysis of structural heterogeneity in monoclonal antibodies using native mass spectrometry.* Nature Protocols, 2014. **9**: p. 967.
150. Sandra, K., et al., *The versatility of heart-cutting and comprehensive two-dimensional liquid chromatography in monoclonal antibody clone selection.* Journal of Chromatography A, 2017. **1523**: p. 283-292.
151. Ren, D., et al., *Detection and identification of a serine to arginine sequence variant in a therapeutic monoclonal antibody.* Journal of Chromatography B, 2011. **879**(27): p. 2877-2884.
152. Capriotti, A.L., et al., *Proteomic study of a tolerant genotype of durum wheat under salt-stress conditions.* Analytical and Bioanalytical Chemistry, 2014. **406**(5): p. 1423-1435.
153. Meyer, M.R., et al., *Identification of main human urinary metabolites of the designer nitrobenzodiazepines clonazolam, meclonazepam, and nifoxipam by nano-liquid chromatography-high-resolution mass spectrometry for drug testing purposes.* Analytical and Bioanalytical Chemistry, 2016. **408**(13): p. 3571-3591.
154. Sinha, A., et al., *In-depth proteomic analyses of ovarian cancer cell line exosomes reveals differential enrichment of functional categories compared to the NCI 60 proteome.* Biochemical and Biophysical Research Communications, 2014. **445**(4): p. 694-701.
155. Selman, M.H.J., et al., *Fc specific IgG glycosylation profiling by robust nano-reverse phase HPLC-MS using a sheath-flow ESI sprayer interface.* Journal of Proteomics, 2012. **75**(4): p. 1318-1329.
156. Mitulović, G., et al., *Preventing Carryover of Peptides and Proteins in Nano LC-MS Separations.* Analytical Chemistry, 2009. **81**(14): p. 5955-5960.
157. Pirmoradian, M., et al., *Rapid and deep human proteome analysis by single-dimension shotgun proteomics.* Molecular & Cellular Proteomics, 2013.
158. Liu, H., et al., *Accurate Determination of Protein Methionine Oxidation by Stable Isotope Labeling and LC-MS Analysis.* Analytical Chemistry, 2013. **85**(24): p. 11705-11709.
159. Folzer, E., et al., *Selective Oxidation of Methionine and Tryptophan Residues in a Therapeutic IgG1 Molecule.* Journal of Pharmaceutical Sciences, 2015. **104**(9): p. 2824-2831.
160. Ji, J.A., et al., *Methionine, tryptophan, and histidine oxidation in a model protein, PTH: mechanisms and stabilization.* Journal of pharmaceutical sciences, 2009. **98**(12): p. 4485-4500.
161. Levine, R.L., et al., *Methionine residues as endogenous antioxidants in proteins.* Proceedings of the National Academy of Sciences, 1996. **93**(26): p. 15036-15040.
162. Stadtman, E., *Oxidation of free amino acids and amino acid residues in proteins by radiolysis and by metal-catalyzed reactions.* Annual review of biochemistry, 1993. **62**(1): p. 797-821.
163. Stadtman, E.R., *Metal ion-catalyzed oxidation of proteins: biochemical mechanism and biological consequences.* Free Radical Biology and Medicine, 1990. **9**(4): p. 315-325.

164. Millán, S., et al., *Investigating process-related post-translational modifications in NISTmAb RM 8671 using high-throughput peptide mapping analysis.* Thermo Fisher Scientific, CA, USA, Technical Note, 2018. **21781**: p. 1-14.
165. Dong, Q., et al., *The NISTmAb tryptic peptide spectral library for monoclonal antibody characterization.* mAbs, 2018. **10**(3): p. 354-369.
166. Waters, *nanoEase M/Z Columns.* White Paper Waters Corporation, 2018. **USRM134941586**(720005931EN): p. 1-11.
167. Eshraghi, J. and S.K. Chowdhury, *Factors affecting electrospray ionization of effluents containing trifluoroacetic acid for high-performance liquid chromatography/mass spectrometry.* Analytical chemistry, 1993. **65**(23): p. 3528-3533.
168. Mirza, U.A. and B.T. Chait, *Effects of anions on the positive ion electrospray ionization mass spectra of peptides and proteins.* Analytical chemistry, 1994. **66**(18): p. 2898-2904.
169. Wang, W., E.Q. Wang, and J.P. Balthasar, *Monoclonal antibody pharmacokinetics and pharmacodynamics.* Clin Pharmacol Ther, 2008. **84**(5): p. 548-58.
170. Sullivan, T.P., et al., *The pig as a model for human wound healing* Wound Repair and Regeneration, 2001. **9**(2): p. 66-76.
171. Zhu, K.Q., et al., *The female, red Duroc pig as an animal model of hypertrophic scarring and the potential role of the cones of skin.* Burns, 2003. **29**(7): p. 649-664.
172. Dashivets, T., et al., *Oxidation in the complementarity-determining regions differentially influences the properties of therapeutic antibodies.* mAbs, 2016. **8**(8): p. 1525-1535.